Porous Polymeric Superstructures as In-Growth Scaffolds for Tissue-Engineered Vascular Prostheses

Dissertation presented for the Degree of Doctor of Philosophy:

Ph.D. (Polymer Science)

At the

University of Stellenbosch

By

Deon Bezuidenhout

Supervisors:

Prof. R.D. Sanderson
Institute for Polymer Science
Stellenbosch University

Prof. P. Zilla
Cardiovascular Research Unit
University of Cape Town

Cape Town
25/11/01

Stellenbosch University http://scholar.sun.ac.za

DECLARATION

I, the undersigned, hereby declare that the work contained in this dissertation is my own original work and that I have not previously in its entirety or in part submitted it at any university for a degree.

Ex Africa semper aliquid novi.

Pliny the Elder

Historia Naturalis II. 8

Stellenbosch University http://scholar.sun.ac.za

Porous Polymeric Superstructures as In-growth Scaffolds for Tissue-Engineered Vascular Prostheses

Ph.D. dissertation by

Deon Bezuidenhout

Supervisor

Prof. R.D. Sanderson

Co-Supervisor

Prof. P. Zilla

Stellenbosch University http://scholar.sun.ac.za

ABSTRACT

Compliance and angio-permissive, three-dimensional ingrowth spaces are important determinants in the healing of vascular prostheses. Conventional ePTFE and Dacron prostheses, as well as experimental polyurethane grafts, fail to provide satisfactory long-term outcomes in small-diameter applications due to a lack of one or both of these criteria. Thus a compliant polyurethane graft containing well-defined, interconnected pores is proposed. These structures were successfully produced by a novel phase inversion/porogen extraction technique using spherical porogens. The pore sizes and interconnectivity could be accurately controlled by variation of the porogen size and the precipitation conditions. Thus pores of 66.1±0.3, 84.2±1.7 and 157.0±2.4μm containing interconnected windows of 30.1±0.8, 41.9±1.5 and 76.4±2.0μm could be produced from 64.5±0.3, 87.5±0.7 and 129.0±0.9μm beads, respectively.

The healing response toward implanted devices often leads to excessive inflammation that, in turn, leads to the formation of unwanted fibrotic scar tissue, and the need to eliminate or reduce this response is obvious. Both pore size and surface characteristics have been shown to influence this response. By increasing the pore size of porous scaffolds from 66 to 157μm, the inflammatory response was reduced by 56% ($p<0.05$). A combination of increased pore size with the pacification of the grafts surfaces with covalently immobilized collagen resulted in an even further decrease in the foreign body response in the rat model (80% decrease; $p<0.002$).

A senescent chacma baboon model was developed for the evaluation of prosthetic vascular grafts. The model consists of an isolated graft segment (between two isolating, low porosity ePTFE segments) and allows for the evaluation of transmural healing in the test segment without interference from transanastomotic outgrowth.

In order to determine whether an increase pore in dimensions alone would result in the desired healing response, very high porosity (150μm IND) ePTFE was compared to standard 30μm material in the isolated primate model. Although the increase in pore size allowed for the ingrowth of capillaries and arterioles, migration to the inner graft surface was inhibited by a dense, impenetrable fibrin layer deposited on the lumenal surface. Elimination of the fibrin layer by the application of a sealant resulted in slightly improved transmural healing, but the node/fibril structure and non-compliant nature of ePTFE was not conducive to cellular re-orientation.

Evaluation of high-porosity polyurethane grafts in the same model showed penetration of capillaries and arterioles, as well as small smooth muscle cell bands throughout most of the thickness of the wall. This response was, however, also limited by the hostile fibrin deposit. The sealing of the lumenal surface in this case led to the desired outcome. Not only did capillaries and arterioles migrate through and populate the entire thickness of the graft wall, but also thick bands of helically oriented smooth muscle cells were observed directly on the outer surface of the lumenal sealant. This is an important milestone in the development of synthetic grafts that would mimic both the structure and function of natural arteries they are to replace.

Stellenbosch University http://scholar.sun.ac.za

OPSOMMING

Meganiese uitsetting as gevolg van gepulseerde druk en 'n oop, drie-dimensionele, porieuse struktuur is belangrike voorvereistes vir die herstel van vaskulêre prostese. As gevolg van 'n gebrek aan een of beide van hierdie vereistes, bied konvensionele ePTFE - en Dacron prostese nie bevredigende lang-termyn resultate in lae deursnit toepassings nie. Hierdie studie ondersoek dus die gebruik van 'n elastomeriese poliuretaan (PU) prostese met goed-gedefineerde, interkommunikerende porieë. 'n Nuut-voorgestelde tegniek, wat die fase-inversie en ekstraksie van sferiese porogene behels, is gebruik om hierdie strukture te vervaardig. Die poriegrotes en interkonnektiwiteit kon akkuraat beheer word deur die variasie van porogeengrote en presipitasiekondisies. Porieë van 66.1±0.3, 84.2±1.7 en 157.0±2.4µm, met interkonneksies van 30.1±0.8, 41.9±1.5 and 76.4±2.0µm kon gevolglik vervaardig word deur die gebruik van PU en 64.5±0.3, 87.5±0.7 and 129.0±0.9µm porogene.

Die reaksie tot prostetiese materiale in vivo, lei dikwels tot oormatige inflammasie wat weer tot die ontwikkeling van fibrotiese letselweefsel lei. Daar word gewys dat beide poriegrote en oppervlakeienskappe die inflammatoriese reaksie beinvloed. 'n Toename in poriegrote van 66 na 157µm het bevoorbeeld gelei tot 'n 56% afname in inflammasie ($p<0.05$), terwyl 'n afname van 80% behaal is ($p<0.002$) deur 'n kombinasie van vergrote porieë en pasifiseering van die oppervakte met kovalent gebonde kollageen.

'n Volwasse femorale chacma bobbejaanmodel is ontwikkel vir die evaluasie van vaskulêre prosteses. Die model behels die interposisionering van die toetsmateriaal tussen twee segmente van 30µm interfiebrielafstand ePTFE. Dit laat die evaluasie van radiale ingroei van weefsel (deur die wand) toe, sonder dat transanastomotiese uitgroei die resultate beinvloed.

Om te bepaal of 'n toename in poriegrote alleen tot die verlangde mate van herstel kan lei, is ePTFE met baie groot porieë (150µm) met standaard 30µm materiaal in die geïsoleerde model vergelyk. Alhoewel die toename in poriegrote die ingroei van kapillêre en arteriole toegelaat het, is migrasie na die binneoppervlak verhinder deur 'n digte, ondeurdringbare fibrienlaag wat deur die bloed gedeponeer is. Eliminasie van hierdie fibrienlaag deur die aanwending van 'n seellaag het gelei tot 'n klein verbetering in radiale weefselingroei, maar die node/fiebriel struktuur en nie-elastomeriese eienskappe van ePTFE het nie sellulêre orientasie toegelaat nie.

Hoë porositeit poliuretaan is ook in die bogenoemde model ge-evalueer. Afgesien van die ingroei van kapillêre en arteriole deur die grootste gedeelte van die wand, is klein bundels gladde spierweefselselle ook waargeneem. Hierdie herstel is egter weereens deur die fibrienlaag beperk. Die aanwending van 'n seellaag op hierdie materiaal (157µm PU) het egter die gewenste uitwerking gehad. Buitenbehalwe die migrasie en besetting van die hele wand deur kapillêre en arteriole, is die vorming van helies-georienteerde bundels gladde spierweefselselle op die buiteoppervlak van die seellaag waargeneem. Dit is 'n belangrike deurbraak in die ontwikkeling van sintetiese vaskulêre prostese wat beide die struktuur en funksie van natuurlike bloedvate naboots.

Stellenbosch University http://scholar.sun.ac.za

ACKNOWLEDGEMENTS

I would like to express my sincere thanks to the following persons and institutions:

Prof. R.D. Sanderson and Prof. Peter Zilla, who supervised this research, for their limitless supply of ideas, advice and enthusiasm, and for the opportunity to undertake this study.

My friends and colleagues at the Cardiovascular Research Unit, University of Cape Town, especially Paul Human, Neil Davies and Terri Dower.

Dmitri Lennert, Zelda Vergotine and Jenny Molde for their expert technical assistance.

Medtronic, Inc: The staff of the Medtronic Center for Biomaterials (MBC, Minneapolis, USA) especially Becky Bergman, Mike Wolf and Paul Trescony and the staff at the Bakken Research Center (BRC, Maastricht, the Netherlands), especially Pat and Linda Cahalan, Marc Hendriks and Michel Verhoeven, for their collaborative and financial support.

Prof. Curt Thies, for the development and supply of the custom-made gelatin microspheres central to the development of well-defined porous scaffolds.

Bruno Orlandi, Eike von Guerard and Christiaan Louw, for help with the design and fabrication of mechanical devices.

Dr. Margaret Hurndall, for proof-reading this dissertation, and for her expert advice on the structure and compilation of the document.

Tom du Toit for help with polymer characterization.

My friends and family for their support.

Stellenbosch University http://scholar.sun.ac.za

GLOSSARY

Term	Definition
anastomosis (-es)	The surgical union of two hollow organs, e.g. blood vessels, to ensure continuity of the passageway
aneurysm	A fluid-filled sac in the wall of an artery that can weaken the wall and lead to excessive localized enlargement
arteriosclerosis	A common arterial disease in which raised areas of degeneration and cholesterol deposits (plaques) form on the inner surface of arteries
autologous	Derived from the patient's own body
axillary artery	Artery located under the armpit
bifurcation	A split or branch into two parts
biodegradable	Made of a substance that will degrade, in this case, in the body
biostable	Made of a substance that will be stable, in this case, in the body
bypass	A surgical operation to redirect the blood around the occlusion via a grafted blood vessel. Carried out when the existing vessel has become blocked
carotid artery	A large artery on either side of the neck that supplies blood to the head
collagen	A fibrous protein found in skin, bone, cartilage, tendon and other connective tissue
compliance	The ability of a vessel to dilate and contract in sympathy with an internal pulsatile pressure
coronary artery	An artery supplying blood to the muscles of the heart.
distal	Further away from the point of reference (e.g. the centre of the body or the heart)
endothelium	A layer of cells that lines the inside of certain body cavities, for example, blood vessels
exogenous	Originating outside an organism or system
femoral artery	Artery located in the thigh
fibrin	An insoluble fibrous protein produced by the polymerisation of fibrinogen during the blood clotting process
fibroblasts	A type of cell that secretes the proteins that form collagen and elastic fibres and the substance between the cells of connective tissue
fibrosis	An abnormal thickening and scarring of connective tissue most often following injury, hypoxia, or surgery
haemorrhage	The loss of blood from a ruptured blood vessel
heparin	A polysaccharide present in living tissue that functions naturally as an anticoagulant and is used medically to treat thrombosis
heterologous	Derived or taken from a different species
homograft	A graft of tissue from one organism to another of the same species
homologous	Corresponding in structure, position and origin etc.
hyperplasia	Abnormal growth in a part of the body, caused by an excessive multiplication of cells
hypoxia	An inadequacy in the oxygen reaching the body's tissues
iliac artery	Artery located in the lower abdomen and pelvis
in vitro	In an artificial environment such as a test tube rather than inside a living organism
in vivo	Existing or carried out inside a living organism, as in a test or experiment
ischemia	An inadequate supply of blood to a part of the body, caused by partial or total blockage of an artery
jugular vein	Any one of the four pairs of veins in the neck that drain blood from the head
ligation	The tying of something with a surgical ligature
macrophage	A cell present in the blood, lymph, and connective tissues, removing waste products, harmful organisms and foreign material
occluded	Blocked
patency (n) patent (adj)	Used to describe an artery, duct or other tube in the body that is naturally open and unblocked
patency rate	The percentage of grafts still patent after a given time
pathological	Relating to , or arising from, disease
pathology	The scientific study of the nature, origin, progress, and cause of disease
pedicle graft	A vessel that is used to bypass an occlusion in another vessel by resecting the distal end of the first but leaving its proximal end attached in its original position
popliteal artery	Artery in the part of the leg behind the knee
porogen	A substance (particle), the use of which is responsible for the creation of pores
proximal	Nearer to the point of reference (e.g. the centre of the body or the heart)
renal artery	An artery that supplies blood to the kidneys
saphenous vein	Vein that runs from the foot to the thigh near the surface of the skin
senescent	Approaching an advanced age
smooth muscle cells	A type of muscle cell that functions involuntarily; found in blood vessels
thromboembolectomy	The removal of a clot from a blood vessel
thromboendarterectomy	Surgical excision of the atheromatous tunica intima of an artery
thrombosis	The formation or presence of blood clots that may partially or completely block an artery or vein
tissue engineering	The culture of living cells to form viable structures or organs
transanastomotic	An event that occurs across the anastomosis (juncture between the natural vessel and the prosthesis)
transmural	An event that occurs through the wall of the prosthesis
tunica adventitia	Outer layer of a blood vessel (also adventitia)
tunica intima	Inner layer of a blood vessel (also intima)
tunica media	Middle layer of a blood vessel (also media)
vascular graft	Vascular prosthesis
vascular prosthesis	An artificial blood vessel
vasculature	The arrangement of blood vessels in the body, an organ, or tissue

Stellenbosch University http://scholar.sun.ac.za

LIST OF ABBREVIATIONS

Abbreviation	Meaning
α-SMCA	Alpha smooth muscle cell actin
AA	Abdominal aorta
AAA	Abdominal aortic aneurysm
Aac	Acrylic acid
Aam	Acrylamide
a-FGF	Acidic fibroblast growth factor
AI	Arteriolar index
AlDI	Aliphatic diisocyanate (generic)
ArDI	Aromatic diisocyanate (generic)
ATIII	Antithrombin III
BA	Brachial artery
BDO	Butanediol
b-FGF	Basic fibroblast growth factor
CABG	Coronary artery bypass graft
CB	Coomassie Blue
CCA	Common carotid artery
CFA	Common femoral artery
CHDI	1,4-Cyclohexane diisocyanate
CoA	Carotid artery
DA	Diamine (generic)
DMAC	Dimethyl acetamide
DO	Diol (generic)
EC	Endothelial cell
ED1	A monoclonal antibody (code ED1)
EDA	Ethylene diamine
EDC	1-(3-dimethylaminopropyl)-3-ethyl carbodiimide
EDO	Ethylene diol
ePTFE	Expanded poly(tetrafluorothylene)
ESC	Environmental stress cracking
ESCR	Environmental stress cracking resistance
ETO	Ethylene oxide
FA	Femoral artery
FBGC	Foreign body giant cell
FBGCI	Foreign body giant cell index
GSL-1	Griffonia simplicifolia lectin
H&E	Hematoxylin and eosin
HA	Hydroxyapatite
HBGF	Heparin binding growth factor
HDO	Hexane diol
HMDI	Hydrogenated methylene bis(p-phenyl isocyanate)
ID	Internal diameter
IPA	Isopropanol
IPDI	Isophorane diisocyanate
IRI	Inflammatory response index
LIMA	Left internal mammary artery
MDI	Methylene bis(p-phenyl isocyanate)
NDI	1,5-Naphthalene diisocyanate
NHS	N-Hydroxy succinimide
NMP	N-Methyl pyrollidone
OD	External (outside) diameter
PBD	Hydrogenated polybutadiene
PCL	Polycaprolactone
PDGF	Platelet derived growth factor
PDMS	Poly(dimethyl siloxane)
PEA	Polyethylene adipate glycol
PED	Polyether diol (generic)
PEO	Poly(ethylene oxide)
PesD	Polyester diol (generic)
PET	Poly(ethylene teraphthalate)
PGA	Poly(glycolic acid)
PHECD	Poly(1,6-hexyl 1,2-ethyl carbonate) diol
PHMC	Polyhexymethylene carbonate glycol
PIB	Hydroxy terminated polyisoprene
PLA	Poly(lactic acid)
PMN	Polymorphnuclear cell
POPG	Polyoxypropylene glycol
PS	Ponceau S
PTFE	Poly(tetrafluoroethylene)
PTMEG	Polytetramethylene glycol
PU	Polyurethane
PVAL	Poly(vinyl alcohol)
RIMA	Right internal mammary artery
RT	Room temperature
SEM	Scanning electron microscope

Stellenbosch University http://scholar.sun.ac.za

SMC	Smooth muscle cell
SV	Saphenous vein
TB	Toluidine blue
TDI	Toluene diisocyanate
TEBV	Tissue engineered blood vessel
TODI	Methylene bis(toluene isocyanate)
TPU	Thermoplastic polyurethane
VAG	Vascular access graft
VI	Vascular index

Stellenbosch University http://scholar.sun.ac.za

LIST OF SYMBOLS

Symbol	Meaning
β	Stiffness parameter
ξ	Surface energy
σ_b	Stress at break
ε_b	Elongation at break
ρ_{Bpol}	Polymer bulk density
ρ_{Bpor}	Porogen bulk density
γ_c	Critical surface tension
δ_d	Dispersive component of solubility parameter
ξ^d	Dispersive component of surface energy
δ_h	Hydrogen bonding component of solubility parameter
δ_p	Polar component of solubility parameter
ξ^p	Polar component of surface energy
ρ_{pol}	Polymer density
ρ_{por}	Porogen density
ρ_{soln}	Solution density
ρ_{solv}	Solvent density
δ_t	Total solubility parameter
γ_w	Contact angle with water
$[M]$	Total concentration of unreacted monomers in the feed at any time.
$[M_1]$	Concentration of M_1.
$[M_1^\bullet]$	Concentration of polymeric species ending in an M_1-type active center.
$[M_1^0]$	Concentration of M_1 in feed at zero conversion.
$[M_2]$	Concentration of M_2.
$[M_2^\bullet]$	Concentration of polymeric species ending in an M_2-type active center.
$[M_2^0]$	Concentration of M_2 in feed at zero conversion.
°C	Degrees Celsius
µm	Micrometer
C_D	Compliance (based on diameter change)
C_V	Compliance (based on volume change)
D_d	Diameter at diastole
D_s	Diameter at systole
E_{100}	Modulus at 100% elongation
E_Y	Young's Modulus
f_1	Mole fraction of unreacted M_1 in feed.
F_1	Instantaneous mole fraction of M_1 entering the copolymer.
f_1^0	Mole fraction of M_1 in feed at zero conversion.
F_{1av}	Average mole fraction of M_1 in the total amount of copolymer formed up to that point.
f_2	Mole fraction of unreacted M_2 in feed.
F_2	Instantaneous mole fraction of M_2 entering the copolymer.
f_2^0	Mole fraction of M_2 in feed at zero conversion.
F_{2av}	Average mole fraction of M_2 in the total amount of copolymer formed up to that point.
g/cm^3	Gram per cubic centimeter
k_{11}	Rate constant for reaction of $M_1^\bullet$ with M_1 (radical first).
k_{12}	Rate constant for reaction of $M_1^\bullet$ with M_2.
k_{21}	Rate constant for reaction of $M_2^\bullet$ with M_1.
k_{22}	Rate constant for reaction of $M_2^\bullet$ with M_2.
M	Molarity (mol/dm^3)
M	Total number of moles of unreacted monomers in the feed at any time.
M^0	Total number of moles of unreacted monomers in the feed at zero conversion.
m%	Percentage by mass
M_1	Monomer 1.
$M_1^\bullet$	Polymeric species ending in an M_1-type active center.
M_1^0	Total number of moles of unreacted M_1 in the feed at zero conversion.
M_2	Monomer 2.
$M_2^\bullet$	Polymeric species ending in an M_2-type active center.
M_2^0	Total number of moles of unreacted M_2 in the feed at zero conversion.
M_n	Number average molecular weight
MPa	Megapascal
m_{por}	Porogen mass
m_{pol}	Polymer mass
m_{solv}	Solvent mass
m_{soln}	Solution mass
M_w	Weight average molecular weight
$N_{1:x}$	Number fraction of sequences of M_1 of length x.
$N_{2:x}$	Number fraction of sequences of M_2 of length x.
P_{11}	Probability that growing radical ending in $M_1^\bullet$ adds to M_1.
P_{12}	Probability that growing radical ending in $M_1^\bullet$ adds to M_2.
P_{21}	Probability that growing radical ending in $M_2^\bullet$ adds to M_1.
P_{22}	Probability that growing radical ending in $M_2^\bullet$ adds to M_2.
P_{Ax}	Porosity by area (cross section)
P_{Ax}	Porosity by area (inner surface)
P_{Ax}	Porosity by area (outer surface)
P_d	Pressure at diastole

Stellenbosch University http://scholar.sun.ac.za

P_{Gcp}	Porosity of closed pores as determined by the gravimetric method
P_{Gop}	Porosity of open pores as determined by the gravimetric method
P_{Gtp}	Total porosity of pores as determined by the gravimetric method
P_i	Pore size (inner surface)
P_o	Pore size (outer surface)
P_s	Pressure at systole
P_{Tmac}	Porosity of macropores as determined by the theoretical method
P_{Tmic}	Porosity of micropores as determined by the theoretical method
P_{Ttp}	Total porosity as determined by the theoretical method
P_V	Porosity by volume
P_{Vcp}	Porosity of closed pores as determined by the volumetric method
P_{Vop}	Porosity of open pores as determined by the volumetric method
P_{Vtp}	Total porosity of pores as determined by the volumetric method
P_x	Pore size (cross section)
r	radius
r_1	Reactivity ratio of M_1.
r_2	Reactivity ratio of M_2.
SR	Suture retention strength
t	Wall thickness
T_g	Glass transition temperature
T_m	Melting temperature
V_d	Volume at diastole
V_{Gcp}	Volume of closed pores as determined by the gravimetric method
V_{Gop}	Volume of open pores as determined by the gravimetric method
V_{Gtp}	Total volume of pores as determined by the gravimetric method
V_{por}	Porogen volume
V_s	Volume at systole
V_{solv}	Solvent volume
V_{Vcp}	Volume of closed pores as determined by the volumetric method
V_{Vop}	Volume of open pores as determined by the volumetric method
V_{Vscaf}	Volume of the polymeric scaffold containing open and closed pores (volumetric method)
V_{Vskel}	Volume of the polymeric skeleton containing the micropores (volumetric method)
V_{Vtp}	Total volume of pores as determined by the volumetric method
W_1	"Relative weight" of M_1 in the copolymer
W_2	"Relative weight" of M_2 in the copolymer
WP	Water permeability
X	Mole conversion of total monomer to polymer.
x_{1av}	Average length of M_1 sequences.
x_{2av}	Average length of M_2 sequences.

Stellenbosch University http://scholar.sun.ac.za

LIST OF FIGURES

Stellenbosch University http://scholar.sun.ac.za

Stellenbosch University http://scholar.sun.ac.za

Stellenbosch University http://scholar.sun.ac.za

Stellenbosch University http://scholar.sun.ac.za

LIST OF TABLES

Stellenbosch University http://scholar.sun.ac.za

TABLE OF CONTENTS

Stellenbosch University http://scholar.sun.ac.za

Stellenbosch University http://scholar.sun.ac.za

Stellenbosch University http://scholar.sun.ac.za

Stellenbosch University http://scholar.sun.ac.za

Stellenbosch University http://scholar.sun.ac.za

Stellenbosch University http://scholar.sun.ac.za

CHAPTER 1

Introduction

1.1 Background

The high demand for vascular grafts (prostheses) used to augment the insufficient functioning of the vascular system may be inferred from the high number of clinical cases that require such devices (estimated to be between 1 million [1] and 1.4 million [2] cases annualy).

The highest demand is for small-diameter vessels (<6mm) used in coronary bypasses and the alleviation of peripheral ischemia. Contemporary small-diameter vascular prostheses (expanded polyterafluoroethylene (ePTFE) and knitted/woven polyethylene teraphthalate (PET, Dacron)) fail to deliver the desired long-term outcomes due to inadequate healing responses and resultant thrombotic events [3]. Although research into the use of alternate porous scaffolds has been underway for the past 30 years, a viable replacement for commercially available Dacron and ePTFE prostheses has not yet been developed.

Tissue engineering, as related to vascular surgery, has been defined by Chaikof [4] as: "An integration of the principles and methods from engineering, chemistry, medicine, and molecular biology in defining biophysical and molecular mechanisms that control the function and morphology of the vascular wall; establishes a framework for the development of improved biologically functional vascular prostheses and enhanced therapeutic options for the treatment of atherosclerosis." It is a field in which a variety of tissue types are cultured both in vitro and in vivo, often using polymeric scaffolds as supports [2].

Although tissue engineering generally relies on the use of biodegradable scaffolds, this study shows how porous, biostable scaffolds may be used in an in vivo tissue engineering approach to improve the fate of hybrid synthetic/biological vascular grafts.

1.2 Scope

This study forms part of a larger research project by a multidisciplinary group at the Cardiovascular Research Unit at the University of Cape Town, aimed at the development of tissue-engineered cardiovascular prostheses. The larger study is aimed at the combination of porous scaffolds with engineered ingrowth matrices (within the porous structure) in order to attain favourable long-term outcomes through suitable healing responses and transmural endothelialisation.

This dissertation contributes to the knowledge pertaining to the preparation, characterization and use of porous scaffolds for use as vascular prostheses. It describes how porous structures useful in this application may be improved by the optimization of pore size, pore structure and surface pacification. It additionally provides information on the use of in vivo methods suitable for the evaluation of porous scaffolds, and healing responses obtained by the use of these methods.

Additional work closely related to this development, namely the computational mechanical analysis by finite element methods and compliance measurements, forms the subjects of theses by various students carried out under the guidance of the author [5-8].

Engineered biological and synthetic matrices, that would further encourage differential ingrowth of the desired cellular and extracellular matrix materials into the porous structure, are being developed in parallel with the scaffolds described in this dissertation.

Stellenbosch University http://scholar.sun.ac.za

The scope of this dissertation includes:

- An historical overview on the need for vascular grafts
- The theoretical considerations influencing vascular graft properties and identification of desirable and undesirable properties
- The development of a concept for novel vascular grafts
- The development of porous scaffolds suitable for use in vascular prostheses
- The development of novel synthetic vascular grafts consisting of:
  - a porous scaffold
  - a chemically modified surface, and
  - a reinforcing structure
- The in vivo evaluation of the healing response towards these grafts.

1.3 Objectives

The ultimate polymeric vascular graft is one that allows for the incorporation of the prosthetic device in a polymer/tissue composite by the ingrowth of cellular material in order to produce a living neo-artery. Such an ingrowth would involve not only the formation of an endothelium on the lumen, but also population of the pores by active, helically-oriented smooth muscle cells (and supporting blood vessels) with accompanying extracellular matrix materials. This research contributes towards the ultimate goal by providing insight into the properties required of structures for the transmural ingrowth and orientation of smooth muscle cells and blood vessels required to support the viability of ingrown cells.

Thus, the objectives of this study were to:

- Review the healing responses associated with experimental and commercially available vascular prostheses and identify variables responsible for the poor performance of these grafts in small-diameter applications
- Provide a concept for a novel vascular graft that would provide improved healing responses by eliminating some of the shortcomings of currently available grafts
- Produce structures containing well-defined, interconnected pores (resembling pentagonal dodecahedra) that would theoretically allow uninterrupted cellular ingrowth.
- Decrease the in vivo inflammatory response normally associated with implanted porous structures by the optimization of pore size.
- Further decrease this inflammatory response by chemical surface-modification of these structures.
- Develop a circulating in vivo model, suitable for the evaluation of porous vascular grafts, that would enable the differentiation between transanastomotic and transmural healing effects.
- Determine the effect of pore size on the healing response of expanded PTFE vascular grafts in the circulating in vivo model, and determine whether large porosity on its own is sufficient for full transmural healing.
- Evaluate the healing response toward experimental polyurethane vascular grafts containing well-defined, interconnected pores that should, theoretically, be conducive to full transmural healing
- Modify experimental polyurethane vascular grafts in order to achieve the population of the porous structure by helically oriented smooth muscle cells and supporting blood vessels, similar to those found in natural arteries.

Stellenbosch University http://scholar.sun.ac.za

1.4 Layout

The document has been structured in the following manner:

- The first four chapters provide an overall introduction and overview of historical and theoretical aspects pertaining to the field of vascular grafts, and a concept for a new graft.
- The subsequent chapters take the form of journal articles. Although some duplication is inevitable, the information contained in these latter chapters is highly specific to each study. This allows for a more detailed analysis of each topic in the relevant section.
- A summary of the results obtained in the various studies, and an overall conclusion, is given.
- An appendix that contains additional details pertaining to various subjects described in the dissertaion is provided.

1.5 References

1. Zdrahala, R., *Small caliber vascular grafts. Part I: State of the art.* J Biomater Appl, 1996. **10**(4): p. 309-29.
2. Niklason, L.E. and Langer, R.S., *Advances in tissue engineering of blood vessels and other tissues.* Transpl Immunol, 1997. **5**(4): p. 303-6.
3. Bezuidenhout, D. and Zilla, P., *Biomaterials in Vascular Surgery*, in *Encyclopedia of Materials: Science and Technology*, K. Boschow, Cahn, R., Flemmings, M., Ilscher, B., Kramer, E., and Mahakan, S., Editors. 2001, Elsevier.
4. Chaikof, E., *Biomaterials that imitate cell microenviroments.* Chemtech, 1996(August): p. 17-22.
5. Millam, R., *Design of an adventitial type reinforcement of prosthetic vascular grafts through mechanically affirmed material and structure modulation.*, in *Faculty of Health Sciences*. 2001, University of Cape Town: Cape Town.
6. Yeoman, M., *Design and optimisation of a fabric reinforced porous prosthetic graft using finite element methods and genetic algorithms*, in *Mechanical Engineering*, University of Cape Town: Cape Town.
7. Hughes, A., *Mechanical design aspects of a small diameter vascular graft with structured porosity*, in *Mechanical Engineering*. 2000, University of Cape Town: Cape Town.
8. MacKellar, I., *The mechanical design aspects of a small diameter vascular prosthesis*, in *Mechanical Engineering*. 1998, University of Cape town: Cape Town.

Stellenbosch University http://scholar.sun.ac.za

CHAPTER 2

Overview on vascular grafting

2.1 The need for vascular intervention

The total length of blood vessels in the average adult human body has been estimated to be 100,000 miles. In addition to the classification of this complex network of vessels into arteries and veins, the vascular tree may be further sub-classified into large elastic arteries, smaller muscular arteries, arterioles, capillaries, venules, medium-bore veins, and large veins. Apart from the obvious function performed by these vessels, namely that of providing a conduit for the flow of blood from the heart to the organs and extremities, and the return of the blood to the heart, each of these vessel types is highly specialised in form and function in order to perform specific tasks to the best effect.

Clinical intervention may be indicated in the treatment of blood vessels affected by pathological conditions and/or traumatic injury resulting in aneurismal dilation, arterial haemorrhage, thrombotic or atherosclerotic occlusion. Although less severe and less critical injuries and pathologies may be treated by alternative methods, all three cases may require surgical intervention to avoid aneurismal failure, prevent excessive blood loss, or restore blood flow to the distal vascalature. Surgical intervention, in turn, may take on many forms, including ligation, suturing, reconstruction, anastomosis, thromboendarterectomy, arterialembolectomy, and grafting (replacement and bypass).

This dissertation will focus on novel prosthetic devices used in replacement and bypass grafting, and specifically on synthetic vascular grafts suitable for replacing or bypassing occluded small-diameter arteries.

2.1.1 Vascular surgery

From antiquity to the eighteenth century, the management of arterial haemorrhage and aneurysms mostly involved the use of manual compression, cauterisation and ligation. It was only in the nineteenth century that laboratory designed techniques for suturing vascular wounds and anastomosing blood vessels were introduced. Matas [1] was one of the first to describe these methods for the management of aneurysms by using a technique in which a new vessel was made out of the old one.

It could be said that the modern era of vascular surgery was ushered in by the work of Carrel [2] in the first decade of the twentieth century. He carried out the basic investigations concerning blood vessel surgery, including the study of functional and histological analysis of preserved homografts. Carrel's innovations had such an impact that he received the Nobel Prize for medicine in 1912 "in recognition of his work on vascular suture and transplantation of blood vessels and organs." [3]

2.1.1.1 The replacement principle

Even though the pioneering efforts of Matas were of great importance during the early phase of vascular surgery, the grafting of vessels was to have an even greater impact on its development. Vascular replacement surgery involves, as the name indicates, the removal of a damaged arterial section and the replacement thereof with a suitable conduit. At about the same time as Carrel carried out his work, Goyanes described the use of a popliteal vein in situ to restore the continuity of the popliteal artery after the excision of an aneurysm [4]. This was closely followed by the use of a free vein graft by Lexer [5] in a similar operation, where an 8-cm defect in an axillary artery was bridged with an autologous segment of saphenous vein. This method was applied with equal success to the replacement of an iliac artery after removal of an aneurysm

Stellenbosch University http://scholar.sun.ac.za

from such a vessel. Despite further successes with the use of free-vein transplantation for the treatment of aneurysms before the first World War, and excellent results achieved in the treatment of traumatic aneurysms by German surgeons during World War I, ligation remained the treatment of choice for similar cases in the American Army, even during the Second World War [6]. This practice remained in use also in the Korean war, when advances in civilian blood vessel surgery were applied to traumatic vascular lesions. Autologous vein grafts are still used today, not only for peripheral vascular reconstructions but also for coronary and cerebral bypass surgery.

The application of the replacement principle to large-bore arteries (notably aorta and aorto-iliac bifurcations) was made possible by two major developments in the 1940s and 1950s that completely revolutionized surgery for cardiac and aortic lesions. The first was the use of hypothermia to lower the body's oxygen consumption and the second the introduction of the heart-lung machine for extra-corporeal circulation and oxygenation. Whereas autologous veins suitable for the reconstruction of small-diameter arteries could be removed and transplanted to the new position in the arterial vasculature, the replacement of large arteries presented surgeons with the added impediment that no autologous veins of suitable size could be removed from the patient without life-threatening implications. Gross et al. were the first to circumvent this problem by using preserved homografts for arterial transplantation [7]. This led to the first successful resection of the aortic bifurcation and replacement with a homograft by Oudot [8] in 1951, and the successful resection of an abdominal aortic aneurysm (AAA) with insertion of a homograft by Dubost et al. [9]. Thereafter, many segments of the thoracic aorta, including the arch, were treated by excision and replacement with homografts.

2.1.1.2 The bypass principle

The bypass principle, involving the bypassing of the diseased or injured vessel with a suitable conduit *while leaving the original vessel intact*, was first advocated by Ernst Jaeger in 1913 for the management of peripheral aneurysms [10]. It was not until 1948, however, that Kunlin [11] reported this procedure for the treatment of femoro-popliteal occlusive arterial disease. This approach was entirely novel and had significant advantages over the replacement procedure; excessive operative trauma and damage to adjacent nerves and veins was avoided, permitting the preservation of collateral vessels. It is interesting to note that this discovery, and historical landmark in vascular surgery, was born out of necessity, when Kunlin's attempt to implant a venous graft after the removal of an occluded femoral artery failed to relieve the ischemia (by peripheral vasodilation). The end-to-end approach was impossible due to pronounced fibrotic reaction in the previous operative area, and a decision was made to perform an end-to-side implantation of the venous graft. Today, the bypass principle is applied to the management of all sorts of arterial lesions and occlusions, especially those below the groin and, notably, in the coronary artery position.

In conclusion it may be said that the replacement principle is utilised in the management of large bore arteries, while the bypass principle is employed to treat pathologies associated with small-bore blood vessels.

2.2 Types of grafts

Grafts used for the replacement and bypassing of blood vessels may be classified into two broad groups: bioprosthetic and synthetic. Bioprosthetic grafts are composed of autologous, homologous or xenogeneic tissue. These tissue grafts may, in some cases, be stabilised by crosslinking with various fixation techniques or by reinforcement with synthetic materials. The second group comprises prosthetic vascular prostheses fabricated entirely (or mostly) from synthetic materials.

Stellenbosch University http://scholar.sun.ac.za

2.2.1 Bioprosthetic grafts

2.2.1.1 Autologous grafts

Fresh, viable autologous veins have been demonstrated to be the preferred graft for use in relieving lower extremity ischemia by, for example, femoropopliteal bypass grafting [12]. Depending on the exact nature and position of the graft vein relative to the position of the bypass, the graft vein may either be excised and re-implanted in a reverse configuration, or left in-situ with only the proximal and distal ends repositioned and anastomosed to the occluded artery. The in-situ use of veins for arterial bypassing requires the removal of venous valves to allow unrestricted blood flow. Autologous veins (saphenous and jugular veins, and veins of the upper extremities) may further be used for carotid, renal, and other sites.

Although dispensable autologous arteries are usually not as readily available as autologous grafts, their use is indicated as preferential grafts. In coronary artery bypass surgery, the pedicle, left, internal-mammary (LIMA) has long been the superior conduit, but its application is generally limited to the left anterior descending (LAD) coronary artery [13]. Depending on the anatomical position of the graft, the age of the patient, and other factors, further stenoses may be bypassed with either the pedicle or free right internal mammary artery (RIMA), radial arteries, gastroepiploic arteries and saphenous vein grafts. Other specific examples of the use of autologous arteries include the application of resected autologous iliac arteries (that are subsequently replaced with a suitable synthetic prosthesis) to a more critical location, and the use of radial arteries in coronary positions of young patients.

2.2.1.2 Homologous grafts

Prior to the development of good synthetic prostheses, homologous arterial tissue used to be the standard clinical large-bore material. This tissue type has been used in various forms: fresh, frozen, refrigerated in physiological solution, freeze-dried, glycerine preserved, alcohol preserved, dried, and preserved in formalin [12]. The order of ascending reactivity elicited by the host (and thus descending acceptability as a vascular graft) is equal to the order in which the types have been listed above. Although arterial homografts are rarely used today, they still find some application as aortic arch replacements.

Glutaraldehyde-fixed homologous umbilical veins have found some application as bypass grafts for small-diameter arteries in the lower extremities. These grafts are typically externally supported with a light Dacron mesh to enhance structural integrity, and may offer a reasonable alternative to autologous veins when the latter are not available [14].

2.2.1.3 Heterologous grafts

Tissue fixation procedures similar to those used for the crosslinking of heterologous bioprosthetic heart valves have also been used with some success to preserve heterologous arterial tissue. Typically, bovine carotid arteries were fixed in dialdehydes to reduce the antigenicity, reinforced with Dacron mesh to improve mechanical strength, and used as vascular access grafts [12]. The use of heterologous vein grafts has not been reported to any great extent.

2.2.2 Synthetic grafts

The development of synthetic vascular grafts dates back to the beginnings of experimental vascular surgery in 1912. Carrel [15] experimented with glass and aluminum tubes, while parafin-coated silver tubes were used by Tufier in WW I [16]. More recently, many other materials, including Vitaluminum tubes, polyethylene tubing, silicone rubber, steel mesh tubes and Ivalon®, have been used as experimental vascular conduits [17]. One of the first polymeric conduits used for arterial substitution in humans was a solid, rigid poly(methyl methacrylate) tube described by Hufnagel in 1947 [18]. These conduits all failed due to thrombosis.

Stellenbosch University http://scholar.sun.ac.za

An observation made by Voorhees of an endothelial-like surface on a silk thread in the ventricle of a dog led to the reasoning that textile fabrics might serve as suitable graft materials [19]. The relative success with poly(acrylonitrile-co-vinyl chloride) (Vinyon-N®) fabric tubes ushered in the concept of the use of textile materials as vascular grafts. In addition to textile and expanded structures, a variety of other fibrillar and foam-type porous structures have been used in the design of experimental vascular grafts. Of the many materials and structures investigated, two major types remain in regular use today. Poly(ethylene terephthalate) (PET) and expanded poly(tetrafluoroethylene) (ePTFE) vascular prostheses are the synthetic conduits currently most widely used for the clinical substitution of natural blood vessels.

2.2.2.1 Poly(ethylene terephthalate) (PET)

Poly(ethylene terephthalate) (PET) is a semi-crystalline polymer derived from the condensation polymerisation of terephthalic acid and ethylene glycol. Although its ester bonds are potentially susceptible to hydrolysis, its high crystalinity in the oriented fibre form renders it relatively stable. Projections from in vivo experiments indicate a period of approximately 30 years for the complete resorption of PET grafts [20]. It is a strong stiff material (tensile strength = 172MPa; modulus = 14.1 GPa) with a high crystalline melting point [21]. Although the textile structure of PET vascular prostheses imparts a small amount of compliance, the stiffness of the constitutive fibres renders the structure much less compliant (C=1.9 %/100mmHg) than natural arteries (C=5.9 %/100mmHg) [22].

PET is extruded and drawn according to well known spinning techniques into filaments of various cross-sections (circular or trilobal) and linear densities (50 to 200 Decitex) corresponding to diameters of approximately 11 to 18 μm. The multifilament yarns used in vascular grafts, typically consisting of 24 and 108 filaments, are readily woven and knitted into various configurations. Most commercially available PET grafts are either plain weaves, single jersey weft knits, 2-bar lockknits, or tricot warp knits, with the knits being either in the standard or reverse configuration [23]. The simplest, namely the taffeta weave, produces the strongest textile, the closest packing of yarns and hence the lowest porosity. The invention of specialized knitting machines by Golaski, Edman and De Bakey afforded the opportunity of increasing the porosity of the textiles. Weft-knit prostheses were often prone to dilation and unravelling, and were often considered too permeable for some applications due to the excessive porosity. The introduction of warp knitting techniques solved many of the problems associated with weft knitting. The addition of the extra yarns decreased the porosity to a value (generally) between that of woven and weft knit grafts, and the predominantly lengthwise threads eliminated the fraying out of the ends. Warp knits have excellent dimensional stability as well as good suturability and handling characteristics. Another method of improving the healing characteristics of PET grafts through the improved anchoring and mechanical interlocking of tissue was initiated by the introduction of velour designs. This roughening of the lumenal and/or external surfaces is achieved by napping the surfaces with wire brushes or the addition of textured yarns in the woven or knitted fabric.

After knitting, the excessively high permeability of knitted and velour prostheses is reduced to within desired levels by chemical or thermal processes that effect compaction through the longitudinal shrinkage of filaments. Concurrent or subsequent helical or circular crimping increases the longitudinal elongation and decreases the tendency to collapse or kink. As dry or moist heat may cause further deformation of PET vascular prostheses, ethylene oxide gas and ionising radiation are the preferred methods of sterilization.

2.2.2.2 Expanded Poly(tetrafluoroethylene) (ePTFE)

Poly(tetrafluoroethylene) is a very inert material due to the large fluorine atoms protecting the hydrocarbon backbone, its high molecular mass and high crystallinity. It has a low coefficient of

Stellenbosch University http://scholar.sun.ac.za

friction, and one of the lowest critical surface tensions of any polymer. The hydrophobicity of PTFE is evident from its high water contact angle and low water absorption (<0.05%). It has a moderate tensile strength of 21 MPa and tensile modulus of 413 MPa [24]. The compliance of ePTFE grafts (C=1.6 %/100mmHg) is typically even lower than that of PET prostheses [22].

Although PTFE is generally classified as a thermoplastic, its melt viscosity is too high for conventional melt processing, and it is too insoluble for conventional solution-processing techniques. Initial PTFE prostheses made from fibres into textile configurations were prone to unravelling and false aneurysm formation, and this type of prosthesis was discontinued by many manufacturers. Expanded PTFE vascular prostheses are produced in an unique process in which PTFE is ram extruded into the desired shape with an extrusion lubricant, typically a hydrocarbon. Removal of the lubricant, stretching at high rates, and subsequent sintering of the tube results in a porous product with a structure that contains PTFE nodules connected by highly oriented thin fibrils. Grafts of this type are often characterized by an internodal distance (IND), which is typically in the order of 30μm, although larger sizes have also been produced. The IND is often a misleading dimension, as the actual spaces available for tissue ingrowth, namely the inter-fibrillar distance, is typically in the 4-5μm size range [25]. ePTFE grafts often contain an additional reinforcing wrap for added strength, as well as spiral or circular reinforcing structures for kink and crush resistance. PTFE is stable under steam, dry heat, and ethylene oxide sterilization regimens, but it is not suited to sterilization by ionising radiation.

2.2.2.3 Other synthetic grafts

Various experimental grafts made from polyurethanes (PU) and other non-degradable materials, as well as from materials that are designed to be resorbed by the host, were developed in an effort to provide alternatives to these commercially available prostheses. A detailed account of the structure and properties of polyurethane grafts is given in Chapter 5.

2.3 Shortcomings of contemporary grafts

2.3.1 Bioprosthetic grafts

Although autologous veins are currently the grafts of choice in small-diameter indications, their use may be compromised by complications such as excessive intimal hyperplasia, late occlusion and dilation. In up to 20-30% of cases these veins are unsuitable due to disease. This percentage can be even higher in re-operative procedures when these veins are unavailable due to prior harvesting [26]. Autologous arterial tissue may, in theory, be seen as the ideal arterial substitute, but in arteriosclerotic patients sufficiently normal, dispensable arteries are at a premium.

The shortcomings of arterial homografts are evident from the changes that occur during the healing response include slow wall lysis, compaction and loss of elastic tissue, ulceration, mural thrombosis, and calcification. Such changes resemble atherosclerosis [27] and result in a poor long-term outcome. Although few non-arterial homograft tissues have been used in the arterial site, experiments evaluating homologous veins for aortic replacement show late fibrotic stenosis. Glutaraldehyde-fixed, homologous umbilical veins have found some use in lower extremity applications, but the general consensus is that they are not as reliable as autologous vein grafts.

Heterologous arterial tissues demonstrate a decidedly accelerated tissue response, due to antigenicity, and are heavily subject to aneurysm formation and rupture. The antigenicity may be reduced or abolished by certain chemical modifications, such as crosslinking, but these grafts remain prone to aneurismal dilation. This shortcoming has been corrected by Dacron reinforcement, and although studies have shown superior long-term fate to that of freeze-dried homografts and some textile prostheses, the use of fixed heterologous arterial tissue is limited mostly to arteriovenous shunts [28].

Stellenbosch University http://scholar.sun.ac.za

2.3.2 Synthetic grafts

PET (Dacron®) is the material of choice for large-diameter, high-flow vascular graft applications, such as aortic replacements. The manufacturing techniques used in the production of PET grafts lend themselves to the inclusion of side branches and bifurcations, and PET grafts are regularly used as aorto-femoral replacements. A secondary patency rate of 93% at 10 years can be achieved with large-diameter grafts of this type [29]. Many large diameter PET grafts are sealed with collagen, gelatin or albumin to render them initially impermeable to blood, thereby obviating the need for the surgeon to pre-clot the device with blood or fibrin glue [30].

Expanded poly(tetrafluoroethylene) (ePTFE) is favoured in medium-bore (6-12mm) applications when autologous veins are unavailable or unsuitable. Patency rates of 40-50% after 4 years of implantation in femoro-popliteal reconstructions are lower that the rates achieved by using reversed saphenous veins (70%-80%) [31].

These graft types fail to perform satisfactorily, however, in smaller-diameter applications (<6mm) due to occlusion caused by thrombosis and intimal hyperplasia. A more detailed account of the shortcomings of commercial grafts in small-diameter applications, is given in Chapter 3.

2.4 The need for alternative small-diameter grafts

The American Heart Association (AHA) estimates that 598,000 coronary artery bypass grafts (CABG, requiring small-diameter grafts) were performed on 367,000 patients in 1996 in the United States alone [32]. This makes CABG probably the most widely performed procedure in which small diameter vascular substitutes are required (Table 2.1). It has been shown, however, that numerous autologous arteries (and veins) may be, and are, successfully used to bypass coronary stenoses. (See section 2.2.1.1)

Table 2.1: Scope, indications and worldwide market for vascular grafts [33].

Graft size Internal diameter	Large diameter ID = 7-30+ mm	Small diameter ID = 6 mm or less	Coronary (CABG) ID = 1-4mm
Utilization	Thoracic cavity, abdominal cavity, above the knee	Across, below the knee, peripheral graft (PG), vascular access graft(VAG)	Coronary arteries
World market	~$150 million	~$200 million	$450 million

The second largest demand for small-diameter grafts is for peripheral grafts (PG) to relieve lower extremity ischemia. The limitations associated with contemporary small-bore grafts of biological or synthetic origin result in an inability of these grafts to provide satisfactory long-term outcomes in the PG position. Although the ratio of coronary:peripheral graft usage has been estimated at 6:1 in the USA, the number of peripheral procedures performed in the United States in 1991 (150,000) attests to the urgent need for a successful alternative conduit [34]. If these figures are projected, then the current need in the USA is in excess of 200,000 peripheral procedures.

In addition to the large peripheral market, there is also a need for small-diameter prostheses to be used as vascular access grafts (VAG) for the treatment of end-stage renal failure.

2.5 Alternative approaches

2.5.1 In vitro tissue engineering

Recent advances in cell-culture techniques have created an opportunity for the in vitro reconstitution of organs from living cells. Weinberg and Bell [35] were the first to apply such

Stellenbosch University http://scholar.sun.ac.za

techniques to produce a completely biological tissue-engineered blood vessel (TEBV) from collagen gels and cultured bovine endothelial cells (ECs) smooth muscle cells (SMC) and fibroblasts. These grafts did not, however, display the required mechanical strength, even when reinforced with Dacron mesh. Similar results were obtained by L'Heureux et al. who employed the techniques with human collagen and vascular cells [36], and by Hirai and Matsuda [37] who used a canine model.

A radically different approach by L'Heureux et al. involved the production of tissue-engineered blood vessels from cultured human cells without the use of exogenous biological material, by allowing the cells to create their own extracellular matrix in the presence of ascorbic acid [38]. Their method involved wrapping successive layers of acellular and cellular materials onto a mandrel to produce a neo-artery. The first layer consisted of an acellular inner membrane produced by the dehydration of a cultured fibroblast sheet. Onto this inner membrane, successive layers consisting of smooth muscle cells and fibroblast (respectively) were wound onto the inner membrane. After maturation of the composite layers in a bioreactor the lumen was seeded with endothelial cells. The vessels were reported to have undergone histological organisation and displayed burst strengths comparable to those of natural blood vessels. Although the approach and results are very exciting, the procedure takes in excess of 4 months to complete.

A slightly different approach was followed by Niklason and Langer [39]. They used temporary synthetic scaffolds of polyglycolic acid (PGA) to produce tissue-engineered blood vessels by seeding tubular non-woven meshes of PGA with high densities of smooth muscle cells. Maturation of the cells in a bioreactor resulted in the proliferation of the cells and the degradation of the PGA mesh. Pulsatile stretch was employed to facilitate proliferation and enhance the contractile properties of the cells. Although the mechanical stretching did improve the physical strength over that obtained during static culture, the vessels were not able to withstand arterial pressure.

The tissue-engineering approaches detailed above offer valuable insight into the culturing techniques required to produce neo-arteries. The in vitro generation of blood vessels holds the distinct advantage that implanted devices consisting of living autologous tissue may be incorporated and remodelled without foreign body response from the host. The problems associated with the use this approach for the production of vascular grafts are, however, not trivial. The techniques employed, namely for cell harvesting and culture, and the engineering of such cells into viable vessels requires expertise generally found only in large centres and academic hospitals. The time required to produce cells of sufficient numbers, together with the time needed to engineer the cells into vascular structure by manipulation and maturation, may be another factor limiting the use of the technique.

2.5.2 Endothelial cell transplantation

The failure of small-diameter, synthetic, vascular grafts may be attributed mostly to surface thrombogenicity and anastomotic intimal hyperplasia. The surface thrombogenicity, in turn, can be ascribed to a persistent lack of endothelial cell coverage, even after extended implant periods. The basic concept behind endothelial cell transplantation is the lining of autologous endothelial cells (EC's) on contemporary synthetic grafts before implantation in order to mask the thrombotic nature of the underlying synthetic material.

2.5.2.1 Single-stage venous EC seeding

This early method involved the single-staged seeding of endothelial cells harvested from subcutaneous veins onto Dacron prostheses, and the subsequent clotting of the cells into the wide-meshed porous structure of the synthetic graft [40]. The general trend at the time towards the use of ePTFE grafts in peripheral reconstructions prompted researchers to attempt the

Stellenbosch University http://scholar.sun.ac.za

application of this approach to an alternative material. The narrow interfibrillar spaces of the ePTFE, however, resulted in the cells being clotted onto the lumenal surface of the graft instead of into the graft structure. Seeding with cell numbers that were too low for the large surface area of long grafts needed for human implantation, together with the high detachment rate of cells after the restoration of blood flow, resulted in sub-optimal seeding densities. Although this probably led to partial endothelialisation and moderate decrease in thrombogenicity [41], the procedure did not result in an improved clinical patency rate [42]. Newer approaches to circumvent the problem of low seeding densities due to low cell numbers include the mass culture of venous endothelial cells [43] and the mass harvest of capillary endothelial cells from fat tissue [44].

2.5.2.2 In vitro endothelialisation

In vitro endothelialisation was pioneered in the 1980s by a number of groups [45]. This is essentially a two-stage method, the first of which is the mass-culture of endothelial cells isolated from a suitable source, (e.g. a section of the jugular or cephalic vein). The large quantity of endothelial cells cultivated in this first step is subsequently seeded at a high density onto the lumenal surface of a suitable synthetic prosthesis, typically an ePTFE graft. Pre-coating of the graft prior to seeding improves the adhesion of the seeded cells. Post-maturation allows for the recovery from injury caused by the seeding procedure, the maturation of the cells' cytoskeleton to better withstand the shear forces exerted upon it by the bloodstream [46], the formation of a confluent layer of cells on the lumenal surface, and the reduction of the inflammatory activation of the endothelium [47].

Clinical trials carried out with the use of in vitro endothelialised grafts as femoropopliteal bypass grafts commenced in 1989 [48]. Since this date, a number of groups have reported their experience with clinical trials with a follow up period of up to 9 years. The overall success of the procedure is evident from the excellent improvement achieved in patency rates when endothelialised grafts are compared to unendothelialised controls. Control groups typically have a 5-year patency rate of 42% for above-knee ePTFE grafts, whereas patency rates in excess of 65% can be achieved when endothelialised grafts were used [45]. This compares favourably to the 70% patency rate achieved by Veith with the use of reversed autologous saphenous veins in the same position [31]. Multicentre clinical trials aimed at the verification of these results are currently underway in Europe. Although in vitro endothelialisation may offer surgeons an excellent and viable alternative to saphenous veins when the latter is unavailable, two factors may stand in the way of its general acceptance as the graft of choice. The first is the relative complexity of the cell-culture procedure that requires approximately 30 days from harvest to implant date, as well as the infrastructure and expertise required to perform the necessary culture and seeding techniques. These requirements limit the procedure to large centres where the resources are available. The second factor revolves around regulatory issues. Although the current preferred choice of protein matrix (fibrin glue) used in the coating of grafts prior to seeding has clinical approval in Europe, approval of its use by the Food and Drug Administration in the United States may prove problematic.

2.5.3 In vivo tissue engineering

In vitro tissue engineering potentially offers the possibility of vascular grafts that are "made to order" [49]. The possible shortcomings of this approach, including infrastructural and time constraints, have been elucidated. The inability of conventional synthetic grafts to offer good, long-term outcomes in small-diameter applications has also been mentioned, and will be further expounded upon in Chapter 3. In short, the failure of contemporary Dacron and ePTFE grafts to perform optimally in small-diameter applications may be attributed to the poor healing response exhibited by the body toward the implanted prostheses. This lack of healing, in turn, may be attributed to a number of factors that prevent the graft from being incorporated into a viable

Stellenbosch University http://scholar.sun.ac.za

composite of synthetic material and living tissue. Although cell transplantation onto (or into) conventional synthetic prostheses has been successful in improving the patency rates of such grafts, the negative aspects associated with both in vitro cell culture and conventional synthetic grafts are maintained.

The concept proposed in this dissertation may be termed in vivo tissue engineering (TE). Whereas in vitro TE involves the culturing and engineering of cells outside of the body, either with or without exogenous biological or synthetic scaffolds, the present study is aimed at the development of a porous, synthetic scaffold that will provide the complex and interrelated chemical, physical and biological properties required to effect the engineering of tissue in vivo. These properties should be tailored to ensure complete healing of prostheses through functional integration of the synthetic material into a tissue/graft composite in order to produce a viable neo-artery. In short, the ultimate aim is to provide a successful "ready to use" or "off the shelf" vascular graft, as opposed to one that is "made to order" (See Chapter 4)

2.6 References

1. Matas, R., *Traumatic aneurism of the left brachial artery.* Med News, 1888. **53**: p. 462.
2. Carrel, A., *Latent life of arteries.* J Exp med, 1910. **12**: p. 460.
3. Haimovici, H., *History of vascular surgery*, in *Vascular surgery. Principles and techniques*, H. Haimovici, Editor. 1984, Appleton-Century-Crofts: Norwark, Connecticut. p. 3-18.
4. Goyanes, J., *Nuevos trabajos de chirurgia vascular, substitucionplastica de las arterias porlas venas o arterioplastia venosa, applicado como nuevo metodo, al tratamiento de los aneurismas.* El Siglo Med, 1906. **52**(446): p. 459.
5. Lexer, E., *Die ideale Operation des arteriellen und des arteriovenosen Aneurysma.* Arch Klin Chir, 1907. **83**: p. 459.
6. DeBakey, M. and Simeone, F., *Battle injuries of the arteries in World War II. An analysis of 2,472 cases.* Ann Surg, 1946. **123**: p. 534.
7. Gross, R., *Preliminary inobservations on the use of human arterial grafts in the trearment of certain cardiovascular defects.* N Engl J Med, 1948. **239**: p. 578.
8. Oudot, J., *La greffe vasculaire dans les thromboses du carrefour aortique.* Presse Med, 1951. **59**: p. 234.
9. Dubost, C., Allary, M., and Oeconomos, N., *A propos du traitement des anevrismes de l'aorte. Ablation de l'anevrisme, retablissement de la continuite d'aorte humaine conservee.* Mem Acad Chir, 1951. **77**: p. 38.
10. Jaeger, E., *Die Chirurgie der Blutgefasse und des Herzens.* 1931, Berlin: A. Hirschwalt.
11. Kunlin, J., *Le traitement de l'arterite oblitarant par la greffe veinueuse.* Arch Mal Coeur, 1949. **42**: p. 371.
12. Wesolow, A., *Biological behaviour of tissue and prosthetic grafts*, in *Vascular surgery. Principles and techniques*, H. Haimovici, Editor. 1984, Appleton-Century-Crofts: Norwark, Connecticut. p. 93-118.
13. Grondin, P., *Small diameter arteries in the aortocoronary position*, in *Vascular grafts*, P. Sawyer and Kaplitt, M., Editors. 1978, Appleton Century Crofts: New York. p. 373-377.
14. Dardik, H., *Biological behaviour of glutaraldehyde-stabilized human umbilical cord vein grafts*, in *Vascular surgery. Principles and techniques*, H. Haimovici, Editor. 1984, Appleton-Century-Crofts: Norwark, Connecticut.
15. Carrel, A., *Permanent intubation of the thoracic aorta.* J Exp med, 1912. **16**(17): p. 17.
16. Tufier, M., *De l'intubation arterielle dans le plaies des grosses arteres.* Bull Acad Nat Med, 1915. **74**: p. 455.
17. Blakemore, A., Lord, J., and Stefko, P., *The severed primary artery in war wounded.* Surgery, 1942. **12**(488): p. 488.
18. Hufnagel, C., *The use of rigid and flexible prostheses for arterial replacement.* Surgery, 1955. **37**: p. 165.
19. Voorhees, A., Jaretzki, A., and AH, B., *The use of tubes constructed from Vinyon "N" cloth in bridging arterial defects.* Ann Surg, 1952. **135**: p. 332.
20. Coury, A., Levy, R., McMillin, C., Pathak, Y., Ratner, B., Schoen, F., Williams, D., and Williams, R., *Degradation of Materials in the Biological Environment*, in *Biomaterials Science: An Introduction to Materials in Medicine.*, B. Ratner, Hoffman, A., Schoen, F., and Lemons, J., Editors. 1996, Academic Press: San Diego. p. 243-281.
21. Rule, M., *Physical Constants of Poly(oxyethylene-oxyterephthaloyl) (Poly(ethylene terephthalate))*, in *Polymer Handbook*, B. J, EH, I., and EA, G., Editors. 1999, John Wiley and Sons: New York. p. 113-118.
22. Seifalian, A., Giudiceandrea, A., and Schmitz-Rixen, T., *Noncompliance: The silent acceptance of a villain*, in *Tissue engineering of vascular prosthetic grafts*, Z. P and HP, G., Editors. 1999, R.G. Landes: Texas.

Stellenbosch University http://scholar.sun.ac.za

23. King, M., Blais, P., Guidoin, R., Prowse, E., Marcois, M., Gosselin, C., and Noel, H., *Polyethylene terephthalate (Dacron) vascular prostheses - material and fabric construction aspects.*, in *Biocompatibility of Clinical Implant Materials*. 1981. p. 177-207.
24. Speranti, C., *Fluorocarbon polymers, polytetrafluoroethylene (PTFE)*, in *Handbook of plastic materials and technology*, I. Rubin, Editor. 1990, John Wiley and Sons: New York.
25. Davids, L., Dower, T., and Zilla, P., *The lack of healing in conventional vascular grafts*, in *Tissue engineering of vascular grafts*, P. Zilla and Greisler, H., Editors. 1999, RG Landes: Austin. p. 3-44.
26. Paris, E., King, M., Guidoin, R., Dolorme, J., Deng, X., and Douville, Y., *Innovations and deviations in therapeutic vascular devices*, in *Polymeric Biomaterials*, S. Dumitriu, Editor. 1994, Marcel Dekker: New York.
27. Sauvage, L. and Wesolowski, S., *Healing and fate of arterial grafts.* Surgery, 1955(38): p. 1090.
28. Butt, K., *Bovine heterograft for arteriovenous fistula*, in *Vascular grafting*, P. Sawyer and Kaplitt, M., Editors. 1978, Appleton-Century-Crofts: New York. p. 278-281.
29. Sladen, J., Gilmour, J., and Wong, R., *Cumulative patency and actual palliation in patients with claudication after aortofemoral bypass. Prospective long-term follow-up of 100 patients.* American Journal of Surgery, 1986. **152**(2): p. 190-195.
30. von Oppell, U. and Zilla, P., *Tissue adhesives in cardiovascular surgery.* Journal of long-term effectsof medical implants, 1998. **8**(2): p. 87-101.
31. Veith, F.J., Gupta, S.K., Ascer, E., White-Flores, S., Samson, R.H., Scher, L.A., Towne, J.B., Bernhard, V.M., Bonier, P., Flinn, W.R., and et al., *Six-year prospective multicenter randomized comparison of autologous saphenous vein and expanded polytetrafluoroethylene grafts in infrainguinal arterial reconstructions.* J Vasc Surg, 1986. **3**(1): p. 104-14.
32. AHA, *http://americanheart.org/statistics/09medicl.html.* American Heart Association, 1999.
33. Zdrahala, R., *Small caliber vascular grafts. Part I: State of the art.* J Biomater Appl, 1996. **10**(4): p. 309-29.
34. Szycher, M., Reed, A., and Siciliano, A., *In vivo testing of a biostable polyurethane.* J Biomater Appl, 1991. **6**(2): p. 110-30.
35. Weinberg, C. and Bell, E., *A blood vessel model constructed from collagen and cultured vascular cells.* Science, 1986. **231**: p. 397-400.
36. L'Heureux, N., Germain, L., Labbe, R., and Auger, F., *In vitro construction of a human blood vessel from cultured vascular cells; a mophologic study.* J Vasc Surg, 1993. **17**(499-509).
37. Hirai, J. and matsuda, T., *Venous reconstruction using hybrid vascular tissue composed of vascular cells and collagen tissue regeneration process.* Cell Transplant, 1996. **5**(93-105).
38. L'Heureaux, N., Paquet, S., Labbe, R., Germain, L., and Auger, F., *A completely biological tissue-engineered human blood vessel.* FASEB, 1998. **12**(47-56).
39. Niklason, L. and Langer, R., *Advances in tissue engineering of blood vessels and other tissues.* Transplant Immunol, 1997. **1997**(5): p. 303-306.
40. Herring, M.B., Dilley, R., Jersild, R.A., Boxer, L., Gardner, A., and Glover, J., *Seeding arterial prostheses with vascular endothelium. The nature of the lining.* Ann Surg, 1979. **190**(1): p. 84-90.
41. Herring, M.B., Compton, R.S., LeGrand, D.R., Gardner, A.L., Madison, D.L., and Glover, J.L., *Endothelial seeding of polytetrafluoroethylene popliteal bypasses. A preliminary report.* J Vasc Surg, 1987. **6**(2): p. 114-8.
42. Zilla, P., Fasol, R., Deutsch, M., Fischlein, T., Minar, E., Hammerle, A., Krupicka, O., and Kadletz, M., *Endothelial cell seeding of polytetrafluoroethylene vascular grafts in humans: a preliminary report.* J Vasc Surg, 1987. **6**(6): p. 535-41.
43. Jarrell, B., Levine, E., Shapiro, S., Williams, S., Carabasi, R.A., Mueller, S., and Thornton, S., *Human adult endothelial cell growth in culture.* J Vasc Surg, 1984. **1**(6): p. 757-64.
44. Jarrell, B., Williams, S., and Stokes, G., *Use of freshly isolated capillary endothelial cells for the immediate establishment of a monolayer on a vascular graft at surgery.* Surgery, 1986. **100**: p. 392-399.
45. Zilla, P., Deutsch, M., and Meinhart, J., *Endothelial cell transplantation.* Semin Vasc Surg, 1999. **12**(1): p. 52-63.
46. Franke, R.P., Grafe, M., Schnittler, H., Seiffge, D., Mittermayer, C., and Drenckhahn, D., *Induction of human vascular endothelial stress fibres by fluid shear stress.* Nature, 1984. **307**(5952): p. 648-9.
47. Gillis-Haegerstrand, C., *Adhesion molecule expression following in vitro lining*, in *Tissue engineering of prosthetic vascular grafts*, P. Zilla and Greisler, H., Editors. 1999, RG Landes: Austin.
48. Zilla, P., Deutsch, M., Meinhart, J., Puschmann, R., Eberl, T., Minar, E., Dudczak, R., Lugmaier, H., Schmidt, P., Noszian, I., and et al., *Clinical in vitro endothelialization of femoropopliteal bypass grafts: an actuarial follow-up over three years.* J Vasc Surg, 1994. **19**(3): p. 540-8.
49. Niklason, L., *Replacement arteries made to order.* Science, 1999. **286**(5444): p. 1493-1494.

Stellenbosch University http://scholar.sun.ac.za

CHAPTER 3
Historical and theoretical considerations

3.1 Introduction

This chapter summarizes the theoretical considerations that need to be taken into account in the design and development of vascular prostheses. It shows the structure and properties of native vessels (that are to be replaced with the prostheses), and then highlights the demands placed on prosthetic devices in order for them to mimic the natural vessels as closely as possible.

3.2 Natural arteries

In order to develop synthetic arterial substitutes intended to mimic natural arteries, an understanding of the basic structure and function of arteries is essential.

3.2.1 Artery size and structure

Most blood vessels consist of three distinct layers, termed the tunica intima, tunica media and tunica adventitia, that are arranged in concentric layers (Figure 3.1). Each of these layers comprises a complex combination of cellular and extra-cellular materials that are specialized in form and function in order to perform specialized tasks.

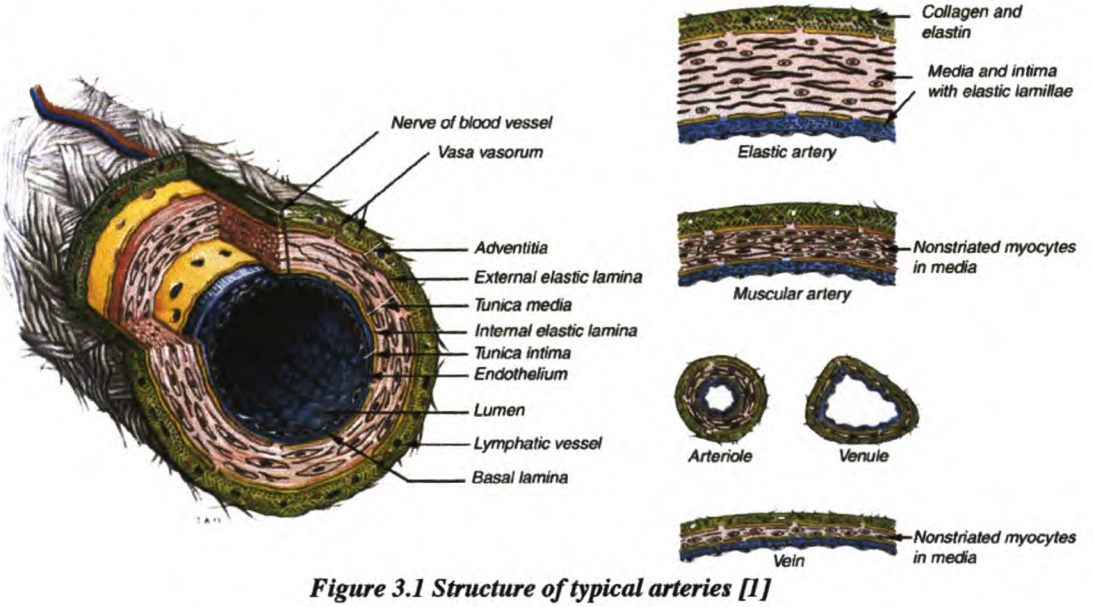

Figure 3.1 Structure of typical arteries [1]

Arteries show considerable variation in structure, size and function along the vascular tree. The large arteries closer to the heart (e.g. the aorta) are termed elastic arteries, and contain a high proportion of elastic material and a proportionally lower amount of contractile muscular tissue (Table 3.1). This allows for the storage of energy by dilation under systolic pressure, and for the release of that energy during diastole. This effect, which is similar to the Windkessel effect, allows for the smoothing of the pressure pulse in distal vessels. Further from the heart, in typical muscular arteries, the relative proportion of smooth muscle cells in the media increases, allowing the vessels to actively constrict and dilate according to physiological stimuli. Capillaries, whose main function of the exchanging of gases with the surrounding tissue prescribes minimum wall thickness, consist of only an endothelium supported by a basal lamina.

Whereas arteries are required to withstand high pressures and to regulate and moderate the blood pressure and flow profiles, the function of the venules and veins is perhaps less complex. Their primary function is to provide a return path for the blood from the capillary bed to the heart. As

Stellenbosch University http://scholar.sun.ac.za

this occurs at pressure that are much reduced from those encountered in the arterial tree, their structures are adapted accordingly. The relative sizes of arteries, arterioles, capillaries, venules and veins are summarized in Table 3.1. The decrease in artery size with increased distance from the heart, and the subsequent increase in size on the venous return is self-evident. The adaptation in the relative size and wall thickness of the different vessels closely follows their function. Large arteries not only have large diameters to deal with the large volumes of blood, but also contain walls that are approximately twice as thick as venous counterparts of similar size.

Table 3.1. Relative dimensions and constitutive tissue of blood vessels. (Adapted from [2])

	Aorta	Artery	Arteriole	Sphincter	Capillary	Venule	Vein	Vena Cava
Vessel Diameter	25mm	4-6mm	30μm	35μm	8μm	20μm	5mm	30mm
Wall thickness	2mm	1mm	20μm	30μm	1μm	2μm	0.5mm	1.5mm
Diameter/ thickness	12.5	4	1.5	1.2	8	10	10	20

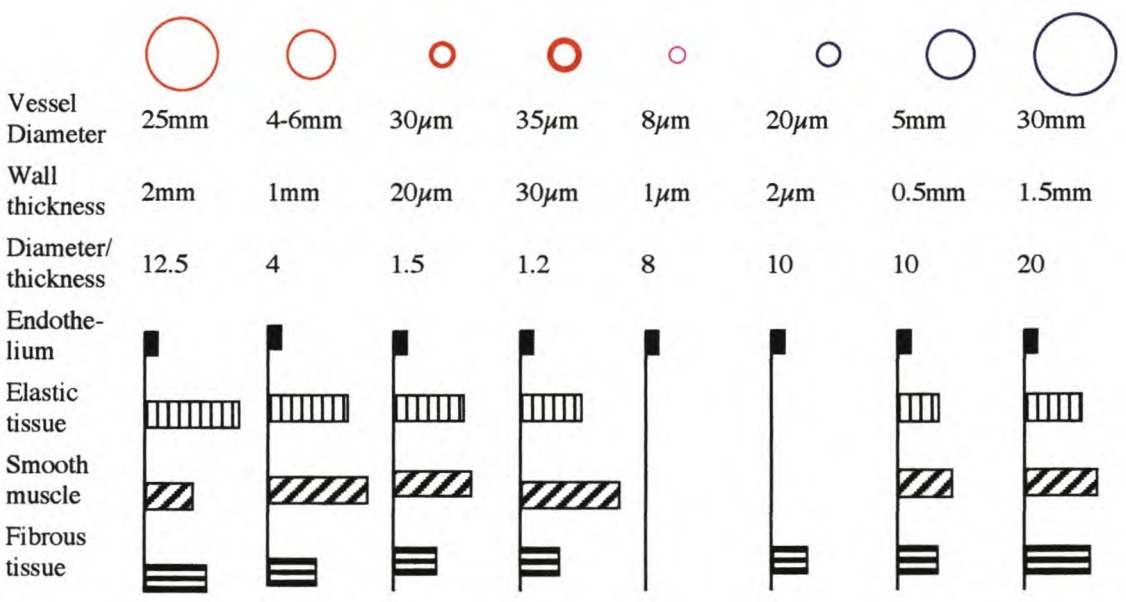

As the development of a suitable substitute for typical muscular arteries is the main goal of this dissertation, their structure will be described in more detail. The intima, consisting of the endothelium attached to a basement membrane, provides a non-thrombogenic, blood-contacting surface. The media contains smooth muscle cells (SMCs) as well as elastic and other intercellular connective and matrix materials, and supplies two other important properties to the blood vessel, namely compliance and contractility. In order to achieve these properties, the tissues are oriented in a helical fashion in this medial layer. It is known that the orientation of smooth muscle cells in the media is closely related to the stresses that these cells experience as a result of pulsatile dilation. Liu [3] has shown that the orientation of these cells may actually be changed by altering the applied stresses. SMCs in the rat aorta and jugular vein are oriented at 85° from the vessel axes (See Fig 3.2). Excision of the jugular vein and using it as an arterial graft results in principle stress changes that result in the re-orientation of the SMCs in the vein graft to 40°.

Another important property, namely structural integrity, is provided by the adventitia. The configuration of elastin and crimped collagen fibres in this layer provides for the "stiffening" of the vessel when subjected to high internal pressures, i.e. the decrease in compliance with increased strain. A more detailed description of the structure and function of blood vessels may be found in Gray's anatomy [1].

Stellenbosch University http://scholar.sun.ac.za

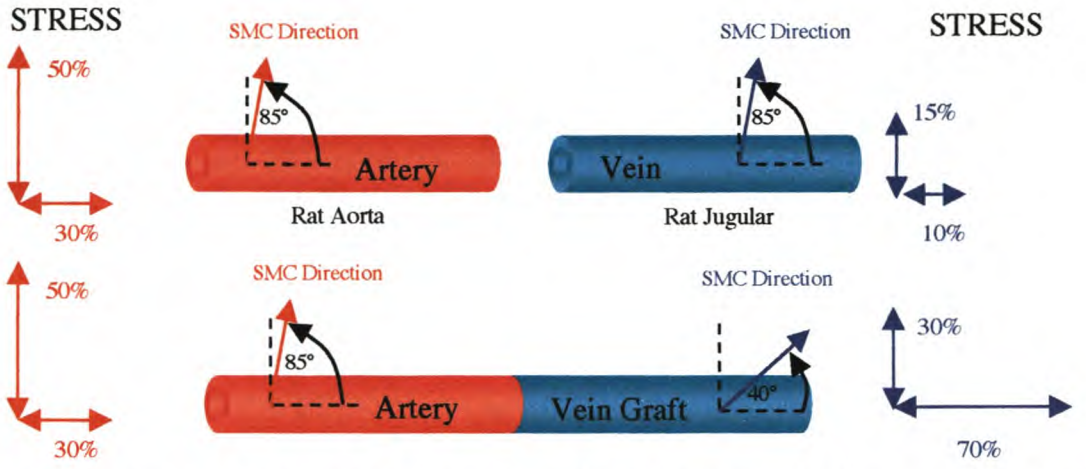

Figure 3.2: Re-orientation of rat jugular vein smooth muscle cells as a result of a change in applied stress due to relocation to an arterial position. [3]

3.2.2 Summary: Artery size and structure

Natural muscular arteries contain:

- An endothelium that provides a **smooth surface** for blood flow and the **active non-thrombogenic properties**
- A medial layer that contains **helically oriented smooth muscle** cells and elastic elements that provides for the contractile behaviour and compliance. The **orientation of SMCs** in the media may be **altered by applying the appropriate stresses**.
- An adventitial layer that consists mainly of elastin and crimped collagen fibres that provide **structural integrity** by **progressively arresting expansion** at high internal pressures
- A typical peripheral muscular artery has a **diameter of 4-6mm** and a wall **thickness of 1mm**.

3.2.3 Mimicking of artery properties

The demands placed on a synthetic vascular prosthesis that would sufficiently mimic the structure and properties of natural arteries to ensure successful long-term outcomes are described in detail in the remainder of this chapter. It is useful to sub-classify these requirements under three headings, namely: general, graft-related and host-related demands. The first relates to the overall structure and function of the replacement vessel, the second to specific demands placed on the physical and chemical properties of the graft, and the third to the response encountered when the device is implanted into living tissue.

3.3 General demands

The desired outcome required from vascular grafting is known. The prosthesis should replace or bypass the diseased or injured vessel, re-establish adequate levels of perfusion to the distal vasculature and organs, and continue to do so for the lifetime of the recipient. Fifty years of research into the use of synthetic biomaterials has highlighted a number of properties that should be exhibited by a vascular graft in order to achieve this goal [4].

The manufacturing processes used for the production of grafts must be economically viable, environmentally acceptable, and must allow for the production of devices of uniform and high quality. Prostheses must then be sterilized and stored for extended periods in a sterile state. In order to satisfy the requirements of vascular surgeons, prostheses should, during implantation,

Stellenbosch University http://scholar.sun.ac.za

display good handling characteristics (drapability without forfeiting dimensional stability) and good suturability. For correct size matching, the surgeon should have a range of diameters and wall thicknesses to choose from, and must be able to trim the prosthesis to the desired length without undue difficulty or adverse consequences to the integrity of the graft. Directly after implantation, the graft should have adequate structural integrity to withstand the internal blood pressure without excessive haemorrhage. Other requirements at this and later stages include kink-resistance around bends and a resistance towards being flattened by surrounding anatomical features.

In order to promote the healing and incorporation of the device into the body, the materials used in its construction should not be toxic, inflammatory, carcinogenic or excessively thrombogenic. Other important requirements, namely material properties, porosity, integrity, compliance matching, biocompatibility and healing will be discussed in further detail below (Section 3.4 and 3.5).

3.4 Graft-related demands

In order to mimic the function of natural arteries, the demands placed on the graft properties are numerous and complexly interrelated. The materials used to fabricate the prosthesis, as well as the structure of the material that comprises the graft wall, determine not only the long-term stability of the implant, but also the mechanical properties and thus function of the device.

3.4.1 Material requirements

Initial investigations into the use of polymeric materials for vascular grafts concentrated on fibrillar materials that showed a high degree of in vivo stability. These studies led to the acceptance of PET and PTFE (initially fibrillar, now expanded) as materials of adequate stability to be used in current commercially available vascular grafts. In addition to the abovementioned polymers, a wide range of other biostable materials have been evaluated for use in vascular graft applications [5, 6]. These include polypropylene (PP), polyethylene (PE), polysiloxanes (specifically polydimethylsiloxane; PDMS) and polyurethanes (PU). The biostable approach is based on the permanent incorporation of the synthetic material into a tissue/polymer composite graft.

Another approach to vascular grafts involves the use of degradable materials in their construction. Typical degradable materials routinely used include poly(glycolic acid), poly(lactic acid) (PLA) and polydioxanone (PDS). Researchers in this field endeavor to effect the generation of a new vessel by the degradation of porous scaffold after ingrowth of sufficient cellular and extracellular materials (before degradation resulted in failure of the graft), followed by complete (or partial) resorption of the polymeric material [7, 8]. The scope of this dissertation is restricted to biostable materials, more specifically polyurethanes, and the demands placed on these materials will be discussed.

3.4.1.1 Chemico-physical stability

It has been recognized that no material is completely inert in the hostile environment found in the human body and even materials that are recognized as being extremely stable (gold, platinum, titanium) are corroded in vivo [9]. Nonetheless, the demands placed on polymeric materials used in durable vascular grafts require them to be chemically stable to the degree that ensures structural integrity, and that prevents the generation of toxic or inflammatory breakdown products. Even if the main component of the material is sufficiently biostable, the possibility and extent of minor components (impurities and additives) leaching from the material must be minimized or eliminated.

Whatever its location in the body, the biomaterial will encounter an aqueous environment containing not only various cations and anions, but also a variety of proteins and cells. All

Stellenbosch University http://scholar.sun.ac.za

polymeric (and other) materials respond continuously to changes in their environment, before and after implantation [5]. All polymers are, to a more or lesser extent, permeable to gasses and liquids. They adsorb, absorb, transmit and desorb components, resulting in changes in surface and/or bulk properties [10]. Thus, degradation of a biomaterial leading to compromised performance may be chemical, physical, or a combination of both.

Physical changes that may occur include swelling, crystallization, de-crystallization, plasticization, fatigue fracture, creep and stress cracking. Chemical degradation is often associated with the scission of covalent bonds, but may also involve ionic bond transformations or even covalent crosslinking [11]. The major modes of chemical degradation in vivo result from hydrolysis, oxidation and mineralization [5]. These modes will now be discussed in more detail.

(A) Hydrolysis

Simple hydrolysis is the scission of susceptible functional groups by reaction with water, and may be catalyzed by acids, bases, salts or enzymes. Polymers that are susceptible to hydrolysis generally contain carbonyl groups bonded to heterochain atoms (O, S, N). The rate of hydrolysis differs among the susceptible groups, and carbonyl group reactivity decreases in the order: anhydride > ester > urethane > amide. Other polymers that are susceptible to hydrolysis under certain conditions contain ether, acetal, nitrile, phosphonate or active methylene groups. The rate of hydrolysis tends to increase with increasing hydrolysable group content, increased hydrophilicity, decreased crystallinity, decreased crosslinking, increased surface-to-volume ratio and increased mechanical stress [12].

The in vivo environment (37 °C, pH 7.4) appears to be a rather mild reaction medium by in vitro standards. Neutral water alone, although capable of hydrolyzing some readily hydrolyzable polymers (e.g. polyglycolic acid etc.), is unlikely to be responsible for significant degradation of more stable heterochain polymers. However, the complex interactions of components present in extracellular fluid produce aggressive responses to foreign bodies. Zaikov has shown that certain ions (e.g. PO_4^{3-}), as well as localized pH changes due to inflammatory response, are effective catalysts of polyester hydrolyzation, and may increase reaction rates by several orders of magnitude [13]. Quite remarkably, certain enzymes are not only able to increase hydrolysis rates of certain polymers, but are able to do so selectively [14, 15].

Polymers that are hydrolytically stable include hydrocarbons, silicones, sulphones, halocarbons and polymers containing isolated carbonyl groups (ketones) [5].

(B) Oxidation

Oxidative degradation of biopolymers results in the modification or destruction of molecular structure by electron-transfer reactions [16]. Polymers that are prone to oxidative attack are generally those that contain groups capable of resonance stabilization of resultant free radicals. They include branched aliphatic hydrocarbons (alkyl, aryl or allyl branch), allylic hydrocarbons, and those that contain aromatic side groups, ether linkages, alcohols (and phenols), aldehydes and secondary amines.

Prior to implant, processes that may induce oxidation include melt processing, γ-sterilization and exposure to light (ultraviolet radiation). Although molecular oxygen may be directly responsible (auto-oxidation) [17], other effective oxidants include metal ions, hypochlorite and hyperoxides [18].

In vivo, biomaterials are susceptible to oxidative attack by powerful oxidizing agents (hydroxyl radicals, peroxynitriles and hypochlorites) resulting from phagocytic activation that occurs during inflammation and foreign-body reaction [16, 18]. In addition, there is some evidence of the limited effect of direct enzymatic catalysis of oxidation [15, 19]. Although the exact mechanisms of in vivo oxidation are not known, it is generally accepted that both

Stellenbosch University http://scholar.sun.ac.za

polymorphnuclear leucocytes (PMNs) and macrophages metabolize oxygen to form the superoxide anion ($O_2^{\bullet-}$). The superoxide may oxidize the polymer directly, or it may be transformed into even more powerful oxidants. Superoxide dismutase (an ubiquitous peroxidase enzyme) can catalyze the conversion of superoxide to hydrogen peroxide, which in turn may be converted to hypochlorous acid (itself a strong oxidant) [20]. Hypochlorite is able to oxidize not only free-amine functionalities (in proteins), but also substituted functional amine groups such as amides, ureas and urethanes [12].

The in vivo oxidation of polyurethanes has been extensively studied. [15-18]. The effect of oxidation usually manifests itself in surface fissuring, deep-crack formation, fragmentation and wear, often in areas of elevated stresses [5].

The mitigation of these structural changes may be achieved by limiting the concentration of stresses, minimising exposure to radiation, the use of antioxidants, isolation of the susceptible polymers from direct phagocytic attack or soluble oxidants, and by the use of polymers that are resistant to oxidation [16-18, 21]. Polymers that are stable to oxidation include straight-chain hydrocarbons (e.g. polyethylene), halocarbons (e.g. PTFE), and those containing fully oxidized groups (e.g. ketones, sulphones, esters, urethanes), although some evidence exists of the susceptibility of carbon atoms next to hetero-atoms in some carbonyl-containing materials [22].

(C) Mineralization

Although mineralization (calcification) may or may not be responsible for significant scission of covalent bonds, it does involve chemical transformation that can cause structural damage to biopolymers. It involves the deposition of insoluble calcium phosphate salt on or in the polymer (extrinsic and intrinsic calcification respectively). The levels of calcification have been shown to be more a function of soluble calcium levels and device function, rather than the chemical composition of the polymer [23, 24]. Although high levels of calcification are associated with devices that undergo high levels of cyclic deformation (such as prosthetic heart valves and heart assist devices), it has been reported to occur in synthetic vascular grafts where deformation levels are more moderate [23].

3.4.1.2 Mechanical Properties

The requirement of compliance (discussed in more detail below, see 3.4.5) further demands that the vascular graft dilates and contracts in sympathy with the internal pressure pulse. This requires that either the polymer from which the device is constructed be of an elastic nature, or that the graft be constructed in such a way that it allows for elastic behaviour (or both). All currently available prosthetic grafts are constructed from highly crystalline materials (PET and PTFE), and they are all undercompliant. In order to overcome this disadvantage, both thermoplastic (e.g. polyurethanes) and thermoset elastomers (e.g. polysiloxanes) have been used to produce a wide range of experimental prostheses that match the compliance of natural blood vessels.

3.4.2 Suitability of polyurethanes for use in medical devices

Due to the almost endless number of formulations that may be used to prepare polyurethanes, they offer the greatest variety of chemical and physical properties of any family of polymers. Their physical properties range from hard, rigid thermosetting materials to those of softer thermoplastic elastomers, while their chemical properties may be tailored to control durability and chemical stability. It is not surprising, therefore, that polyurethanes have been extensively studied over the past four decades for use in medical applications [20, 25].

The total use of plastics in medical and pharmaceutical applications has been estimated at 830,000 metric tons in 1989 [25]. Although thermoplastic polyurethanes (TPU) account for only 4,500 tons of that total (in comparison to that of the most commonly used plastic, PVC: 220,000

Stellenbosch University http://scholar.sun.ac.za

tons), this figure does not reflect the versatility of the materials and their relative success as biomaterials.

A number of TPUs in particular exhibit a unique combination of biocompatibility, toughness, biostability and surface functionality [26] that has led to widespread use in implantable medical device such as pacemaker leads, blood bags, catheters, bladders and artificial hearts [25]. The elastomeric properties of certain PUs also make them good potential candidates for applications where interaction with and mimicking of soft tissue is required. This is particularly true for vascular grafts [26], where the matching of compliance has been highlighted as an important factor governing the fate of prostheses [27].

3.4.3 Polyurethane classification

Depending on the combination of raw materials used in their synthesis, it is possible to sub-classify polyurethanes into a variety of subgroups. Firstly, these polymers may be divided into two groups, namely aromatic or aliphatic. This distinction is based on the nature of the diisocyanate employed in the synthesis as the polyols and chain extenders are generally aliphatic. A second distinction is based on the nature of the polymeric diol, i.e. whether it contains polyester, polyether, polycarbonate, siloxane or hydrocarbon linkages. Thirdly, it is useful to distinguish between polyurethanes and polyurethane ureas, based on whether diols or diamines (respectively) were employed as the chain extender. Thus aliphatic polyether urethane ureas would be polymers derived from aliphatic diisocyanates, polyether diols, and diamine chain-extenders.

3.4.3.1 PU synthesis: Reaction conditions

In order to discuss the material properties and the effect of polymer structure on such properties, a brief introduction to segmented polyurethane synthesis is required. Although polyurethanes may be produced by a simple one-step process, segmented polyurethane elastomers intended for use in medical applications are generally synthesised in a two-step process to gain more control over stoichiometry. Briefly, (see Fig. 3.3) a macromolecular diol is reacted with an excess of diisocyanate to form an isocyanate end-capped prepolymer (M_n up to 15000-120000). The prepolymer (and the remaining unreacted diisocyanate form the first step) is then further reacted with a chain extender to produce the desired segmented multiblock copolymer of type $(AB)_n$, where A denotes the soft segment and B represents the hard segment.

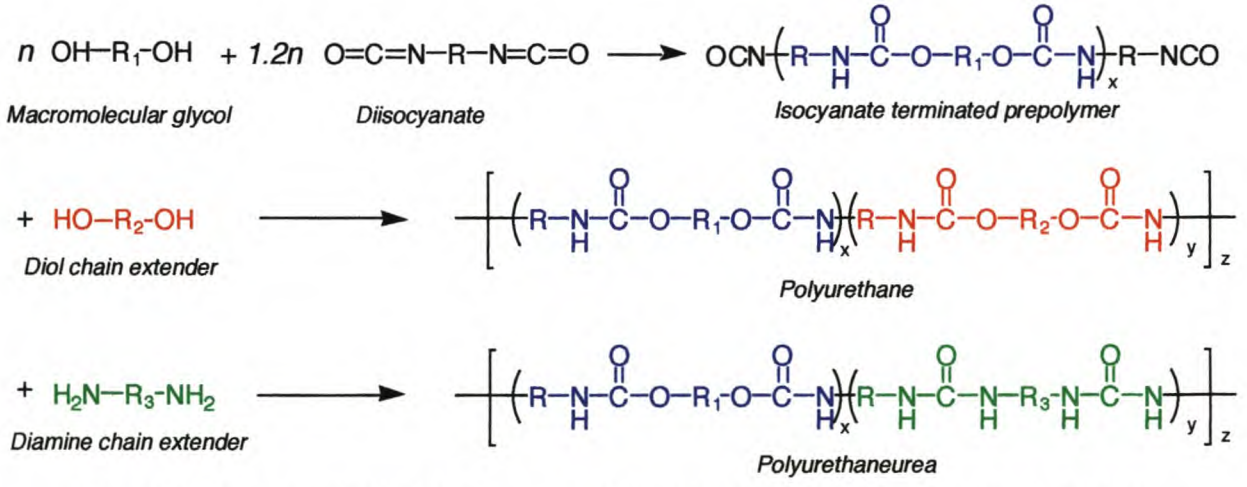

Figure 3.3: Two-step process for the synthesis of segmented polyurethanes and polyurethane ureas

Stellenbosch University http://scholar.sun.ac.za

Great care must be taken in the choice of reaction conditions, as the reactive diisocyanates group may further react with:

- urethane groups to form allophanate linkages (that may result in covalent crosslinking)
- urea groups to form biuret linkages (that may result in covalent crosslinking)
- water to form carbamic acid (that may dissociate into amines and carbon dioxide)
- amines from carbamic acids degradation to form ureas
- with another diisocyanate to form uretidiones
- with another diisocyanate to form carbodiimides
- with two more diisocyanates to form isocyanurates

Apart from accurate stoichiometry, the reaction temperature, catalyst choice and reaction medium may influence the reaction products. Generally, low temperatures (<50°C) favour chain extension, while higher temperatures (50-150°C) promote crosslinking and branching reactions. Higher temperatures (>150°C) lead to dissociation of biuret and allophanate linkages and degradation of aromatic polyurethanes, while temperatures in excess of 220°C will result in the decomposition of aliphatic urethanes. Catalysts that promote the reaction of isocyanates include sodium hydroxide, tertiary amimes and organo-metallic (especially tin) compounds. Careful choice of catalysts must be employed to promote the preferential reaction of isocyanates with the preferred species (such as diols) and minimise the reaction with others (e.g. urethanes and ureas) or vice versa. Although bulk polymerisation is often used, solution polymerisation in N,N-dimethylacetamide (DMAC), dimethylformamide (DMF), tetrahydrofuran (THF) and dimethylsolphoxide(DMSO) may also be employed [25]. Some polymer grades are sold as concentrated solutions (<25%) in these solvents.

3.4.3.2 Raw materials

The chemical and physical properties of polyurethanes are also determined by the nature of the raw materials (diisocyanates, polymeric diols, and diamine/diol extenders) used in the production. Polymeric diols used in the synthesis of elastomeric polyurethanes include polyesters, polyethers, hydrocarbons, and polydimethylsiloxanes. Both aromatic and aliphatic diisocyanates and chain extenders (diols or diamines) can be used. A list of commonly used raw materials is given in Table 3.2. This is followed by a comprehensive list of medical-grade polyurethanes (Table 3.3).

Stellenbosch University http://scholar.sun.ac.za

Table 3.2: Chain extenders, diisocyanates and polymeric diols used in the production of medical-grade polyurethanes

Structure of compound	Name	Abbreviation
	DIOL EXTENDERS	
HO-R-OH	generic diol	DO
$HO-(CH_2)_2-OH$	ethane diol	EDO
$HO-(CH2)_4-OH$	butane diol	BDO
$HO-(CH2)_6-OH$	hexane diol	HDO
	DIAMINE EXTENDERS	
$H_2N-R-NH_2$	generic diamine	DA
$H_2N-(CH_2)_2-NH_2$	ethylene diamine	EDA
	AROMATIC DIISOCYANATES	
O=C=N−R_1−N=C=O R_1 = aromatic	generic aromatic diisocyanate	ArDI
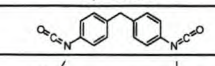	methylene bis(p-phenyl isocyanate)	MDI
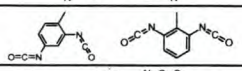	2,4 toluene diisocyanate 2,6 toluene diisocyanate	2,4 TDI 2,6-TDI
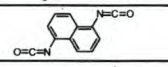	1,5-naphthalene diisocyanate	NDI
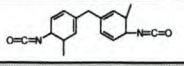	methylene bis (toluene isocyanate)	TODI
	ALIPHATIC DIISOCYANATES	
O=C=N−R_2−N=C=O R_2 = aliphatic	generic aliphatic diisocyanate	AlDI
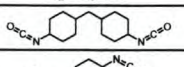	methylene bis(4,4-cyclohexyl isocyanate)	HMDI
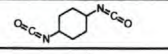	1,4-cyclohexane diisocyanate	CHDI
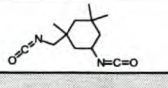	3-isocyanatomethyl-3,5,5-trimethylcyclohexyl isocyanate (isophorone diisocyanate)	IPDI
	POLYESTER DIOLS	
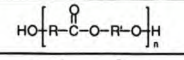	generic polyester diol	PesD
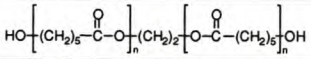	polyethylene adipate glycol	PEA
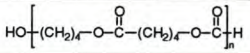	polycaprolactone	PCL
	POLYETHER DIOLS	
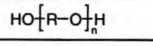	generic polyether diol	PED
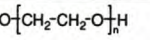	poly(ethyleneoxide) glycol poly(oxyethylene) glycol	PEO
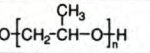	polypropylene oxide glycol poly(oxypropylene) glycol	POPG
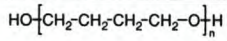	poly(oxytetramethylene)glycol poly(tetramethylene oxide) glycol	PTMEG
	POLYCARBONATE DIOLS	
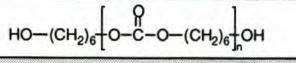	polyhexamethylene carbonate glycol	PHMC
	POLYSILOXANE DIOLS	
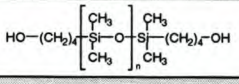	hydroxybutyl terminated poly(dimethylsiloxane)	PDMS
	HYDROCARBON DIOLS	
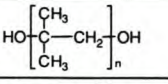	hydroxy terminated polyisobutylene	PIB
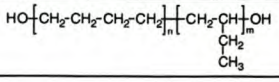	hydrogenated polybutadiene	PBD

Stellenbosch University http://scholar.sun.ac.za

Table 3.3: Listing and properties of medical grade polyurethanes.

AROMATIC POLYETHER URETHANES																
#	Name	Producer	Diisocyanate	Soft Segment	Extender	Shore	γ_c	T_g	T_{mh}	M_w (x10^3)	M_n (x10^3)	σ_b (MPa)	E_Y (MPa)	ε_b (%)	E_{100} (MPa)	ρ (g/cm^3)	Ref
1	Pellethane 2363	Dow	MDI	PTMEG	BDO	80A-55D					35-48	3.6-14		350-600		1.15	[20, 28-30]
	55D					55D			156	81		40-48	87	328-390	17.2		
	75D																
	80A					82A		-36				31-34	13.2	430-550	6		
	90																
2	Vialon 510X	Becton Dickenson	MDI	PTMEG	BDO												[20, 30]
3	Cardiomat 610	Kontron	MDI	PED	DO	80A					27.6	8.1*	500				[20]
	Corplex																[20]
4	Erythrothane	Biosearch	ArDI	PED	DO												[20]
5	Renathane	Renal Syst's	ArDI	PED	DO												[20]
6	SRI series	Stanford Res. Inst.	MDI	PED	DO												[20]
7	Estane 5714	BF Goodrich	MDI	PED	DO												[20, 30]
8	Texin	Mobay (Bayer)	MDI	PED	DO												[20]
9	Techothane	Thermedics	MDI	PTMEG													[31, 32]
	TT-1074A					75A	81	-51	220	100		41.3		550	3.4	1.10	
	TT-1085A					85A						48.2		450	5.5	1.12	
	TT-1095A					94A						62.1		440	9.0	1.15	
	TT-1055D					54D						66.1		350	17.2	1.16	
	TT-1065D					64D						68.9		300	19.3	1.18	
	TT-1069D					69D						60.7		310	22.1	1.18	
	TT-1072D					74D						62.1		275	25.5	1.18	
	TT-1075D					75D						57.2		150	24.8	1.19	
10	Tecoplast TP-470	Thermedics				82D						68.9		50			[32]
11	Elasthane 55D	PTG	MDI	PTMEG	BDO	55D						55.2		490	14.9	1.16	[33]
12	Chronothane 80A	CT Biomaterials	MDI	PTMEG								35.2		550	5.9		[34]
						80A											
13	Elast-Eon 1	Elastomedic	ArDI	PHMO		80A-75D						31±2	54.5±6	580±45	9.1±0.2		[35]

AROMATIC POLYETHER URETHANE UREAS																
#	Name	Producer	Diisocyanate	Soft Segment	Extender	Shore	γ_c	T_g	T_{mh}	M_w (x10^3)	M_n (x10^3)	σ_b (MPa)	E_Y (MPa)	ε_b (%)	E_{100} (MPa)	ρ (g/cm^3)	Ref
1	Biomer SolG	Ethicon	MDI	PTMEG	EDA/DAC	75A		-73	295	157	31-41	2.8-5.5	600-800				[30, 36, 37]
2	Biomer ExtG	Ethicon	MDI	PTMEG	water	75A					28-35	12.4Flx					[20]
3	Mitrathane	Polymedica	MDI	PTMEG	EDA												[20, 38]
4	Surethane	Cardial Con Sys	MDI	PTMEG	DA												[20]
5	SRI series	Stanford Res	MDI	PED	DA												[20]
6	Mod.PUU	Mercor	ArDI	PED	DA/Surf.												[20]
7	Univ. Utah	Univ. Utah	MDI	POPG	EDA												[20]
8	Lycra	DuPont	MDI	PTMEG	DA												[20]
9	Biospan	PTG	MDI	PTMEG	DA												[30, 33]
	70A					70A		-65	180	180	41	41.3	5.9	850			
10	TM5	Toyobo	MDI	PTMEG	PDA												

AROMATIC POLYCARBONATE POLYURETANE																
#	Name	Producer	Diisocyanate	Soft Segment	Extender	Shore	γ_c	T_g	T_{mh}	M_w (x10^3)	M_n (x10^3)	σ_b (MPa)	E_Y (MPa)	ε_b (%)	E_{100} (MPa)	ρ (g/cm^3)	Ref
1	Chronoflex AR	Cardiotech Inc.	MDI	PCDO	EDA/DAC	72A-67D	86	-34	240	140							[30, 31, 34, 37]
	75A	(Polymedica)										51.7		500			
2	Bionate (Corethane)	PTG (Corvita)	MDI	PHECD	BD												[28, 30, 31, 33]
	80A					80A	81	-18	240	130	45-52	48.3	400-490	570	6.8	1.19	
	90A					90A						53.8		420	12.6	1.20	
	55D					55D	96	-78.3	140	75	48-59	62.1	365-440	380	18.3	1.21	
	75D					75D					48-63	68.9	255-320	260	37.9	1.22	
3	Chronoflex C	Cardiotech Inc.													secant		[34]
	80A	(Polymedica)				80A						37.9-44.8		400-490	5.3-8.6		
	55D					55D						41.4-51.7		365-440	12.8-15.2		
	75D					75D						48.3-55.2		255-320	36.5-39.3		

Stellenbosch University http://scholar.sun.ac.za

ALIPHATIC POLYETHER URETHANES

#	Name	Producer	Diisocyanate	Soft Segment	Extender	Shore	γ_w	T_g	T_{mh}	M_w (x10^3)	M_n (x10^3)	σ_b (MPa)	E_Y (MPa)	ε_b (%)	ε_{100} (MPa)	ρ (g/cm^3)	Ref
1	Tecoflex	Thermedics	HMDI	PTMEG	BDO		81	-70					580-800				[20, 30-32]
	EG-80A					72A						40.0		660	2.1	1.04	
	EG-85A					77A						42.7		550	4.1	1.05	
	EG-93A					87A						53.1		390	6.9	1.08	
	EG-100A					94A						56.5		370	11.0	1.09	
	EG-60D					51D						57.2		360	12.4	1.09	
	EG-65D					60D					42	57.2		360	15.2	1.10	
	EG-68D					63D						57.2		350	17.9	1.10	
	EG-72D					72D					55	55.8		310	23.4	1.11	
2	Techophilic	Thermedics												wet/dry			[32]
	HP-60D-20					43D								430/390			
	HP-60D-35					42D								450/390			
	HP-60D-60					41D								500/300			
	HP-93A-100					83A								1040/620			
3	SRI series	Stanford Res. Inst.	HMDI	PED	DO												[20]
4	Southern RI	Southern Res. Inst.	IPDI	PTMEG	BDO												[20]
5	Akzo	Akzo	AlDI	PED	DO												[20]

ALIPHATIC POLYETHER URETHANE UREAS

#	Name	Producer	Diisocyanate	Soft Segment	Extender	Shore	γ_w	T_g	T_{mh}	M_w (x10^3)	M_n (x10^3)	σ_b (MPa)	E_Y (MPa)	ε_b (%)	E_{100} (MPa)	ρ (g/cm^3)	Ref
1	SRI series	Stanford Res. Inst.	HMDI	PED	DA												[20]

ALIPHATIC POLYCARBONATE POLYURETANE

#	Name	Producer	Diisocyanate	Soft Segment	Extender	Shore	γ_w	T_g	T_{mh}	M_w (x10^3)	M_n (x10^3)	σ_b (MPa)	E_Y (MPa)	ε_b (%)	E_{100} (MPa)	ρ (g/cm^3)	Ref
1	Chronoflex AL	Cardiotech Inc.	HMDI???	PCDO	EDA/DAC												[30, 34]
	80A	(Polymedica)				80A						37.9		585	4.5		
	55D					55D						57.9		325	20.0		
	65D					65D						62.1		300	22.1		
2	Carbothane	Thermedics	HMDI	PCDO	BD												[31, 32]
	PC-3570A						96	-29	140	75							
	PC-3575A					73A						36.5		470	2.1	1.15	
	PC-3585A					84A						41.4		410	4.1	1.15	
	PC-3595A					95A						49.0		380	6.9	1.15	
	PC-3555D					60D						50.3		370	10.3	1.15	
	PC-3572D					71D						58.6		360	22.8	1.15	

SILOXANE URETHANE COPOLYMERS

#	Name	Producer	Diisocyanate	Soft Segment	Extender	Shore	γ_w	T_g	T_{mh}	M_w (x10^3)	M_n (x10^3)	σ_b (MPa)	E_Y (MPa)	ε_b (%)	E_{100} (MPa)	ρ (g/cm^3)	Ref
1	Cardiothane 51	Avcothane	MDI	PED	DO PDMS	72A					43		580				[20]
2	Rimplast	Petrarch	AlDI	PED	DO PDMS												[20]
3	Elasteon 2	Aortec	ArDI	PDMS		80A-55D											[35]
	85A	(Elastomedic)c				85A						28±0.7	33	580±5	10±0.3		
4	Elasteon 3	Aortec		PDMS/PHMO		65A-80A											[29, 35, 39]
	70A	(Elastomedic)				70A						25±1	7.0±0.6	490±11	5.0±0.1		
	H-O			0% PDMS		89A		-41				13±1	38±4	225±35			
	H-20			20% PDMS		85A		NA/-46				16±1	24±1	393±50			
	H-20 opt			20% PDMS		85A						25.5	25±2	460			
	H-50			50% PDMS		82A		-116/-46				15±2	23±3	361±60			
	H-80			80% PDMS		82A		-112/-31				18±1	20±1	473±25			
				100% PDMS		85A		-112				28±2	17±1	472±25			
5	PurSil AR	PTG	MDI	PTMO	DO												[33]
	AR 10-80A			10 wt% PDMS				-68				34.5		770	5.6	1.11	
	AR 20-80A			20 wt% PDMS				-74				33.7		770	6.2	1.11	
	AR 30-80A			30 wt% PDMS				-86				24.8		620	7.2	1.11	
6	PurSil AL	PTG	AlDI	PTMO +	DO												[33]
	AL-5-75A			5 wt% PDMS								36.5		900	1.9	1.06	
	AL-10 75A			10 wt% PDMS								33.8		700	1.9	1.07	
	AL-20 75AA			20 wt% PDMS								28.3		730	2.0	1.07	
7	CarboSil	PTG	MDI	PCDO+													[33]
	10 90A			10 wt% PDMS								39.8		420	10.1	1.18	
	20 90A			20 wt% PDMS								42.6		530	8.8	1.16	
	40 90A			40 wt% PDMS								29.6		530	9.0	1.14	

Stellenbosch University http://scholar.sun.ac.za

HYDROPHILIC POLYURETHANES																	
#	Name	Producer	Diisocyanate	Soft Segment	Extender	Shore	γ_w	T_g	T_{mh}	M_w (x10^3)	M_n (x10^3)	σ_b (MPa)	E_Y (MPa)	ε_b (%)	E_{100} (MPa)	ρ (g/cm^3)	Ref
1	Hydromer	Hydromer	ArDI	PED/PEst	H2O												[20]
2	ORI	Ontario Res. Inst.	HMDI	POADA	PEG												[20]
3	MIT	MIT	CHDI	PEO	DEG												[20]

OTHER POLYURETANES																	
#	Name	Producer	Diisocyanate	Soft Segment	Extender	Shore	γ_w	T_g	T_{mh}	M_w (x10^3)	M_n (x10^3)	σ_b (MPa)	E_Y (MPa)	ε_b (%)	E_{100} (MPa)	ρ (g/cm^3)	Ref
1	M48	Medtronic	MDI/dimer	dimerDI/BDO/ dimerDO	BDO/dimer DO	85-90A				220	120	29 MPa	21 MPa				[36]
2	Hydrothane 80A 93A	[20]	AlDI									53.8		580			[34]
2	Hydroslip C	[20]													1.16		[34]
3	Elast-Eon 4 85D					55D-85D 85D						77	648	23	---		[35]
4	Enka PUR 817 923 947 981	ENKA AG polyetherurethane Ditto + PDMS Polyesterurethane Polyesterurethane															[20]
5	Thoralon	Thoratec		PED	DA												

Diisocyanates		Extenders		Soft segments		Property	
ArDI	Aromatic diisocyanate	DA	Diamine	PED	Polyether diol	γ_w	Water contact angle
AlDI	Aliphatic Aromatic diisocyanate	EDA	Ethylene Diamine	PTMEG	Polytetrameth Ether Glyc	T_g	Glass transition temperature
MDI	Methyl Diphenyl Isocyanate	POADA	Polyoxyalkylene DA	PEO	Polyoxyethylene oxide	T_m	Melt temperature of hard segment
HMDI	Hydrogenated MDI	DO	Diol	POPG	Polyoxypropylene oxide	M_w	Number average molecular mass
CHDI	1,4-Cyclohexane diisocyanate	BDO	Butane diol	PO	Polyol	M_n	Weight average molecular mass
IPDI	Isopherone diisocyanate	DEG	Diethylene diol	PesD	Polyester polyol	σ_b	Stress at break
TDI	Toluene diisocyanate	DAC	Diaminocyclohexane	PBD	Polybutadiene glycol	E_Y	Young's modulus
TODI	Methylene bis (toluene diisocyanate)	HMOD	Hydroxymethyl octadecanol	PHECD	Poly(1,6-hyxyl 1,2-ethyl carbonate) diol	ε_b	Elongation at break
		HDO	Hexane diol	PDMS	Poly(dimethyl siloxane)	E_{100}	Modulus at 100% extension
				PCDO	Polycarbonate diol	ρ	Density

Stellenbosch University http://scholar.sun.ac.za

3.4.3.3 Structure of polyurethanes

The properties of segmented polyurethanes depend not only on their chemical nature and constitutive elements, but also on the manner in which these hard and soft segments are arranged in the bulk of the material, and on the nature of the interaction between these phases. It is now generally agreed that the hard segments form glassy or semicrystalline domains dispersed in an amorphous or semicrystalline soft segment matrix, and that the hard domains act as reversible physical crosslinking sites and reinforcing fillers. It is for this reason that segmented PUs exhibit high moduli and elastic behaviour normally associated with covalently crosslinked polymers.

In general, hard segments are responsible for tensile strength, hardness, permanent elongation and compression set associated with the polymer, while soft segments determine the elastic expansion and glass transition temperature (T_g).

3.4.3.4 Effect of diisocyanate on properties

Polyurethanes that contain aromatic diisocyanates in their hard segments generally have superior mechanical properties to PUs derived from their aliphatic counterparts. MDI, an example of an aromatic diisocyanate, has a rigid planar structure that provides stiffness, strength and hard-segment character to polyurethanes. HMDI (the fully hydrogenated version of MDI), on the other hand, provides for weaker hard-segment aggregation and yield weaker polyurethanes with poorer dynamic performance such as shorter flex life, larger stress hysteresis, and lower impact and abrasion resistance [21]. Polyurethanes based on aliphatic isocyanates also tend to possess poorer high-temperature properties and lower solvent resistance. The symmetry of the diisocyanate is also an important determinant of physical properties. Increased symmetry favours the crystallisation and degree of phase segregation, which in turn results in increased modulus, hardness, and abrasion resistance [25].

The major advantage of the use of aliphatic diisocyanates is the increase in chemical stability imparted to the polymer. Aromatic isocyanate-based PUs tend to turn yellow with even mild exposure to UV radiation (e.g. due to diquinone-imide formation), while aliphatic polyurethanes are non-yellowing. Aliphatic urethanes are more stable when subjected to alkaline hydrolysis [40] and have shown to have greater thermal stability than aromatic analogues [41]. Certain harsh treatments, such as steam sterilisation can also liberate amines by hydrolysis of urethane and urea groups [42]. The aromatic amines originating from MDI are suspected carcinogens, while those of its aliphatic analogues (HMDI) have not been implicated in a carcinogenic response.

3.4.3.5 Effect of polymeric diol on properties

The polymeric diol, which constitutes the soft segment, is responsible for the flex life and the ultimate elongation of the material. As the molecular weight of the macroglycol increases (with equivalent proportions of other reagents) the elongation and resilience increases, while the hardness, modulus and tensile strength will be lower [21]. Increased macroglycol length also decreases the T_g of the polyurethane. Increased phase separation leads to increased backbone rotation and a decrease in the T_g to levels closer to those of the macroglycol itself. When the polymers are formulated with equal hard-segment weight ratios, however, increased hard-segment length will improve phase separation and thus increase the modulus.

The chemical stability of polyurethanes is closely linked to the chemical nature of the macroglycol that constitutes its soft segment. Early polyurethane implants failed due to degradation of the hydrolytically unstable polyester macroglycols used in their synthesis. Replacement of the polyester-based soft segments with those based on polyethers provided the required in vivo hydrolytic stability while retaining most of the desired mechanical properties [18]. Subsequent studies have shown, however, that, although hydrolytically stable, certain

Stellenbosch University http://scholar.sun.ac.za

polyether urethanes are susceptible to oxidative degradation in the presence of metal ions and other strong oxidants [20]. This realisation has spurred extensive research into alternative formulations, that continues to this day. Although polyether urethanes are still available and useful in certain applications, the trend toward the full or partial replacement of the polyether functionalities with those consisting of polymeric carbonates [30-32, 34, 37], siloxanes [29, 33, 35, 39], hydrocarbons [36], and fluorinated ethers [43, 44] continues. The use of polycarbonate soft segments has been reported to increase chemical stability (especially ESCR) when compared to PUs containing polyethers [28, 45, 46], but possibly at the risk of decreased hydrolytic stability. Siloxane soft segments increase the oxidative stability of urethanes without an accompanying decrease in hydrolytic stability [39]. These polymers do tend, however, to have lower tear strengths than their polyether soft-segment counterparts. Medtronic Inc. eliminated the use of polyester, polyether and polycarbonates by basing an experimental urethane of hydrocarbon soft segments. Takahara et al. [36] compared the in vitro oxidative resistance of this polymer ("Biostable PUR" = M48) to a number of urethanes containing PEO, PTMEG, PBT, HPBT and PDMS soft segments (all with the same MDI-BDO based hard segment).

Their findings include:

- "Biostable PUR" and PUs containing PBT and HPBT showed minimal oxidative degradation
- PDMS-based PUs also showed high oxidative resistance, but degraded rapidly under oxidative conditions in the presence of an organic carboxylic acid salt
- PEO and PTMEG-based PUs showed degradation in oxidative environments, and that it was the ether linkages that were oxidized.

The mechanism of oxidative degradation of polyetherurethanes was further elucidated by Schubert et al. [47] and Stokes et al. [17]

3.4.3.6 Effect of extender on properties

Both the chemical nature and proportion of chain extender used in the formulation of a segmented polyurethane influences its chemical and physical properties. Generally, the use of aliphatic extenders leads to polymers that are softer than those obtained with aromatic extenders. The use of diamines instead of diols yields polymers with more polar urea functionalities that increases phase separation and hydrogen bonding between hard segments, thus resulting in improved physical properties. The nucleophilic character of diamines also provide for a more rapid reaction with the diisocyanate, and catalysts are not needed for this reaction. The strong hydrogen bonding associated with urea linkages, however, decreases solubility and melt-processability, and a very high urea content may render the polymer unsuitable for melt processing in its dry form without the risk of thermal decomposition [21].

3.4.3.7 Summary: Graft-related demands

In order for a vascular graft to withstand the chemical and physical requirements placed on it when implanted into the hostile environment encountered in the body, and in order to achieve the compliant properties believed to be essential in vascular graft design, the following required material properties are proposed:

A) Manufacturability: The material(s) should be

- readily processed into **uniform, high quality** devices of the desired size and structure in an **economically feasible** manner without excessive negative environmental impact.
- readily **sterilizable** by conventional means without negative impact on its integrity and other properties

Stellenbosch University http://scholar.sun.ac.za

B) Biostability: The material(s) should not be excessively

- **toxic, inflammatory, or thrombogenic**, either in itself, or by the release of toxic, inflammatory or thrombogenic additives or degradation products
- **succeptable toward oxidative and hydrolytic attack**, and not prone to environmental stress cracking or excessive calcification

C) Mechanical properties: The material(s) should:

- display good **handling characteristics** and **suturability**
- be **amenable to trimming** without adversely affecting mechanical properties
- be **elastomeric**

In order for these requirements to be filled by polyurethanes, the PU should preferably contain:

- **aromatic hard segments** for good microphase separation and thus improved dynamic performance
- **hydrocarbon** or **siloxane**-based soft segments for oxidative and stress cracking resistance.

3.4.4 Porosity

3.4.4.1 The need for porosity

Porosity has long been known to be a determining factor in the fate of prosthetic vascular grafts. Initial attempts to replace arteries with solid tubes of synthetic material were unsuccessful due to thrombotic occlusion [48-52]. Wesolowski affirmed the importance of porosity when he screened a variety of materials and showed that synthetic polymers — successful as porous prostheses — were not successful as solid-wall prostheses [6]. Subsequent efforts by prosthetic vascular graft pioneers to achieve complete graft healing through porosity were unsuccessful [53-55].

The complete surface healing of arterial prostheses became possible with the advent of highly porous ePTFE grafts, and then only in a juvenile animal model. Clowes et al. showed that higher porosities may allow for surface endothelialization [56, 57]. However, if the intent of tissue engineering of prosthetic vascular grafts is to emulate functional arteries, the narrow focus on endothelial cells will need to be broadened to a more comprehensive concept in which the other constitutive elements of natural arteries are also encouraged to populate the pores.

Researchers were long puzzled why interstitial graft spaces of particular prostheses were sufficient to allow macrophages and other inflammatory cells to migrate in, whereas connective tissue cells of similar dimensions were often conspicuously absent [58-61]. Today it is understood that certain of these connective tissue cells like smooth muscle cells, mainly follow the ingrowing endothelial cells [62, 63]. Therefore, one important determining dimension for complete graft healing is that which mechanically allows capillaries to sprout into the meshwork of a synthetic graft and still leave some space for accompanying cells. Thus, although the average diameter of a capillary is 8-10μm, the diameter of a functional arteriole, i.e. an endothelium, and at least one layer of smooth muscle cells is approximately 30μm [2, 64-66].

3.4.4.2 Porosity measurement

The attempt to determine porosity requirements for graft healing is complicated by material-specific characteristics and structural uniqueness. The complex three-dimensional structure of contemporary grafts results in a wide range of voids between the synthetic surfaces, which makes precise definition of ingrowth spaces difficult (See Figure 3.4). Dacron manufacturers

Stellenbosch University http://scholar.sun.ac.za

circumvented this problem by defining water permeability in lieu of porosity. Grafts were then distinguished not only on the basis of being knitted and woven, but further characterised as being of high porosity (1500 to 4000 ml.cm^{-2}.min^{-1}) or low porosity (200-1000 ml.cm^{-2}.min^{-1}) [67].

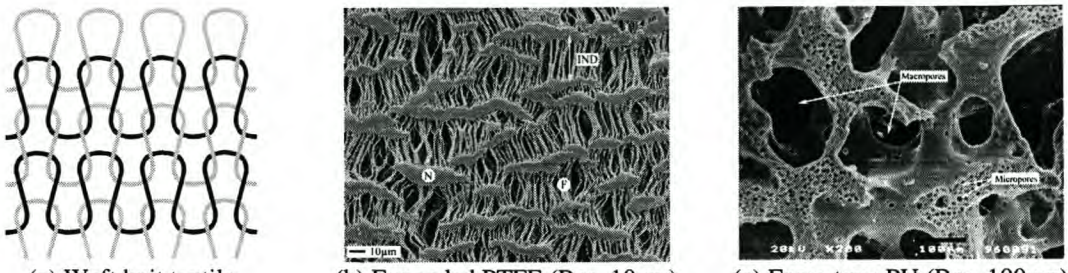

(a) Weft knit textile (b) Expanded PTFE (Bar=10μm) (c) Foam type PU (Bar=100μm)

Figure 3.4: Typical pore structures of three commonly encountered vascular prostheses. (a) a schematic representation of a weft knit textile, (b) scanning electron micrograph of a typical low porosity ePTFE prosthesis, and (c) scanning electron micrograph of a foam-type PU prosthesis

The porosity of ePTFE grafts is generally characterized by average distances between the centres of adjacent nodes of the expanded material, the so-called internodular distance (IND). For most commercially available ePTFE grafts this value is typically in the order of 30μm, although larger sizes have been produced. The IND distance is often a misleading dimension, as the actual spaces available for tissue ingrowth, namely the inter-fibrillar distance, is typically in the 4-5μm size range [68]. The morphology of foam-type porous scaffolds used in experimental polyurethane grafts is potentially more definable in terms of actual pore size. This would be true for foams in which the pores and inter-pore windows are clearly discernable. However, the use of salts and other irregularly shaped porogens, together with the premixing methods used during graft production, generally result in irregularly shaped pores and limited pore interconnectivity [69]. Thus the porosities of these graft type are also generally expressed either in terms of water permeability or, indirectly by stating the average size of the porogens used in their production.

Although these values serve as useful parameters in characterising the materials, they are not helpful with regards to healing. The poorly defined space dimensions made it impossible to come to a conclusive answer concerning the role porosity plays in the mitigation of tissue ingrowth into prosthetic vascular grafts. If one attempts to gain a better understanding of the relationship between porosity and healing one needs to make a clear distinction between porosity and permeability in order to avoid a confusion of terminology. It is important to understand that these terms are not synonymous, because a highly porous material may have a low permeability and vice versa.

The water permeability of a graft is defined as the volumetric flow-rate of water through a unit area of graft wall in a unit time at a predefined pressure; it is usually measured at 120mmHg and expressed in ml.cm^{-2}.min^{-1} [70]. Porosity, on the other hand, is traditionally described as the void volume of the structure as a percentage of the total graft volume. It is generally expressed as a percentage, and may be determined by planimetric, gravimetric or volumetric methods [70].

A third, and arguably best, way of describing the porous nature of a vascular prosthesis involves the actual measurement of openings available for tissue ingrowth. Unfortunately, hardly any information is available regarding the dimensions of porous structures in commercial vascular grafts. In order to get a better insight into this critical parameter for tissue incorporation, the interstitial space dimensions in a few typical contemporary grafts have been evaluated, both before and after implantation [68].

Stellenbosch University http://scholar.sun.ac.za

3.4.4.3 Further requirements

Although the voids within a material will allow water to flow through them, numerous pores may well be dead-ends that fail to provide an open corridor from the ablumenal to the lumenal surface. Moreover, vascular prostheses are not designed to be rigid structures. They are compressible for ease of handling and can be readily deformed by radial and longitudinal tensions as well as by internal pressures, even in the relatively non-compliant contemporary grafts. Such stresses not only change the dimensions of the prostheses, but also lead to a redistribution of the yarns and fibres within the material. Naturally, the change in textile structure by both circulatory stress and compression by ingrowing tissue itself affects the distribution, size and tortuosity of the channels that run from one side of the graft to the other. Since the limiting factor for tissue ingrowth is the bottle-neck of the narrowest part of a transmural space, it is further important to look at interstitial spaces throughout their three - dimensional course. Thus it is not only the pore dimensions that are important, but also the arrangement of the pores in the three-dimensional structure. This is especially true when not only radial ingrowth of capillaries and accompanying tissue is required, but also the circumferential arrangement of connective tissue is thought to be of importance (for the mimicking of a natural vessel structure).

3.4.4.4 Summary: Porosity

Although porosity is generally agreed to be a crucial factor in the design of vascular prostheses, the exact nature and dimensions of the porosity required for proper healing is neither clearly understood nor have they been clearly defined or measured.

It may be deduced, however, that the minimum porosity requirements for a tissue-engineered graft that would heal in a way that mimics the natural artery are:

- **Continuous ingrowth spaces** from the ablumenal to the lumenal surface.
- **Pore "channels"** that are at least as large as the **size of an arteriole**, and possibly appreciably larger, to accommodate for the narrowing effect of the three-dimensional structure.
- A porosity that allows for not only the **radial ingrowth of capillaries**, but also for the **ingrowth and circumferential orientation of smooth muscle cells and connective tissue**.

3.4.5 Compliance

3.4.5.1 Definitions

Both the complex function and the structure of blood vessels require unique mechanical properties. One parameter used to describe the mechanical properties, namely the compliance, is a measure of the expansion and contraction a vascular graft undergoes as a result of the pressure and flow changes occurring between diastole and systole. The diameter compliance (C_D) is defined in eq. (3.1), where D and P are the internal diameter and pressure, and subscripts *s* and *d* denote systole and diastole, respectively [27]. It is usually expressed as %/100mmHg.

$$C_D = \frac{(D_s - D_d)}{(P_s - P_d) \times D_d} \tag{3.1}$$

The compliance of a tube is indirectly proportional to the modulus of the material constituting the tube wall, and is related to it by eq. (3.2), where r is the inner radius of the tube, t is the wall thickness, and E_w is the circumferential tensile modulus of the wall.

Stellenbosch University http://scholar.sun.ac.za

$$C_D = \frac{r}{t}\frac{1}{E_w} \tag{3.2}$$

For isotropic solid-walled tubes, the wall tensile modulus (E_w) equals the tensile modulus of the material (E_m). In porous walls, the constitutive elements defining the wall (e.g. fibres) fill only a fraction of the wall volume. Additionally, these elements are not completely aligned in the circumferential direction, and the deformation is not purely tensile. In such cases the modulus of the vessel also depends on the frictional forces involved in the relative movement between individual elements, as well as the flexural and shear moduli of the elements themselves. It is for this reason that prostheses constructed from very stiff materials such as PET fibres may exhibit only some, but not adequate, compliance. A mismatch in the compliance of the synthetic graft and the host vessel has been implicated in the inability of conventional grafts to have long-term patencies, especially in small-diameter prostheses. This phenomenon is illustrated by a significant correlation between compliance and patency [27, 71, 72]. Increased impedance and decreased capacitance, causing disturbed flow patterns, have been cited as causes for intimal hyperplasia that results in the failure of under-compliant grafts.

Compliance measurement has also been based on the change in volume of a test specimen instead of its internal diameter. Thus, the volumetric compliance is defined as C_v, with V_s and V_d the systolic and diastolic internal volumes of the vessel, respectively (See Appendix 1):

$$C_V = \frac{(V_s - V_d)}{(P_s - P_d)\times V_d} \approx 2C_D \tag{3.3}$$

Since blood vessels have non-linear elastic properties (they stiffen with increasing pressure), the compliance decreases with increasing pressure. Most compliance values quoted in the literature have been determined in the physiological pressure range of P_s=120 mmHg and P_d = 80 mmHg.

Blood vessels are also viscoelastic, and compliance values depend on the strain rate applied during compliance testing. It is therefore also important to distinguish between static and dynamic testing. During static testing, the pressure is incrementally increased and the corresponding diameter (or volume, as the case may be) measured while the pressure remains constant. Dynamic testing involves the real-time acquisition of diameter (or volumetric) data under pulsatile internal pressure. Due to the viscoelastic nature of the vascular tissue, there is a phase shift between the pressure and diameter (volume) change, and dynamic compliance values are generally lower than those obtained by the static method. In this dissertation, the subscripts *dyn* and *stat* will be used to infer dynamic and static compliance, respectively, while the pressure range at which the compliance was determined will be indicated by a superscript P_d-P_s. Thus, a dynamic volumetric compliance determined between 80 and 120mmHg may be indicated with the symbol C_{Vdyn}^{80-120}.

The distensibility of a vessel under internal pressure may also be described by a stiffness parameter, β, defined in [73-76]:

$$\beta = \frac{D_d \ln(P_s - P_d)}{D_s - D_d} \tag{3.4}$$

The stiffness parameter is an attempt to linearise the non-linear response observed with natural arteries (and elastomeric vascular prostheses), and is thus independent of pressure.

3.4.5.2 Compliance measurement

The foregoing definitions of the various parameters used to describe the pulsatile behaviour of arteries have in common that they are all based on the accurate measurement of vessel size (diameter or volume) and the internal pressure at both diastolic and systolic pressure without

Stellenbosch University http://scholar.sun.ac.za

undue influence on these parameters due to the measuring technique. Both in vivo and in vitro techniques have been developed.

(i) In vivo assessment

Standard pressure transducers, available in surgical theatres, are commonly used for measuring pressure profiles. As catheterisation may influence the pressure profile, these probes are typically inserted proximal or distal to the test section (where diameter measurement is performed), and it may be argued that the difference in pressure between the test section and measuring point may introduce errors. In order to minimise the error, an average of proximal and distal reading may be used. Alternatively, more specialised microtransducers, inserted to the exact point of diameter measurement, are advocated. Diameter measurements may be obtained by invasive techniques involving the use of strain gauges but, ideally, non-invasive techniques (Doppler, ultrasound) are preferred [77].

(ii) In vitro assessment

Whereas the pressure pulse in the in vivo assessment of compliance is provided by the host, the in vitro measurement of compliance provides the additional challenge of mimicking the pressure and flow patterns (as encountered in vivo) by artificial means. The demands and limitations on pressure measurement are similar to those encountered in the in vivo case, whereas the measurement of diameter (or volume) lends itself to more varied approaches due to the accessibility of the test section. Cantilevered strain gauges, video monitoring, and non-contact laser micrometry are examples of methods that may be employed [77].

3.4.5.3 Compliance of human arteries

As the structure and function of blood vessels change along the vascular tree, so do their mechanical properties. Table 3.4 shows compliance and stiffness parameter data for human blood vessels.

It is also important to note that, in addition to variation of compliance between healthy individuals within the same age group, the compliance is also a function of age, and may be further influenced by disease (notably atherosclerosis, hypertension, diabetes). The effect of the age of the patient is clearly demonstrated by Kawasaki et al. [73], who showed significant stiffening of arteries with increased age. They were able to derive a linear function to predict the stiffness parameter, β, as a function of age. Thus, for the human femoral artery: $\beta = 106x + 7.6$, where x is the age of the patient (fit: r=0.58). The extent and significance of an age-related increase in arterial stiffness can further be seen from the actual average stiffness values listed in Table 3.5.

Stellenbosch University http://scholar.sun.ac.za

Table 3.4: Compliance and stiffness parameters for typical blood vessels in humans. (CD in %/100mmHg; β: dimensionless)

Blood Vessel	Stiffness parameter,β	Compliance C_D (%/100mmHg)	Determination method	Patient age (years)	Reference
CCA	5.9	-	in vivo, ultrasound	29	[73]
CCA	3.2	-	in vivo, ultrasound	28	[78]
CFA	10.6	-	in vivo, ultrasound	29	[73]
CFA	10.5	-	in vivo, ultrasound	28	[79]
AA	4.3 - 9.8	-	in vivo, ultrasound	<19 - >60 yrs	[73]
BA	8.6 – 13.7	-	in vivo, ultrasound	<19 - >60 yrs	[73]
CCA	19.84	-	-	-	[80]
CFA	5.25	-	-	-	[80]
CCA	~5	-	-	-	[81]
FA	~20	-	-	-	[81]
CoA	~39	-	-	-	[81]
CCA	-	6.6	ultrasound	-	[82]
SFA	-	1.8	ultrasound	-	[82]
FA	-	5.9	-	-	[77]
SV	-	4.4	-	-	[77]
MA	-	8.0	in vitro, ultrasound	-	[74]
SV	-	5.0	in vitro, ultrasound	-	[74]
CFA	-	14.1	in vivo, ultrasound	-	[83]
DSFA	-	2.2	in vivo, ultrasound	-	[83]
MPA	-	4.7	in vivo, ultrasound	-	[83]
CCA	-	5.18	in vitro, TV camera	-	[76]
FA	-	19.8	-	-	[76]

CCA: Common Carotid Artery
CFA: Common Femoral Artery
SFA: Superficial femoral Artery
FA: Femoral Artery
DSFA: Distal Superficial Femoral Artery
MPA: Midgenicular Poplitial Artery
MA: Muscular Artery
CoA: Carotid Artery
BA: Brachial Artery
AA: Abdominal Aorta
SV: Saphenous Vein

Table 3.5: Influence of age on the stiffness of human femoral arteries [73]

Age (years)	Stiffness parameter (β)	Significance (β)	*Compliance
1-19	9.41±2.71	(a); (b)	14.4
20-39	10.6±3.32		11.6
40-59	12.63±3.77	(a)	9.2
>60	15.31±4.52	(b)	7.3
* Calculated from average data		(a)$p<0.01$ (b) $p<0.001$	

The effect of disease and drugs on the compliance has also been investigated. Smilde et al. showed a significant improvement in CFA compliance with a lowering of cholesterol levels in hypercholesterolemic patients with statins [84]. Similarly, the compliance of arteries could be increased by administration of converting enzyme inhibitors and calcium entry blockers [85]. Estrogen and antiandrogens significantly reduced both FA and BA compliance in men. Testosterone had no observed effect on the compliance of these arteries in women, but an inverse correlation between fasting insulin levels and compliance was observed in this test group [86]. Surprisingly, Giltay et al. also found a positive correlation between arterial compliance and fat mass variables [87]. Other factors that negatively affect arterial compliance include smoking, hyperhomocysteinemia and hypertension [88].

3.4.5.4 Sub Summary: Compliance

The following factors are important in compliance measurement and matching:

- **Compliance matching** of graft with host vessel is an **important determinant in the patency** of the prosthesis
- Various parameters have been defined to describe the compliant characteristics of grafts

Stellenbosch University http://scholar.sun.ac.za

- The **dynamic compliance or stiffness parameter** is the **most accurate measure** as its definition accounts for the dynamic pulsatile pressure encountered in vivo
- Artery compliance is **affected by age, disease and drugs**, and these factors should be taken into account when matching is undertaken
- In order to match the **compliance of peripheral arteries** (e.g. femoral arteries), a dynamic diameter-compliance of the prosthesis should be approximately **10%/100mmHg** (the average values for femoral arteries are shown in Table 3.5)

3.5 Host-related demands

3.5.1 Biocompatibility

3.5.1.1 Introduction

Complete inertness, a property that has been shown to be unattainable with current materials, may actually be an undesirable property as it may cause incomplete functional incorporation and healing of the device due to limited interaction with the living tissue. It is for this reason that biomaterials are now being rendered "bioactive" by a variety of surface and bulk modification techniques in order to promote constructive interaction between the implant and the host tissue.

3.5.1.2 Tissue/Polymer interaction

The nature of the reaction elicited by the implantation of a vascular graft determines not only the short-term fate of the implant, but also its long term stability and function. The sequence of events that follow implantation is summarized in Fig. 3.5, and briefly described below [89, 90]:

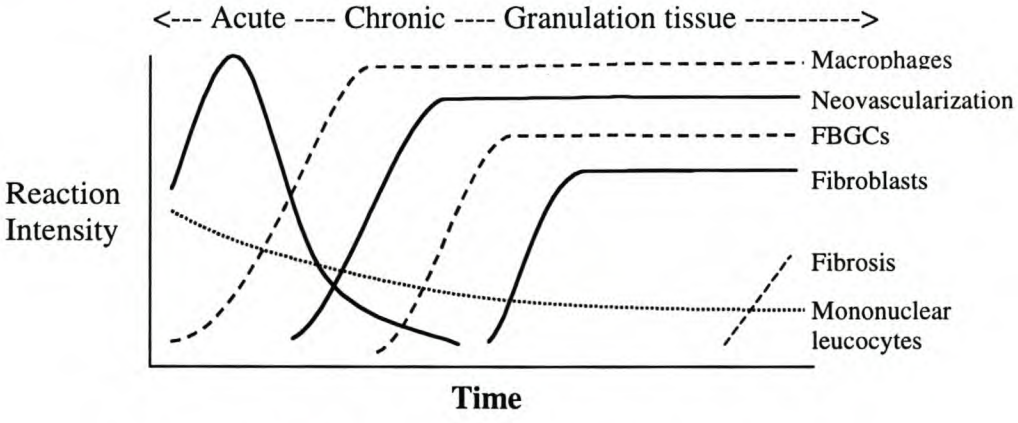

Figure 3.5: Chronology of events after implantation (Adapted from [90])

- **Injury**, causing the release of fluid, proteins and blood cells into the injured area. Blood proteins adsorb to the lumenal, peri-adventitial and interstitial spaces of the implanted device, and facilitate the adhesion of infiltrating cells.
- **Acute inflammation**, a relatively short phenomenon (minutes to days), characterized by the exudation of fluids and proteins, and the immigration and adhesion of leucocytes (predominantly neutrophils).
- **Chronic inflammation**, characterized by the presence of monocytes, macrophages and lymphocytes with the proliferation of blood vessels and connective tissue. The chronic inflammatory response may be influenced by the physical and chemical properties of the implant, and also by motion in the implant site.

Stellenbosch University http://scholar.sun.ac.za

- The formation of **granulation tissue**, characterized by the proliferation of fibroblasts and vascular endothelial cells. Fibroblasts also synthesise collagen and proteoglycans in the developing granulation tissue.
- **Foreign body reaction**, characterized by the formation of foreign body giant cells (FBGC). FBGCs are multinucleated cells derived from the coalescence of activated macrophages.
- **Fibrosis and fibrous encapsulation.** Repair of implant sites can involve two distinct processes:
  - regeneration, the replacement of injured tissue by cells of the same type, or
  - replacement by connective tissue that constitutes the fibrous capsule. This is generally the end-stage healing response towards implanted biomaterials.

3.5.1.3 Surface modification

Surface modification is a useful tool that allows for the alteration or masking of the chemical nature of the implant that is exposed to the surrounding tissue, as it may be used to alter this property without undue influence on physical properties that may have been optimised for the intended application. The wide variety of surface modification techniques employed includes overcoating, deposition of surface gradients, self-assembly, addition of surface-active bulk additives, surface roughening and chemical reaction [91]. Chemical modification with synthetic reagents (monomeric or polymeric) rely on the alteration of functional surface-groups and hence physico-chemical properties such as hydrophilicity, charge etc.) to alter the in vivo response. Modification agents also include materials of biological origin that may render the material bioactive, i.e. actively interact with the host tissue by mimicking naturally occurring materials. Other approaches rely on the immobilization of oligopeptide sequences (identified as being the active binding sites in proteins) to obtain the desired effect.

The surfaces of biomaterials may be modified for a number of reasons, all intended to improve the biocompatibility of the material. The reasons include: to decrease the adhesion of proteins and/or inflammatory cells, to decrease the thrombogenicity of the material, and to increase the adhesion, proliferation or migration of desired cell types on or in the material.

Leucocyte and macrophage adhesion (and differentiation of macrophages into FBGCs) play a pivotal role in the inflammatory response. The adhesion of these cell types has been shown to depend on several factors that include surface chemistry, hydrophilicity and protein adsorption [92]. Smetna et al. [93] demonstrated how the incorporation of $-SO_3H$ and –COOH groups could inhibit both the spreading of macrophages and the formation of FBGCs, while Bruil showed an increase in leukocyte adhesion to PU surfaces modified with amino and carboxyl groups [94]. Yun et al. modified FEP surfaces by grafting neutral (polyacrylamide, PAam), partially anionic (acrylic acid/acrylamide copolymer, PAam-co-PAac), anionic (acrylic acid, PAac) and cationic (polyetheleneimine, PEI) hydrogels. They found optimal (minimum) adhesion of human macrophages on neutral or partially anionic surfaces [92].

Polyethylene glycols are shown to be a very versatile polymer in surface modification applications. Not only have they been shown to decrease protein and macrophage adhesion [95-97] and bacterial adhesion [98], but also to be effective antithrombotic agents [99-101]. This antithrombotic effect was attributed to a thermodynamic restriction effect and high mobility of the immobilized PEG chains (effectivity increased with chain length).

Thrombotic events have also been decreased by the immobilization of a number of active anti-thrombogenic agents. These include acetyl salicylic acid (ASA or aspirin) [102], hirudin [103, 104], dipyridamole [105-107], lumbrokinase [108, 109] and heparin [110-118]. The immobilization of heparin will be discussed in more detail in Chapter 8.

Stellenbosch University http://scholar.sun.ac.za

The improved incorporation of synthetic devices may be facilitated by the immobilization of extracellular matrix materials such as collagen [119-124]. Collagen and other extracellular matrix materials contain distinct peptide sequences that have been identified as the adhesion sites for certain cells. These include the well-known RGD sequence, as well as the YIGSR and IKVAV sequences. These oligopeptides (with flanking sequences) have all been covalently immobilized on biomaterials with the aim of improving tissue interaction [125-131]

3.5.1.4 Summary: Biocompatibility and surface modification

The following are important factors relating to the biocompatibility of materials:

- **The minimization of the inflammatory response,** by:
  - decreasing the leukocyte adhesion,
  - decreasing the macrophage adhesion and proliferation, and
  - decreasing the differentiation of macrophages into FBGCs
- Mimicking the extracellular conditions by presenting a **naturally occurring macromolecule** (or active part thereof) to the host.

These objectives may be met to some extent by **surface modification** techniques, by keeping the following principles in mind:

- **polymeric hydrogels** are effective in that they not only change the surface chemistry, but also provide a hydrophilic barrier
- protein, leukocyte and macrophage adhesion may be decreased by the use of **neutral to anionic surfaces**.
- tissue incorporation may be improved by the immobilization of **collagen** or specific **oligopeptide sequences** responsible for adhesion.

3.5.2 Healing

In order to understand the in vivo response to vascular grafts, it is important to distinguish between the different modes of healing. Tissue originating from the native vessel may grow across the anastomosis, either on the graft surface or into the porous structure. This mode of healing is termed *transanastomotic healing*. The tissue surrounding the graft is a second source of tissue. In order for this tissue to form part of the implant, a second mode of healing, namely *transmural healing*, is required. In the past, very little distinction was made between these modes of healing, and healing patterns were described without specific reference to the source of the tissue. Due to the differences in healing responses observed in different animal models, it will be shown that knowledge of the tissue source is of critical importance. A graft that may show complete surface healing (and even complete surface endothelialization) in one model due to transanastomotic effects, will not necessarily show the same favourable response in the clinical applications.

3.5.2.1 Transanastomotic healing

Shortly after implantation of a vascular graft, smooth muscle (and other) cells in the media of the native artery start to proliferate and migrate through the damaged internal elastic lamina into the intima [132]. This hyperplastic tissue subsequently migrates and proliferates onto the graft (from each anastomosis), toward the midgraft area, forming a "tongue" of tissue generally referred to as the *pannus*. (See Figure 3.6) Even before the proliferation of the pannus, smooth muscle cells (SMC) start migrating onto the graft [133-135]. Thus the leading endothelium (EC) grows on the exposed (or fibrin covered) graft even before the layer of smooth muscle cells grow in underneath it [136-139]. This layer, consisting of smooth muscle cells, fibroblasts, collagen and macrophages [56, 140-142], gradually thickens with time. The subendothelial layer lacks,

Stellenbosch University http://scholar.sun.ac.za

however, the features of a native artery (e.g. elastic fibres between the SMCs and an internal elastic lamina [143, 144].

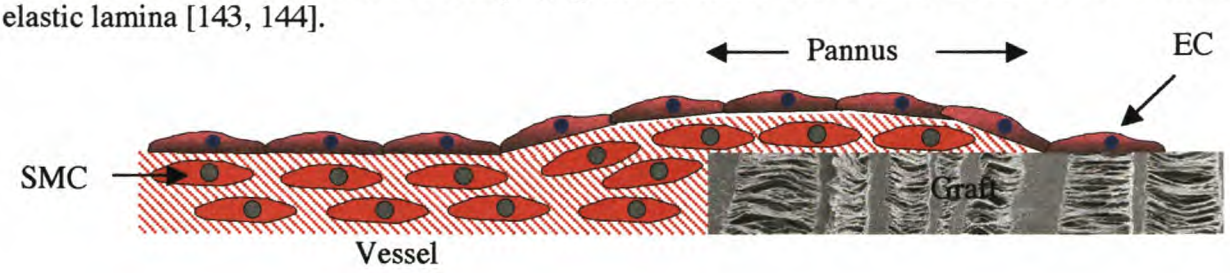

Figure 3.6: Transanastomotic healing showing the migration of endothelial cells and the pannus tissue onto the graft surface.

A number of factors influence the thickness on synthetic grafts. These include the anatomical position [145, 146], variations in flow conditions [147, 148], shear stress [148] and also whether the anastomosis in question is the proximal or distal anastomosis [146, 149, 150].

Three major factors influence the extent of pannus growth. The first two, namely the porosity of the graft and the presence of tissue under the inner fibrinous capsule, may be closely interrelated. Although the fibrin layer on woven and knitted Dacron grafts are of equal thickness [51, 53, 60, 140, 141, 151-153], the presence of an almost continuous layer of tissue under the fibrin layer in knitted grafts results in faster outgrowth [53, 60, 142, 145, 154, 155] than is that observed with woven prostheses [156] (that contain minimal tissue in this location). Faster outgrowth also occurs with high porosity ePTFE grafts that have been externally wrapped with tissue. This may be due to the facilitated transmural ingrowth that provides the sub-fibrin tissue layer that in turn allows for increased transanastomotic outgrowth [134].

The third factor affecting transanastomotic outgrowth is the animal model. Although the proliferative capacity of human endothelial cells does not differ significantly between experimental animals [157], there is a marked difference in the extent of endothelialization observed in vivo between the human and experimental animal models. For reasons unknown, transanastomotic endothelialization stops after only a short distance from the anastomosis in humans [53, 158, 159].

In the dog (the most commonly used model), the transanastomotic endothelialization proceeds for approximately 2cm on ePTFE grafts [60, 160-165] and more than 3cm on Dacron grafts [53, 60, 145, 166-168]. Due to the limited length of grafts used in many studies, it is not possible to gauge the further progress of the endothelium on these grafts, as most of them were completely endothelialized after this time-point. Similar 3-month distances are observed with the second most common model, the yellow baboon (papio cynocephalus). [57, 135, 151, 169-171].

On standard porosity ePTFE (30μm), the coverage achieved in humans in 56 weeks occurs in dogs, the yellow baboon, and the chacma baboon in 3.5, 5.6 and 7.6 weeks respectively [60, 161, 162, 164, 165]. The difference between the baboon models may well be related to the fact that the yellow baboon is a juvenile model (10kg), while the chacma baboon with a body weight of up to 40kg is a senescent model.

Thus, the chacma baboon, in which transanastomotic outgrowth is 2.1 times slower than in the most commonly used model (the dog), seems to be the best choice for the evaluation of transanastomotic endothelialization of grafts intended for man.

3.5.2.2 Transmural healing

Peripheral vascular grafts used to alleviate lower extremity ischemia (femero-popliteal) may be up to 60 cm in length. This fact, combined with the very short distance the endothelium is able to migrate (in humans) onto the surfaces of such grafts by transanastomotic surface healing, indicates that future grafts intended for clinical use should rely more on transmural healing. If

Stellenbosch University http://scholar.sun.ac.za

full transmural healing could be achieved, it would not only lead to the formation of a viable endothelium, but would also result in the formation of viable tissue in the graft wall, and thus to the improved incorporation of the prosthetic material in the host. The mural tissue should consist, as previously indicated, not only of smooth muscle cells and accompanying extracellular matrix, but also of a fully developed vasa vasorum capable of sustaining the viability of the cells.

The ability of tissue to migrate through the graft wall is, again dependent on both the structure of the graft and the proliferative and migratory capacity of the cells of the host. The need for sufficient porosity to accommodate cellular ingrowth has been introduced in Section 3.4.4. The healing patterns observed with standard (30μm) and large (60μm) porosity ePTFE prostheses will be described in detail in Chapter 10; these historical results will be compared to results obtained by the author on very large porosity materials (150μm). It is useful, however, at this stage to give a few general observations on the effect of graft type and animal model on the transmural healing.

The full endothelialization of vascular grafts in the dog model due to transanastomotic healing has been shown, and although the researchers typically discussed the transmural ingrowth into the graft walls, this mode of lumenal surface healing has generally precluded investigation into the contribution of transmural ingrowth. Standard porosity ePTFE, due to its restricted ingrowth spaces, does not allow for significant transmural ingrowth, irrespective of the animal model used. It is interesting to note, however, that the differences regarding this type of healing between the two baboon models is even more pronounced than that observed with transanastomotic healing. In 60μm ePTFE, transmural ingrowth of capillary vessels leads to the surface endothelial in as little as two weeks in the yellow baboon, whereas the perigraft tissue does not even penetrate the outer two-thirds of these grafts in the chacma baboon [68].

The healing of Dacron grafts is also greatly affected by porosity. Low-porosity Dacron prostheses (woven) show perigraft incorporation similar to the standard (30μm) ePTFE during the initial period after implantation. Subsequently, some fibroblast and capillary infiltration into the narrow spaces between the Dacron yarns is observed [156, 172]. In dogs, this can occur after 2-3 weeks of implantation [156], whereas in humans this may be observed after 5 months [159] or absent even after 18 years [152, 158, 173]. Even if the tissue does manage to grow through the tight interfibrillar spaces, however, it is unable to penetrate the compact inner fibrin layer deposited on the graft surface [174]. In high-porosity Dacron (knitted), transmural tissue reaches the compact lumenal fibrin layer within 3-4 weeks in the calf [53], the yellow baboon [171] and the dog [60, 166] and 3-6 months in humans [53, 175]. The complete endothelialization of long prostheses, comparable to that one in highly porous ePTFE grafts, is occasionally seen in knitted prostheses. [154, 176]. In the yellow baboon, for instance, knitted Dacron grafts may form complete endothelial linings although not as readily and consistently as in 60μm ePTFE [57, 171, 177, 178]. However, in contrast to high-porosity ePTFE grafts it remains unclear whether this endothelium is derived from transmural tissue ingrowth, facilitated transanastomotic outgrowth or fall-out healing [179, 180]. The latter is a phenomenon predominantly observed in Dacron grafts where - apparently independent from transmural tissue ingrowth and with some delay - endothelial islands emerge on the surface of the compacted fibrin.

3.5.2.3 Summary: Healing

The following factors are important in the design of spontaneously healing synthetic grafts;

- Conventional **Dacron and ePTFE** vascular grafts **do not generally permit uninterrupted transmural ingrowth** of endothelial smooth muscle cells.
- Even when transmural ingrowth is achieved, ingrowing cells are blocked by an **impenetrable fibrin matrix** deposited on the lumenal surface.

Stellenbosch University http://scholar.sun.ac.za

- **Transanastomotic healing** in the **human** stops near to the anastomosis, and may not be relied upon to achieve endothelialization of the full length of the prosthesis.
- The **dog and yellow baboon** model is **not representative** of what could be expected in humans, as they allow for complete transanastomotic and a greater degree of transmural healing.
- The adult **chacma baboon** should be the **model of choice** for vascular graft evaluation.

3.6 References

1. Gray, H., in *Gray's anatomy*, P. Williams, Warwick, R., Dyson, M., and Bannister, L., Editors. 1989, Churchill Livingston: London. p. 685.
2. Frasher, W. *What is known about the physiology of larger blood vessels.* in *Biomechanics : Applied Mechanics Division of the ASME.* 1966. New York.
3. Liu, S., J . Biomed. Mater. Res, 1998. **120**.
4. Bezuidenhout, D. and Zilla, P., *Biomaterials in Vascular Surgery*, in *Encyclopedia of Materials: Science and Technology*, K. Boschow, Cahn, R., Flemmings, M., Ilscher, B., Kramer, E., and Mahakan, S., Editors. 2001, Elsevier.
5. Coury, A., *Biostable Polymers as Durable Scaffolds for Tissue Engineered Vascular Prostheses.*, in *Tissue engineering of vascular prosthetic grafts*, Z. P and HP, G., Editors. 1999, R.G. Landes: Texas. p. 469-480.
6. Wesolowski, S., *Foundations of modern vascular grafts*, in *Vascular Grafts*, P. Sawyer and Kaplitt, M., Editors. 1978, Appleton Century Croft: New York.
7. Fox, D., Vorp, D., and HP, G., *Bioresorbable Grafts: A Counterintuitive Approach*, in *Tissue engineering of vascular prosthetic grafts*, Z. P and HP, G., Editors. 1999, R.G. Landes: Texas. p. 489-503.
8. van der Lei, B. and Wildevuur, C., *Microporous, compliant, biodegradable small-calibre vascular grafts*, in *Current perspectives on implantabel devices*, G. Williams, Editor. 1990, Jai Press: London.
9. Williams, D., *Bioinertness: An outdated principle*, in *Tissue engineering of vascular prosthetic grafts*, Z. P and HP, G., Editors. 1999, R.G. Landes: Texas. p. 459-467.
10. Coury, A., *Preparation of specimens for blood compatibility testing.* Cardiovasc Pathol, 1993. **2(3) (Suppl)**: p. 1015-1105.
11. Coury, A., *Factors and interactions affecting the performance of polyurethane elastomers in medical devices.* J Biomater Appli, 1988. **3**: p. 130-179.
12. Coury, A., Levy, R., McMillin, C., Pathak, Y., Ratner, B., Schoen, F., Williams, D., and Williams, R., *Degradation of Materials in the Biological Environment*, in *Biomaterials Science: An Introduction to Materials in Medicine.*, B. Ratner, Hoffman, A., Schoen, F., and Lemons, J., Editors. 1996, Academic Press: San Diego. p. 243-281.
13. Zaikov, G., *Quantitative aspects of polymer degradation in the living body.* JMS-Rev Macromol Chem Phys, 1985. **C25(4)**: p. 551-597.
14. Labow, R.S., Erfle, D., and Santerre, J.P., *Neutrophil-mediated degradation of segmented polyurethanes.* Biomaterials, 1995. **16**: p. 51-59.
15. Santerre, J., Labow, R., Duguay, D., Erfle, D., and Adams, G., *Biodegradation evaluation of polyether and polyester-urethanes with oxidative and hydrolytic enzymes.* J Biomed Mater Res, 1994. **28**(10): p. 1187-99.
16. Coury, A., *Chemical and biochemical degradation of polymers*, in *Biomaterials Science*, B. Rattner, Hoffman, A., Schoen, F., and JE, L., Editors. 1996, Academic Press: San Diego. p. 243-260.
17. Stokes, K., Coury, A., and Urbanski, P., *Autooxidative degradation of implanted polyether polyurethane devices.* J Biomater Appl, 1987. **1**(4): p. 411-48.
18. Coury, A., Stokes, K., Cahalan, P., and Slaikeu, P., *Biostability considerations for implantable polyurethanes.* Life Support Syst, 1987. **5**(1): p. 25-39.
19. Santerre, J.P., Labow, R.S., and Adams, G.A., *Enzyme-biomaterial interactions: effect of biosystems on degradation of polyurethanes.* J Biomed Mater Res, 1993. **27**(1): p. 97-109.
20. Coury, A., Slaikeu, P., Cahalan, P., and Stokes, K., *Medical applications of implantable polyurethanes: current issues.* Progress in Rubber and Plastics tecnology, 1987. **3**(4): p. 24-37.
21. Coury, A., Slaikeu, P., Cahalan, P., Stokes, K., and Hobot, C., *Factors and interactions affecting the performance of polyurethane elastomers in medical devices.* J Biomater Appl, 1988. **3**(2): p. 130-79.
22. Sutherland, K., Mahoney, J.R., 2nd, Coury, A.J., and Eaton, J.W., *Degradation of biomaterials by phagocyte-derived oxidants.* J Clin Invest, 1993. **92**(5): p. 2360-7.
23. Pathak, Y., Schoen, F., and Levy, R., *Pathological calcification of biomaterials*, in *Biomaterials Science, an introduction to materials in medicine*, B. Rattner, Editor. 1996, Academic Press: San Diego.
24. Joshi, R., Frautschi, J., and Phillips, R. *Immobilized heparin and heparin-biphosphonateprevent polyurethane calcification and thrombosis.* in *5th world Biomaterials Conference.* 1996.

Stellenbosch University http://scholar.sun.ac.za

25. Lamba, N., Woodhouse, K., and Cooper, S., *Polyurethanes in Biomedical applications*. 1997, Boca Raton: CRC Press.
26. Zdrahala, R., *Small caliber vascular grafts. Part II: Polyurethanes revisited.* J Biomater Appl, 1996. **11**(1): p. 37-61.
27. Seifalian, A., Giudiceandrea, A., and Schmitz-Rixen, T., *Noncompliance: The silent acceptance of a villain*, in *Tissue engineering of vascular prosthetic grafts*, Z. P and HP, G., Editors. 1999, R.G. Landes: Texas.
28. Tanzi, M., Mantovani, D., Petrini, P., Guidoin, R., and Laroche, G., *Chemical stability of polyether urethanes versus polycarbonate urethanes.* J Biomed Mater Res, 1997. **36**(4): p. 550-9.
29. Martin, D., Warren, L., Gunatillake, P., McCarthy, S., Meijs, G., and Schindhelm, K., *Polydimethylsiloxane/polyether-mixed macrodiol-based polyurethane elastomers: biostability.* Biomaterials, 2000. **21**(10): p. 1021-9.
30. Zdrahala, R. and Zdrahala, I., *Biomedical applications of polyurethanes: a review of past promises, present realities, and a vibrant future.* J Biomater Appl, 1999. **14**(1): p. 67-90.
31. Yang, M., Zhang, Z., Hahn, C., Laroche, G., King, M., and Guidoin, R., *Totally implantable artificial hearts and left ventricular assist devices: selecting impermeable polycarbonate urethane to manufacture ventricles.* J Biomed Mater Res, 1999. **48**(1): p. 13-23.
32. www.thermedics.com, *Medical grade resins- A selection guide*. 2001, Thermedice Inc.
33. www.polymertech.com, *The polymer technology group*. 2001.
34. www.cardiotech-inc.com, *Polyurethane biomaterials from CT biomaterials*. 2001.
35. www.elastomedic.com, *Guide to Elast-Eon medical polymers*. 2001.
36. Takahara, A., Coury, A., Hergenrother, R., and Cooper, S., *Effect of soft segment chemistry on the biostability of segmented polyurethanes. I. In vitro oxidation.* J Biomed Mater Res, 1991. **25**(3): p. 341-56.
37. Reed, A., Potter, J., and Szycher, M., *A solution grade biostable polyurethane elastomer: ChronoFlex AR.* J Biomater Appl, 1994. **8**(3): p. 210-36.
38. Gilding, D., Reed, A., Askill, I., and Briana, S., *Mitrathane. A new polyether urethane urea for critical medical application.* Trans Am Soc Artif Intern Organs, 1984. **30**: p. 571-6.
39. Gunatillake, P., Meijs, G., MCCarty, S., and Adhikari, R., *Poly(dimethylsiloxane)/Poly(hexamethylene oxide) mixed macrodiol based polyurethane elastomers. 1. Synthesis and properties.* J Appl Polym Sci, 2000. **76**.
40. Matuzak, M., Frisch, K., and Reegen, S., *Hydrolysis of linear polyurethanes and model monocarbamates.* J. Pol. Sci., Pol. Chem. Ed., 1973. **11**: p. 1683-1690.
41. Fabris, H., *Thermal and oxidative stability of polyurethanes*, in *Advances in urethane science and technology*, K. Frisch and Reegen, S., Editors. 1976, Technomic: lancaster, PA.
42. Mazzu, A. and Smith, C., *Determination of extractable methylene dianiline in thermoplastic polyurethanes by HPLC.* J. Biomed. Mater. Res., 1984. **18**: p. 961-968.
43. delGuerra, R., Lelli, L., Tonelli, C., Trombetta, T., Cascone, M., Taveri, M., Narducci, P., and Giusti, P., *In vitro biocompatibility of fluorinated polyurethanes.* Journal of Materials Science: Materials in Medicine, 1994. **5**: p. 452-456.
44. Tonelli, C., Trombetta, T., Scicchitano, M., Simeone, G., and Ajroldi, G., *New fluorinated thermoplastic elastomers.* Journal of Aplied Polymer Science, 1996. **59**: p. 31-327.
45. Szycher, M., Reed, A., and Siciliano, A., *In vivo testing of a biostable polyurethane.* J Biomater Appl, 1991. **6**(2): p. 110-30.
46. Capone, C., *Biostability of a non-ether polyurethane.* J Biomater Appl, 1992. **7**(2): p. 108-29.
47. Schubert, M., Wiggins, M., Anderson, J., and Hiltner, A., *Role of oxygen in biodegradation of poly(etherurethane urea) elastomers.* J Biomed Mater Res, 1997. **34**(4): p. 519-30.
48. Carrel, A., *Permanent intubation of the thoracic aorta.* J Exp med, 1912. **16**(17): p. 17.
49. Tufier, M., *De l'intubation arterielle dans le plaies des grosses arteres.* Bull Acad Nat Med, 1915. **74**: p. 455.
50. Hufnagel, C., *The use of rigid and flexible prostheses for arterial replacement.* Surgery, 1955. **37**: p. 165.
51. Harrison, H., *Synthetic materials as vascular prostheses. Ia. A comparative study in small vessels of nylon, dacron, orlon, ivalon sponge and teflon.* Amer J Surg, 1958. **95**: p. 3-15.
52. Wesolowski, S., Fries, C., Karlson, K., Debakey, M., and Sawyer, P., *Porosity: Primary determinant of ultimate fate of synthetic vascular grafts.* Surgery, 1961. **50**: p. 91-96.
53. Sauvage, L., Berger, K., Wood, S., Nakagawa, Y., and Mansfield, P., *An external velour surface for porous arterial prostheses.* Surgery, 1971. **70**(6): p. 940-53.
54. DeBakey, M., Jordan, G.J., Beall, A., O'Neal, R., Abbott, J., and Halpert, B., *Basic biologic reactions to vascular grafts and prostheses.* Surg Clin North Am, 1965. **45**: p. 477.
55. DeBakey, M., Jordan, G.J., Abbott, J., Halbert, B., and O'Neal, R., *The fate of dacron vascular grafts.* Arch Surg, 1964. **89**: p. 757-82.

Stellenbosch University http://scholar.sun.ac.za

56. Clowes, A., Kirkman, T., and Clowes, M., *Mechanisms of arterial graft failure. II. Chronic endothelial and smooth muscle cell proliferation in healing polytetrafluoroethylene prostheses.* J Vasc Surg, 1986. **3**(6): p. 877-84.
57. Clowes, A., Zacharias, R., and Kirkman, T., *Early endothelial coverage of synthetic arterial grafts: porosity revisited.* Am J Surg, 1987. **153**(5): p. 501-4.
58. Bellon, J.M., Bujan, J., Contreras, L.A., Hernando, A., and Jurado, F., *Similarity in behavior of polytetrafluoroethylene (ePTFE) prostheses implanted into different interfaces.* J Biomed Mater Res, 1996. **31**(1): p. 1-9.
59. Campbell, C., Goldfarb, D., and Roe, R., *A small arterial substitute: expanded microporous polytetrafluoroethylene: patency versus porosity.* Ann Surg, 1975. **182**(2): p. 138-43.
60. Herring, M., Baughman, S., Glover, J., Kesler, K., Jesseph, J., Campbell, J., Dilley, R., Evan, A., and Gardner, A., *Endothelial seeding of Dacron and polytetrafluoroethylene grafts: the cellular events of healing.* Surgery, 1984. **96**(4): p. 745-55.
61. Mathisen, S., Wu, H., Sauvage, L., Usui, Y., and Walker, M., *An experimental study of eight current arterial prostheses.* J Vasc Surg, 1986. **4**(1): p. 33-41.
62. Beck, L.J. and D, A.P., *Vascular development: cellular and molecular regulation.* FASEB J, 1997. **11**(5): p. 365-73.
63. Hirschi, K., Rohovsky, S., and D, A.P., *Cell-cell interactions in vessel assembly: a model for the fundamentals of vascular remodelling.* Transpl Immunol, 1997. **5**(3): p. 177-8.
64. Cheresh, D., Berliner, S., Vicente, V., and Ruggeri, Z., *Recognition of distinct adhesive sites on fibrinogen by related integrins on platelets and endothelial cells.* Cell, 1989. **58**(5): p. 945-53.
65. Dvorak, H., Nagy, J., Berse, B., Brown, L., Yeo, K., Yeo, T., Dvorak, A., van, d.W.L., Sioussat, T., and Senger, D., *Vascular permeability factor, fibrin, and the pathogenesis of tumor stroma formation.* Ann N Y Acad Sci, 1992. **667**: p. 101-11.
66. Gamble, J., Matthias, L., Meyer, G., Kaur, P., Russ, G., Faull, R., Berndt, M., and Vadas, M., *Regulation of in vitro capillary tube formation by anti-integrin antibodies.* J Cell Biol, 1993. **121**(4): p. 931-43.
67. Tabbara, M. and White, R., *Biologic and prosthetic materials for vascular conduits.*, in *Vascular Surgery: Principles and Practice.*, F. Veith, Hobson, R., Williams, R., and Wilson, S., Editors. 1994, McGraw-Hill, Inc: USA. p. 523-35.
68. Davids, L., Dower, T., and Zilla, P., *The lack of healing in conventional vascular grafts*, in *Tissue engineering of vascular grafts*, P. Zilla and Greisler, H., Editors. 1999, RG Landes: Austin. p. 3-44.
69. Nam, Y. and Park, T., *Porous biodegradable polymeric scaffolds prepared by thermally induced phase separation.* J Biomed Mater Res, 1999. **47**(1): p. 8-17.
70. *Cardiovascular implants - Vascular prostheses.* 1994, Association for the advancement of medical instrumentation: Arlington, VA.
71. Abbott, W.M., Megerman, J., Hasson, J.E., L'Italien, G., and Warnock, D.F., *Effect of compliance mismatch on vascular graft patency.* J Vasc Surg, 1987. **5**(2): p. 376-82.
72. Walden, R., L'Italien, G.J., Megerman, J., and Abbott, W.M., *Matched elastic properties and successful arterial grafting.* Arch Surg, 1980. **115**(10): p. 1166-9.
73. Kawasaki, T., Sasayama, S., Yagi, S., Asakawa, T., and Hirai, T., *Non-invasive assessment of the age related changes in stiffness of major branches of the human arteries.* Cardiovasc Res, 1987. **21**: p. 678-687.
74. Tai, N., Salacinski, H., Edwards, A., Hamilton, G., and Seifalian, A., *Compliance properties of conduits used in vascular reconstruction.* Br J Surg, 2000. **87**(11): p. 1516-24.
75. Hayashi, K., Takamizawa, K., Saito, T., Kira, K., Hiramatsu, K., and Kondo, K., *Elastic properties and strength of a novel small-diameter, compliant polyurethane vascular graft.* J Biomed Mater Res, 1989. **23**(A2 Suppl): p. 229-44.
76. Gupta, B.S. and Kasyanov, V.A., *Biomechanics of human common carotid artery and design of novel hybrid textile compliant vascular grafts.* J Biomed Mater Res, 1997. **34**(3): p. 341-9.
77. Millam, R., *Design of an adventitial type reinforcement of prosthetic vascular grafts through mechanically affirmed material and structure modulation.*, in *Faculty of Health Sciences*. 2001, University of Cape Town: Cape Town.
78. Arndt, J., Klauske, J., and Mersch, F., *The diameter of the intact carotid artery in man and its change with pulse pressure.* Pfluegers Arch, 1968. **30**: p. 230-240.
79. Mozersky, D., Sumner, D., Hokanson, D., and Strandness, D., *Transcutaneous measurement of the elastic properties of the human femoral artery.* Circulation, 1972. **46**: p. 948-955.
80. Hayashi, K., Handa, H., Nagasawa, S., Okumura, A., and Moritake, K., *Stiffness and elastic behavior of human intracranial and extracranial arteries.* J Biomech, 1980. **13**(2): p. 175-84.
81. Doi, K., Nakayama, Y., and Matsuda, T., *Novel compliant and tissue-permeable microporous polyurethane vascular prosthesis fabricated using an excimer laser ablation technique.* J Biomed Mater Res, 1996. **31**(1): p. 27-33.
82. Rosset, E., Brunet, C., and Rieu, R., *Viscoelastic properties of human arteries.* Surgical and Rodiological Anatomy, 1996. **18**: p. 89-96.

Stellenbosch University http://scholar.sun.ac.za

83. Tai, N., Giudiceandrea, A., Salacinski, H., Seifalian, A., and Hamilton, G., *In vivo femoropopliteal arterial wall compliance in subjects with and without lower limb vascular disease.* J Vasc Surg, 1999. **30**(5): p. 936-45.
84. Smilde, T.J., van den Berkmortel, F.W., Wollersheim, H., van Langen, H., Kastelein, J.J., and Stalenhoef, A.F., *The effect of cholesterol lowering on carotid and femoral artery wall stiffness and thickness in patients with familial hypercholesterolaemia.* Eur J Clin Invest, 2000. **30**(6): p. 473-80.
85. Lafleche, A., Gautier, S., Topouchian, J., Wilmet, C.S., Girerd, X., Safar, M.E., and Benetos, A., *Differential responses of the heart and vasculature to chronic blood pressure reduction in essential hypertension.* Clin Pharmacol Ther, 1998. **64**(1): p. 96-105.
86. Giltay, E.J., Lambert, J., Gooren, L.J., Elbers, J.M., Steyn, M., and Stehouwer, C.D., *Sex steroids, insulin, and arterial stiffness in women and Men.* Hypertension, 1999. **34**(4 Pt 1): p. 590-7.
87. Giltay, E.J., Lambert, J., Elbers, J.M., Gooren, L.J., Asscheman, H., and Stehouwer, C.D., *Arterial compliance and distensibility are modulated by body composition in both men and women but by insulin sensitivity only in women.* Diabetologia, 1999. **42**(2): p. 214-21.
88. Smilde, T.J., van den Berkmortel, F.W., Boers, G.H., Wollersheim, H., de Boo, T., van Langen, H., and Stalenhoef, A.F., *Carotid and femoral artery wall thickness and stiffness in patients at risk for cardiovascular disease, with special emphasis on hyperhomocysteinemia.* Arterioscler Thromb Vasc Biol, 1998. **18**(12): p. 1958-63.
89. Anderson, J., Gristina, A., Hanson, S., Harker, L., Johnson, R., Merritt, K., Naylor, P., and Schoen, F., *Host reaction to biomaterials and their evaluation*, in *Biomaterials science: An introduction to materials in medicine*, B. Ratner, Hoffman, A., Schoen, F., and Lemons, J., Editors. 1996, Academic Press: San Diega.
90. Anderson, J., *Inflammatory reaction: The nemesis of implants*, in *Tissue engineering of vascular prosthetic grafts*, Z. P and HP, G., Editors. 1999, R.G. Landes: Texas.
91. Rattner, B. and Hoffman, A., *Thin films, grafts and coatings*, in *Biomaterials Science. An Introduction to Material in Maedicine*, B. Ratner, Hoffman, A., Schoen, F., and Lemons, J., Editors. 1996, Academic Press: San Diego. p. 105-118.
92. Yun, J., DeFife, K., Colton, E., Stack, S., Azeez, A., Cahalan, L., Verhoeven, M., Cahalan, P., and Anderson, J., *Human monocyte/macrophage adhesion and cytokine production on surface-modified poly(tetrafluoroethylene/hexafluoropropylene) polymers with and without protein preadsorption.* J Biomed Mater Res, 1995. **29**(2): p. 257-68.
93. Smetna, K., Vacik, J., Souckova, D., Krcova, Z., and Suic, J., *The influence of hydrogel functional groups on cell behaviour.* J. Biomed. Mater. Res., 1990. **24**: p. 463-470.
94. Bruil, A., Terlingen, G., Beugeling, T., van Aken, W., and Feijen, J., *In vitro leukocyte adhesion to modified polyurethane surfaces.* Biomaterials, 1992. **13**: p. 915-923.
95. Pavey, K. and Olliff, C., *SPR analysis of the total reduction of protein adsorption to surfaces coated with mixtures of long- and short-chain polyethylene oxide block copolymers.* Biomaterials, 1999. **20**(9): p. 885-90.
96. Quinn, C., Connor, R., and Heller, A., *Biocompatible, glucose-permeable hydrogel for in situ coating of implantable biosensors.* Biomaterials, 1997. **18**(24): p. 1665-70.
97. Han, D., Park, K., Ryu, G., Kim, U., Min, B., and Kim, Y., *Plasma protein adsorption to sulfonated poly(ethylene oxide)-grafted polyurethane surface.* J Biomed Mater Res, 1996. **30**(1): p. 23-30.
98. Park, K., Kim, Y., Han, D., Kim, Y., Lee, E., Suh, H., and Choi, K., *Bacterial adhesion on PEG modified polyurethane surfaces.* Biomaterials, 1998. **19**(7-9): p. 851-9.
99. Lee, J., Ju, Y., Lee, W., Park, K., and Kim, Y., *Platelet adhesion onto segmented polyurethane surfaces modified by PEO- and sulfonated PEO-containing block copolymer additives.* J Biomed Mater Res, 1998. **40**(2): p. 314-23.
100. Amiji, M. and Park, K., *Surface modification of polymeric biomaterials with poly(ethylene oxide), albumin, and heparin for reduced thrombogenicity.* J Biomater Sci Polym Ed, 1993. **4**(3): p. 217-34.
101. Llanos, G. and Sefton, M., *Does polyethylene oxide possess a low thrombogenicity?* J Biomater Sci Polym Ed, 1993. **4**(4): p. 381-400.
102. San, R.J., Bujan, J., Bellon, J., Gallardo, A., Escudero, M., Jorge, E., de, H.J., Alvarez, L., and Castillo, -.O.J., *Experimental study of the antithrombogenic behavior of Dacron vascular grafts coated with hydrophilic acrylic copolymers bearing salicylic acid residues.* J Biomed Mater Res, 1996. **32**(1): p. 19-27.
103. Phaneuf, M., Berceli, S., Bide, M., Quist, W., and LoGerfo, F., *Covalent linkage of recombinant hirudin to poly(ethylene terephthalate) (Dacron): creation of a novel antithrombin surface.* Biomaterials, 1997. **18**(10): p. 755-65.
104. Seifert, B., Romaniuk, P., and Groth, T., *Covalent immobilization of hirudin improves the haemocompatibility of polylactide-polyglycolide in vitro.* Biomaterials, 1997. **18**(22): p. 1495-502.
105. Aldenhoff, Y., Pijpers, A., and Koole, L., *Synthesis of a new photoreactive derivative of dipyridamole and its use in the manufacture of artificial surfaces with low thrombogenicity.* Bioconjug Chem, 1997. **8**(3): p. 296-303.

Stellenbosch University http://scholar.sun.ac.za

106. Aldenhoff, Y., Blezer, R., Lindhout, T., and Koole, L., *Photo-immobilization of dipyridamole (Persantin) at the surface of polyurethane biomaterials: reduction of in-vitro thrombogenicity.* Biomaterials, 1997. **18**(2): p. 167-72.
107. Aldenhoff, Y. and Koole, L., *Studies on a new strategy for surface modification of polymeric biomaterials.* J Biomed Mater Res, 1995. **29**(8): p. 917-28.
108. Ryu, G., Han, D., Park, S., Kim, M., Kim, Y., and Min, B., *Surface characteristics and properties of lumbrokinase-immobilized polyurethane.* J Biomed Mater Res, 1995. **29**(3): p. 403-9.
109. Ryu, G., Park, S., Kim, M., Han, D., Kim, Y., and Min, B., *Antithrombogenicity of lumbrokinase-immobilized polyurethane.* J Biomed Mater Res, 1994. **28**(9): p. 1069-77.
110. Larm, O., Larsson, R., and Olsson, P., *A new non-thrombogenic surface prepared by selective covalent binding of heparin via a modified reducing terminal residue.* Biomater Med Devices Artif Organs, 1983. **11**(2-3): p. 161-73.
111. Larsson, R., Larm, O., and Olsson, P., *The search for thromboresistance using immobilized heparin.* Ann N Y Acad Sci, 1987. **516**: p. 102-15.
112. Marconi, W., Benvenuti, F., and Piozzi, A., *Covalent bonding of heparin to a vinyl copolymer for biomedical applications.* Biomaterials, 1997. **18**(12): p. 885-90.
113. West, R., Paul, A., Hibbert, S., Cahalan, P., Cahalan, L., Verhoeven, M., Hendriks, M., and Fouache, B., *Correlation of the surface chemistries of polymer bioactive coatings, with their biological performances.* Journal of Materials Science: Materials in Medicine, 1995. **6**: p. 63-67.
114. Olsson, P. and Larm, O., *Biologically active heparin coating in medical devices [editorial].* Int J Artif Organs, 1991. **14**(8): p. 453-6.
115. Nojiri, C., Park, K., Grainger, D., Jacobs, H., Okano, T., Koyanagi, H., and Kim, S., *In vivo nonthrombogenicity of heparin immobilized polymer surfaces.* ASAIO Trans, 1990. **36**(3): p. M168-72.
116. Lindhout, T., Blezer, R., Schoen, P., Willems, G., Fouache, B., Verhoeven, M., Hendriks, M., Cahalan, L., and Cahalan, P., *Antithrombin activity of surface-bound heparin studied under flow conditions.* J Biomed Mater Res, 1995. **29**(10): p. 1255-66.
117. Sapatnekar, S., Kieswetter, K., Merritt, K., Anderson, J., Cahalan, L., Verhoeven, M., Hendriks, M., Fouache, B., and Cahalan, P., *Blood-biomaterial interactions in a flow system in the presence of bacteria: effect of protein adsorption [published erratum appears in J Biomed Mater Res 1995 May;29(5):679].* J Biomed Mater Res, 1995. **29**(2): p. 247-56.
118. Esquivel, C., Bjorck, C., Bergentz, S., Bergqvist, D., Larsson, R., Carson, S., Dougan, P., and Nilsson, B., *Reduced thrombogenic characteristics of expanded polytetrafluoroethylene and polyurethane arterial grafts after heparin bonding.* Surgery, 1984. **95**(1): p. 102-7.
119. Huang, L., Lee, P., Chen, L., and Hsieh, K., *Comparison of epoxides on grafting collagen to polyurethane and their effects on cellular growth.* J Biomed Mater Res, 1998. **39**(4): p. 630-6.
120. Shimizu, Y., Miyamoto, Y., Teramatsu, T., Okamura, S., and Hino, T., *Studies on composites of collagen and a synthetic polymer. Second report - mode of reaction of a laminar composite with living tissue, and results of long-term implantation.* Biomater Med Devices Artif Organs, 1978. **6**(4): p. 375-91.
121. Lee, S., Hsiue, G., Chang, P., and Kao, C., *Plasma-induced grafted polymerization of acrylic acid and subsequent grafting of collagen onto polymer film as biomaterials.* Biomaterials, 1996. **17**(16): p. 1599-608.
122. Okada, T. and Ikada, Y., *Tissue reactions to subcutaneously implanted, surface-modified silicones.* J Biomed Mater Res, 1993. **27**(12): p. 1509-18.
123. Kinoshita, Y., Kuzuhara, T., Kirigakubo, M., Kobayashi, M., Shimura, K., and Ikada, Y., *Soft tissue reaction to collagen-immobilized porous polyethylene: subcutaneous implantation in rats for 20 wk.* Biomaterials, 1993. **14**(3): p. 209-15.
124. Shimizu, Y., Abe, R., Teramatsu, T., Okamura, S., and Hino, T., *Studies on copolymers of collagen and a synthetic polymer. First report- -experimental study on biocompatibility of laminar copolymers of collagen and a synthetic polymer.* Biomater Med Devices Artif Organs, 1977. **5**(1): p. 49-66.
125. Anderheiden, D., Klee, D., Hocker, H., Heller, B., Kirkpatrick, C., and Mittermayer, C., *Surface modification of a biocompatible polymer based on polyurethane for artificial blood vessels.* Journal of Materials Science; Mataerials in Medicine, 1992. **3**: p. 1-4.
126. Sugawara, T. and Matsuda, T., *Photochemical surface derivatization of a peptide containing Arg-Gly-Asp (RGD).* J Biomed Mater Res, 1995. **29**(9): p. 1047-52.
127. Lin, H., Sun, W., Mosher, D., Garcia, -.E.C., Schaufelberger, K., Lelkes, P., and Cooper, S., *Synthesis, surface, and cell-adhesion properties of polyurethanes containing covalently grafted RGD-peptides.* J Biomed Mater Res, 1994. **28**(3): p. 329-42.
128. Barrera, D., Zylstra, E., Lansbury, P., and Langer, R., *Synthesis and RGD peptide modification of new biodegradable copolymer: poly(lactic acid-co-lysine).* J Am Chem Soc, 1993. **115**: p. 11010-11011.
129. Cook, A., Hrkach, J., Gao, N., Johnson, I., Pajvani, U., Cannizzaro, S., and Langer, R., *Characterization and development of RGD-peptide-modified poly(lactic acid-co-lysine) as an interactive, resorbable biomaterial.* J Biomed Mater Res, 1997. **35**(4): p. 513-23.

Stellenbosch University http://scholar.sun.ac.za

130. Porte-Durrieu, M., Labrugere, C., Villars, F., Lefebvre, F., Dutoya, S., Guette, A., Bordenave, L., and Baquey, C., *Development of RGD peptides grafted onto silica surfaces: XPS characterization and human endothelial cell interactions.* J Biomed Mater Res, 1999. **46**(3): p. 368-75.
131. Kao, W., Lee, D., Schense, J., and Hubbell, J., *Fibronectin modulates macrophage adhesion and FBGC formation: the role of RGD, PHSRN, and PRRARV domains.* J Biomed Mater Res, 2001. **55**(79-88).
132. Hamdan, A., Misare, B., Contreras, M., LoGerfo, F., and Quist, W., *Evaluation of anastomotic hyperplasia progression using the cyclin specific antibody MIB-1.* Am J Surg, 1996. **172**(2): p. 168-70; discussion 170-1.
133. van der Lei, B. and Wildevuur, C., *Improved healing of microvascular PTFE prostheses by induction of a clot layer: an experimental study in rats.* Plast Reconstr Surg, 1989. **84**(6): p. 960-8.
134. Bull, D., Hunter, G., Holubec, H., Aguirre, M., Rappaport, W., and Putnam, C., *Cellular origin and rate of endothelial cell coverage of PTFE grafts.* J Surg Res, 1995. **58**(1): p. 58-68.
135. Clowes, A., Gown, A., Hanson, S., and Reidy, M., *Mechanisms of arterial graft failure. 1. Role of cellular proliferation in early healing of PTFE prostheses.* Am J Pathol, 1985. **118**(1): p. 43-54.
136. Bartels, H., van, d.L.B., and Robinson, P., *Prosthetic microvenous grafting in the rat femoral vein.* Lab Anim, 1993. **27**(1): p. 47-54.
137. Douville, E., Kempczinski, R., Birinyi, L., and Ramalanjaona, G., *Impact of endothelial cell seeding on long-term patency and subendothelial proliferation in a small-caliber highly porous polytetrafluoroethylene graft.* J Vasc Surg, 1987. **5**(4): p. 544-50.
138. Kenney, D., Tu, R., and Peterson, R., *Evaluation of compliant and noncompliant PTFE vascular prostheses.* ASAIO Trans, 1988. **34**(3): p. 661-3.
139. van der Lei, B. and Wildevuur, C., *Microvascular polytetrafluoroethylene prostheses: the cellular events of healing and prostacyclin production.* Plast Reconstr Surg, 1988. **81**(5): p. 735-41.
140. Burkel, W., Ford, J., Vinter, D., Kahn, R., Graham, L., and Stanley, J., *Fate of knitted dacron velour vascular grafts seeded with enzymatically derived autologous canine endothelium.* Trans Am Soc Artif Intern Organs, 1982. **28**: p. 178-84.
141. Baitella, -.E.G., Groscurth, P., Zilla, P., Lachat, M., Muller, -.G.W., Schneider, J., Neudecker, A., von, S.L., Dardel, E., and Turina, M., *Long-term results of tissue development and cell differentiation on Dacron prostheses seeded with microvascular cells in dogs.* J Vasc Surg, 1993. **18**(6): p. 1019-28.
142. Sottiurai, V., Sue, S., Rau, D., and Tran, A., *Comparative analysis of pseudointima biogenesis in Gelseal coated Dacron knitted graft versus crimped and noncrimped graft.* J Cardiovasc Surg (Torino), 1989. **30**(6): p. 902-9.
143. Florian, A., Cohn, L., Dammin, G., and Collins, J.J., *Small vessel replacement with gore-tex (expanded polytetrafluoroethylene).* Arch Surg, 1976. **111**(3): p. 267-70.
144. Nomura, Y., *The ultra-structure of the pseudointima lining synthetic arterial grafts in the canine aorta with special reference to the origin of the endothelial cell.* J Cardiovasc Surg (Torino), 1970. **11**(4): p. 282-91.
145. Hertzer, N., *Regeneration of endothelium in knitted and velour dacron vascular grafts in dogs.* J Cardiovasc Surg (Torino), 1981. **22**(3): p. 223-30.
146. Wu, M., Shi, Q., Kouchi, Y., Onuki, Y., Ghali, R., Yoshida, H., Kaplan, S., and Sauvage, L., *Implant site influence on arterial prosthesis healing: a comparative study with a triple implantation model in the same dog.* J Vasc Surg, 1997. **25**(3): p. 528-36.
147. Binns, R., Ku, D., Stewart, M., Ansley, J., and Coyle, K., *Optimal graft diameter: effect of wall shear stress on vascular healing.* J Vasc Surg, 1989. **10**(3): p. 326-37.
148. Kraiss, L., Geary, R., Mattsson, E., Vergel, S., Au, Y., and Clowes, A., *Acute reductions in blood flow and shear stress induce platelet-derived growth factor-A expression in baboon prosthetic grafts.* Circ Res, 1996. **79**(1): p. 45-53.
149. Wu, M., Kouchi, Y., Onuki, Y., Shi, Q., Yoshida, H., Kaplan, S., Viggers, R., Ghali, R., and Sauvage, L., *Effect of differential shear stress on platelet aggregation, surface thrombosis, and endothelialization of bilateral carotid-femoral grafts in the dog.* J Vasc Surg, 1995. **22**(4): p. 382-90; discussion 390-2.
150. Margolin, D., Kaufman, B., DeLuca, D., Fox, P., and Graham, L., *Increased platelet-derived growth factor production and intimal thickening during healing of Dacron grafts in a canine model.* J Vasc Surg, 1993. **17**(5): p. 858-66; discussion 866-7.
151. Shepard, A., Eldrup, -.J.J., Keough, E., Foxall, T., Ramberg, K., Connolly, R., Mackey, W., Gavris, V., Auger, K., Libby, P., and et, a., *Endothelial cell seeding of small-caliber synthetic grafts in the baboon.* Surgery, 1986. **99**(3): p. 318-26.
152. Wu, M., Shi, Q., Wechezak, A., Clowes, A., Gordon, I., and Sauvage, L., *Definitive proof of endothelialization of a Dacron arterial prosthesis in a human being.* J Vasc Surg, 1995. **21**(5): p. 862-7.
153. Schmidt, S., Hunter, T., Hirko, M., Belden, T., Evancho, M., Sharp, W., and Donovan, D., *Small-diameter vascular prostheses: two designs of PTFE and endothelial cell-seeded and nonseeded Dacron.* J Vasc Surg, 1985. **2**(2): p. 292-7.
154. Noishiki, Y., *Pattern of arrangement of smooth muscle cells in neointimae of synthetic vascular prostheses.* J Thorac Cardiovasc Surg, 1978. **75**(6): p. 894-901.

Stellenbosch University http://scholar.sun.ac.za

155. Wu, X. and Trinkaus, -.R.V., *The expression of integrin subunits alpha 6 and beta 4 by corneal epithelial cells on modified hydrogel surfaces.* J Biomed Mater Res, 1997. **37**(2): p. 166-75.
156. Stewart, G., Essa, N., Chang, K., and Reichle, F., *A scanning and transmission electron microscope study of the luminal coating on Dacron prostheses in the canine thoracic aorta.* J Lab Clin Med, 1975. **85**(2): p. 208-26.
157. Zilla, P., Fasol, R., Dudeck, U., Siedler, S., Preiss, P., Fischlein, T., Muller, -.G.W., Baitella, G., Sanan, D., Odell, J., and et, a., *In situ cannulation, microgrid follow-up and low-density plating provide first passage endothelial cell masscultures for in vitro lining.* J Vasc Surg, 1990. **12**(2): p. 180-9.
158. Szilagyi, D., Smith, R., Elliott, J., and Allen, H., *Long-term behavior of a dacron arterial substitute: clinical, roentgenologic and histologic correlations.* Ann Surg, 1965. **162**(3): p. 453-77.
159. Sottiurai, V., Yao, J., Flinn, W., and Batson, R., *Intimal hyperplasia and neointima: An ultrastructural analysis of thrombosed grafts in humans.* Surgery, 1983. **93**(6): p. 809-17.
160. Boyd, K., Schmidt, S., Pippert, T., and Sharp, W., *Endothelial cell seeding of ULTI carbon-coated small-diameter PTFE vascular grafts.* ASAIO Trans, 1987. **33**(3): p. 631-5.
161. Graham, L., Burkel, W., Ford, J., Vinter, D., Kahn, R., and Stanley, J., *Expanded polytetrafluoroethylene vascular prostheses seeded with enzymatically derived and cultured canine endothelial cells.* Surgery, 1982. **91**(5): p. 550-9.
162. Hussain, S., Glover, J., Augelli, N., Bendick, P., Maupin, D., and McKain, M., *Host response to autologous endothelial seeding.* J Vasc Surg, 1989. **9**(5): p. 656-63; discussion 663-4.
163. Kaufman, B., DeLuca, D., Folsom, D., Mansell, S., Gorman, M., Fox, P., and Graham, L., *Elevated platelet-derived growth factor production by aortic grafts implanted on a long-term basis in a canine model.* J Vasc Surg, 1992. **15**(5): p. 806-15; discussion 815-6.
164. Koveker, G., Burkel, W., Graham, L., Wakefield, T., and Stanley, J., *Endothelial cell seeding of expanded polytetrafluoroethylene vena cava conduits: effects on luminal production of prostacyclin, platelet adherence, and fibrinogen accumulation.* J Vasc Surg, 1988. **7**(4): p. 600-5.
165. Ombrellaro, M., Stevens, S., Kerstetter, K., Freeman, M., and Goldman, M., *Healing characteristics of intraarterial stented grafts: effect of intraluminal position on prosthetic graft healing.* Surgery, 1996. **120**(1): p. 60-70.
166. Burkel, W., Vinter, D., Ford, J., Kahn, R., Graham, L., and Stanley, J., *Sequential studies of healing in endothelial seeded vascular prostheses: histologic and ultrastructure characteristics of graft incorporation.* J Surg Res, 1981. **30**(4): p. 305-24.
167. Graham, L., Vinter, D., Ford, J., Kahn, R., Burkel, W., and Stanley, J., *Endothelial cell seeding of prosthetic vascular grafts: early experimental studies with cultured autologous canine endothelium.* Arch Surg, 1980. **115**(8): p. 929-33.
168. Schmidt, S., Monajjem, N., Evancho, M., Pippert, T., and Sharp, W., *Microvascular endothelial cell seeding of small-diameter Dacron vascular grafts.* J Invest Surg, 1988. **1**(1): p. 35-44.
169. Golden, M., Au, Y., Kenagy, R., and Clowes, A., *Growth factor gene expression by intimal cells in healing polytetrafluoroethylene grafts.* J Vasc Surg, 1990. **11**(4): p. 580-5.
170. Kraiss, L., Raines, E., Wilcox, J., Seifert, R., Barrett, T., Kirkman, T., Hart, C., Bowen, -.P.D., Ross, R., and Clowes, A., *Regional expression of the platelet-derived growth factor and its receptors in a primate graft model of vessel wall assembly.* J Clin Invest, 1993. **92**(1): p. 338-48.
171. Zacharias, R., Kirkman, T., and Clowes, A., *Mechanisms of healing in synthetic grafts.* J Vasc Surg, 1987. **6**(5): p. 429-36.
172. Wesolow, A., *Biological behaviour of tissue and prosthetic grafts*, in *Vascular surgery. Principles and techniques*, H. Haimovici, Editor. 1984, Appleton-Century-Crofts: Norwark, Connecticut. p. 93-118.
173. Shi, Q., Wu, M., Onuki, Y., Ghali, R., Hunter, G., Johansen, K., and Sauvage, L., *Endothelium on the flow surface of human aortic Dacron vascular grafts.* J Vasc Surg, 1997. **25**(4): p. 736-42.
174. Berger, K., Sauvage, L., Rao, A., and Wood, S., *Healing of arterial prostheses in man: its incompleteness.* Ann Surg, 1972. **175**(1): p. 118-27.
175. Wesolowski, S., Fries, C., Gennigar, G., Fox, L., Sawyer, P., and Sauvage, L., *Factors contributing to long-term failures in human vascular prosthetic grafts.* Cardiovas Surg, 1964. **38**: p. 544-67.
176. Shi, Q., Wu, M., Hayashida, N., Wechezak, A., Clowes, A., and Sauvage, L., *Proof of fallout endothelialization of impervious Dacron grafts in the aorta and inferior vena cava of the dog.* J Vasc Surg, 1994. **20**(4): p. 546-56; discussion 556-7.
177. Kohler, T., Stratton, J., Kirkman, T., Johansen, K., Zierler, B., and Clowes, A., *Conventional versus high-porosity polytetrafluoroethylene grafts: clinical evaluation.* Surgery, 1992. **112**(5): p. 901-7.
178. Sauvage, L., Berger, K., Wood, S., Yates, S.d., Smith, J., and Mansfield, P., *Interspecies healing of porous arterial prostheses: observations, 1960 to 1974.* Arch Surg, 1974. **109**(5): p. 698-705.
179. Hammond, W., *Surface population with blood-borne cells.*, in *Tissue Engineering of Prosthetic Vascular Grafts*, P. Zilla and Greisler, H., Editors. 1998, Landes Bioscience: Austin.
180. Stumb, M., Jordan, G., and DeBakey, M., *Endothelium growth from circulating blood on isolated intravascular Dacron hub.* Amer J Path, 1963. **43**: p. 361-68.

Stellenbosch University http://scholar.sun.ac.za

CHAPTER 4

Vascular graft concept

The proposed design concept for a vascular graft may conveniently be discussed by the use of illustrations below. First, an overview of the overall concept will be presented, after which more details on the individual concepts will be given. Although the overall concept includes components that fall outside the scope of this dissertation, they are included in the interest of completeness, and to highlight where the current research fits into the ultimate goal of producing a fully functional vascular graft by in vivo tissue engineering.

4.1 Overall concept

The overall concept of the vascular graft proposed in this dissertation involves the fabrication and evaluation of a tubular structure comprising (See Fig 4.1):

- An internal diameter of 4-6mm and a wall thickness of 0.5-1mm,
- An openly-porous wall that will be permissive to cellular infiltration and re-orientation.
- An external reinforcing structure consisting of helically wound fibres (optimization of alternative adventitial reinforcing structures is part of the overall concept, but falls outside the scope of this dissertation),
- A surface pacification layer lining the exposed graft material,
- A temporary lumenal sealant to prevent the ingress of blood products into the structure and prevent the deposition of fibrin on the lumenal surface (permanent sealants will be used in this dissertation to prove this concept), and
- An ingrowth matrix optimised for preferential ingrowth of preferred cell types (the development of these matrixes is the subject of parallel research in our laboratories, and does not fall within the scope of this dissertation).

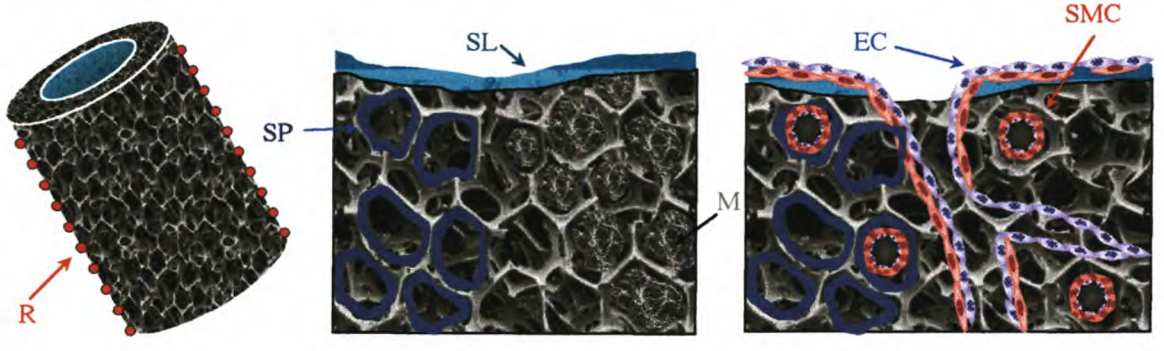

Figure 4.1: Overall vascular graft design concept showing (a) complete structure; (b) wall cross-section highlighting the surface pacification (SP), lumenal surface layer (SL) and ingrowth matrix (M); and (c) the proposed ingrowth of endothelial cells (EC) and smooth muscle cells (SMC).

Stellenbosch University http://scholar.sun.ac.za

4.2 Porosity

4.2.1 Dodecahedral unit-cell foams

The units defining foamed structures are often idealized by open-faced pentagonal dodecahedra. Figure 4.2 (a) shows a side view of such a pore. Figure 4.2 (d) relates the diameter of the pentagonal interconnecting window (W) with the height of the pore for the two routes indicated by the coloured lines in Figure 4.2 (a). The green and red dashed lines indicate the approximate size of capillaries and arterioles respectively. A three-dimensional view of a dodecahedral pore is depicted in (b). In reality, the struts defining the pores as well as the interconnecting windows between pores are often rounded, as shown in (c). This structure offers the least restriction to infiltration in three dimensions. Cells growing into a foam of this structure are equally free to migrate or orient themselves in all directions (e).

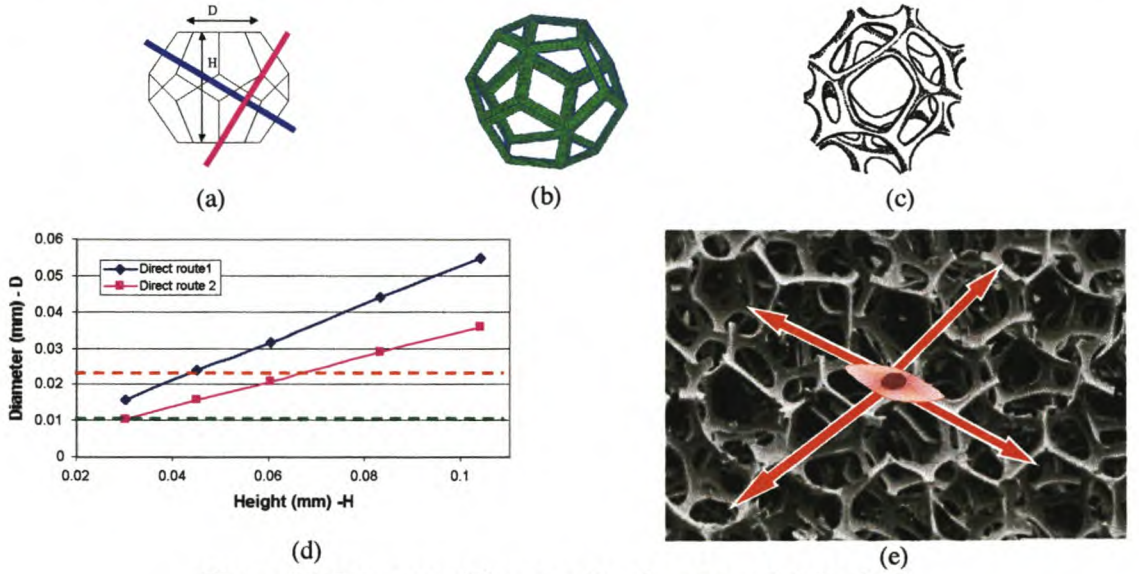

Figure 4.2: Pores resembling open-faced pentagonal dodecahedra.

Low-porosity ePTFE (Fig 4.3 (a)) does not allow for considerable cellular ingrowth due to limited ingrowth spaces. High porosity ePTFE (Fig 4.3 (b)) and loosely knitted Dacron grafts (Fig 4.3 (c)) may allow for the radial ingrowth of cells, but the re-orientation of cells into the circumferential direction is clearly not feasible due to their structures. In order to differentiate between the effect of increased ingrowth spaces alone and the effect obtainable with dodecahedral structures (that allow for improved ingrowth and circumferential orientation), ePTFE grafts with very large internodal distances will also be evaluated.

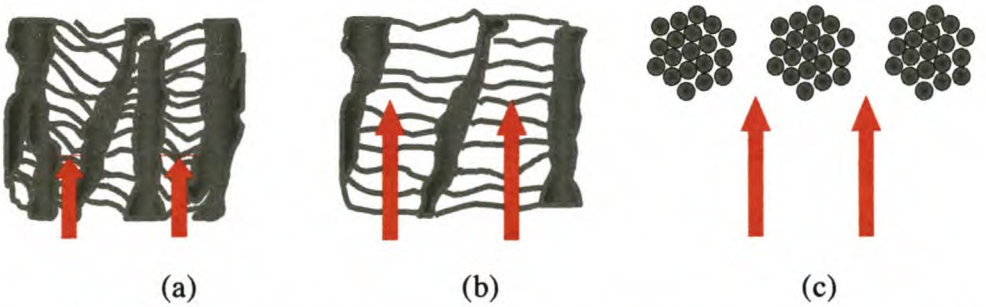

Figure 4.3: Possible ingrowth directions obtainable with ePTFE and Dacron vascular grafts.

Stellenbosch University http://scholar.sun.ac.za

4.2.2 Circumferential orientation

It is well known that smooth muscle cells exist in natural arteries in helically-wound bundles or sheets. The reorientation of these cells in sympathy with applied stresses has also been shown. It is thus proposed that helical orientation of ingrowing (ingrown) smooth muscles cells should occur when the graft is subjected to pulsatile dilation (resulting in circumferential stresses). As the proposed foam structure is equally amenable to growth in all directions, the structure should not impede orientation (Fig. 4.4).

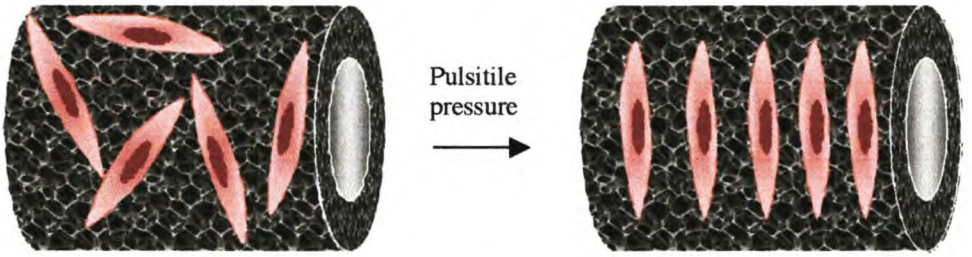

Figure 4.4: Circumferential orientation of smooth muscle cells as a result of pulsatile pressure.

4.2.3 Helical ingrowth channels

In the event that smooth muscle cells are not able to orient themselves circumferentially despite open porosity provided by the foams described above, an alternative is proposed. The alternative configuration comprises interconnecting helical channels in the graft wall. Consider the model in Figure 4.5 (a) (the channel spacing in this model is larger than proposed for ease of visualization). If the helical channels have openings where the successive layers cross, radial cellular ingrowth could occur if the cells were to follow the interconnections from the ablumenal to the lumenal surface. This concept is further illustrated in Fig 4.5 (b), which shows a cross-sectional view of the proposed graft wall (again the number of channels and helical angle are exaggerated). The arrows clearly indicate the route cells may follow to migrate from the ablumenal to the lumenal surface, and further indicate how cells may also be "forced" to orient themselves in the circumferential direction.

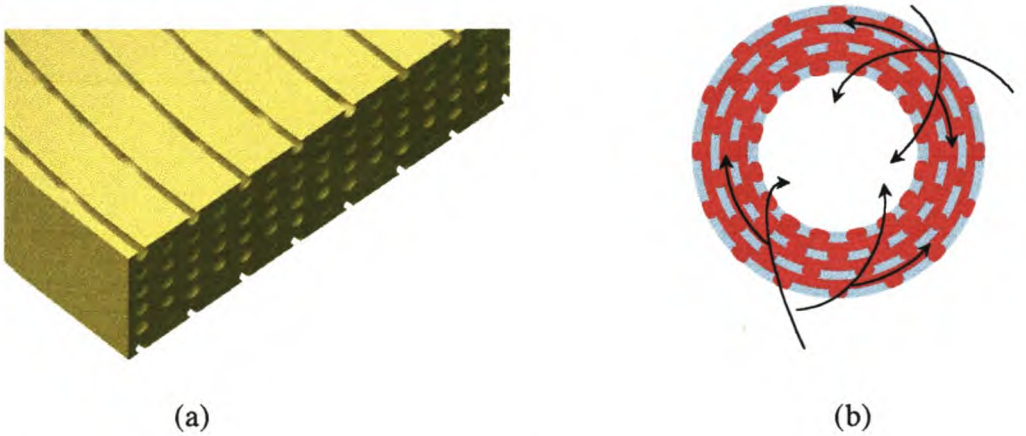

Figure 4.5: Schematic representation of interconnected helical channels in the wall of a conceptual vascular graft.

Stellenbosch University http://scholar.sun.ac.za

4.3 Production materials and methods

Polyurethanes have been selected as materials of choice due to their processability, biocompatibility and elastomeric properties. The majority of the work will be done with a proprietary PU developed by Medtronic Inc (Code M48), although other PUs will also be considered during the development process (notably Elast-Eon 2). The choice of these two materials was based on their superior biostability (See Chapter 3).

Phase inversion with extractable porogens is proposed as the primary method by which the porous structures are to be fabricated. Although many variations on this method have been previously employed to produce porous polyurethane grafts, the use of irregular porogens and premixing techniques have resulted in ill-defined structures, often with limited interconnectivity.

As the idealised dodecahedral pore structure may be considered as consisting of spherical pores, the use of spherical pores will be evaluated. In order to improve the interconnectivity between pores, the porogen will be pre-packed into an annular mould prior to infiltration of the interstices with the polymer solution. This concept is illustrated (in 2 dimensions) in Figure 4.6 below. It is evident that the combination of spherical porogens and the pre-packing technique should yield pores of a more regular shape and increased interconnectivity.

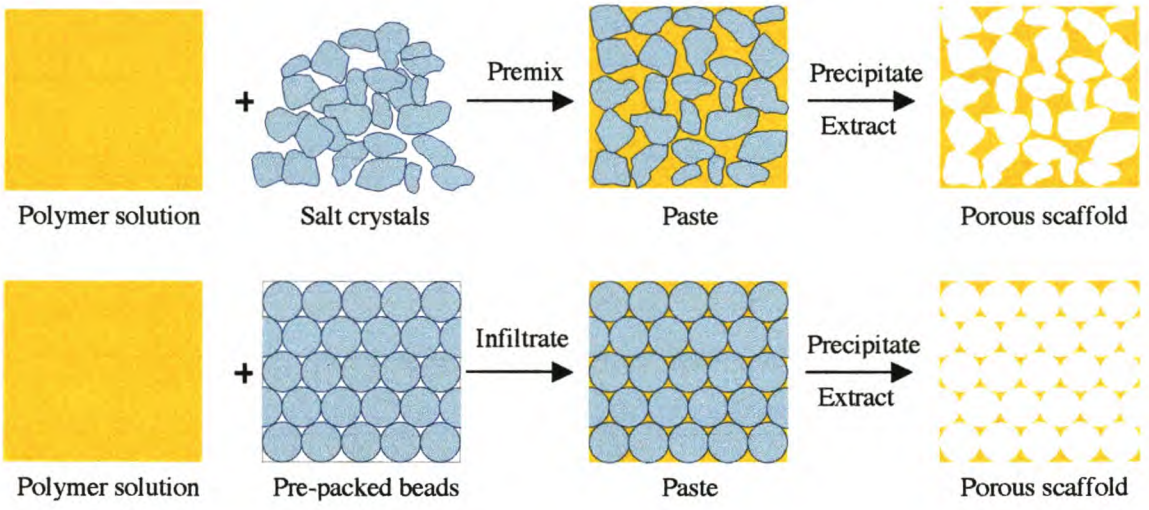

Figure 4.6: Proposed use of pre-packed spherical porogens for the creation of interconnected pores (lower scematic) vs. a conventional technique of pre-mixing salt crystals (upper schematic).

Alternate methods will include melt processing techniques whereby pores are created either by extraction of porogens, or by the use of chemical blowing agents.

Two methods for the formation of interconnected helical channels are proposed:

- the winding of polyurethane-coated extractable fibres on a rotating mandrel, followed by precipitation of the polymer and extraction of the fibres.
- the combination of particulate and fibrillar porogens to render a graft containing both foam-type pores and helical channels.

Stellenbosch University http://scholar.sun.ac.za

4.4 Surface modification

Surface modification techniques will involve the covalent attachment of collagen (a protein known to improve tissue/device integration), and heparin (a polysaccharide known for its thromboresistant and growth factor binding capabilities). Attachment will be performed via a poly(acrylic acid-co-acrylamide) hydrogel layer covalently attached to the polyurethane by graft copolymerisation (Fig 4.7).

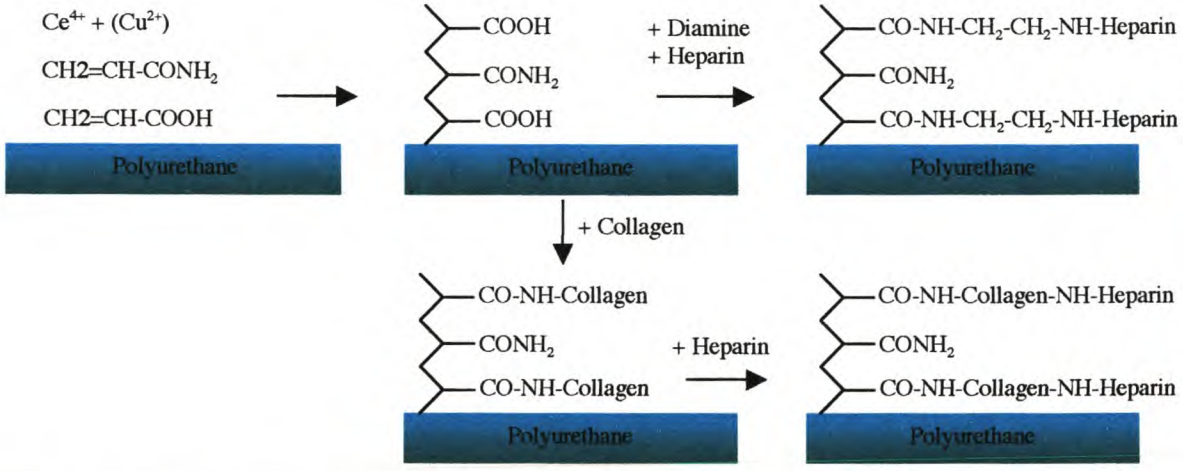

Figure 4.7: Schematic representation of techniques used for the surface modification of polyurethanes.

4.5 Lumenal surface sealant

The lack of healing throughout the walls of large-porosity ePTFE and PU grafts may be attributed to the formation of impenetrable fibrin layers deposited on the lumenal surface and in the inner portion of the graft wall. A proposed method of testing this hypothesis involves the application of a lumenal sealant (Fig 4.8). This sealant would prevent the deposition of the impenetrable layer, and thus allow cells to penetrate the full thickness of the graft wall (from the tissue surrounding the graft). If the sealant was engineered to degrade at a time point after full transmural ingrowth has been accomplished, the cells would be able to also populate the lumen of the graft.

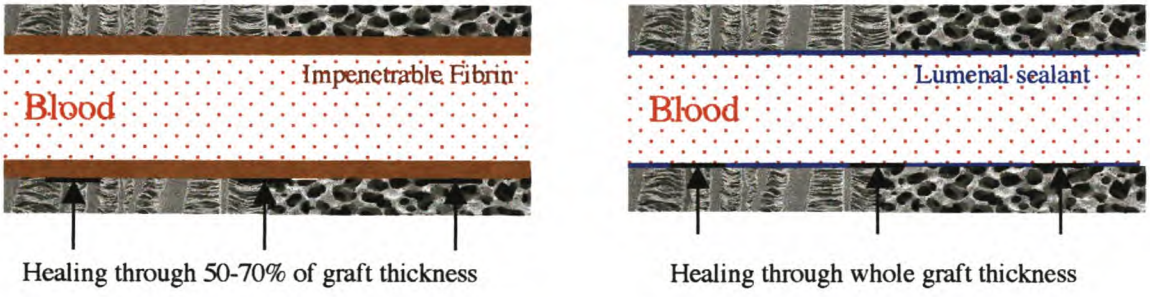

Figure 4.8: Schematic representation of the lumenal sealant concept

Stellenbosch University http://scholar.sun.ac.za

CHAPTER 5

Effect of porogen structure and incorporation technique on the structure and properties of porous vascular prostheses

5.1 Introduction

The importance of porosity in the long term healing response toward vascular grafts has been elucidated (See Chapter 3). Commercially available vascular grafts are mostly limited to expanded structures and textile structures (woven, knitted, velour etc). Over the past 30 years, a large variety of alternative techniques have been used to create porous structures from polyurethanes in efforts to overcome the inherent drawbacks associated with the structures and properties of the commercial products.

One class of techniques used in graft development of the polymer comprised the processing of fibres into wound or woven tubes, resulting in the formation of fibrillar structures containing a porosity defined by the interfibrillar spaces. Another method, of which a number of variants, have been evaluated, is termed phase inversion/porogen extraction. It involves the shaping of a polymeric solution containing porogen particles, precipitating the polymer in a non-solvent, and subsequently extracting the porogen to yield a structure in which a macroporosity, roughly the size and shape of the porogen, is superimposed on the microporous structure resulting from the phase-inversion process. These micro and macropores were mostly ill-defined and lacking in the degree of interconnectivity needed for full transmural ingrowth of tissue upon implantation into the host.

In an attempt to improve on the structures obtained by the phase-inversion/porogen extraction technique, the different methods of porogen incorporation were reinvestigated, and a novel method of incorporating spherical porogens for the creation of well-defined, interconnected macropores is proposed.

The use of crystalline porogens and historical techniques of porogen incorporation resulted in structures that will be shown to be similar to those obtained by previous researchers. The first adaptation of these techniques involved the pre-packing of the porogen into annular moulds before impregnation with the polymer solution. This resulted in an improvement in the interconnectivity of the macropores, but the pore structures remained ill-defined. The second adaptation consisted of the use of spherical porogens in place of angular salt crystals. By using the spherical porogens in the column impregnation technique, well-defined, spherical pores (approximating pentagonal dodecahedral pores observed in idealized foams) could be produced.

In addition, a novel method of producing vascular grafts containing interconnected, helically-oriented channels by the extraction of extractable fibres is introduced.

5.2 Introduction

In describing the structure and porosity of polyurethane vascular prostheses, it is useful to distinguish between two major categories, namely those that have a fibrillar composition and those that resemble cellular or foamed structures.

5.2.1 Fibrillar PU grafts

Fibrillar structures have been produced by the electrostatic spinning [1] (Fig 5.1a,b) or winding processes [2, 3] (Fig5.1c-f) by which PU filaments (molten or dissolved) are deposited onto rotating mandrels. Cooling or solvent evaporation lead to a coherent structure containing voids defined by the interstices between adjacent fibres. Accurate control over fibre orientation, fibre thickness, density, and wall thickness allowed for the tailoring of the porosity and optimization of mechanical properties. The use of the winding method led to the development of the

Stellenbosch University http://scholar.sun.ac.za

Vascugraft® vascular graft (Fig 5.1g,h), a product of B Braun Melsungen AG (Germany) that made it to clinical trials in below-knee indications. The graft was, however, withdrawn by the manufacturers [4]. Another method of producing fibrillar grafts involved the use of conventional knitting and weaving techniques generally applied to Dacron vascular grafts. Gupta et al. [5] used this method to produce PU/PET textile grafts by weaving a combination of PU and PET fibres into textile structures (Fig. 5.1i,j).

5.2.2 Foam type grafts

5.2.2.1 Phase precipitated PU grafts

Phase precipitation of polyurethane solutions by the addition of a non-solvent, the evaporation of the solvent, or by the lowering of the temperature, is a versatile technique that has been used extensively in the production of porous grafts. These processes generally lead to the formation of small (1-10μm) pores, although larger pores and pore gradients have been reported.

Figure 5.2 shows various structures obtained by this method. Dip-coating, followed by phase inversion led to the creation of 10-20μm micropores [6] (Fig 5.2a,b) or the formation of the laminar structures seen in Fig 5.2c and d [7, 8]. An alternative method, termed the flotation method, involves the deposition of a PU solution onto the surface of a non-solvent, and subsequent winding of the precipitating polymer onto a mandrel. This procedure leads to laminar structures [9] (Fig 5.2e,f) similar to those obtained by the use of Lommen's dip-coating method (Fig 5.2c). A third method of fashioning a tubular structure before phase precipitation is the extrusion of the polymer solution into the non-solvent [10-12]. Figure 5.2g-j shows the variety of porosities obtained by this method.

Stellenbosch University http://scholar.sun.ac.za

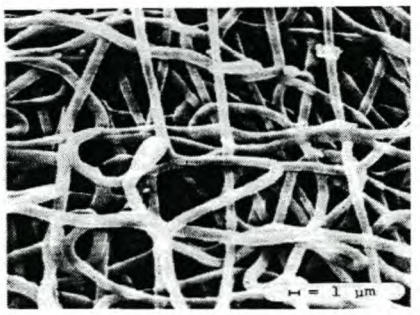

(a) Electrostatically spun graft (A) Annis [1]

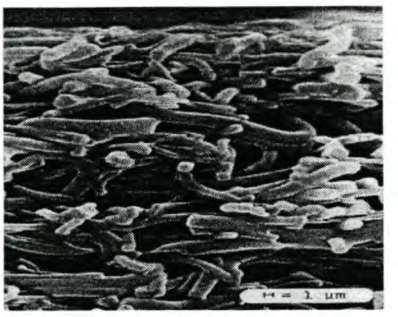

(b) Electrostatically spun graft (X) Annis [1]

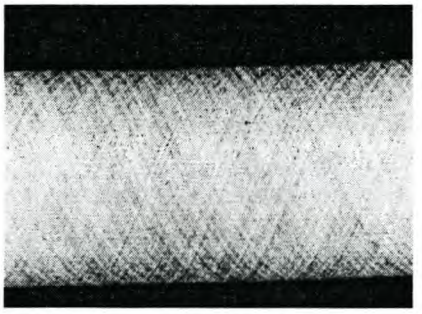

(c) Wound graft (A) Wilson[2]

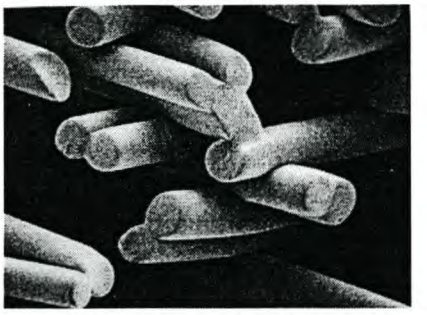

(d) Wound graft (X) Wilson [2]

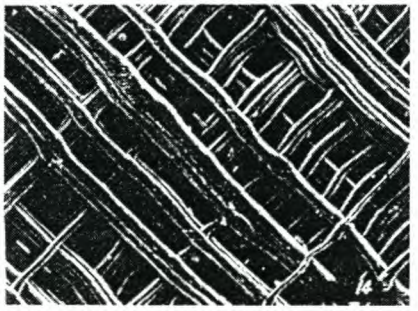

(e) Wound graft (L) Leidner [3]

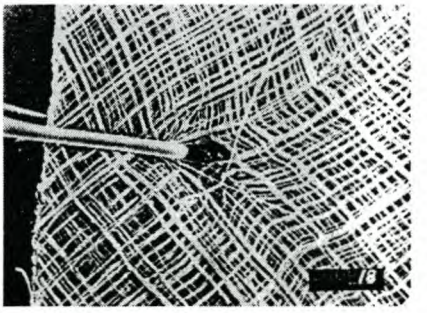

(f) Wound graft (A) Leidner [3]

(g) Vascugraft (L) Zhang [4]

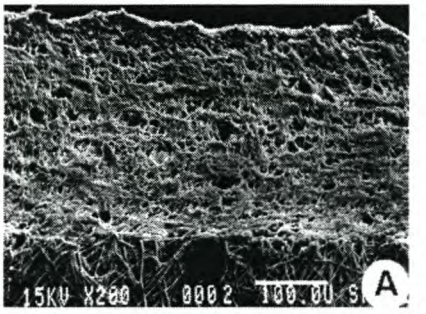

(h) Vascugraft (X) Lamba [12]

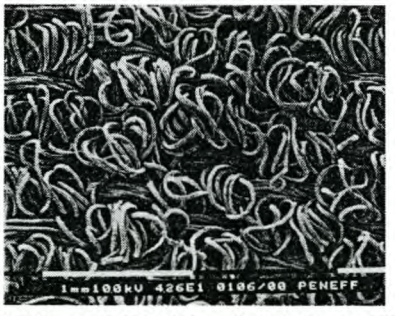

(i) Woven PU/PET graft (A) Gupta [5]

(j) Woven PU/PET graft (L) Gupta [5]

Figure 5.1: Fibrillar polyurethane grafts.
L=lumenal surface; A=ablumenal surface; X=cross-section; 3D=three-dimensional reconstruction

Stellenbosch University http://scholar.sun.ac.za

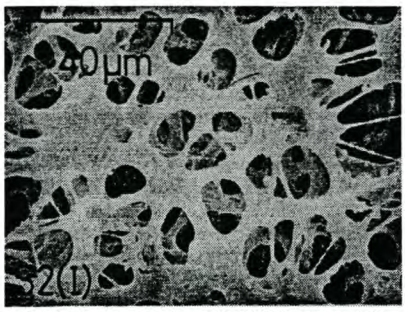

(a) Dip-coated graft (L) Lamba [6]

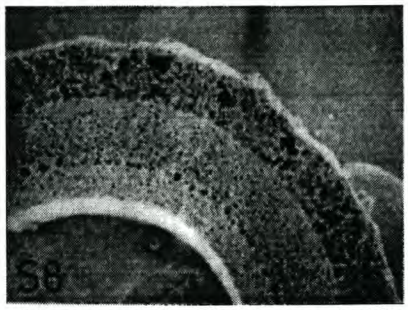

(b) Dip-coated graft (X) Hayashi [6]

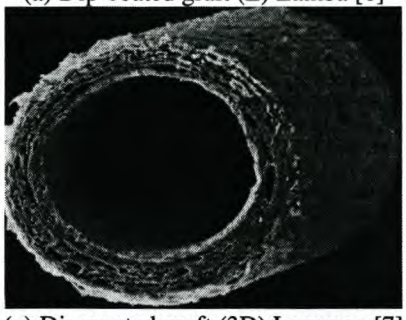

(c) Dip-coated graft (3D) Lommen [7]

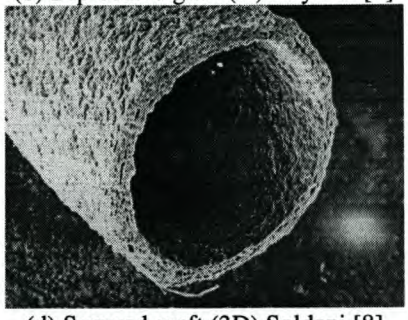

(d) Sprayed graft (3D) Soldani [8]

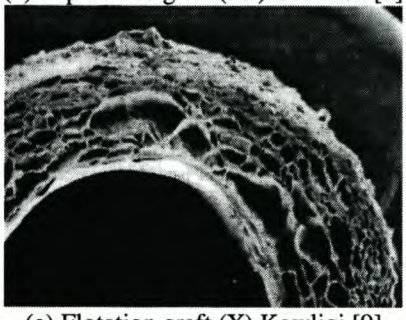

(e) Flotation graft (X) Kowligi [9]

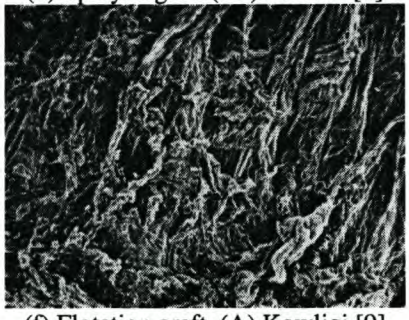

(f) Flotation graft (A) Kowligi [9]

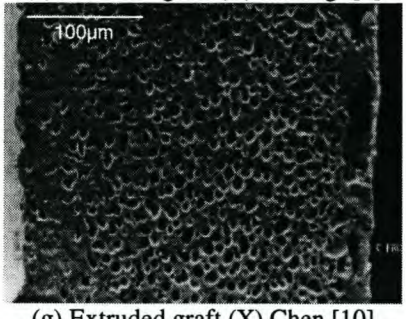

(g) Extruded graft (X) Chen [10]

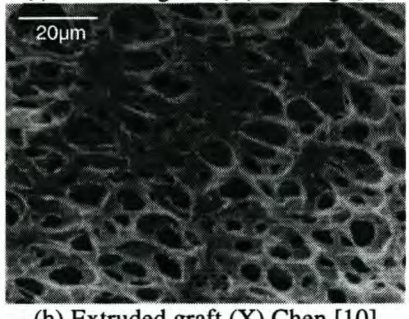

(h) Extruded graft (X) Chen [10]

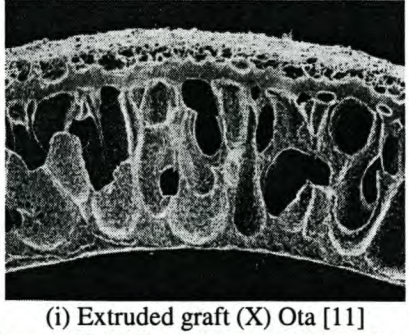

(i) Extruded graft (X) Ota [11]

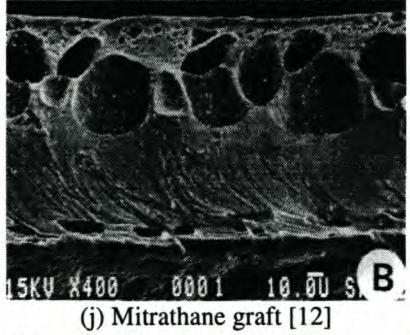

(j) Mitrathane graft [12]

Figure 5.2: Polyurethane grafts produced by phase precipitation without the addition of porogens.
L=lumenal surface; A=ablumenal surface; X=cross-section

Stellenbosch University http://scholar.sun.ac.za

5.2.2.2 Reticulated foam grafts

A number of processes have been evaluated for suitability in the production of grafts containing larger pores (than those obtainable by phase precipitation alone). The first vascular grafts of this nature were produced in the early 1970s by fashioning existing porous polyurethanes into tubular structures. Examples of these grafts include grafts produced from BF Goodrich VC sponge [13] and grafts prepared by rolling a reticulated sheet (Scottfoam®) into a tubular structure [14]. Figure 5.3 shows the structures of Scottfoam before and after reticulation (heat treatment to transform a closed-celled foam into an open-celled structure).

(a) Unreticulated Scottfoam (b) Reticulated Scottfoam

Figure 5.3: Structure of Scottfoam in its unreticulated and reticulated forms. [14].

5.2.2.3 Replamineform grafts

"Replamineform", an ingenious process by which the microstructure of sea urchin spines is replicated, was used to yield PU grafts with interconnected (open-cell) structures. A wide variety of pore sizes could be achieved by using the spines of different sea urchins, and although fault-lines present in the calcite structures could be eliminated to a certain degree, laborious machining processes were involved in this process. Figure 5.4 shows examples of machined spines (a), a cuboid section showing the pore structure (b), and a close-up view of the porosity (c).

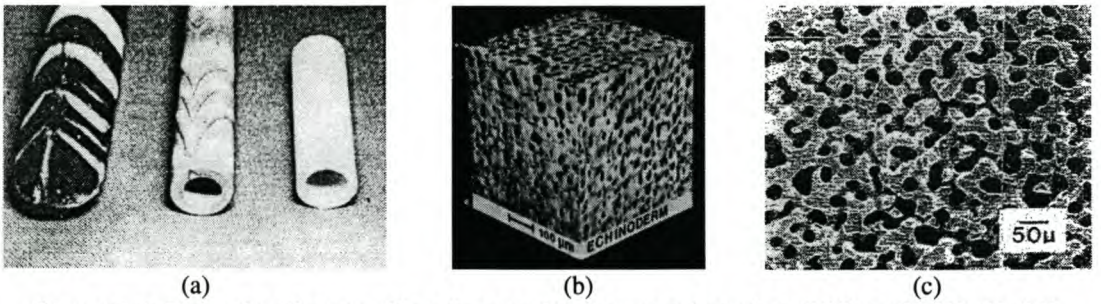

(a) (b) (c)

Figure 5.4: Examples of sea-urchin spines used in the manufacturing of PU grafts [12, 15, 16]

5.2.2.4 Phase-precipitated grafts with extracted porogens

Large pores (typically 25-150µm) can also be introduced by the inclusion of extractable porogens to the PU solution prior to precipitation. The porogens (typically salt crystals) are added to the polymer solution and extracted concurrent with, or subsequent to, the precipitation of the polymer. A macroporosity of roughly the dimensions of the porogen is thereby superimposed on the microporosity achieved by the phase-inversion process. Depending on the conditions used during processing, the macropores may be either open or closed. The ChronoFlex® vascular access graft (VAG) graft depicted in Figure 5.5 is an example of the structure obtainable by this method. It was produced by the extrusion of a polyurethane solution

Stellenbosch University http://scholar.sun.ac.za

containing suspended salt particles onto a mandrel and subsequently precipitating the polymer and extracting the salt.

Similar structures were obtained by Kambic [17], Murabayashi [18] and Uchida [19], who used a dip-coating method to apply the paste to the mandrel.

(a) Cross section (b) Unreinforced graft (c) Reinforced graft

Figure 5.5: Scanning electron micrographs of the ChronoFlex vascular graft made by phase inversion of polyurethane solutions containing extractable porogens. [12, 20, 21]

The dip-coating process was also employed by der Lei [22] and Hinrichs [23] to fabricate the experimental grafts from PU/PLA blends (Figure 5.6). Porosity gradients may be achieved by altering the porogen size and/or loading in successive coatings.

(a) van der Lei [22] (b) Hinrichs [23]

Figure 5.6: Polyurethane grafts produced by phase inversion of PU/PLA solutions containing extractable porogens.

5.3.2.5 Other PU grafts

Two more methods of creating macropores in polyurethane structures merit further discussion. Doi et al. [24] used laser ablation techniques to create transmural, cylindrical pores in solid polyurethane tubes produced by dip-coating followed by air drying (Fig 5.7a). The final method, employed by Kowligi et al. [25], involves the deposition of a polyurethane solution with pressurized nitrogen gas, followed by drying at elevated temperatures. A vascular graft containing large, closed pores is thus produced (Fig 5.7b).

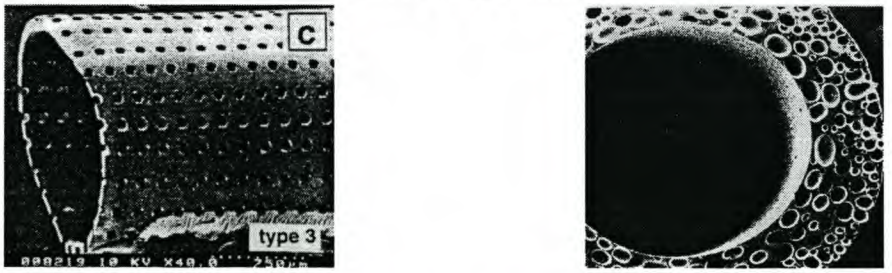

(a) Laser perforation [24] (b) Nitrogen blowing [25]

Figure 5.7: Polyurethane grafts produced by (a) laser perforation of dip-coated polyurethane tubes and (b) spraying with nitrogen.

Stellenbosch University http://scholar.sun.ac.za

5.2.3 Contemporary polyurethane grafts

The Corvita® graft (Corvita Corp., Miami FL) is a helically-wound graft (Chronoflex AR wound at 45°) [26] that contains a sealed external PET mesh (Fig. 5.8a,b). The process is thought to be based on the methods of Leidner [3].

Two companies have used phase inversion to produce vascular grafts. The Thoratec® graft (Thoratec Lab Corp., Berkeley, CA) was produced by a multilayer casting technique, whereby material was sequentially added to a rotating/transversing mandrel. The graft contained an impermeable layer (sandwiched between two porous layers of varying porosity) and helical, reinforcing monofilaments within the wall (Fig 5.8 c,d). The Pulse-Tec® (Newtec vascular products Ltd., Clwyd, UK; now Polymedica Industries Inc., Woburn, Mass) has a higher and more irregular porosity than the Thoratec® graft. It contains a skin on both the lumenal and ablumenal surfaces, with porosities much lower than in the bulk (Fig 5.8e,f). The exact conditions used in the production of these two proprietary grafts (i.e. whether porogens were used) are not known to the author.

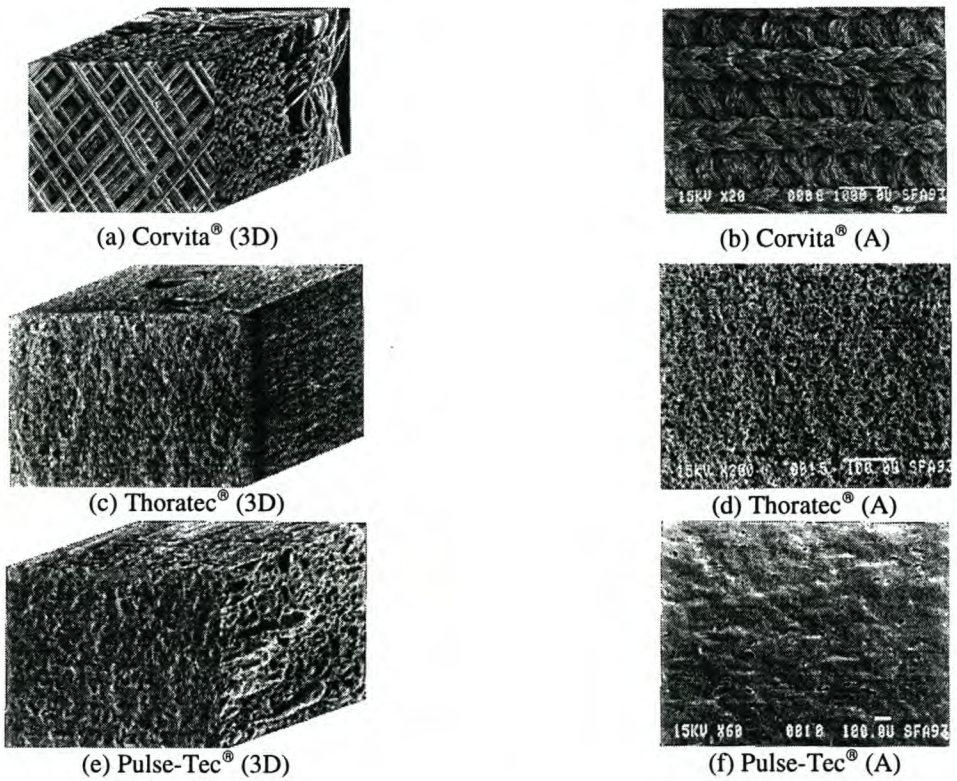

Figure 5.8: Contemporary polyurethane grafts produced by Corvita Corporation, Thoratec Laboratries and Newtec vascular products. [26] A=ablumenal surface; 3D=three-dimensional reconstruction

5.2.4 PU graft porosity

The size of voids or pores in vascular grafts, i.e. the spaces between adjacent fibres (fibrillar grafts), the microvoids resulting from the phase-inversion process, or the macrovoids resulting from extracted fillers or other porosifying agents, are not always readily quantified. This can be attributed to the irregular and ill-defined shape of these spaces. It is, however, possible to give a semi-quantitative account of these pore sizes (as measured by researchers).

For fibrillar grafts, the pore size depends on the fibre thickness, the winding angle used during fabrication, the regularity of the deposition and extent of coagulation of fibres in the melt or

Stellenbosch University http://scholar.sun.ac.za

solution. Although these parameters may be readily varied, the fibre size is usually limited by other considerations (if the fibres are too thick, the graft will be stiff and drapability will be compromised). Thus, fibres ranging from 1-30μm were reported [1, 27], with resultant pore sizes the pore sizes in the 10-60μm range [1, 26-28]. Leidner [27] gave a detailed theoretical analysis of the effect of wind angle on pore size, and further reported a volumetric porosity of 60% (the percentage of volume occupied by pores).

Phase precipitation (without the inclusion of extractable porogens) has been shown to lead to a variety of structures, and may thus lead to the formation of pores with various shapes and sizes. Apart from the ±100μm closed pores produced in the outer layer of the Mitrathane graft [29], micropore sizes are generally smaller than 15μm [6, 10, 26, 29].

The addition of extractable porogens offers the opportunity of increasing the porosity of grafts prepared by the phase-inversion technique. Pores of 30-75μm [23], 40μm [17, 18] and up to 200μm [30] have been obtained by the use of suitable porogens. A pore-size gradient (10-100μm) has also been achieved by changing the size of the porogen in successive layers used to build up a graft [22].

The ability to produce foam-type structures of various pore sizes by the use of the replamineform process was discussed in section 5.2.2.3. Although the vascular graft produced by Hiratzka [15] contained pores ranging from 18 to 25μm, this process has been applied to the fabrication of square samples containing distinctly different pore sizes (18-28, 30-45, 75-95, 60-120 and 120-180μm).

The closed-cell foams produced by Kowligi [25] by solution spraying and nitrogen expansion contained the largest reported pore (up to 475μm). These pores were, however, not intercommunicating. The pore sizes obtainable by the use of pre-existing reticulated foams naturally depend on the processing conditions used. Besides the observation that pore sizes of the Scottfoam used by Berkowitz et al. had a pore size of 190-250μm [14]), these foams will not be discussed further.

5.2.5 Mechanical properties

One of the main driving forces behind the control of porosity was the effect that pore shape and size have on the mechanical properties of grafts. Graft compliance is, however, also dependent on a number of other factors such as material properties, wall thickness, the presence of solid layers or skins and reinforcing structures. The methods used to measure the compliance of vascular grafts are also not standardised [31]. For these reasons, a direct comparison between the compliances of grafts made by different techniques is not always meaningful.

It may be said, however, that a wide range of compliances, ranging from levels lower than that of the intended host artery to levels far exceeding that value, may be produced by all of the methods discussed thus far. Diameter-compliance values, for example, range from 5% [32] to 49.5%/100mmHg [18] for grafts produced by phase inversion and porogen extraction, whereas phase inversion alone (without porogen incorporation/extraction) yielded grafts, in two cases, with compliances of 1.4-2.4% [29] and 4.2-9.5%/100mmHg [10].

A more meaningful comparison may be drawn between grafts evaluated in the same study. Eberhart et al. [26] compared the Corvita®, Thoratec® and Pulse-Tec® grafts in a recent review on the properties of these three commercially available PU grafts, and found their static diameter-compliances to be 1.2-1.9, 2.1-3.1 and 2.5-3.5 %/100mmHg respectively. A full chronological summary of vascular grafts produced over the past 30 years, including production methods, porosities, mechanical properties and in vivo evaluations is presented in Table 5.1.

Stellenbosch University http://scholar.sun.ac.za

Table 5.1: Chronological listing of polyurethane grafts, showing manufacturing methods, properties and in vivo assessment.

Reference Author ID ;Wall (mm)	Material	*Designation / trade name (manufacturer)* Fabrication Method	Pore structure; Porosity (P_V) Pore size (μm): P_x, P_i, P_o Pore area (%): P_{Ax}, P_{Ai}, P_{Ao} Water Perm (ml/min/cm$_2$)	Mechanical Properties E_{100}, ε_b, σ_b, β, C_D, C_V, E_p, SR, P_b, E_{circ}, E_{long}	In vivo assessment	Year
[13] Marinescu 6.8-12 ;	BF Goodrich PU	*Preformed foam* Graft fabricated from BF Goodrich VC sponge	N/A	N/A	7.6 to 10 year dog aortic implants (n=9) 4-7cm 100% patency rates. Fully endothelialized. Slight to no dilation.	1971
[14] Berkowitz 8 ; 300μm	Scottfoam	*Preformed foam* Reticulated foam glued to Dacron (knit/felt) and fashioned into tube	Open cell foam P_x = 190-250μm	N/A	7-240 day dog infrarenal aorta interposition (n=25) 3.8cm Pseudointimal lining (290μm formed) Full EC coverage assumed but not confirmed	1972
[15] Hiratzka 6; 1	Bioelectric polyurethane (BEP)	*Replamineform* Impregnation of PU into porous tubes fashioned from sea-urchin spines	Open cell foam P_x=18-25μm P_V=32%	N/A	1-32 week dog infrarenal aorta implants (n=24) 3cm 100% patency rate Full endothelialization after 8wks (3cm grafts) Minimal inflammatory response	1972
[33] White 4; 1	Bioelectric PU (BEP); Biomer	*Replamineform* Impregnation of PU into porous tubes fashioned from sea-urchin spines	N/A	N/A	3-15 day dog carotid and femoral implants (n=10) 3cm 90% patency rate Well-formed neo-intima	1976
[34] Lyman 4 ;	PEUU MDI/PPO/EDA	*Dip coating sans porogen* 7-10% PU in DMF; phase inversion, PET reinforcing sock	WP=67	DMA results given	10-111 day dog femoral. 33% patency rate (n=9) 5cm No loss of compliance after implant (patent grafts). Hypertrophic healing at anastomoses (occluded grafts)	1977
[1] Annis, 10 ; 0.65	PEU MDI/PTMEG/ BDO	*Electrostatic spinning* 12.5% PU (DMF/Butanone) ejected near charged rotating mandrel.	Fibrous mesh (1-1.6μm fibres) P_x=10μm ρ=280 WP=25	σ_b=4.9MPa ε_b =400 % SR=4N E_Y=1.1MPa	1-12 month pig thoracic aorta interposition (n=52) 8cm 4 early graft related failures 100% patency 1.5cm pannus	1978
[35] Lyman, 1978 4 ;	Biomer	*Dip coating sans porogen* 7-10% PU in DMF; phase inversion; PET reinforcing sock	N/A	N/A	2-77 day dog aortic and femoral implants (5+5) 6/9 compliant grafts patent vs. 0/7 for non-compliant controls.	1978
[7] Lommen, 1.5 ; 0.7	PU/PLA blend	*Dip-coating sans porogen* PU/PLA solution coated onto mandrel; phase inversion	Ill-defined foam P_x = 40-50μm	N/A	3/6/12 week rat aorta interposition (n=18) Complete EC lining, elastogenesis 100% patency	1983
[2] Wilson 10 ; 0.5	Pellethane 75D	*Fibre winding* PU fibres spun from DMF solution; wound on rotating mandrel; evaporation	Fibrous mesh	E_{circ}=12.1-14.5MPa E_{long}=0.309-0.507MPa	3month-1year dog infrarenal aorta interposition (n=8+6) 5cm 100% patency (6months) 0.2μm neo-intima with slight thickening at anastomoses (hyperplasia)	1983
[3] Leidner 4-10 ; 0.82-0.86	Pellethane	*Fibre winding* Winding of fibres (molten PU or PU solution) wound on rotating mandrel; evaporation	Fibrous mesh (13-30μm fibre) Detailed pore size calc P_x=21-120μm P_V=60%	Detailed information on wind-angle vs. properties	3 month dog aorta and carotid artery (n=1+1) 5cm Outer encapsulation Smooth glistening neo-intima formed	1983
[36] Hess 1.6	PU	*Vascugraft®* Fibres spun from PU solution spun with air pressure onto rotating mandrel; evaporation	N/A	N/A	1-25 month rat aorta interposition (n=47) 1cm Time course description of healing Full endothelial covering by 12 weeks. Neo-media with circularly arranged SMC	1983

Stellenbosch University http://scholar.sun.ac.za

Reference Author ID ;Wall (mm)	Material	*Designation / trade name (manufacturer)* Fabrication Method	Pore structure; Porosity (P_V) Pore size (μm): P_x, P_i, P_o Pore area (%): P_{Ax}, P_{Ai}, P_{Ao} Water Perm (ml/min/cm$_2$)	Mechanical Properties E_{100}, ε_b, σ_b, β, C_D, C_V, E_p, SR, P_b, E_{circ}, E_{long}	In vivo assessment	Year
[17] Kambic 4 ; 0.6	Biomer Tecoflex 80A Heksyn Siloxane	*Dip coating with porogen* PU soln in DMAC containing NaCl coated onto mandrel; evaporation; porogen extraction	Salt cast foam P_A=3.5-40μm Impermeable to cells	ε_b=70 %	GA crosslinked gelatin impregnated grafts 3d-6m dog carotid implants (n=30) 5cm Psuedo-neointima formed after 6 months.	1984
[37] Ives, 5.5 ;	PEUU	*Mitrathane® graft (type 1)* Phase inversion (sans porogen)	Microporous foam		Dog femoral and iliac implants (n=14) All femoral occluded after 4 weeks 3/5 patent after iliac implants	1984
[18] Murabayashi	Biomer	*Dip coating with porogen* 10% PU in DMAC containing 1:2 to 1:10 salt/PU NaCl (<37μm); phase inversion; extraction	Ill-defined open porosity P_x < 40μm	C_D=49.5 C_D=3-4 (biolized))	Biolized grafts: Gelatin impregnation 3day-13month dog carotid (n=30) 5cm 77% patency (1month) Unhealed psuedo-intima formed.	1985
[11] Ota	Mitrathane clone	*Solution extrusion* Tube drawn from PU solution; phase inversion	Lumenally skinned foam WP = 0 IC = 15-26% (200 - 300mmHg)	P_b > 500mmHg	1-12 week dog carotid interposition (n=10) membranous surface covering; anastomotic hyperplasia. Limited clinical VAG trial for puncture resistance: bleeding stops <5min	1987
[22] van der Lei 1.5 ; 0.3	PU/PLA blend	*Dip coating with porogen* PU/PLA solution in DMAC containing NaCl; evaporation; extraction	Ill-defined foam P_V = 10-100μm gradient		1h-12 week rat abdominal aorta interposition (n=28) 1cm Transanastomotic neo-intima formation. Circularly arranged SMC after 12 wks (growth from media of aorta)	1987
[29] Martz 3-8 ;	PEUU	*Mitrathane® graft (type 1)* Phase inversion (sans porogen)	3 layer foam P_x(outer): 100μm closed cell P_x(middle): no voids P_x(inner): 10-0μm	C_V=2.8-4.8 σ_b=9.3MPa	N/A	1987
[9] Kowligi 3-5 ; 0.55-1	Surethane	*Foam flotation* 2-5% PU solution in DMAC sprayed onto water surface with N_2; rolled onto mandrel	Ill–defined foam WP = 0-6.65	σ_b=0.05-2.3MPa ε_b=150-600 %	N/A	1988
[25] Kowligi 3-6 ; 0.5-1.2	Tecoflex 80A	*Solution spraying* PU solution sprayed onto rotating mandrel with N_2; evaporation	Closed cell foam P_x = 13-475μm	SR=8N (4/0, 1mm) C=4.9	N/A	1988
[38] Muller-Glauser 4 ;	PU/Siloxane copolymer	N/A	Microporous foam	σ_b=4.9MPa C_D=13.2 PB>5 bar	Pre-lined with EC 24 hour dog arteriovenous shunts. No thrombus.	1988
[39] [Underwood 4 ; 1	N/A	N/A	N/A	N/A	3-7 month sheep carotid (n=21) 6cm 100% patency (0-3 months) 78% patency (3-7 months)	1988
[6] Hayashi 3 ; 0.8	PU MDI/PTMEG Siloxane/EDO	*Dip Coating sans porogen* PU solution coated on mandrel; phase inversion; PET felt outer reinforcement	Open cell foam P_x=7-9μm; P_{Ax}=35-40% WP=34-58	E_{100}=0.6-0.8 kPa σ_b=3.9-4.6 kPa β=22.9	N/A	1989
[40] Kogel	PU	*Vascugraft® (B. Braun Melsungen)* Fibres spun from PU solution spun with air pressure onto rotating mandrel; evaporation	Fibrous mesh	N/A	1week-12month dog vena cava implants (n=11) 6cm 43% patency at 12 months	1989

Stellenbosch University http://scholar.sun.ac.za

Reference Author ID ;Wall (mm)	Material	*Designation / trade name (manufacturer)* Fabrication Method	Pore structure; Porosity (P_V) Pore size (μm): P_x, P_i, P_o Pore area (%): P_{Ax}, P_{Ai}, P_{Ao} Water Perm (ml/min/cm$_2$)	Mechanical Properties E_{100}, ε_b, σ_b, β, C_D, C_V, E_p, SR, P_b, E_{circ}, E_{long}	In vivo assessment	Year
[41] Kogel	PU	*Vascugraft® (B. Braun Melsungen)* Fibres spun from PU solution spun with air pressure onto rotating mandrel; evaporation	Fibrous mesh	N/A	6-12 week dog infrarenal vena cava implants (n=12) 6cm Neo-intimal pannus (2-3cm) No transmural EC ingrowth	1989
[42] Uchida	Biomer	*Dip coating with porogen* PU solution with salt crystals salt coated onto mandrel; phase inversion; extraction	Macroporous foam	C_D=13.5	N/A	1989
[43] Therrien 5;	PEUU	*Mitrathane® graft (2)* Electrostatic spinning	Fibrous mesh	N/A	(2) 24hour-6month dog infrarenal aortic implants (n=8) Thin inner capsule Infiltration of blood elements	1989
[44] Brothers 4.8 ;	Estane 5714	*Dip coating with porogen* PU solution with salt crystals coated onto mandrel; phase inversion; extraction	Macroporous foam P_V=70% WP=30	230% dilation (6months)	6 month dog end-to side infrarenal aorta and external iliac. Aneurismal dilation detected. 75% patency (n=8). Higher thrombogenicity that ePTFE (59% vs. 22%)	1990
[28] Wilson	Corethane	*Fibre winding* PU fibres spun from DMAC solution onto rating mandrel; warp knit PET outer reinforcing	Fibrous composite P_x = 30-60μm (inner)		Gelatin ± heparin filled 1-12 m dog femoral interposition (n=20) 5cm 100% patency (n=10) vs. 60% for non gelatin/heparin filled controls (n=10)	1991
[8] Soldani 1.5 ; 0.3	PU blend with PAAc, PAAm, PVAL, collagen, etc	*Solution spraying* Spraying of PU solution onto mandrel; phase inversion	Ill-defined foam	N/A	N/A	1991
[23] Hinrichs 1.3-1.5 ; 0.3-0.6	Various PU/PLA etc blends	*Dip coating with porogen* PU solution with citrate crystals coated onto mandrel; evaporation; extraction	Ill-defined foam Px=30-75μm ρ=0.11-0.31 P_V=70-90%	F_{100}=0.5-1.9 (long) σ_b andε_b after implant	6 week rat abdominal aorta interposition 1cm 12 types of prosthesis implanted (n=3) 100% patency	1992
[45] Huang, 3 ; 0.7	PU	*Vascugraft® (B. Braun Melsungen)* Fibres spun from PU solution spun with air pressure onto rotating mandrel; evaporation	Fibrous mesh	N/A	1-12 week peritoneal cavity in rats (n=24) FBGC surrounding prostheses. Cellular penetration (fibroblasts) limited to outer portion.	1992
[46] Hess 3	PU	*Vascugraft® (B. Braun Melsungen)* Fibres spun from PU solution spun with air pressure onto rotating mandrel; evaporation	Fibrous mesh	N/A	1.5week-53month dog carotid / femoral implants (n=72) Complete transanastomotic endothelialization after 6 months (3cm)	1992
[47] Hess 3mm ;	PU	*Vascugraft® (B. Braun Melsungen)* Fibres spun from PU solution spun with air pressure onto rotating mandrel; evaporation	Fibrous mesh 1μm fibres	N/A	Fibronectin coating / gelatin coating Grafts pre-seeded with EC in vitro No implants	1992
[30] Williams 4 ;	Terathane 2000 + MDI/EDA	*Dip coating with porogen* PU solution with salt crystals extruded into water; phase inversion; extraction	3 layer foam outer: mid: ±100-200μm inner: 0.5μm WP=50	ε_b =930%	Grafts pre-seeded with EC in vitro (n=9) 6cm 5 week dog carotid interposition. 67% patency (6/9) Multicellular lining on lumen formed (detached after 5 weeks)	1992

Stellenbosch University http://scholar.sun.ac.za

Reference Author ID ;Wall (mm)	Material	*Designation / trade name (manufacturer)* Fabrication Method	Pore structure; Porosity (P_V) Pore size (μm): P_x, P_i, P_o Pore area (%): P_{Ax}, P_{Ai}, P_{Ao} Water Perm (ml/min/cm$_2$)	Mechanical Properties E_{100}, ε_b, σ_b, β, C_D, C_V, E_p, SR, P_b, E_{circ}, E_{long}	In vivo assessment	Year
[48] Gershon	Lycra + Pellethane	*Fibre winding* Lycra fibres wound onto mandrel after coating with Pellethane matrix	N/A	N/A	N/A	1992
[49] Cohn - ; 0.44	Lycra + Pellethane + PELA	*Fibre winding* Lycra fibres wound onto mandrel after coating with Pellethane/PELA matrix	P_x= 0 (initial) P_x= 50μm (1 week)	PB>1000mmHg SR = 6.5-18.6N C=2,5% initial	90 day dog carotid implants (n=13) 6cm 12/13 patent (same as ePTFE controls) Smooth glistening neo-intima formed	1992
[50] Guidoin	PU (Mitrathane1; Mitrathane 2)	*Vascugraft® (B. Braun Melsungen)* Fibres spun from PU solution spun with air pressure onto rotating mandrel; evaporation	Fibrous mesh	N/A	N/A	1992
[19] Uchida 4 ; 0.5	Biomer	*Dip coating with porogen* 15% PU solution with salt crystals (6:1) coated onto mandrel; phase inversion; extraction	Macroporous foam	C_D = 10.3 Decrease with implant time	Gelatin sealed grafts (n=14) 5cm 6 wk dog carotid implants 64% patency (vs. 50% for non-compliant controls)	1993
[51]	Tecoflex	*Univ of Texas-Arlington graft (UTA)*			N/A	
[52] Stansby	Chronoflex	*Pulse-Tec® graft* Low temp phase inversion	Open cell foam	C_D= ±6	No implant. EC lining in vitro	1994
[12, 32] Edwards 5-6 ; 0.9	Chronoflex	*Extrusion with porogen* PU solution with salt crystals extruded into water; phase inversion; extraction	Macroporous foam, skinned P_V=70% Wp< 5	σ_b=2.14 kPa C_V=5-10% SR > 2.5N	6 week dog carotid interposition 24wk patency = 50% (n=4) Neo-intimal lining	1995
[24] Doi 2 ; 0.1	Cardiomat 610	*Laser ablation* Dip coating of solution on mandrel; evaporation Laser holes	Translumenal cylindrical holes PA = 3.4 – 13.6% # = 6-24 / circumference	β=37.7-80.5	N/A	1996
[53] Poole-Warren 4 ;	Polycarbonate-urethane	*Fibre winding (Vascugraft®)* Fibres spun from PU solution spun with air pressure onto rotating mandrel; evaporation	Fibrous structure	N/A	Grafts prelined with EC. 1-6 week ovine carotid implants. 4cm Slightly higher patency of seeded vs. control grafts. Decrease in EC coverage before recovery to 80% at 3wks.	1996
[54] Allen	Thoralon	*Thoratec® VAG graft (Thoratec Lab)*			Multicentre VAG clinical trial (n=145) 44.9% primary patency (1yr) 64.5% secondary patency (1yr) Graft loss: thrombosis (17%) and infection (11%)	1996
[55] Marois	PU	*Vascugraft® (B. Braun Melsungen)* Fibres spun from PU solution spun with air pressure onto rotating mandrel; evaporation	Fibrous mesh		4-6 month dog abdominal aortic bypass Low thrombogenicity towards platelet and fibrin deposits Breaks in microfibrous structure observed	1996
[5] Gupta 4-6 ; 0.42-1.23	PU and PET Fibres 8-9 tex	*Fibre weaving* PU and PET fibres woven into textile graft	Open woven WP=0.18-2.06	E_p=61-88 kPa β=4.8-7.8 C_V=0.31-0.43	1-12 month dog carotid interposition thin internal layer, no thrombus EC coverage	1997
[56] Akiyama	Chronoflex	*Corvita® graft (Corvita Corp)* Filament wound Sealed external PET mesh			3-6 month dog abdominal aorta 100% patency (6 months) vs. 50% for ePTFE controls Intimal thickening less than ePTFE controls	1996

Stellenbosch University http://scholar.sun.ac.za

Reference Author ID ;Wall (mm)	Material	*Designation / trade name (manufacturer)* Fabrication Method	Pore structure; Porosity (P_V) Pore size (μm): P_x. P_i, P_o Pore area (%): P_{Ax}, P_{Ai}, P_{Ao} Water Perm (ml/min/cm$_2$)	Mechanical Properties E_{100}, ε_b, σ_b, β, C_D, C_V, E_p, SR, P_b, E_{circ}, E_{long}	In vivo assessment	Year
[4] Zhang 5-16 ;	Polycarbonate urethane	Fibres spun from solution onto rotating mandrel	Fibrous mesh	N/A	21-358 day human femoral-popliteal interposition (n=4) 3-5cm All failed due to thrombosis Withdrawn by B Braun Melsungen	1997
[10] Chen 4.9-5.2; 0.16-0.39	Segmented polyether urethane	*Solution extrusion sans porogen* Tube drawn from PU solution; phase inversion	Microporous foam P_V=20-44% P_x =±10μm	C_{Dstat}=4.2-9.5 C_{Ddyn}=4.4-9.7	N/A	1999
[26] Eberhart	Chronoflex	*Corvita® graft (Corvita Corp)* Filament wound Sealed external PET mesh	Fibrous mesh 10-15μm interconnected pores fibre spacing = 24-200μm wind angle = 45°	C_{Dstat}=1.2-1.9 @40mmHg C_{Dstat} =2.4-2.5 @ 200mmHg	N/A	1999
[26] Eberhart	Thoralon	*Thoratec® VAG graft (Thoratec Lab)* Low temperature coagulation of material sequentially added to rotating/transversing mandrel	Micoporous foam P_x=15μm solid middle layer (70μm) helical reinforcement (200μm)	C_{Dstat}=2.1-3.1 @40 C_{Dstat} =1.8-2.2 @ 200mmHg	N/A	1999
[26] Eberhart	Chronoflex	*Pulse-Tec® graft (Newtec Vasc Prod)* Low temp phase inversion	Micoporous foam Inner: 28-140μm pores Outer: 28μm pores Surfaces skinned	C_{Dstat} =2.5-3.5	N/A	1999
[57] Farrar 2.5-3mm	Thoralon	*Aria® CABG graft*			Clinical CABG trials (27 patients) Data incomplete: So far no device related serious injury, symptom free	
[21] Tai	PU MDI/PCDO EDA	*ChronoFlexc® graft* Low temperature coagulation of PU solution containing porogens	Micoporous foam	C_D=8.1 β=20	N/A	2000

P_V = Porosity by volume (%)	E_{100} = 100% modulus	C_D = Diameter compliance	EC = Endothilial cell
P_x. = Pore size (cross-section)	E_{circ} = Circumferential modulus	C_V = Volumetric compliance	CABG = Coronary artery bypass graft
P_i,= Pore size (inner surface)	E_{long} = Longitudinal modulus	C_{dyn} = Dynamic compliance	VAG = Vascular access graft
P_o = Pore size (outer surface)	σ_b = Stress at break	C_{stat} = Static compliance	PET = Polyethylene teraphthalate
P_{Ax}, P_{Ai}, P_{Ao} = pore area	ε_b = Extension at break	SR = Suture retention force (N)	DMF = Dimethyl formamide
WP = Water Permeability (ml/min/cm$_2$)	β = Stiffness parameter	PB = Burst pressure	DMAC = Dimethyl acetamide

Stellenbosch University http://scholar.sun.ac.za

5.2.6 Scope

In this study some of the historical methods used for foam-type scaffold production (including both solution and melt techniques) are described and alternate approaches evaluated. This was done in an effort to produce vascular grafts and porous scaffolds containing well-defined interconnected porosities (approximating pentagonal dodecahedra). These approaches may be sub-classified according to:

- The technique used to process the polymer, i.e. solution or melt processing,
- The porosifying agents used, i.e. particulate porogens, fibrous porogens or blowing agents,
- The technique by which the porosifying agents and polymers were combined, i.e. premixing of polymer solution (or polymer melt), infiltration of polymer solution into a packed column of porogen,
- The shape and size of the porogen, and
- The various parameters that influence the phase-inversion process or melt extrusion process

The following organizational chart is useful to distinguish the different techniques evaluated in this study:

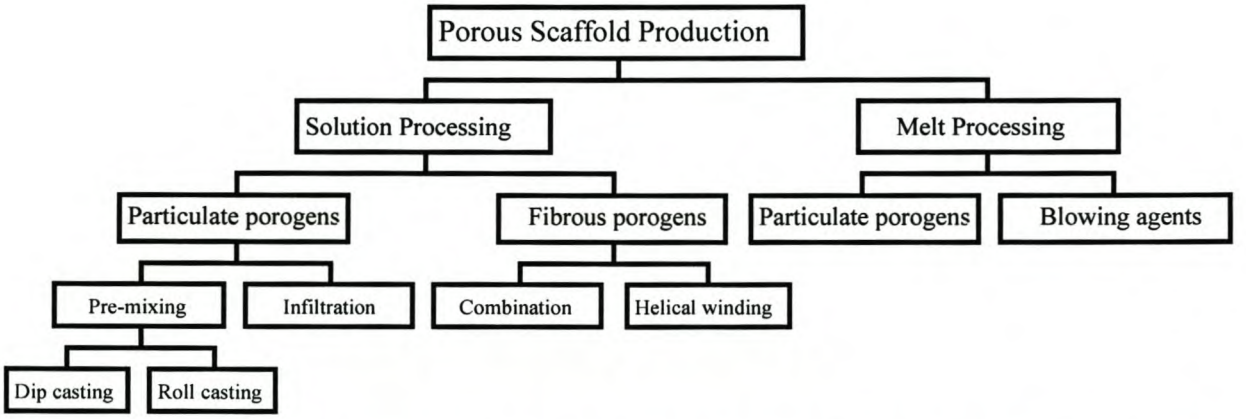

Figure 5.9: Organizational chart illustrating the techniques used to evaluate the effect of processing conditions on the structure of porous scaffolds.

Stellenbosch University http://scholar.sun.ac.za

5.3 Materials and methods

Two techniques were used to incorporate particulate porogens in polymer solutions, with the goal of producing foam-type structures:

- **Pre-mixing:** This method consisted of premixing the porogen and polymer solution to form a paste that is subsequently formed into the desired shape. This method of porogen incorporation was used in the production of *dip-cast grafts* and *roll-cast grafts*.
- **Infiltration casting**: In this method the porogen is pre-packed into a mould of the desired shape and the polymer solution infiltrates the interstices between the individual particles. *vacuum/pressure-cast rods* and *vacuum/pressure-cast grafts* were produced by this method.

Two methods for the incorporation of fibrous porogens, with the goal of creating synthetic grafts with interconnected helical channel porosities, were also evaluated:

- **Combination casting**: This is achieved by incorporating of soluble fibre into roll cast grafts to produce a structure containing both open pores and helical channels (*combination grafts*).
- **Helically Winding**: This method involved the coating of water-soluble fibres with a polyurethane solution and winding the coated fibre onto a mandrel to produce *helically-wound grafts*.

Two further methods, based on the melt extrusion techniques, were also evaluated:

- **Melt extrusion/porogen extraction:** Particulate fillers were compounded with polymer melts, extruded into tubes, and subsequently extracted to form *melt-extracted grafts*.
- **Melt extrusion/blowing agents**: Chemical blowing agents were used in this method to create pores in melt-extruded tubes (*melt-blown-grafts*).

5.3.1 Porogen properties

5.3.1.1 Porogen types

The three types of particulate porogens evaluated in this study were: sodium bicarbonate crystals (Saarchem Holpro, RSA), hydroxyapatite beads (Biorad) and custom-made gelatin microspheres (Thies Technologies, St Louis, USA). All porogen types were dried in vacuo (-700mmHg, RT, 48h) before use, to remove traces of water that could initiate the precipitation of the polymer solution during scaffold manufacture. The bicarbonate salt and gelatin beads were sieved to obtain fractions of the desired size range while the hydroxyapatite beads, due to high cost and limited original size fraction available, were used without further size classification. In addition to the particular porogens described above, water-soluble fibrous porogens were obtained for use in the production of vascular grafts containing oriented helical channels as opposed to the foam-type structures prepared with particular porogens. Soluble poly(vinyl alcohol) (PVAL) fibres (Sanyo ML45, 45 denier), nominal diameter 85μm, were used in the winding process.

5.3.1.2 Particulate porogen size fractionation

Fractionation of the porogens to the desired size fractions was achieved by passing them through graded sieves of known mesh sizes. The relationship between mesh size and sieve opening is illustrated in Figure 5.10.

Stellenbosch University http://scholar.sun.ac.za

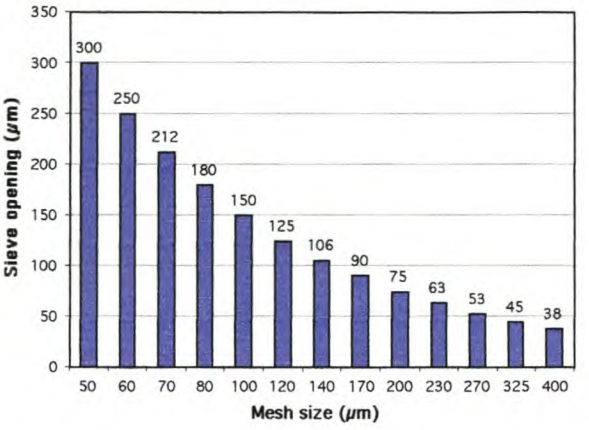

Figure 5.10: Mesh sizes and corresponding sieve openings for a series of standard sieves

5.3.1.3 Porogen size determination

The porogen size distributions were also determined by standard image analysis techniques (by scanning electron micrography after size classification), and are quoted as mean±standard error of the means (Fig 5.11). Particulate porogen sizes are quoted as being either nominal sizes (according to the sizes of the two sieves between which they were collected), or as actual (determined by image analysis). The diameters of fibrous porogens were determined by image analysis of SEM micrographs.

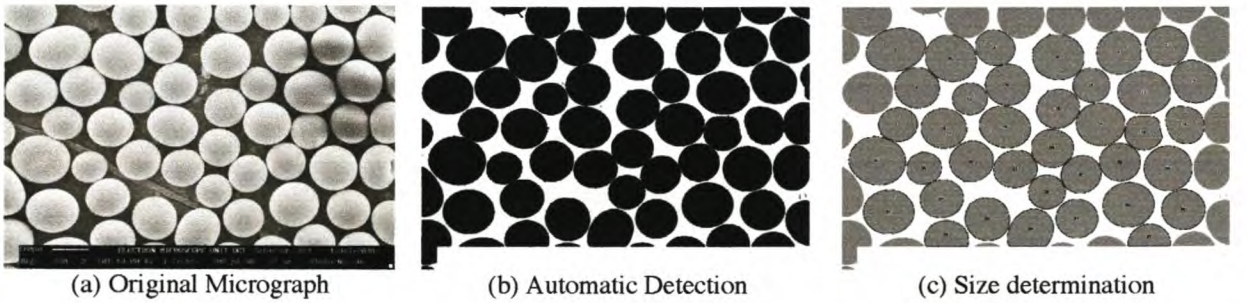

(a) Original Micrograph (b) Automatic Detection (c) Size determination

Figure 5.11: Determination of porogen size by automatic feature detection and size analysis using NIH Image software (Gelatin Microbeads, 150-180μm fraction, Mag=350x)

5.3.1.4 Porogen density determination

The absolute density of a particulate porogen fraction (ρ_{por}) was determined by a volume displacement method. A volumetric flask was about half-filled with a known mass of porogen, m_{por}, and the remainder of the flask filled with a liquid that does not swell or dissolve the porogen. The density of the porogen was determined from the mass of porogen, mass of liquid added, and the volume of the flask. Thus:

$$\rho_{por} = \frac{m_{por}}{V_{por}} \tag{5.1}$$

$$\rho_{por} = \frac{m_{por}}{V_f - V_{solv}} = \frac{m_{por}}{V_f - (m_{solv}/\rho_{solv})} \tag{5.2}$$

where V_f is the volume of the flask, V_{por} the volume of the porogen, and m_{solv} and ρ_{solv} the mass and density of the solvent, respectively. The bulk density (ρ_{Bpor}) was determined by filling a

Stellenbosch University http://scholar.sun.ac.za

measuring cylinder with porogen particles (with agitation to ensure close packing), noting the mass of porogen needed to fill the cylinder to known volume (V_{cyl}), and calculation by:

$$\rho_{Bpor} = \frac{m_{por}}{V_{cyl}} \tag{5.3}$$

5.3.2 Material properties

5.3.2.1 Materials used

Seven medical-grade polyurethanes were originally evaluated in this study (Table 5.2). As different polyurethanes were used in different applications, depending on availability and suitability, evaluation of the different properties was selectively performed. The Medtronic M48 turned out to be the polyurethane used to produce most of the grafts shown in this study, and should be assumed as the graft material unless otherwise indicated.

Table 5.2: Medical grade polyurethanes used in the production of porous scaffolds.

Number	Material	Supplier
1	M48	Medtronic
2	Pellethane 80A	Dow
3	Chronoflex AL 55D	Cardiotech
4	Chronoflex AL 75D	Cardiotech
5	Hydrothane	CT Biomaterials
6	Elast-Eon 2 85A	Aortech
7	Texin	Bayer

5.3.2.2 Solubility determination

The solubility parameters of polyurethanes were determined by the solvent spectrum method described by Hansen [58]. Ampoules containing 1.00 ml of solvent and 0.10 g of dried polyurethane were shaken for 7 days at room temperature. The liquids were then classified, by visual assessment, as good solvents, good swelling agents, poor swelling agents or non-solvents. Hansen divided the total solubility parameter (δ_t) into polar (δ_p), dispersion (δ_d) and hydrogen bonding (δ_h) forces:

$$\delta_t^2 = \delta_p^2 + \delta_d^2 + \delta_h^2 \tag{5.4}$$

These solubility parameters can be represented in three-dimensional vector space and may be depicted by the point (δ_p, δ_d, δ_h) in the center of a solubility sphere. The solubility parameters of the polyurethanes were calculated by using the mean value of the liquids that acted as good solvents.

5.3.2.3 Surface tension determination

Three methods, namely the Zisman plot method, the Geometric multi-liquid method and the Harmonic/Geometric two-liquid method, were used to study the surface characteristics of polyurethanes. The Zisman plot method involves plotting the cosine of advancing contact angles at liquid /surface interfaces against the surface tension of that liquid for a series of liquids [59]. The linear relationship between these values is then extrapolated to $\cos\theta = 1$ (or $\theta = 0°$), at which point the critical surface tension (γ_c) is defined. Liquids with a surface tension greater than γ_c will not spread on the subject solid and liquids with surface tensions less than the γ_c will exhibit a 0° contact angle or, more likely, spread spontaneously. The geometric multi-liquid method used is an adaptation of a method developed by Kaelble [60]. The essential assumption is the additivity of the different molecular interactions that determine the surface tension and surface energies of liquids or solids, i.e., dispersion forces, dipole and induced dipole interactions and

Stellenbosch University http://scholar.sun.ac.za

hydrogen bonding. By making a further few assumptions the following relation for surface tension can be derived:

$$\xi = \xi^d + \xi^p \tag{5.5}$$

where ξ^d and ξ^p represent dispersion and polar interactions. The harmonic mean two-liquid method is an adaptation of the method used by Wu [61].

Flat sheets of Chronoflex AL 55D, Pellethane and Medtronic were cast from 20 % solutions of these polymers in N-methyl-2-pyrrolidone. The sheets were air dried for two days followed by 5 days drying at 60 °C in vacuo. Blocks of 22 x 30 mm were cut and the contact angles determined by the Wilhelmy plate method on a Cahn Dynamic Contact Angle Analyser 322. Water, glycerol and di-iodomethane were used as wetting liquids.

5.3.2.4 Density determination

The density and bulk density of polymers were determined by methods similar to those used for porogens. (See 5.3.1.4)

5.3.3 Graft production

5.3.3.1 Solution processing

(A) Dip-cast grafts

Dip cast grafts were produced by methods adapted from those employed by various researchers [17, 18, 22, 23, 42]. Briefly, cleaned glass mandrels (6mm) were dipped into a paste (salt:polymer ratio = 10:1) consisting of porogen particles (90-106μm $NaHCO_3$) suspended in a polyurethane solution (10% M48 in NMP). After removal of the coated mandrel from the suspension, the polymer was solidified by solvent evaporation, after which the dipping/solidification process was repeated until the desired wall thickness had been achieved (measured by image analysis of scanning electron micrographs). Final solidification was followed by the extraction of the porogen to yield the vascular graft (Fig 5.12)

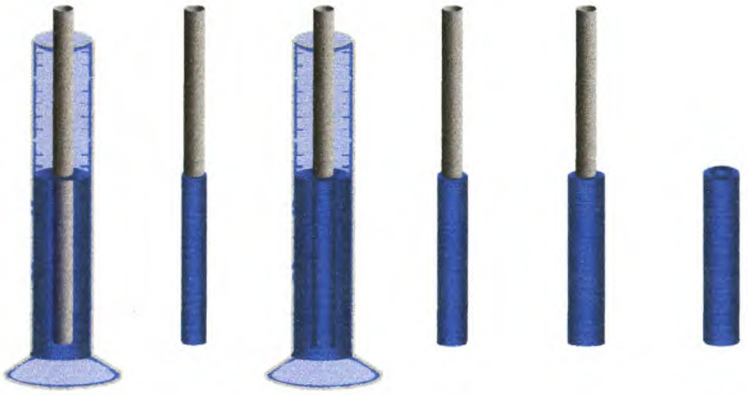

Figure 5.12: Schematic representation of the dip-casting method used in the production of porous polyurethane grafts.

Stellenbosch University http://scholar.sun.ac.za

(B) Roll-cast grafts

For the production of roll-cast grafts, a paste was first prepared by premixing a polymer solution (20% M48 in NMP) with various quantities of $NaHCO_3$ crystals of desired size fraction. The porogen loading was expressed as the porogen:polymer ratio (or porogen: solution ratio). The paste was subsequently extruded by means of a 50ml syringe onto a polished stainless steel mandrel (of desired diameter) containing, at both ends, an annular PTFE spacer of a thickness equivalent to the wall thickness of the graft to be produced (Fig 5.13). The rolling of the extruded paste around the mandrel on a glass plate, followed by precipitation of the polymer (and subsequent or simultaneous extraction of the porogen) resulted in the prototype vascular graft.

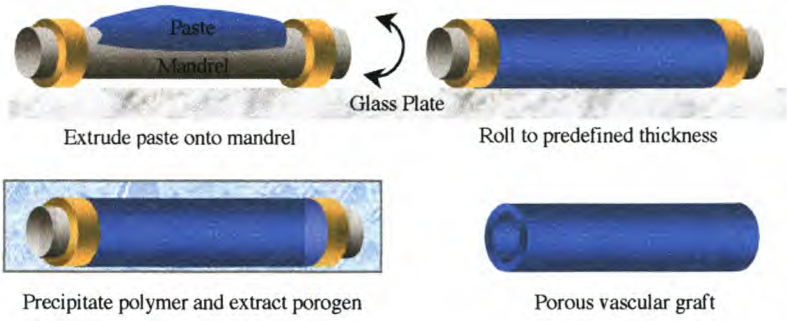

Figure 5.13: Schematic representation of the method used in preparing Roll Cast Grafts

(C) Vacuum/pressure-cast grafts

Porogen particles were packed into the annular space between cylindrical glass tubes (ID=5.4mm, length =180mm) and central stainless steel mandrels vertically mounted in a custom-made manifold containing upper and lower reservoirs. The upper reservoirs were filled with a polyurethane solution, after which a pressure of 750kPa and a vacuum of 100kPa were applied to the upper and lower manifolds, respectively.

After complete infiltration of the entire length of the packed bead column, the resultant polymer/solvent/porogen grafts were demoulded and the polymer precipitated by phase inversion. Subsequent or simultaneous extraction of the porogen beads, extensive washing to remove traces of porogen and solvent, and drying resulted in the porous scaffold. Initially, the centering mechanism depicted on the left hand side of Fig. 5.14 was employed. This mechanism relied on centering the mandrel in the upper reservoir and lower manifold. An improved centering mechanism (Fig 5.14b) using laser cut spacers (see insert) to align the mandrel inside the glass tube was later employed. The complete rig, capable of producing 6 grafts, is shown in Fig. 5.15.

During the adaptation of the vacuum/pressure casting technique to the use of gelatin microspheres, several alternative techniques were evaluated. These techniques may be differentiated according to the technique used to demould the graft. The first demoulding method consisted of removing the central mandrel, whereafter the polymer was precipitated (in water) while residing in the glass tube. In the second method, a custom-made device was used to remove both the central mandrel and the graft from the glass tube, after which the polymer was precipitated on the mandrel (in ethanol).

Figure 5.16 shows sequential steps of vacuum-cast graft production (second method) after removal of (A) a single mould from the rig, (B) the upper reservoir, (C) the graft (on the mandrel) from the mould and subsequent phase inversion, (D) the porogen by extraction in a suitable solvent, and (E) the graft from the mandrel and drying.

Stellenbosch University http://scholar.sun.ac.za

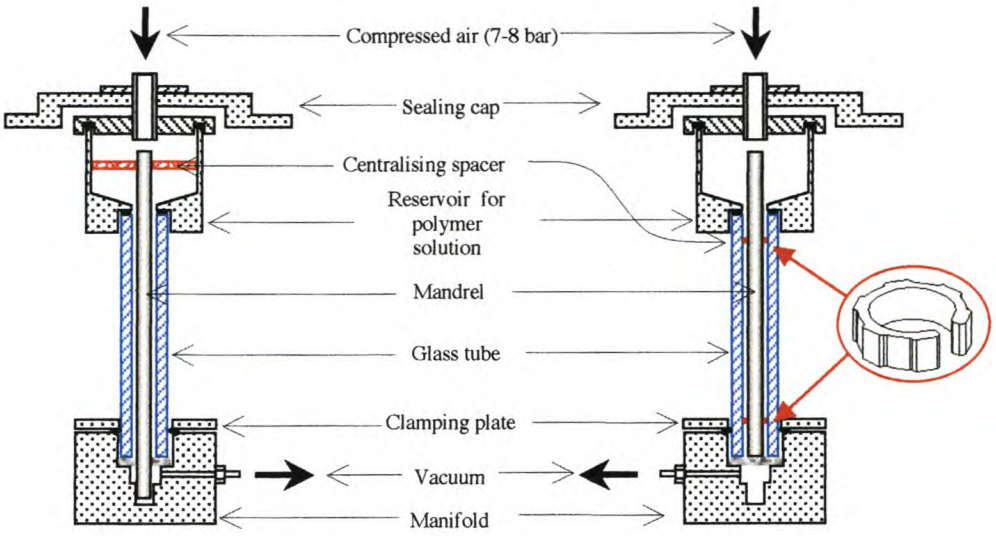

Figure 5.14: Schematic representation of the device used in the production of vacuum cast grafts, highlighting the two centring mechanisms.

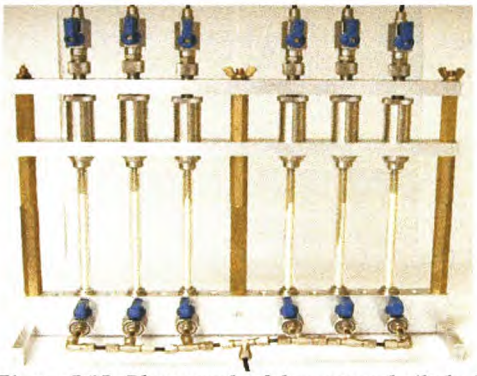

Figure 5.15: Photograph of the custom-built device used in the production of vacuum/pressure cast grafts

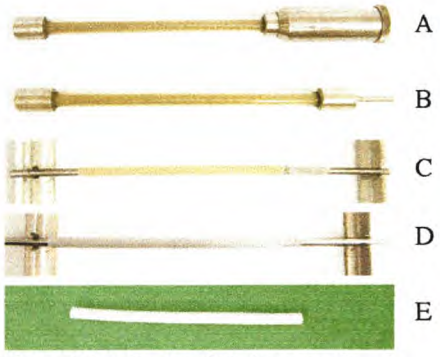

Figure 5.16: Sequential photographs of vacuum/pressure cast graft production

(D) Combination Grafts

Prototype grafts containing a combination of foam-type pores and helical channels were manufactured by a multi-layering technique involving the successive winding of soluble PVAL fibres and impregnating the interstices with a polymer/solvent/porogen paste (Fig 5.17). Subsequent precipitation of the polymer and extraction of both the particulate and fibrous porogens resulted in the desired graft.

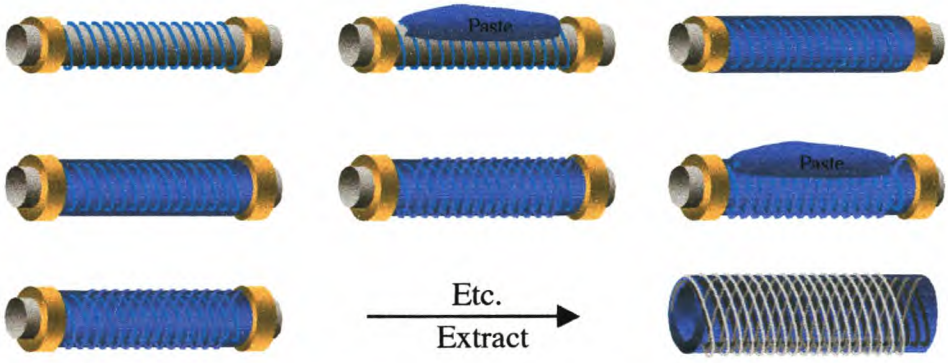

Figure 5.17: Schematic representation of the method used in the production of composite grafts.

Stellenbosch University http://scholar.sun.ac.za

(E) Helically-wound grafts

Grafts containing helical channels were prepared on a custom-built winding device. A soluble poly(vinyl alcohol) fibre from a spool was passed through a syringe containing a 20% M48 polyurethane solution and wound onto a stainless steel mandrel (Fig 5.18 and 5.19). The winding device consisted of two stepper motors fitted in a frame in such a manner that the first provided for rotation of the mandrel containing the graft, while the other was mounted to a screw that could provide for translational movement of a carriage containing the fibre spool and syringe. Application of multiple layers by the to-and-fro winding (multiple traverses) the vascular graft was built up on the mandrel. Specialised software provided for accurate control of the two motors through the computer interface, thereby allowing for the accurate and reproducible winding at the desired pitch. Precipitation of the polymer, extraction of the PVAL fibre and subsequent drying resulted in a graft that contained the helical channels.

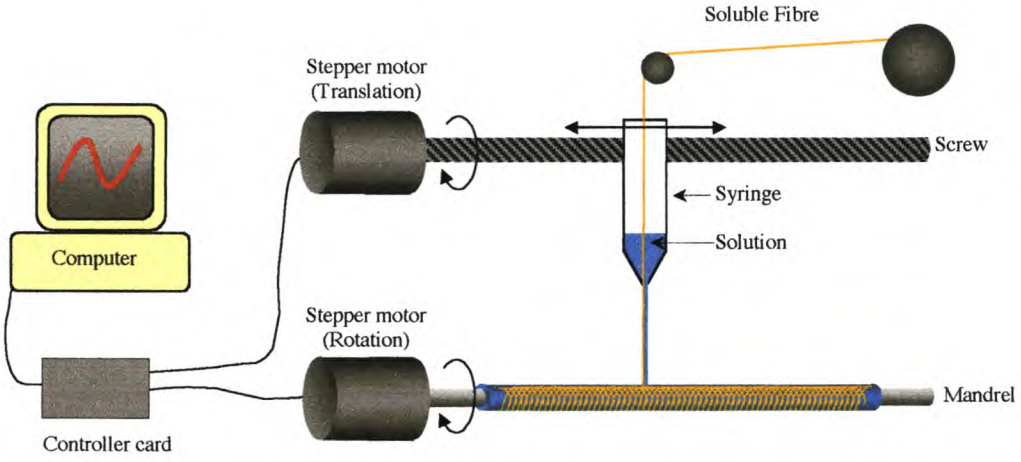

Figure 5.18: Schematic representation of winding technique used in the winding of helically wound grafts

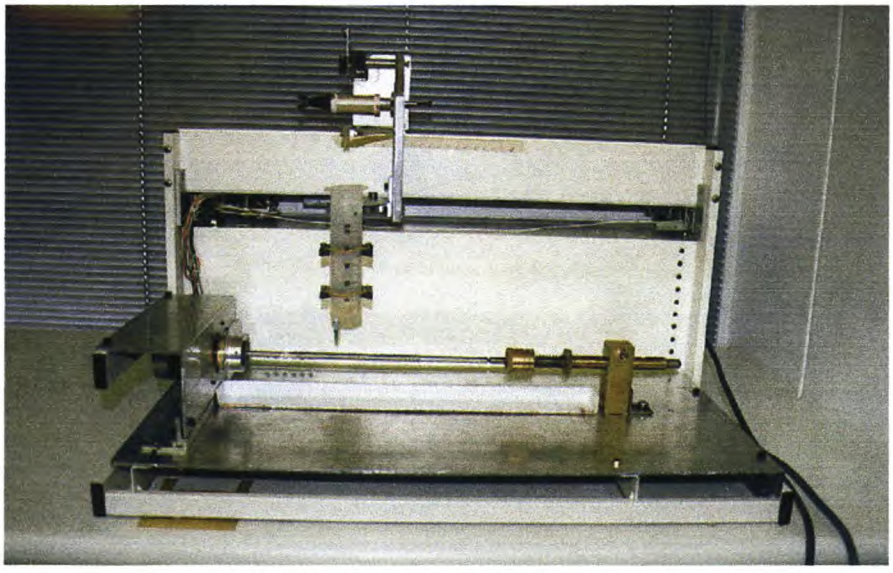

Figure 5.19: Photograph of the production of porous polyurethane grafts containing helical porosities with the use of computer-controlled winding apparatus using soluble PVA fibres.

Stellenbosch University http://scholar.sun.ac.za

5.3.3.2 Melt processing

(A) Melt-extracted grafts

Polyurethane (M48) was compounded with various loadings of dried inorganic filler (NaCl, 90-106μm) on a twin roll mill (Brabender attachment) at 180°C for 10min. The sheet of filled material was then cooled, pelletised, and extruded (Brabender single screw; 160/170/180/140°C) through a tubular die (6x8mm). The NaCl was subsequently extracted by extensive washing in hot water to produce a porous graft.

(B) Melt-blown grafts

Polyurethanes were premixed with chemical blowing agents (Genitron VKA 9164 and Genitron DP 35/22) with the use of a small quantity of mineral oil (to facilitate homogeneous dispersion) and subsequently extruded through a 6x8mm tubular die. Various blowing agent loadings and temperature profiles were used to produce porous structures.

5.3.3.3 Graft reinforcement

A Brabender extruder was fitted with a 2mm circular die and M48 was extruded from the die and drawn to the desired dimensions by winding on a spool. The temperature profile, from the feed zone to the die, was 160/170/180/140°C. Fibres of different diameters could be produced by varying the relative speed of winding to the extrusion rate.

Helical reinforcement was performed on the custom-built winding device shown in Fig 5.20. When the device was used for reinforcement, fibres that are non-soluble in the polymer precipitant were used. Precipitation in water (RT, 24hr), washing in water to remove traces of solvent introduced during the winding process, and subsequent drying resulted in a helical reinforcement that was firmly attached to the outer surface of the graft. A helical pitch of 2.5mm was used unless otherwise indicated.

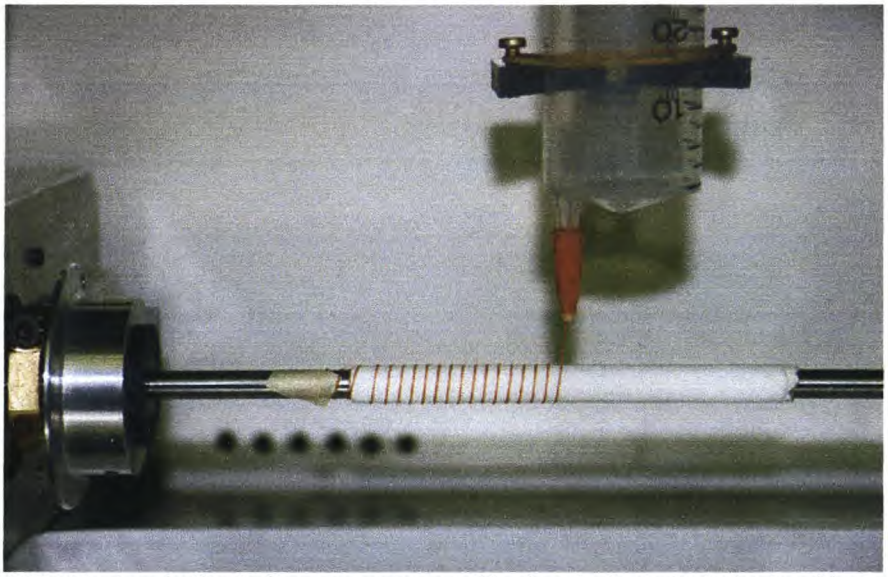

Figure 5.20: Custom-built winding apparatus used in the winding of reinforcing fibres onto the outer surface of porous polyurethane grafts.

Stellenbosch University http://scholar.sun.ac.za

5.3.4 Porosity determination

5.3.4.1 Pore size measurement

Pore (D_p) and interconnecting window (D_w) sizes were determined from scanning electron micrographs by image analysis using NIH Imaging software for the Macintosh. Depending on the orientation of the windows relative to the cut plane of the section, circular features may appear to be elliptical. Thus the long axes of the ellipses were quantified, and the features were assumed to be of a circular shape with a radius equalling the long axis.

5.3.5 Residual porogen determination

Residual porogen determination was performed on scaffolds prepared by using gelatin microbead porogens. Gelatin content was evaluated by an adaptation of a method of Sarin et al. [62] for quantitative monitoring of solid-phase peptide synthesis reactions. Briefly, to 2-5mg porous sample in an Epindorf tube, 100μl of solution A (a mixture of: 40g phenol, 10ml EtOH, stirred with 4g Amberlite resin and filtered; and 65mg of KCN in 100ml water, 2ml of which is diluted to 100ml in pyridine and stirred with 4g Amberlite resin and filtered) and 25μl of solution B (2.5g ninhydrin in 50ml absolute EtOH; kept in dark under N_2) was added.

The samples were mixed and heated to 95°C in a heating block for 10min, cooled by immersion in cold water, and 1ml of 60% EtOH was added. The suspensions were subsequently filtered through a Pasteur pipette containing a glass-wool plug, rinsed twice with 0.2ml of 0.5M Et_4NCl in CH_2Cl_2, and made up to 2ml with 60% EtOH. Absorbance was measured at 570nm against a reagent blank. The standard curve depicted in Fig 5.21 was produced by using known quantities of gelatin.

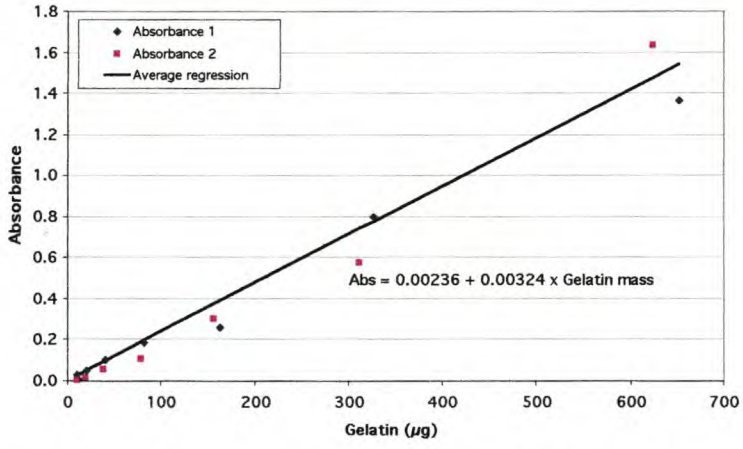

Figure 5.21: Standard curve for the determination of residual gelatin content in porous structures by the ninhydrin method.

The porogen content of grafts based on dry mass before porogen extraction was calculated from eq 5.6 below (See Appendix 4)

$$Por = \frac{\rho_{Bpor}}{\rho_{Bpor} + x\rho_{so\,\ln}\left(1-\left(\rho_{Bpor}/\rho_{por}\right)\right)} \tag{5.6}$$

where *Por* is the mass fraction of porogen present in the dried, precipitated structure (before porogen extraction), ρ_{Bpor} and ρ_{por} the bulk and absolute densities of the porogen, respectively, x the concentration of the polymer (mass%) and ρ_{por} the density of the polymer solution.

Stellenbosch University http://scholar.sun.ac.za

5.4 Results and discussion

5.4.1 Porogen properties

5.4.1.1 Porogen types

Figure 5.22 shows the shapes of the three particulate porogens used in the fabrication of foam-type scaffolds, as well as the water-soluble poly(vinyl alcohol) (PVAL) fibre used in the production of vascular grafts containing oriented helical channels. The sodium bicarbonate crystals depicted in Fig. 5.22 (a) are from the 90-106 μm size-fraction. The irregularity of the crystals and their large aspect ratios (length: width) make the sieving of narrow size distribution difficult, as elongated crystals may pass through the sieve opening in certain directions (orientations) only. The hydroxyapatite beads approximated rough spheres, and are more conducive to narrow fractionation by sieving techniques. It was found however, that a large percentage of the beads were smaller than 80μm, and the beads were used in their unfractionated state due to limited availability. The gelatin microbeads (Figure 5.22c) were smooth and spherical, and although a small percentage of the particles were ellipsoid or thoroid in shape, they were readily fractionated into the desired size ranges. The fibrous porogen was a poly(vinyl alcohol) (PVAL) fibre, shown in Fig. 5.22 (d).

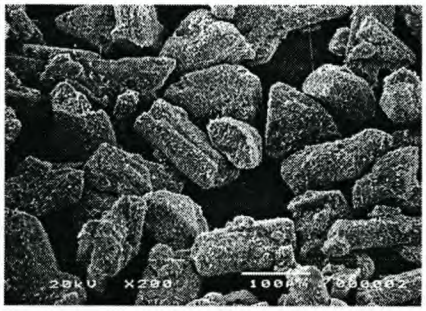

(a) Sodium Bicarbonate (Mag=200X)

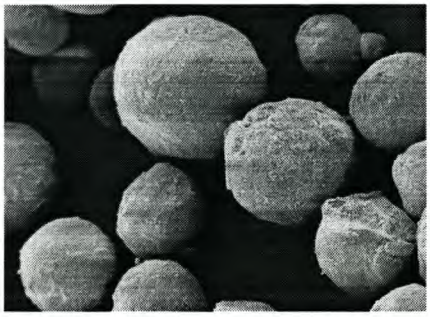

(b) Hydroxyapatite (Mag=1.45KX)

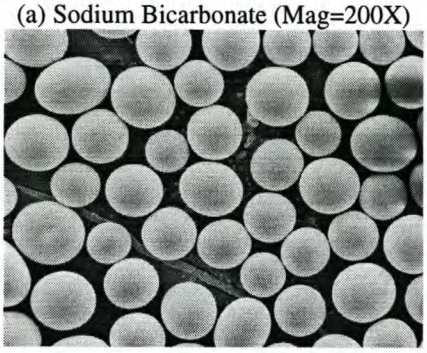

(c) Gelatin microbeads (Mag=350X)

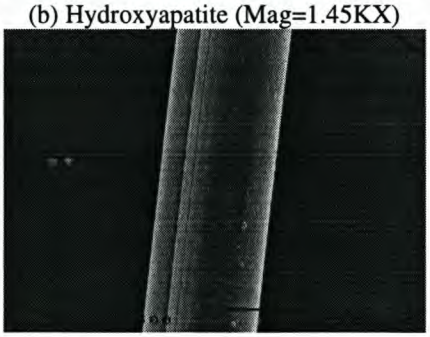

(d) PVAL fibre (Mag=500KX)

Figure 5.22: Scanning electron micrographs of three types of particulate and fibrous porogens used in the production of porous scaffolds.

5.4.1.2 Porogen size

The dimensions of the $NaHCO_3$ crystals, hydroxyapatite beads and gelatin microspheres are given in Table 5.3. The irregularity of the bicarbonate crystals is confirmed by the large aspect ratio of this porogen type. The hydroxyapatite beads had a much lower aspect ratio, while the sherical shape of the gelatin beads is confirmed by an aspect ratio close to unity.

Stellenbosch University http://scholar.sun.ac.za

Table 5.3: Dimensions (Mean±SEM; μm) and aspect ratios of the three particulate porogens.

Porogen	Sieve Fraction	Count	Long axis	Short axis	Diameter	Aspect ratio
$NaHCO_3$	63-75	50	79.0±2.5	46.8±1.8	60.1±1.7	1.80±0.1
$NaHCO_3$	90-106	60	148.5±5.5	82.0±2.6	109.1±3.1	1.89±0.09
$NaHCO_3$	150-180	50	246.5±8.1	139.1±6.4	182.6±6.2	2.00±0.1
HA	all	85	87.4±1.8	71.0±1.9	74.1±2.5	1.27±0.03
Gelatin	63-75	241	66.3±0.4	62.8±0.3	64.5±0.3	1.06±0.01
Gelatin	90-106	208	90.3±0.5	84.7±0.5	87.4±0.4	1.07±0.01
Gelatin	150-180	207	134.0±1.0	124.5±0.9	129.0±0.9	1.08±0.01

The actual porogen size distributions of gelatin microspheres (for the three sieve fractions indicated) are shown in Fig. 5.23. From the shape of the histogram (and the standard errors of the means) it is evident that narrower size distributions were obtained with the smaller beads. A possible explanation of this phenomenon pertains to the production process. It was originally optimised for 90-106μm beads and thus conducive to the production of small beads of narrow size distribution. The larger beads are less stable during the manufacturing process, hence larger size distributions are obtained (personal correspondence with Curt Thies, Thies Technologies). Thus, although beads were re-sieved in our laboratories, problems encountered with the manual re-sieving (high blocking rates), the distributions could not be narrowed further than those shown below. The bead sizes will be referred to by the sieve fractions in most cases; actual sizes are given only when specifically determined.

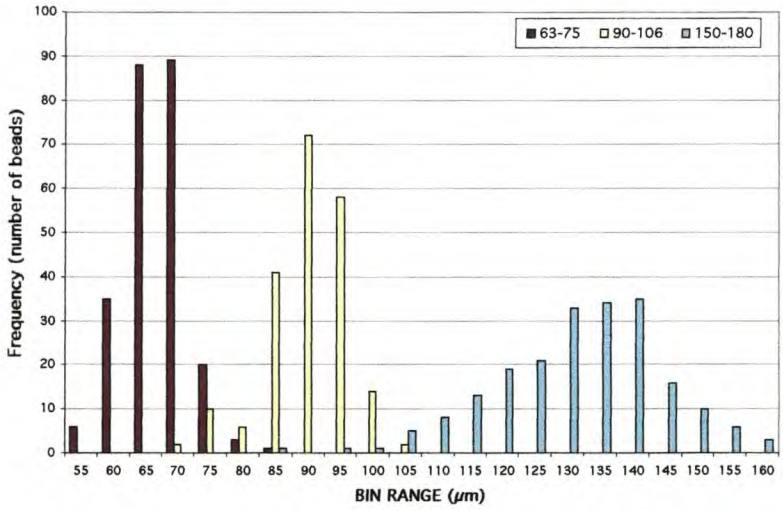

Figure 5.23: Histogram of gelatin microbead size distributions after sieving and collection of the 63-75, 90-106 and 150-180μm sieve fractions.

5.4.1.3 Particulate porogen densities

The bulk and absolute densities of the particulate porogens, as determined by methods described in 5.3.1.4, are listed in Table 5.4. These values were used to determine the theoretical porosities.

Table 5.4: Bulk and absolute densities of particulate porogens.

Porogen Type	Sieve Fraction	Bulk Density (g/cm^3)	Absolute Density (g/cm^3)
$NaHCO_3$	63-75	1.15	2.16 *
	90-106	1.18	2.16
	150-180	1.20	2.16
Hydroxyapatite	<80	0.58	
Gelatin	63-75	0.83	1.32
	90-106	0.82	1.33
	150-180	0.81	1.31
* [63]			

Stellenbosch University http://scholar.sun.ac.za

5.4.2 Polymer properties

5.4.2.1 Solubility parameters

The values for the Hansen three-dimensional solubility parameters, as calculated from the averages of good solvents (Tables 5.5; data Appendix 2). Chloroform, N,N-dimethyl acetamide (DMAC), N-methyl pyrrolidone (NMP) and pyridine proved to be good solvents for all four of the polyurethanes evaluated. Although the dispersive component of the solubility parameter was slightly higher for M48 than for the other three polymers, both the polar and hydrogen-bonding components were lower, resulting in a lower total solubility parameter. These lower values may be explained by the nature of the soft-segments of the polyurethanes. The soft segment of M48 contains hydroxymethyl octadecanol that can be expected to be less polar and less capable of hydrogen bond formation than the polycarbonate diols used in Chronoflex. The author does not know the soft-segment chemistry of Hydrothane.

Table 5.5: The three-dimensional solubility parameters of polyurethanes.

Material	δ_d ($MPa^{1/2}$)	δ_p ($MPa^{1/2}$)	δ_h ($MPa^{1/2}$)	δ_t ($MPa^{1/2}$)
M48	18.0	6.4	6.8	20.3
Chronoflex AL 55D	17.5	8.2	9.4	21.5
Chronoflex AL 75D	17.0	9.3	8.6	21.9
Hydrothane	17.1	8.2	9.7	21.3

5.4.2.2 Surface tension

The critical surface tensions of Medtronic and Chronoflex are very close to one another with the value for Pellethane nearly double the latter. This implies that water (surface tension 72.8 dynes/cm) spreads better on Pellethane than on the other two polyurethanes (Table. 5.6).

Table 5.6: Critical surface tension (γ_c), and dispersive (ξ^d) and polar (ξ^p) components of the surface energy of polyurethanes (units: dynes/cm).

MATERIAL	Zisman	Geometric multi-liquid			Geometric/Harmonic two liquid			
		Geometric			Geometric		Harmonic	
	γ_c	ξ^d	ξ^p	ξ_{total}	ξ^d	ξ^p	ξ^d	ξ^p
Medtronic M48	28.54	24.01	0.93	24.94	24.80	1.17	23.76	4.58
Chronoflex AL 55D	27.07	24.69	4.30	28.99	26.32	5.00	23.87	10.38
Pellethane	45.89	38.69	1.13	39.82	44.47	2.35	38.90	8.34

5.4.2.3 Density determination

The densities of various polyurethanes under investigation at the time are given in Table 5.7. The density of a 20% M48 solution (the solution used in a majority of cases) is 1.04 g/cm^3, while the density of NMP is 1.03g/cm^3.

Table 5.7: Densities of polyurethanes (g/cm^3).

M48	Pellethane	Chrono AL55	Chrono AL75	Hydrothane	Texin
1.025±0.005	1.135±0.025	1.145±0.015	1.125±0.005	1.115±0.005	1.105±0.005

Stellenbosch University http://scholar.sun.ac.za

5.4.3 Reinforcing fibres

An example of an extruded fibre with an average diameter of 220μm is given in Figure 5.24.

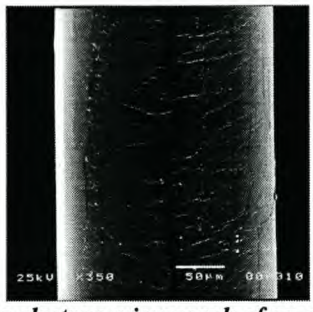

Figure 5.24: Scanning electron micrograph of an extruded polyurethane fibre used in graft reinforcement (Mag=150X; bar=50μm)

5.4.4 Solution processing

5.4.4.1 Dip-cast grafts

Figure 5.25 illustrates grafts produced by the dip-casting method. The structures resulting from this casting method were similar to those obtained by Murabayashi [18]. Grafts consisted of randomly distributed, ill-defined pores, with limited interconnectivity.

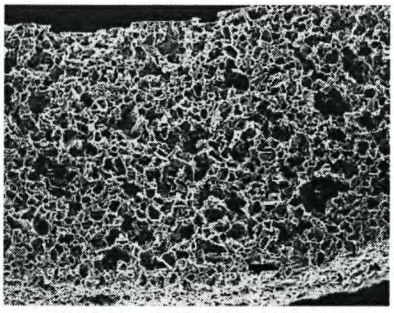

(a) Mag=75X; bar=100μm

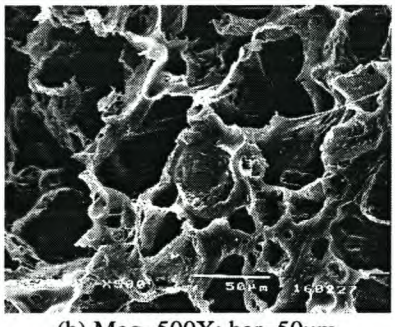

(b) Mag=500X; bar=50μm

Figure 5.25: Structure of porous polyurethane grafts produced by the dip-casting method (90-106μm $NaHCO_3$ porogen).

5.4.4.2 Roll-cast grafts

Premixing of the porogen and polymer solution resulted in the porous structures shown in Fig 5.26. When $NaHCO_3$ was used as porogen, the structure contained macrovoids resembling the size and shape of the bicarbonate crystals. A high degree of microporosity was observed, but the interconnectivity between macropores was low (Fig 5.26 a).

Since the optimal shape of a porogen for the creation of a well-defined pore is spherical, hydroxyapatite (HA) porogens were employed. Although the structure depicted in Fig 5.26 (b) contained some irregular, large voids (possibly the result of HA bead clusters), it gave the first indication that well-defined, spherical pores may be produced by the use of spherical porogens. Gelatin microspheres failed to produce the desired spherical porosity (Fig 5.26 c) when the roll-cast method was used.

Stellenbosch University http://scholar.sun.ac.za

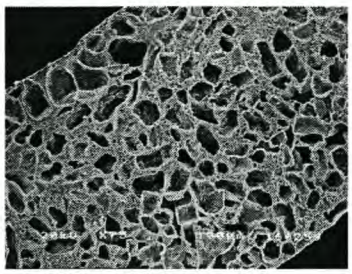
(a) Mag=75X; bar=100μm

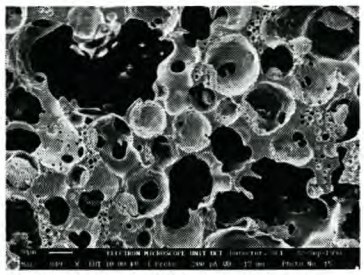
(b) Mag=849X; bar=30μm

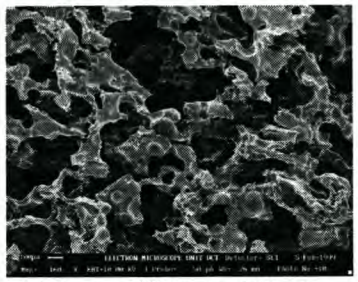
(c) Mag=160X; bar=100μm

Figure 5.26: Micrographs of porous vascular grafts produced from 20% M48 in NMP by roll casting. Porogens: (a) 90-106μm $NaHCO_3$, (b) HA and (c) 90-106μm gelatin microspheres.

5.4.4.3 Vacuum/Pressure-cast grafts

(A) $NaHCO_3$ crystals and HA beads as porogens

Attempts at using the vacuum/pressure-cast method with $NaHCO_3$ particles as porogens were successful in that an openly porous structure, that would allow for the uninterrupted passage of material through the graft wall, could be produced (Fig 5.27 a,b), The pore structure was, however, quite random, as the material surrounding the pores did not define clear "cells", but was randomly constructed and "finger-like".

Figure 5.27c shows a porous structure obtained by the use of HA beads in combination with the vacuum/pressure casting technique. The beads were only partially extracted to show how the pore formed around the porogen. Complete extraction of the beads yielded the structure depicted in Fig 5.27d.

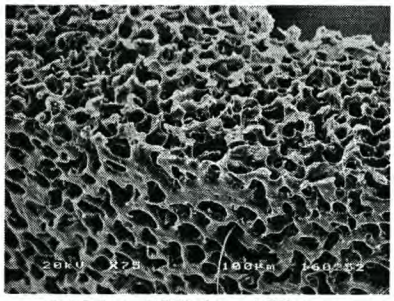
(a) Mag=75X; bar=100μm

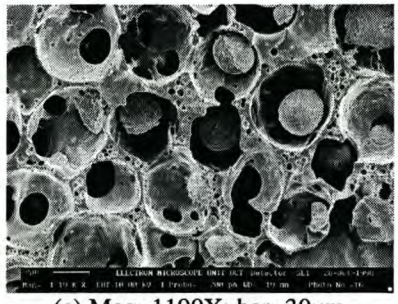
(c) Mag=1190X; bar=30μm

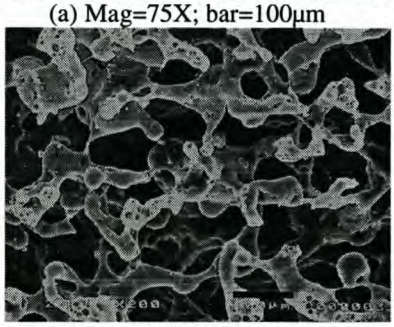
(b) Mag=200X; bar=100μm

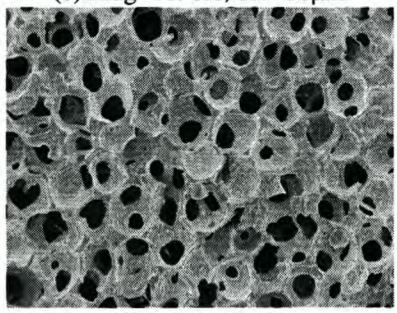
(d) Mag=500X

Figure 5.27: Micrographs of porous vascular grafts produced from 20% M48 in NMP by vacuum/pressure-casting. Porogens: (a,b) 90-106μm $NaHCO_3$, (c,d) hydroxyapatite beads.

(B) Gelatin Microspheres as Porogens

(i) Water Precipitation

Initial attempts to use gelatin microspheres as porogens in the vacuum/pressure casting method used water as both the precipitation and porogen-extraction solvent. Grafts produced in this manner contained interconnected pores approximating the size of the spherical porogen used, but

Stellenbosch University http://scholar.sun.ac.za

the pores were not as well-defined as those obtained with the HA porogen. Precipitation in water had a number of other disadvantages. The swelling of the grafts (while constrained on the ablumenal surface by the mould) caused thickening of the graft wall (Figure 5.28a) and the undulation of the lumenal surface (Figure 5.28b). Figure 5.8 (c and d) show cross-sectional views of the same graft.

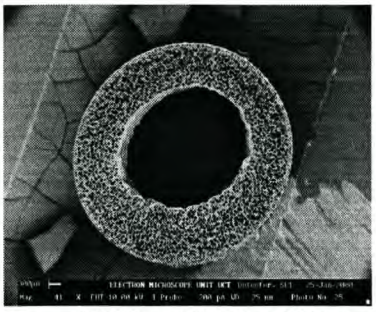

(a) Mag=41X; bar=300μm

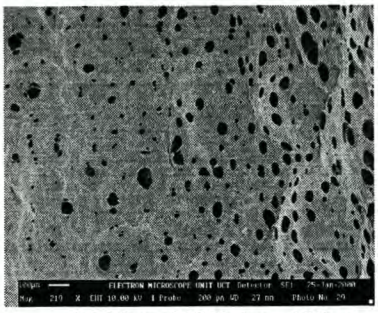

(b) Mag=219X; bar=100μm

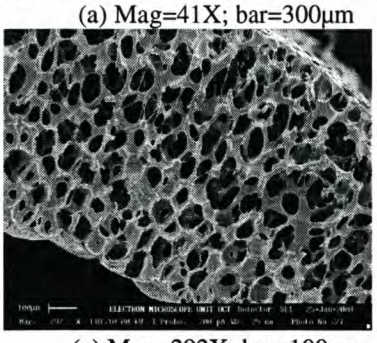

(c) Mag=292X; bar=100μm

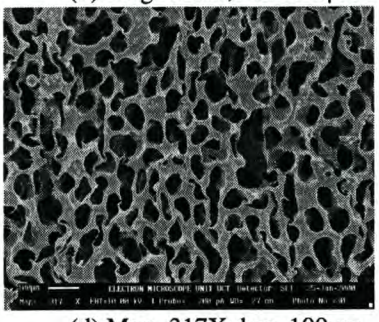

(d) Mag=317X; bar=100μm

Figure 5.28: Micrographs of porous vascular grafts produced from 20% M48 in NMP by vacuum/pressure-casting followed by water precipitation . Porogen: 90-106μm gelatin microspheres.

(ii) Ethanol Precipitation

The swelling of precipitating grafts seen during precipitation in water (due, in part to the swelling of the gelatin microbeads) was eliminated by the use of an alternative precipitant, i.e. one that would not swell the porogen before the solidification of the polymer was complete. Thus the precipitation of the graft in ethanol resulted in the desired structure. The well-defined spherical pores, interconnected by multiple windows, are evident in Figure 5.29. Examples of grafts produced by this method, using gelatin microbeads of distinctly different pore sizes, are shown in Figure 5.30. The effect of the increase in porogen size on the size of the pores and interconnecting windows is evident, and will be quantified in a later section. (See 5.4.4.4)

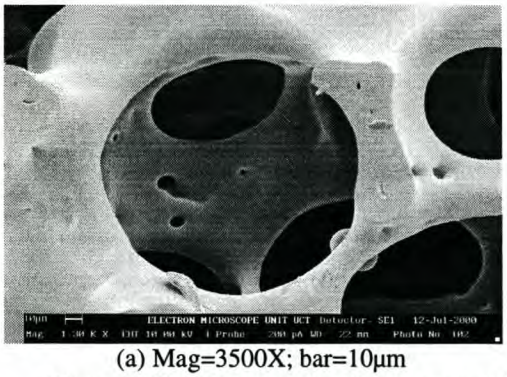

(a) Mag=3500X; bar=10μm

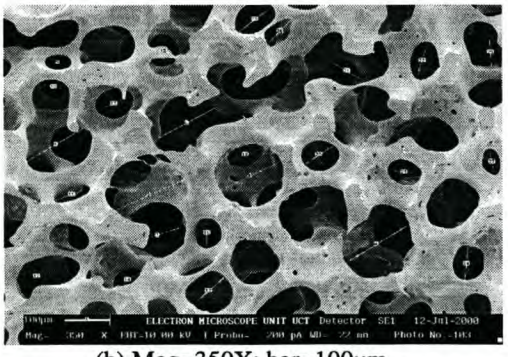

(b) Mag=350X; bar=100μm

Figure 5.29: Micrographs of porous vascular grafts produced from 20% M48 in NMP by the vacuum/pressure-casting followed by ethanol precipitation. Porogen: 150-180μm gelatin microspheres

Stellenbosch University http://scholar.sun.ac.za

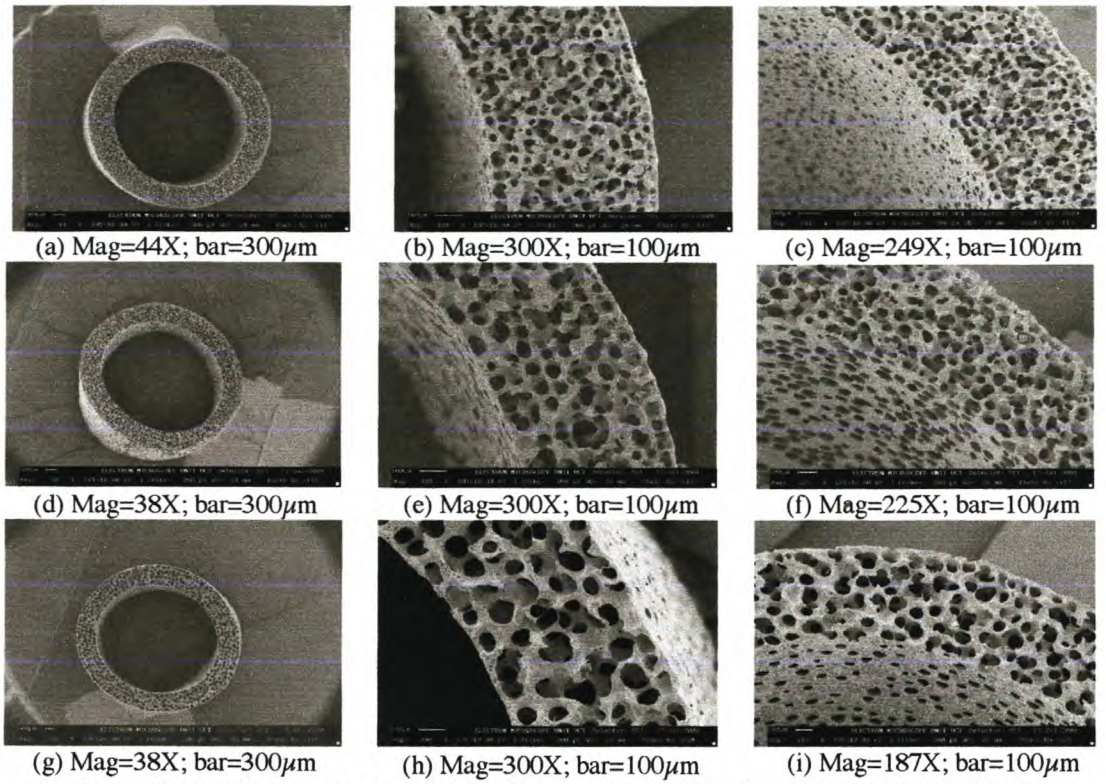

Figure 5.30: Micrographs of porous vascular grafts produced from 20% M48 in NMP by vacuum/pressure-casting followed by ethanol precipitation . Porogens: (a-c) 63-75μm, (d-f) 90-106μm and (g-i) 150-180μm gelatin microspheres.

5.4.4.4 Porosity determination

The porogen sizes of the 63-75, 90-106 and 150-180 sieve fractions were 55.8±0.5, 84.8±0.6 and 137.9±1.1μm respectively. On average, the pores created were 1.21±0.07 times the diameter of the porogens from which they were formed, and the interconnecting windows were approximately half the size of the pores (window:pore = 0.52±0.04). The intrafeature porogen, pore and window sizes obtained from the three sieve fractions were distinctly different ($p<0.15$).

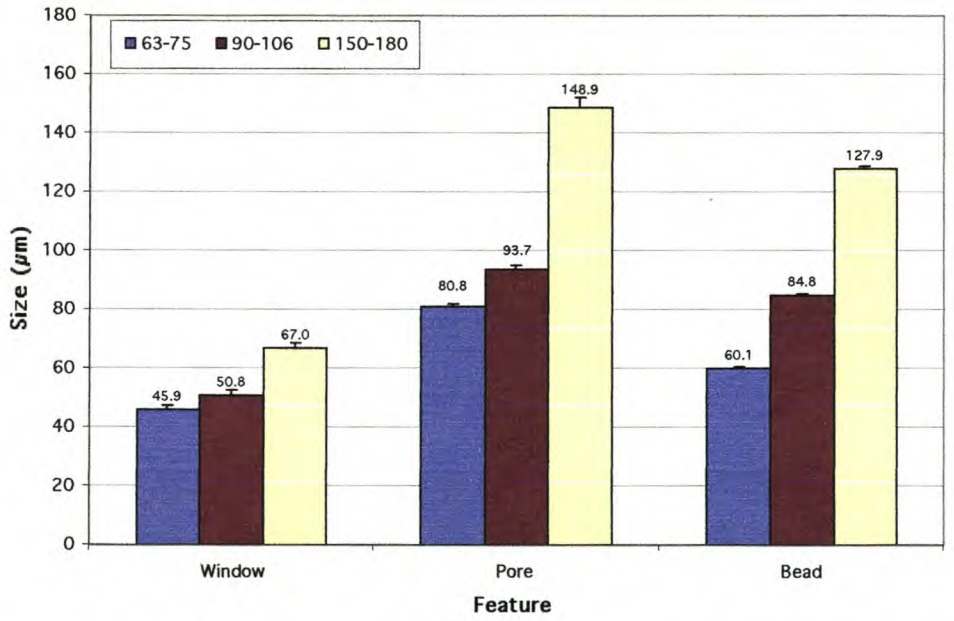

Figure 5.31: Pore and interconnecting window sizes of porous polyurethane grafts produced by vacuum/pressure casting with gelatin microspheres and subsequent phase inversion and porogen extraction (Average±SEM; μm)

Stellenbosch University http://scholar.sun.ac.za

5.4.4.5 Residual porogen determination

The calculated percentage of porogen present in the precipitated graft (before porogen extraction) was 94%. Washing of the grafts for a period of 172hrs at 55°C in water was able to remove the gelatin (used as porogen) to the extent that the porogen percentage decreased to 0.52%. The blue diamonds in Fig. 5.32 represent the gelatin content of five grafts produced subsequent to the establishment of the 172hr minimum extraction procedure (all less than 1%).

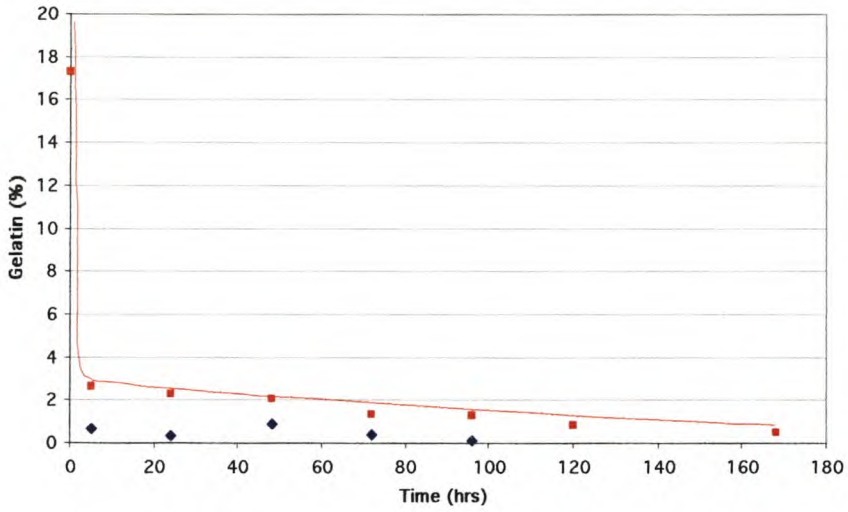

Figure 5.32: Elution curve (red) showing the residual gelatin content of porous polyurethane grafts after extraction in water at 55°C over a period of 172 hours. Blue diamonds represent the gelatin content of five subsequently produced grafts washed for 172 hrs.

5.4.4.6 Graft reinforcement

The winding of polyurethane fibres onto the ablumenal graft surface resulted an evenly-spaced reinforcement. The pre-coating of the fibres prior to application resulted in the bonding and slight penetration of the fibres into the lumenal surface, as seen in Fig. 5.33.

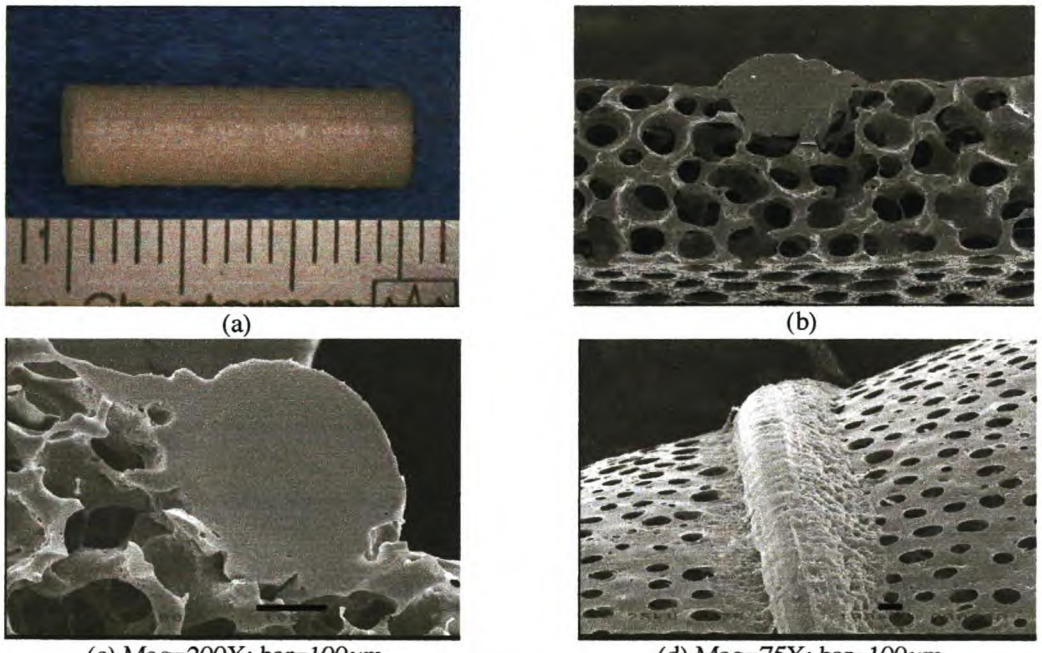

(a) (b)

(c) Mag=200X; bar=100μm (d) Mag=75X; bar=100μm

Figure 5.33: Macro and microphotographs showing porous grafts containing helical reinforcement consisting of bound polyurethane fibres.

Stellenbosch University http://scholar.sun.ac.za

5.4.4.7 Elast-Eon grafts

As Medtronic had ceased production of the M48 polyurethane, an alternative source of biostable material was sought. Elast-Eon 2 (Elastomedics, Australia), a polyurethane containing a siloxane based soft segment, was selected due to its excellent biostability. This section describes the efforts to replicate the structures obtained with M48 with the new material.

(A) Ethanol Precipitation

Standard ethanol precipitation of Elast-Eon 2 grafts resulted in the formation of well-defined spherical pores in the graft wall, but the interconnectivity between the pores, as well as that to the lumenal and ablumenal surfaces, was poor (See Fig. 5.34). The poor interconnectivity was ascribed to the relative instability of the Elast-Eon 2 solution. Due to the high siloxane content of this polymer, precipitation occurred before the interconnecting windows could be formed by the minimization of surface area. The measures taken to increase the inter-pore connectivity, and the results obtained by these methods, are given in subsequent sections.

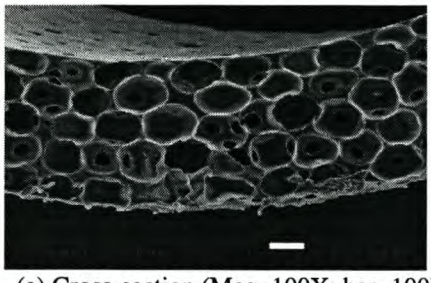

(a) Cross-section (Mag=100X; bar=100)

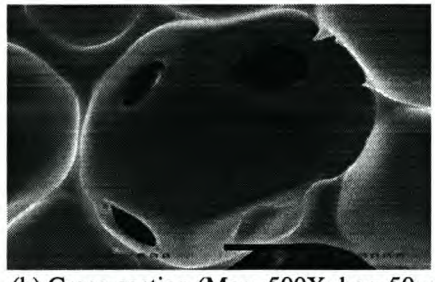

(b) Cross-section (Mag=500X; bar=50μm)

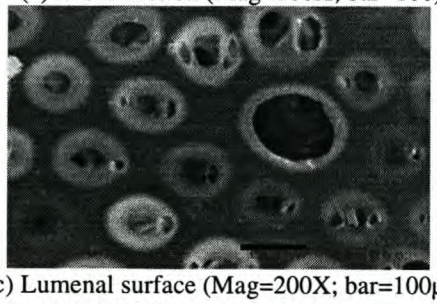

(c) Lumenal surface (Mag=200X; bar=100μm)

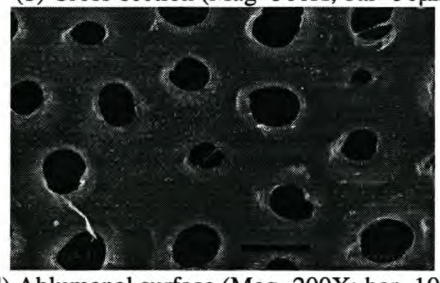

(d) Ablumenal surface (Mag=200X; bar=100μm)

Figure 5.34: Micrographs of porous vascular grafts produced from 20% Elast-Eon in DMAC by the vacuum/pressure-casting followed by ethanol precipitation . Porogen: 125-150μm gelatin microspheres.

(B) Reticulation

The first method used to increase interconnectivity is based on the reticulation of standard ethanol precipitated structures. Representative structures of samples subjected to heat treatment (160 to 190°C, 10 minutes) are shown in Figure 5.35. The unreticulated control (Fig 5.35 a) shows the typical, poorly connected porous structure. After heating at 160°C, the melting of the interpore windows is clearly evident. The increase in temperature to 170°C had no visible additional effect on the porous structure. At 180°C, the deformation of the spherical pores is evident, and a further increase in temperature to 190°C resulted in the complete collapse of the porous structure. Thus an increase in interpore connectivity could be achieved by reticulation. Some evidence of polymer degradation (yellowing of the samples) was observed at temperatures above 170°C. As a difference in structure between samples treated at 160 and 170°C was not observed, the temperature of 160°C was concluded to be the optimum temperature for reticulation.

Stellenbosch University http://scholar.sun.ac.za

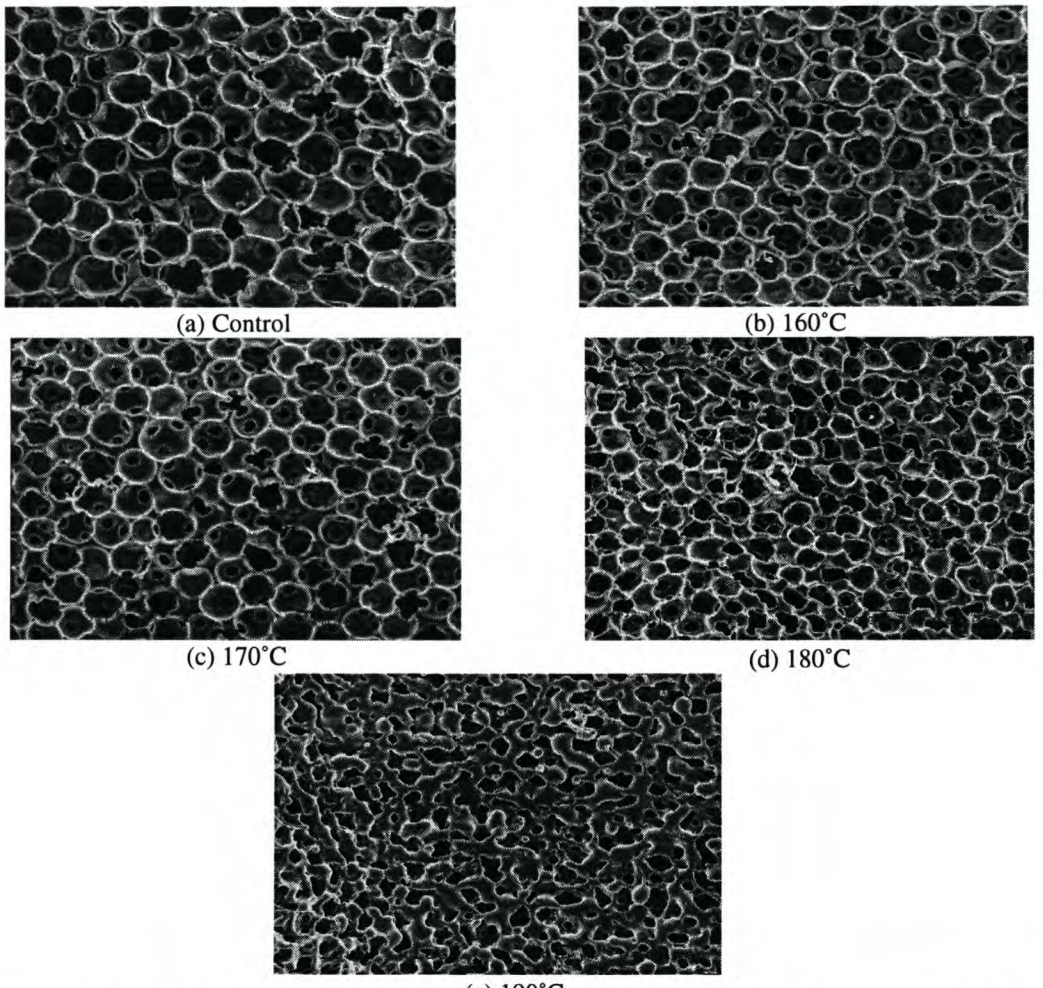

Figure 5.35: Micrographs of porous vascular grafts produced from 20% Elast-Eon in DMAC by the vacuum/pressure-casting followed by ethanol precipitation and reticulation at the indicated temperature. Porogen: 125-150μm gelatin microspheres. (original Mag: 100X)

(C) Alternative alcohols as precipitants

The use of alternative alcohols (C_1 to C_{12}), both at ambient and low temperature (4°C), and the addition of a surfactant to the polymer solution, failed to have the desired effect. The reasoning behind the use of these conditions was that the mobility of the precipitant, and thus the speed at which the precipitant enters the precipitating solution, would decrease due to increased chain length and decreased temperature. The polymer solution would then have more time to decrease its surface area (due to surface tension), and thereby increase the interconnecting window size. Figure 5.36 shows selected structures obtained by the use of the conditions indicated in the figure. The use of methanol, cold ethanol and propanediol as precipitants had no beneficial effect on the interconnectivity. Similar structures to these (Fig. 5.36 a-c) were obtained with alcohols with increased chain length (C_{12}). An interesting honeycomb structure was obtained when the casting solution contained 5% sodium lauryl sulphate (SDS), but although an increase in the microporosity could be observed, the macropore interconnectivity remained poor (Fig. 5.36 d).

Stellenbosch University http://scholar.sun.ac.za

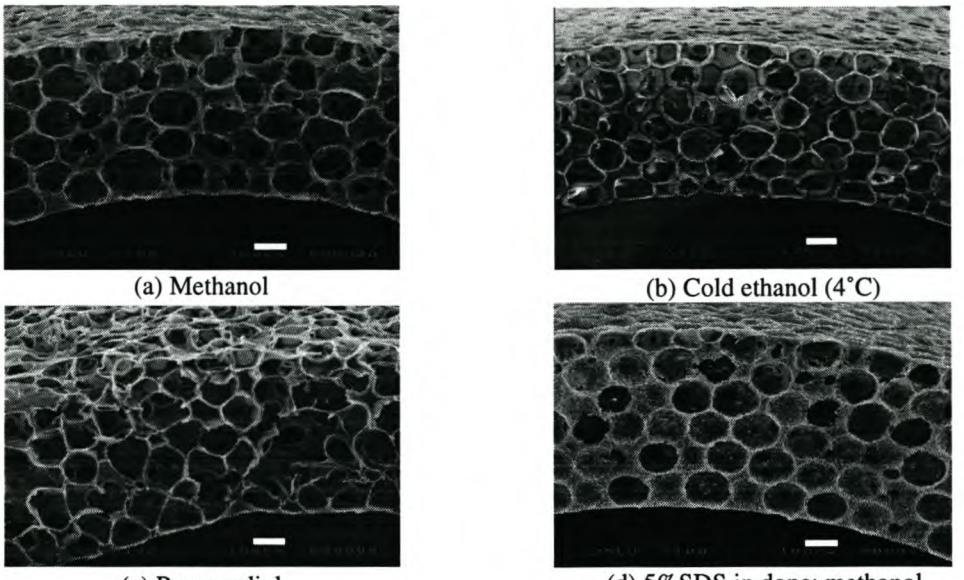

(a) Methanol (b) Cold ethanol (4°C)

(c) Propanediol (d) 5%SDS in dope; methanol

Figure 5.36: Micrographs of porous vascular grafts produced from 20% Elast-Eon in DMAC by the vacuum/pressure-casting followed by precipitation in various solvents . Porogen: 125-150μm gelatin microspheres. (Orig Mag=100X; bar=100μm)

(D) Dual precipitation

The addition of solvents to the non-solvent used for the precipitation is known to decrease the rate at which the polymer precipitates form solution. The failure to obtain the desired interconnected structures with the addition of various amounts of DMAC (the solvent used for Elast-Eon) to the ethanol precipitation bath (results not shown), prompted investigation into the use of other non-solvent combinations. The best results were obtained by the use of a dual-precipitation regimen, in which the polymer is partly precipitated in DMSO, and thereafter fully precipitated in ethanol (Figure 5.37). Structures containing well-defined pores of high interconnectivity could be produced by using this method.

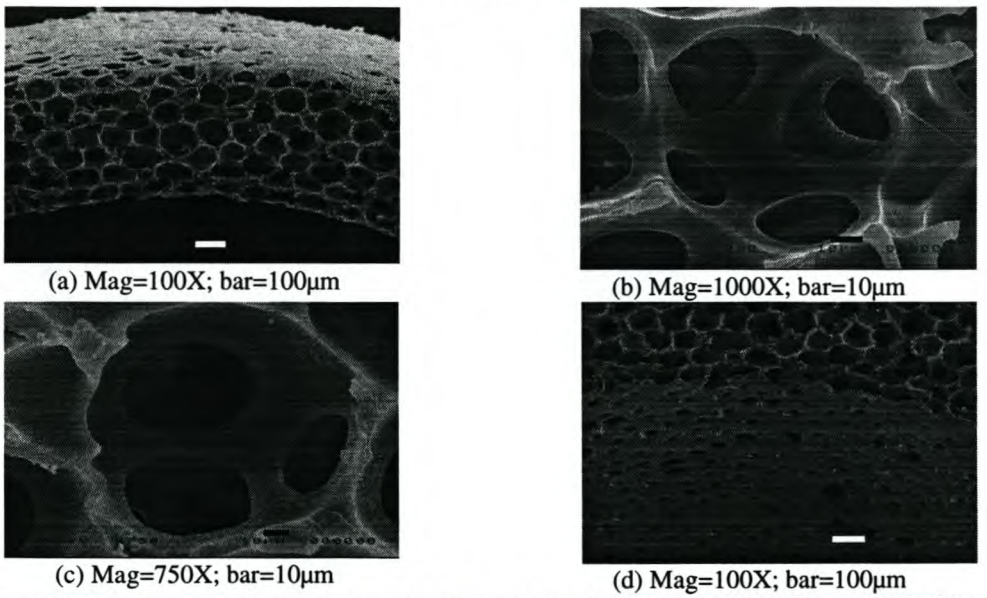

(a) Mag=100X; bar=100μm (b) Mag=1000X; bar=10μm

(c) Mag=750X; bar=10μm (d) Mag=100X; bar=100μm

Figure 5.37: Micrographs of porous vascular grafts produced from 20% Elast-Eon in DMAC by the vacuum/pressure-casting followed by dual precipitation (2hr DMSO followed by 18hr EtOH). Porogen: 125-150μm gelatin microspheres.

Stellenbosch University http://scholar.sun.ac.za

5.4.4.8 Grafts containing helical channels

Grafts containing helical channels and interconnected pores could be produced by using a combination of particulate and fibrous porogens (see 5.3.3.1 D). Figure 5.38 shows an example of such a graft containing concentric layers of helical channels. The interconnectivity between the channels and the pores are evident from Figure 5.38 b. Figure 5.38 c-f shows a prototype grafts containing helical channels (without additional macropores) produced by the winding process described in 5.3.3.1 (E).

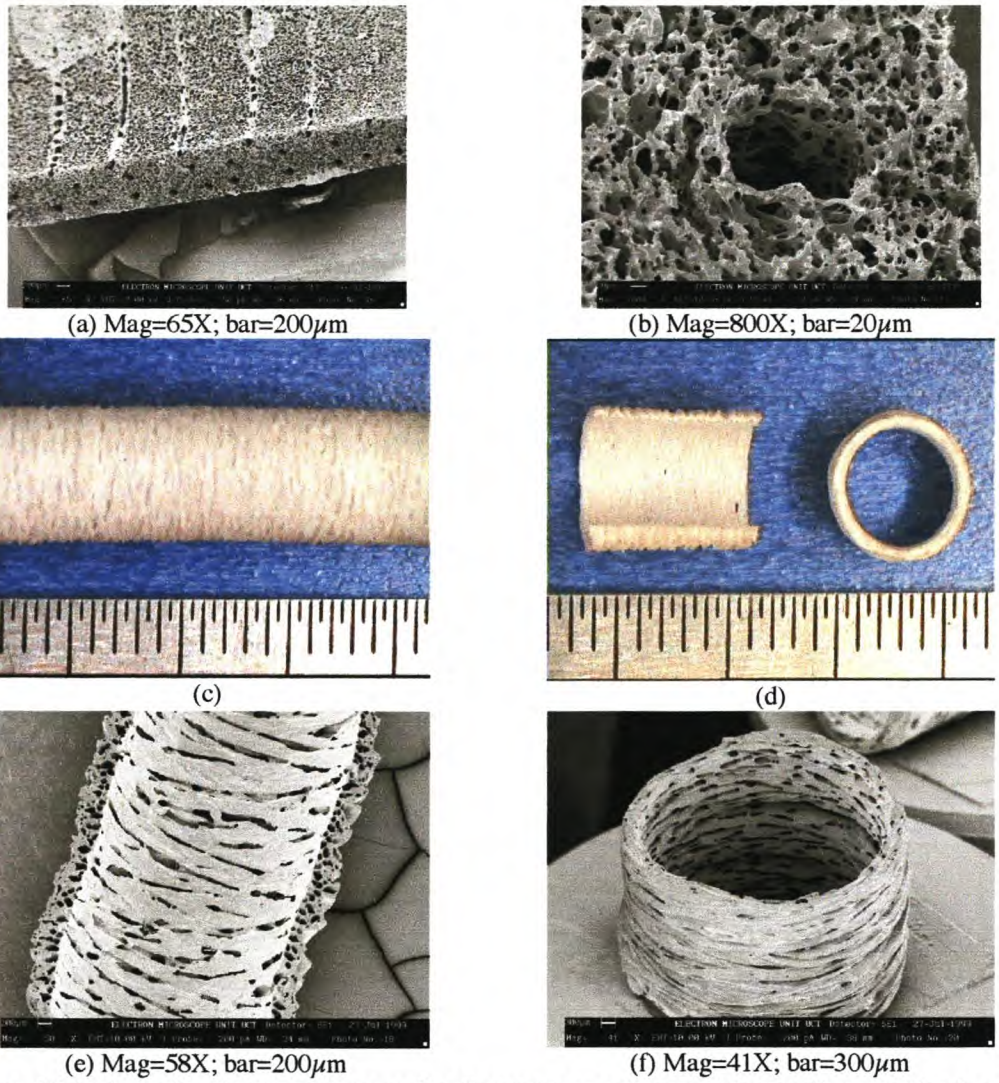

(a) Mag=65X; bar=200μm (b) Mag=800X; bar=20μm

(c) (d)

(e) Mag=58X; bar=200μm (f) Mag=41X; bar=300μm

Figure 5.38: Scanning electron micrographs of prototype grafts containing (a,b) a combination of helical channels and pores, and (c-f) helical channels without additional macropores

5.4.5 Melt Processing

5.4.5.1 Melt-extracted grafts

The melt processing of polyurethanes with salt crystals (and subsequent extraction of the crystals) resulted in structures not unlike those obtained by solution techniques in which the porogen and particulate porogen were premixed. The pores were ill-defined (See Figure 5.39) and the interpore connectivity was low.

Stellenbosch University http://scholar.sun.ac.za

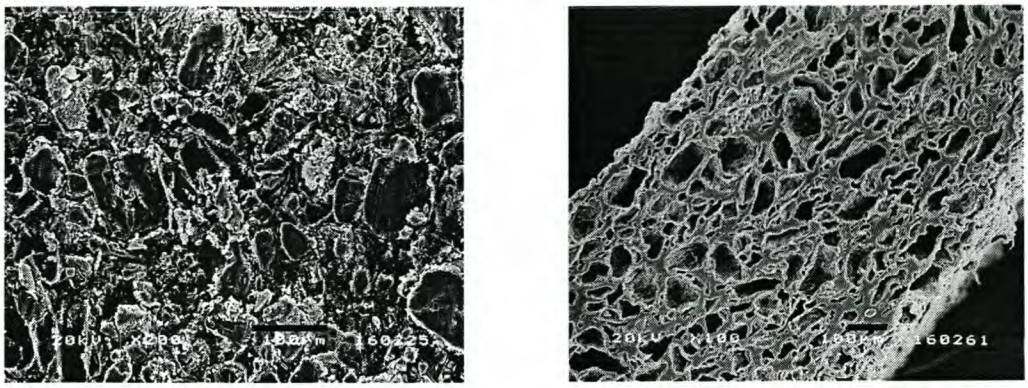

(a) Before extraction (Mag=200X; bar=100μm) (b) After extraction (Mag=100X; bar=100μm)

Figure 5.39: Micrographs of structures obtained by extruding M48 after compounding with 50% NaCl (90-106μm)

5.4.5.2 Melt -blown grafts

Melt extrusion of polyurethanes with chemical blowing agents resulted in the formation of non-connected pores similar to those obtained by Soldani [8]. Although the porosity could be influenced by changing the type and quantity of blowing agent, open-cell foams could not be produced by this method. Two representative samples of the structures obtained with two polyurethanes using two different blowing agents are shown in Figure 5.40. Further attempts to increase the porosity were accompanied by the collapse of the foam structures.

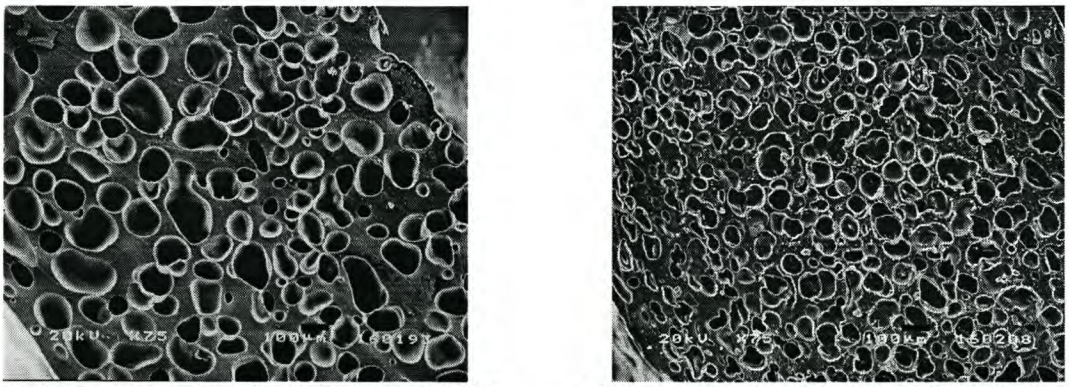

Texin + 1phr Genitron VKA 9164 (175/190/205/125°C)
(Mag=75X; bar=100μm)

M48 + 3phr Genitron DP 35/22 (145/160/170/125°C)
(Mag=75X; bar=100μm)

Figure 5.40: Micrographs of the pore structures obtained by the melt extrusion of polyurethanes with chemical blowing agents.

Stellenbosch University http://scholar.sun.ac.za

5.5 Summary

The different techniques that have been used to produce porous vascular grafts resulted in the formation of a wide variety of structures that may be classified as being either

- fibrillar (polyurethane fibres constructed into a tube by winding or weaving techniques),
- microporous (structures containing pores in the 5-15μm, range resulting from the phase inversion techniques), or
- macroporous (larger pores produced by the addition of porogens prior to phase inversion, or by reticulation, replamineform, or gas spraying methods).

Reinvestigation of the porogen leaching techniques involving the pre-mixing of particulate porogens (salt crystals) resulted in foam-type structures similar to those obtained by previous researchers. The pores in these structures were ill-defined and contained poor interconnectivity. Although the interconnectivity of these structures was improved by a technique whereby the porogens were pre-packed into annular moulds prior to impregnation with the polymer solution, the structures remained ill-defined due to the shape of the porogens used. Spherical porogens were subsequently used to obtain structures containing both well-defined dodecahedral pores and a high degree of interconnectivity. The size of the pores could be controlled by the use of porogens of well-defined, narrow size distributions.

A rigorous porogen extraction procedure ensured the removal of the porogen. This was confirmed by a ninhydrin protein determination assay. Graft reinforcement was achieved by the helical winding and bonding of a polyurethane fibre to the ablumenal surface.

The application of the technique to an alternative polyurethane was not without problems, but the desired structures could be obtained by reticulation or optimization of the precipitation conditions.

Although the production of grafts containing helical porosities were not taken beyond the prototype stage, novel techniques for the fabrication of such structures were demonstrated.

5.6 References

1. Annis, D., Bornat, A., Edwards, R.O., Higham, A., Loveday, B., and Wilson, J., *An elastomeric vascular prosthesis.* Trans Am Soc Artif Intern Organs, 1978. **24**: p. 209-14.
2. Wilson, G.J., MacGregor, D.C., Klement, P., Lee, J.M., del Nido, P.J., Wong, E.W., and Leidner, J., *Anisotropic polyurethane nonwoven conduits: a new approach to the design of a vascular prosthesis.* Trans Am Soc Artif Intern Organs, 1983. **29**: p. 260-8.
3. Leidner, J., Wong, E.W., MacGregor, D.C., and Wilson, G.J., *A novel process for the manufacturing of porous grafts: process description and product evaluation.* J Biomed Mater Res, 1983. **17**(2): p. 229-47.
4. Zhang, Z., Marois, Y., Guidoin, R.G., Bull, P., Marois, M., How, T., Laroche, G., and King, M.W., *Vascugraft polyurethane arterial prosthesis as femoro-popliteal and femoro-peroneal bypasses in humans: pathological, structural and chemical analyses of four excised grafts.* Biomaterials, 1997. **18**(2): p. 113-24.
5. Gupta, B.S. and Kasyanov, V.A., *Biomechanics of human common carotid artery and design of novel hybrid textile compliant vascular grafts.* J Biomed Mater Res, 1997. **34**(3): p. 341-9.
6. Hayashi, K., Takamizawa, K., Saito, T., Kira, K., Hiramatsu, K., and Kondo, K., *Elastic properties and strength of a novel small-diameter, compliant polyurethane vascular graft.* J Biomed Mater Res, 1989. **23**(A2 Suppl): p. 229-44.
7. Lommen, E., Gogolewski, S., Pennings, A.J., Wildevuur, C.R., and Nieuwenhuis, P., *Development of a neo-artery induced by a biodegradable polymeric vascular prosthesis.* Trans Am Soc Artif Intern Organs, 1983. **29**: p. 255-9.
8. Soldani, G. and Mercogliano, R., *Bioartificial polymeric materials obtained from blends of synthetic polymers with fibrin and collagen.* Int J Artif Organs, 1991. **14**(5): p. 295-303.
9. Kowligi, R.R., von Maltzahn, W.W., and Eberhart, R.C., *Synthetic vascular graft fabrication by a precipitation-flotation method.* ASAIO Trans, 1988. **34**(3): p. 800-4.

Stellenbosch University http://scholar.sun.ac.za

10. Chen, J., Laiw, R., Jiang, S., and Lee, Y., *Microporous segmented polyetherurethane vascular graft: I. Dependency of graft morphology and mechanical properties on compositions and fabrication conditions.* J Biomed Mater Res, 1999. **48**(3): p. 235-45.
11. Ota, K., Sasaki, Y., Nakagawa, Y., and Teraoka, S., *A completely new poly(ether-urethane) graft ideal for hemodialysis blood access.* ASAIO Trans, 1987. **33**(3): p. 129-35.
12. Lamba, N., Woodhouse, K., and Cooper, S., *Polyurethanes in Biomedical applications.* 1997, Boca Raton: CRC Press.
13. Marinescu, V., Pausescu, E., and Carnaru, S., *Long-term biological fate of polyurethane aortic prostheses.* Thorax, 1971. **26**(1): p. 108-11.
14. Berkowitz, H.D., Perloff, L.J., and Roberts, B., *Pseudointimal development on microporous polyurethane lattices.* Trans Am Soc Artif Intern Organs, 1972. **18**(0): p. 25-9.
15. Hiratzka, L.F., Goeken, J.A., White, R.A., and Wright, C.B., *In vivo comparison of replamineform, Silastic, and bioelectric polyurethane arterial grafts.* Arch Surg, 1979. **114**(6): p. 698-702.
16. White, R., Hirose, F., Sproat, R., Lawrence, R., and Nelson, R., *Histopathologic observations after short-term implantation of two porous elastomers in dogs.* Biomaterials, 1981. **2**(3): p. 171-6.
17. Kambic, H., Murabayashi, S., Yozu, R., Morimoto, T., Furuse, M., Harasaki, H., George, C., Helmus, M., Snyder, R., and Nose, Y., *Small vessel replacement with elastomeric protein composite materials: preliminary studies.* Trans Am Soc Artif Intern Organs, 1984. **30**: p. 406-10.
18. Murabayashi, S., Kambic, H., Harasaki, H., Morimoto, T., Yozu, R., and Nose, Y., *Fabrication and long-term implantation of semi-compliant small vascular prosthesis.* Trans Am Soc Artif Intern Organs, 1985. **31**: p. 50-4.
19. Uchida, N., Kambic, H., Emoto, H., Chen, J.F., Hsu, S., Murabayshi, S., Harasaki, H., and Nose, Y., *Compliance effects on small diameter polyurethane graft patency.* J Biomed Mater Res, 1993. **27**(10): p. 1269-79.
20. Seifalian, A., Giudiceandrea, A., and Schmitz-Rixen, T., *Noncompliance: The silent acceptance of a villain*, in *Tissue engineering of vascular prosthetic grafts*, Z. P and HP, G., Editors. 1999, R.G. Landes: Texas.
21. Tai, N., Salacinski, H., Edwards, A., Hamilton, G., and Seifalian, A., *Compliance properties of conduits used in vascular reconstruction.* Br J Surg, 2000. **87**(11): p. 1516-24.
22. van der Lei, B., Wildevuur, C.R., Dijk, F., Blaauw, E.H., Molenaar, I., and Nieuwenhuis, P., *Sequential studies of arterial wall regeneration in microporous, compliant, biodegradable small-caliber vascular grafts in rats.* J Thorac Cardiovasc Surg, 1987. **93**(5): p. 695-707.
23. Hinrichs, W.L., Kuit, J., Feil, H., Wildevuur, C.R., and Feijen, J., *In vivo fragmentation of microporous polyurethane- and copolyesterether elastomer-based vascular prostheses.* Biomaterials, 1992. **13**(9): p. 585-93.
24. Doi, K., Nakayama, Y., and Matsuda, T., *Novel compliant and tissue-permeable microporous polyurethane vascular prosthesis fabricated using an excimer laser ablation technique.* J Biomed Mater Res, 1996. **31**(1): p. 27-33.
25. Kowligi, R.R., von Maltzahn, W.W., and Eberhart, R.C., *Fabrication and characterization of small-diameter vascular prostheses.* J Biomed Mater Res, 1988. **22**(3 Suppl): p. 245-56.
26. Eberhart, A., Zhang, Z., Guidoin, R., Laroche, G., Guay, L., De La Faye, D., Batt, M., and King, M.W., *A new generation of polyurethane vascular prostheses: rara avis or ignis fatuus?* J Biomed Mater Res, 1999. **48**(4): p. 546-58.
27. Leidner, J. and Wong, E., *A novel process for the manufacturing of porous grafts: Process description and product evaluation.* J. Biomed. Mater. Res., 1983. **17**: p. 229-247.
28. Wilson, G.J., MacGregor, D.C., Klement, P., Dereume, J.P., Weber, B.A., Binnington, A.G., and Pinchuk, L., *The composite Corethane/Dacron vascular prosthesis. Canine in vivo evaluation of 4 mm diameter grafts with 1 year follow-up.* ASAIO Trans, 1991. **37**(3): p. M475-6.
29. Martz, H., Beaudoin, G., Paynter, R., King, M., Marceau, D., and Guidoin, R., *Physicochemical characterization of a hydrophilic microporous polyurethane vascular graft.* J Biomed Mater Res, 1987. **21**(3): p. 399-412.
30. Williams, S.K., Carter, T., Park, P.K., Rose, D.G., Schneider, T., and Jarrell, B.E., *Formation of a multilayer cellular lining on a polyurethane vascular graft following endothelial cell sodding.* J Biomed Mater Res, 1992. **26**(1): p. 103-17.
31. Millam, R., *Design of an adventitial type reinforcement of prosthetic vascular grafts through mechanically affirmed material and structure modulation.*, in *Faculty of Health Sciences*. 2001, University of Cape Town: Cape Town.
32. Edwards, A., Carson, R.J., Bowald, S., and Quist, W.C., *Development of a microporous compliant small bore vascular graft.* J Biomater Appl, 1995. **10**(2): p. 171-87.
33. White, R.A., White, E.W., Hanson, E.L., Rohner, R.F., and Webb, W.R., *Preliminary report: Evaluation of tissue ingrowth into experimental Replamineform vascular prostheses.* Surgery, 1976. **79**(02): p. 229-32.

Stellenbosch University http://scholar.sun.ac.za

34. Lyman, D.J., Albo, D., Jr., Jackson, R., and Knutson, K., *Development of small diameter vascular prostheses.* Trans Am Soc Artif Intern Organs, 1977. **23**: p. 253-61.
35. Lyman, D.J., Fazzio, F.J., Voorhees, H., Robinson, G., and Albo, D., Jr., *Compliance as a factor effecting the patency of a copolyurethane vascular graft.* J Biomed Mater Res, 1978. **12**(3): p. 337-45.
36. Hess, F., Jerusalem, C., and Braun, B., *The endothelialization process of a fibrous polyurethane microvascular prosthesis after implantation in the abdominal aorta of the rat. A scanning electron microscopic study.* J Cardiovasc Surg (Torino), 1983. **24**(5): p. 516-24.
37. Ives, C.L., Zamora, J.L., Eskin, S.G., Weilbaecher, D.G., Gao, Z.R., Noon, G.P., and DeBakey, M.E., *In vivo investigation of a new elastomeric vascular graft (Mitrathane).* Trans Am Soc Artif Intern Organs, 1984. **30**: p. 587-90.
38. Muller-Glauser, W., Lehmann, K.H., Bittmann, P., Bay, U., Dittes, P., von Segesser, L., and Turina, M., *A compliant small-diameter vascular prosthesis lined with functional venous endothelial cells.* ASAIO Trans, 1988. **34**(3): p. 528-31.
39. Underwood, C.J., Tait, W.F., and Charlesworth, D., *Design considerations for a small bore vascular prosthesis.* Int J Artif Organs, 1988. **11**(4): p. 272-6.
40. Kogel, H., Vollmar, J.F., Cyba-Altunbay, S., Mohr, W., Frosch, D., and Amselgruber, W., *New observations on the healing process in prosthetic substitution of large veins by microporous grafts--animal experiments.* Thorac Cardiovasc Surg, 1989. **37**(2): p. 119-24.
41. Kogel, H., Amselgruber, W., Frosch, D., Mohr, W., and Cyba-Altunbay, S., *New techniques of analyzing the healing process of artificial vascular grafts, transmural vascularization, and endothelialization.* Res Exp Med, 1989. **189**(1): p. 61-8.
42. Uchida, N., Emoto, H., Kambic, H., Harasaki, H., Chen, J.F., Hsu, S.H., Murabayashi, S., and Nose, Y., *Compliance effect on patency of small diameter vascular grafts.* ASAIO Trans, 1989. **35**(3): p. 556-8.
43. Therrien, M., Guidoin, R., Adnot, A., and Paynter, R., *Hydrophobic and fibrillar microporous polyetherurethane urea prosthesis: an ESCA study on the internal and external surfaces of explanted grafts.* Biomaterials, 1989. **10**(8): p. 517-20.
44. Brothers, T.E., Stanley, J.C., Burkel, W.E., and Graham, L.M., *Small-caliber polyurethane and polytetrafluoroethylene grafts: a comparative study in a canine aortoiliac model.* J Biomed Mater Res, 1990. **24**(6): p. 761-71.
45. Huang, B., Marois, Y., Roy, R., Julien, M., and Guidoin, R., *Cellular reaction to the Vascugraft polyesterurethane vascular prosthesis: in vivo studies in rats.* Biomaterials, 1992. **13**(4): p. 209-16.
46. Hess, F., Jerusalem, C., Steeghs, S., Reijnders, O., Braun, B., and Grande, P., *Development and long-term fate of a cellular lining in fibrous polyurethane vascular prostheses implanted in the dog carotid and femoral artery. A scanning and light microscopical study up to 53 months after implantation.* J Cardiovasc Surg (Torino), 1992. **33**(3): p. 358-65.
47. Hess, F., Jerusalem, R., Reijnders, O., Jerusalem, C., Steeghs, S., Braun, B., and Grande, P., *Seeding of enzymatically derived and subcultivated canine endothelial cells on fibrous polyurethane vascular prostheses.* Biomaterials, 1992. **13**(10): p. 657-63.
48. Gershon, B., Cohn, D., and Marom, G., *Compliance and ultimate strength of composite arterial prostheses.* Biomaterials, 1992. **13**(1): p. 38-43.
49. Cohn, D., Elchai, Z., Gershon, B., Karck, M., Lazarovici, G., Sela, J., Chandra, M., Marom, G., and Uretzky, G., *Introducing a selectively biodegradable filament wound arterial prosthesis: a short-term implantation study.* J Biomed Mater Res, 1992. **26**(9): p. 1184-204.
50. Guidoin, R., Sigot, M., King, M., and Sigot-Luizard, M.F., *Biocompatibility of the Vascugraft: evaluation of a novel polyester urethane vascular substitute by an organotypic culture technique.* Biomaterials, 1992. **13**(5): p. 281-8.
51. Sigot-Luizard, M.F., Sigot, M., Guidoin, R., King, M., von Maltzahn, W.W., Kowligi, R., and Eberhart, R.C., *A novel microporous polyurethane blood conduit: biocompatibility assessment of the UTA arterial prosthesis by an organo-typic culture technique.* J Invest Surg, 1993. **6**(3): p. 251-71.
52. Stansby, G., Berwanger, C., Shukla, N., Schmitz-Rixen, T., and Hamilton, G., *Endothelial seeding of compliant polyurethane vascular graft material.* Br J Surg, 1994. **81**(9): p. 1286-9.
53. Poole-Warren, L.A., Schindhelm, K., Graham, A.R., Slowiaczek, P.R., and Noble, K.R., *Performance of small diameter synthetic vascular prostheses with confluent autologous endothelial cell linings.* J Biomed Mater Res, 1996. **30**(2): p. 221-29.
54. Allen, R.D., Yuill, E., Nankivell, B.J., and Francis, D.M., *Australian multicentre evaluation of a new polyurethane vascular access graft.* Aust N Z J Surg, 1996. **66**(11): p. 738-42.
55. Marois, Y., Paris, E., Zhang, Z., Doillon, C.J., King, M.W., and Guidoin, R.G., *Vascugraft microporous polyesterurethane arterial prosthesis as a thoraco-abdominal bypass in dogs.* Biomaterials, 1996. **17**(13): p. 1289-300.
56. Akiyama, N., Esato, K., Fujioka, K., and Zempo, N., *A comparison of CORVITA and expanded polytetrafluoroethylene vascular grafts implanted in the abdominal aortas of dogs.* Surg Today, 1997. **27**(9): p. 840-5.

Stellenbosch University http://scholar.sun.ac.za

57. Farrar, D.J., *Development of a prosthetic coronary artery bypass graft.* Heart Surg Forum, 2000. **3**(1): p. 36-40.
58. Hansen, C., Journal of Paint Technology, 1967. **39**: p. 505-510.
59. Bascom, W., *The wettability of polymer surfaces and the spreading of polymer liquids.* Advances in Polymer Science, 1988. **85**: p. 89.
60. Kaeble, D., *The chemistry of adhesion*. 1971, New York: Wiley Interscience.
61. Wu, S., Journal of Adhesion, 1973. **5**: p. 39.
62. Sarin, V., Kent, S., Tam, J., and Merrifield, R., *Quantitative monitoring of solid-phase peptide synthesis by the ninhydrin reaction.* Anal Biochem, 1981. **117**(1): p. 147-57.
63. *Physical constants of inorganic compounds*, in *CRC Handbook of Chemistry and Physics*, R. Weast, Editor. 1985, CRC Press: Boca Raton, Florida. p. B142.

Stellenbosch University http://scholar.sun.ac.za

CHAPTER 6

Effect of well-defined dodecahedral porosity on inflammation and neo-vascularization

6.1 Abstract

Porosity is an important factor in the healing of prosthetic devices. To better understand this phenomenon, porous polyurethane scaffolds were produced by a variation of the phase inversion/porogen-extraction technique in which a pre-packed column of spherical porogen particles was infiltrated with a polymer solution prior to polymer precipitation and porogen extraction. Scaffolds contained pores of well-defined shape (approaching open-faced, pentagonal dodecahedra), narrow size distributions (66.1±1.3, 84.2±1.7 and 157.0±2.4μm) and high interconnectivity (interconnecting windows of 30.1±0.8, 41.9±1.5 and 76.4±2.0μm respectively). A high degree of accessible macroporosity (greater than 80%) could be achieved while limiting the inaccessible microporosity to below 2%.

The neo-vascularization and inflammatory responses to the scaffolds were evaluated in the subcutaneous rat model for 4 weeks. The inflammatory response index (IRI) and foreign-body giant-cell index (FBGCI) could be reduced by 56% ($p<0.05$) and 21% ($p<0.02$) respectively when the pore size was increased from 66 to 157μm, while the vascularization index (VI) and arteriolar index (AI) remained unchanged.

Thus a significant decrease in inflammatory response could be achieved without adversely affecting the degree of neo-vascularization by increasing the size of the pores.

6.2 Introduction

Porous polymeric scaffolds have been widely employed in organ regeneration, structural tissue repair and prosthetic devices. In order to fulfil the requirements posed by such applications, scaffolds should exhibit a highly interconnected and uniformly distributed pore structure throughout the matrix [1]. High porosity values and large interconnected pores have consequently been identified as essential characteristics for tissue ingrowth, vascularization and the diffusion of nutrients [2].

In addition to expanded structures created by the stretching of crystalline materials (e.g. ePTFE), porous scaffolds are conveniently divided into two classes, based on their morphology, i.e. fibrillar structures and foams. Fibrillar scaffolds may be produced by knitting and weaving [3], melt or solution spinning [4], electrostatic spinning [5], and other non-woven techniques [2]. Several techniques are also available for the production of the second class, termed foamed structures. Replamineform [6], thermal inversion [1], blowing/reticulation [7] and gas expansion [8] are among those reported. Liquid-liquid phase inversion of polymeric solutions is another versatile technique that has been used extensively in the production of porous scaffolds [9, 10]. This method is typically restricted to the production of pores in the 1-10μm range. Larger pores (typically 25-200μm) can be introduced by the addition of extractable porogens to the polymer solution prior to precipitation [11-13]. The porogens are added to polymer solutions and extracted concurrent with or subsequent to the precipitation of the polymer. A macroporosity of roughly the dimensions of the porogen is thereby superimposed on the microporosity achieved by the phase inversion process. The use of salts and other irregularly shaped porogens, together with the premixing methods used during production, generally result in irregularly shaped pores, limited pore interconnectivity, and residual porogen remaining in the structure [1].

The effect of pore size on the ingrowth of tissue into porous devices has been studied by various workers. Structures with pores smaller than 0.5μm allow for the passage of fluids but prevent

Stellenbosch University http://scholar.sun.ac.za

the ingrowth of cells and bacteria, and are preferred for wound dressing applications [14]. An increase in pore size to 5-10μm allows only limited cell ingrowth [15]. In addition to cellular ingrowth, structures with interconnected pores of 10-30μm have been reported to additionally support the ingrowth of fibrohistiocytic tissue and capillaries [6, 16]. Organised fibrous tissue forms in pores of 30-100μm [17], while fibrocartilaginous tissue has been reported to form in pores of 18-180μm [18].

The objectives of the present study were to produce porous structures containing regularly shaped pores of well-defined size distribution and high interconnectivity, and to evaluate the effect of pore size on the neo-vascularization and inflammatory response to such scaffolds in the subcutaneous rat model. The lowest of the three pore sizes used in this study has interconnecting windows (the limiting dimension for ingrowth) of 30μm, which corresponds with the lower porosity range that has been reported to support capillary ingrowth. The largest pore size was chosen to fall in the >100μm range, that has been reported to support fibrocartilaginous tissue formation, while the mid-range pore size was chosen to correspond to the 100μm divide described above.

6.3 Materials and methods

6.3.1 Porous scaffold production

Spherical gelatin beads (Thies Technologies, St Louis, USA) were fractionated into the desired size ranges by passing them through graded sieves The 63-75μm, 90-106μm and 150-180m fractions were collected. The beads were packed into the lumens of cylindrical glass tubes (ID=5.4mm, length =180mm) vertically mounted in a custom-made manifold containing upper and lower reservoirs. The upper reservoirs were filled with a 20% (m/m) solution of segmented polyurethane (in N-methyl pyrollidone, NMP, Sigma-Aldrich, RSA), after which a pressure of 750kPa and a vacuum of 100kPa were applied to the upper and lower manifolds, respectively. After complete infiltration of the entire length of the packed bead column, the resultant polymer/solvent/porogen rods were demoulded and the polymer precipitated by phase inversion achieved in a non-solvent for both the polymer and the porogen (24hrs, RT, 96% ethanol, Saarchem Holpro, Krugersdorp, RSA). Extraction of the porogen beads (5x1h, 60°C, water), extensive washing (5 days, 60°C, water) to remove traces of porogen and solvent, and drying, resulted in the porous scaffold (Figure 6.1). The rods were skinned by applying a 5% solution of the polyurethane in chloroform (Sigma-Aldrich, RSA) to the outer surface (in order to limit tissue ingrowth to the longitudinal direction) and subsequent drying at elevated temperatures (Fig 6.2b). After slicing disks of uniform thickness (2mm) from the rods, sterilization by ethylene oxide (ETO) exposure, and removal of residual ETO at low pressure (24hr, RT, -750mmHg), the morphological and in vivo evaluations were performed.

6.3.2 Porogen, pore and window size measurement

Standard image analysis techniques, using NIH image software (for Macintosh), were used to determine porogen, pore and interconnecting window sizes from scanning electron micrographs.

Stellenbosch University http://scholar.sun.ac.za

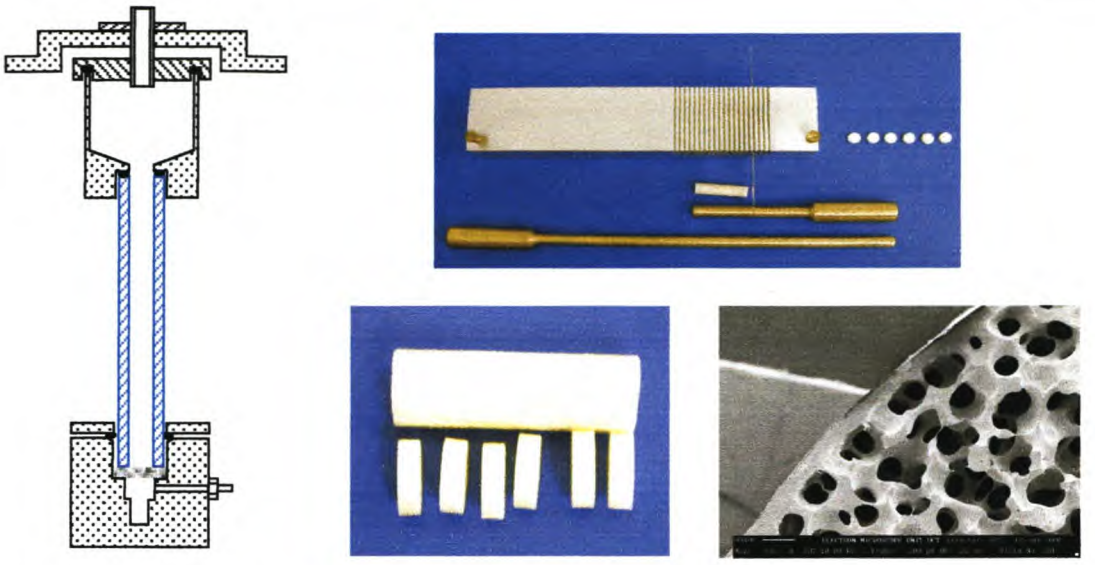

Figure 6.1: Graphic representation of the methods used in the production of porous disks.

6.3.3 Porosity determination

6.3.3.1 Volumetric method

Porosities were determined by a volumetric liquid displacement technique similar to that described by Zhang and Zhang [19]. A scaffold sample of a given mass (m_{scaf}) was immersed in a graduated cylinder containing a known volume (V_1) of ethanol. After a series of evacuation/re-pressurization cycles, to ensure penetration of the ethanol into all the accessible pores, the volume (V_2) was recorded. The ethanol-impregnated scaffold was subsequently removed and the residual volume (V_3) recorded. The porosity of the open pores (P_{Vop}) was calculated from equation (6.1):

$$P_{Vop} = V_{Vop} / V_{Vscaf} = (V_1 - V_3)/(V_2 - V_3) \tag{6.1}$$

where V_{Vscaf} is the volume of the scaffold and V_{Vop} the volume of the open pores. In addition, the porosity of the closed pores (P_{Vcp}) was calculated by (See appendix 3):

$$P_{Vcp} = \left(1 - \frac{m_{scaf}}{\rho_{pol}(V_2 - V_1)}\right)\left(\frac{V_2 - V_1}{V_2 - V_3}\right) \tag{6.2}$$

where m_{scaf} is the mass of the scaffold and ρ_{pol} the density of the polymer (1.025g/cm^3). The total porosity of the scaffold (P_{Vtp}), as determined by the volumetric method, follows from:

$$P_{Vtp} = P_{Vop} + P_{Vcp} \tag{6.3}$$

6.3.3.2 Gravimetric method

The total porosity of the scaffold was also calculated directly from the mass and volume of the scaffold according to:

$$P_{Gtp} = \frac{V_{Gtp}}{V_{Gscaf}} = \frac{V_{Gscaf} - V_{Gpol}}{V_{Gscaf}} = 1 - \frac{V_{Gpol}}{V_{Gscaf}} = 1 - \frac{m_{scaf}}{\rho_{pol} V_{Gscaf}} = 1 - \frac{m_{scaf}}{\rho_{pol}(\pi r^2 l)} \tag{6.4}$$

where P_{Gtp} is the total porosity and V_{Gtp} is the total volume of pores (V_{Gop} + V_{Gcp}), as determined by the gravimetric method, r and l are the radius and length of the porous rod, and other variables as defined elsewhere, with the exception that they refer to those obtained via the gravimetric method (subscript *G*)

Stellenbosch University http://scholar.sun.ac.za

6.3.3.3 Theoretical method

If one assumes that the volume of the skeleton defined by the polymer solution in a packed bed method remains constant during phase inversion, it is possible to derive the theoretical macro (P_{Tmac}), micro (P_{Tmic}) and total porosity (P_{Ttp}) from basic principles based on physical characteristics of the constitutive elements (polymer, solvent, solution, porogen) alone. It can be shown that (See appendix 4):

$$P_{Ttp} = 1 - \left[\left(\frac{x\rho_{soln}}{\rho_{pol}}\right)\left(1 - \frac{\rho_{Bpor}}{\rho_{por}}\right)\right] \tag{6.5}$$

$$P_{Tmac} = \frac{\rho_{Bpor}}{\rho_{por}} \tag{6.6}$$

and hence:

$$P_{Tmic} = P_{Ttp} - P_{Tmac} \tag{6.7}$$

where x is the concentration of the polymer solution (m/m) and ρ_{soln}, ρ_{pol}, and ρ_{por} the densities (g/cm^3) of the solution, polymer, and porogen, and ρ_{Bpor} is the bulk density of the porogen.

6.3.4 Rat subcutaneous implants

All animal experiments described in this dissertation were performed after approval by the Animal Research and Ethics Committee of the University of Cape Town, and in compliance with the "Principles of Laboratory Care" and the guidelines for the care and use of laboratory animals (NIH publication no. 86-23).

Disks were prepared from each porogen size fraction (63-75, 90-106 and 150-180 μm) as described above and implanted subcutaneously in young male Wistar rats (+ 200 g). Following induction of general anaesthesia with an intramuscular injection of a ketamine/xylazine mixture, the dorsal side of the animal was shaved. Using an aseptic technique, three 1 cm longitudinal incisions were made through the skin at either side of the dorsal midline. A subcutaneous pocket for each disk was prepared by gentle blunt dissection with a pair of curved artery forceps. Three disks were implanted on each side (i.e. 6 per animal) and the skin incision was closed with single 3/0 prolene stitches (Fig 6.2a). After 28 days of implantation, the animals were killed by inhalation of carbon dioxide. Disks were explanted with their surrounding fibrous capsules and fixed overnight in 10% buffered formalin.

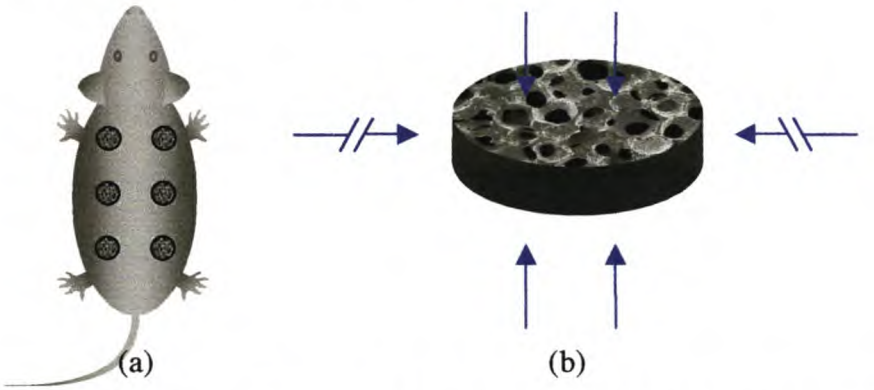

Figure 6.2: Schematic representation of rat subcutaneous implant model showing possible ingrowth directions and circumferential sealant.

Stellenbosch University http://scholar.sun.ac.za

6.3.5 Evaluation of neovascularisation and inflammatory response.

One half of each disk (Fig. 6.3B) was then transferred to a 70% ethanol solution for storage, while the other half (A) was embedded in paraffin wax (C,D) after dehydration in ascending grades of alcohol and clearing with iso-octane. The embedded samples were subsequently sectioned to a thickness of 5 μm (E), mounted on microscope slides (E), and excess wax removed by incubation at elevated temperatures (60°C, 1h) and clearing (iso-octane) (F).

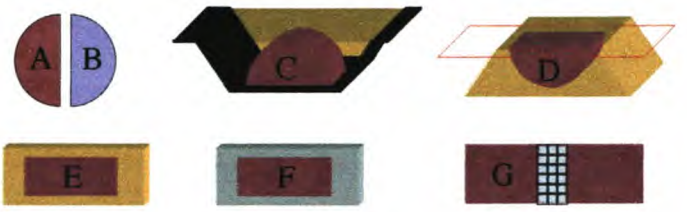

Figure 6.3: Schematic representation of explant sample preparation steps.

Sections were deparaffinised and stained with a biotinylated Griffonia simplicifolia lectin (GSL-1) (Vector Laboratories, Burlingame, CA, USA) which shows specificity for endothelial cells, monoclonal anti-rat smooth muscle cell actin antibody (α-SMCA) (Research Diagnostics, Flanders, NJ, USA) which shows specificity for vascular smooth muscle cells, and monoclonal antibody ED1 (Serotec Ltd, Oxford, UK) which shows specificity for tissue macrophages. Multinucleated foreign body giant cells (FBGC) were identified on hematoxylin and eosin stained sections.

To quantify the inflammatory response (ED1 positive cells), FBGC content, neovascularisation (GSL-1 positive cells) and arteriolarization (a-SMCA positive cells), the relevant stained sections were subjected to image analysis. For each section, a blinded observer captured 18 regions (Fig 6.3 F; 300 X 350μm: neovascularisation, arteriolarization; 150 X 175 μm: inflammatory response, FBGC content) with a Leitz DM RB microscope. The areas of positively identified elements were quantified with Qwin image analysis software and normalised to the available ingrowth area, generating a vascularisation index (VI), arteriolarization index (AI), FBGC index (FBGCI) and an inflammatory response index (IRI)

6.3.6 Statistical analysis

Data are expressed as means ± standard error of means (SEM). The comparisons of porogen, pore and interconnecting window sizes, as well as VI, AI, FBGCI and IRI between groups, were made by Student's unpaired t-tests. One-sided p-values were determined in all cases. A significance level of 0.05 or less was accepted as being statistically significant.

6.4 Results

6.4.1 Structure

Figure 6.4 a-c shows low magnification scanning electron micrographs of hemicircular sections of disks produced from the three porogen size fractions (63-75μm, 90-106μm and 150-180μm), as well as the thin polyurethane skin around the circumference. The increase in pore size with increased porogen size, and the uniformity of the pores sizes, is clearly seen in the higher magnification micrographs (Fig 6.4 d-f).

Stellenbosch University http://scholar.sun.ac.za

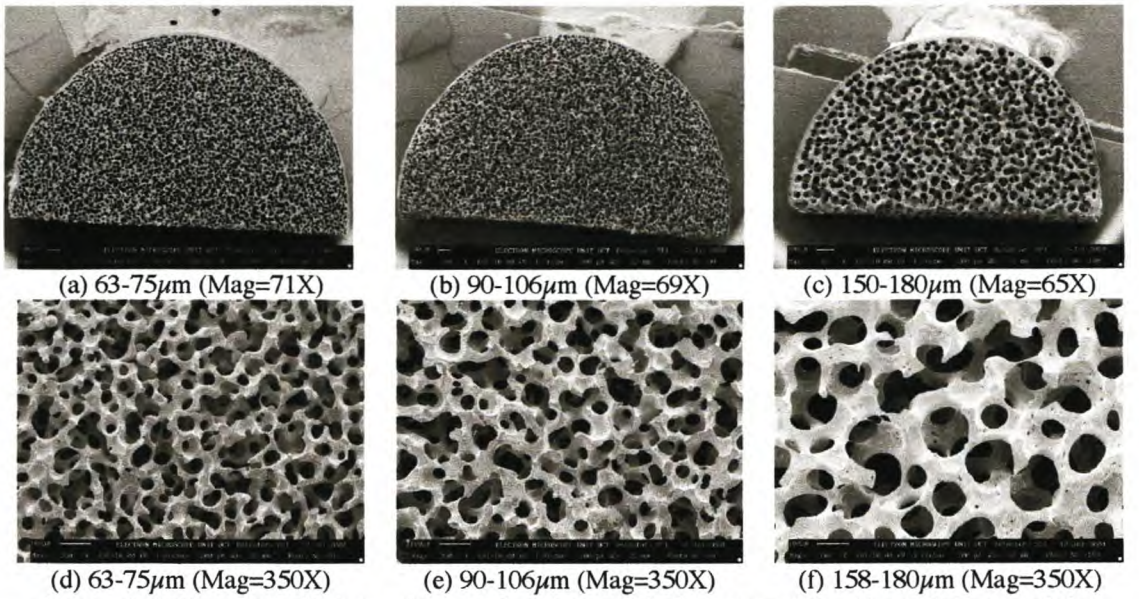

(a) 63-75μm (Mag=71X) (b) 90-106μm (Mag=69X) (c) 150-180μm (Mag=65X)

(d) 63-75μm (Mag=350X) (e) 90-106μm (Mag=350X) (f) 158-180μm (Mag=350X)

Figure 6.4: Scanning electron micrographs of unmodified porous polyurethane disks containing pores of uniform and discrete size distributions.

6.4.2 Porogen, pore and window sizes

The actual porogen sizes were within 14% of the lower value of the sieve ranges from which they were collected (64.5±0.3μm for 63-75μm range, 87.5±0.7μm for 90-106 range and 129.0±0.9μm for the 150-180μm range). The use of these porogens resulted in the formation of macropores of 66.1±1.3μm, 84.2±1.7μm and 157.0±2.4μm. The respective sizes of the interconnecting windows were 30.1±0.8μm, 41.9±1.5μm and 76.4±2.0μm (Figure 6.5). The differences in intra-feature porogen, pore and window sizes were statistically highly significant ($p < 10^{-8}$). The window-to-bead size ratio was relatively constant at an average of 51.3±4.0%, while the pore to bead size ratio was found to be either close to unity (smaller bead sizes), or above unity (large beads). The window-to-pore size ratio averaged at 48.0±1.3%, and increased as the porogen size increased.

6.4.3 Porosity

A comparison of the porosities obtained by the three methods employed is depicted in Figure 6.6. It shows that the porosity of the scaffolds is independent of the size of the porogen used in its production. According to the volumetric method, the average open porosity of 84.2±0.1% contributes 99.8% of the total porosity (85.2±0.0%). The gravimetric method produces a slightly lower total porosity of 81.2±0.0%. A theoretical calculation of the porosities, under the assumption of constant polymer/polymer solution volume and no contraction or expansion during phase inversion, yields a much lower value for the macroporosity (61.9±0.3%), and higher values for the micro and total porosities (30.4±0.3% and 92.3±0.1%, respectively).

Stellenbosch University http://scholar.sun.ac.za

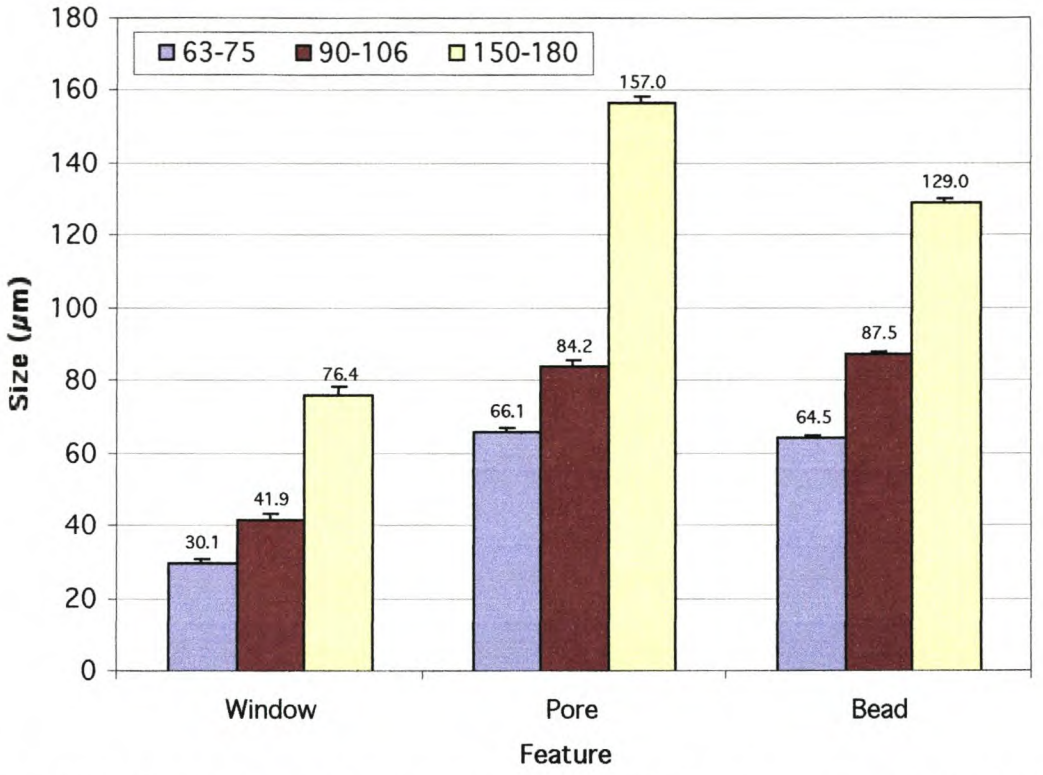

Figure 6.5: The sizes of gelatin porogen beads after fractionation into 63-75, 90-106 and 150-180µm fractions and the sizes of macropores and interconnecting windows of porous scaffolds prepared by the use of these particulate porogens (Mean ± SEM).

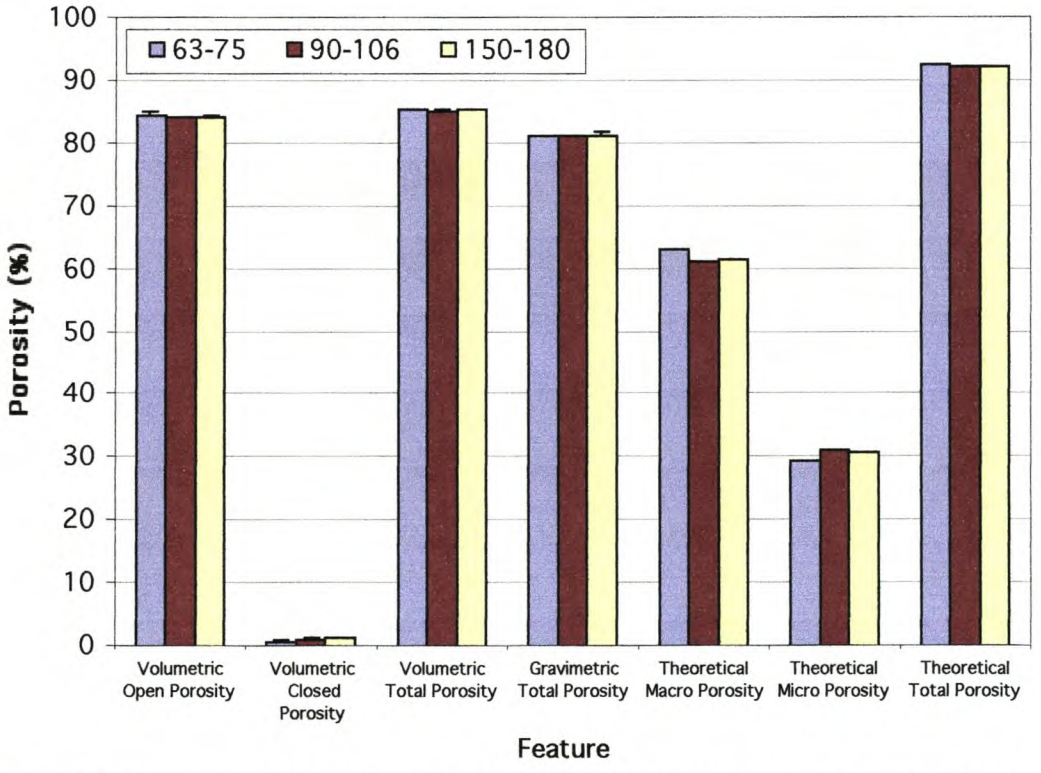

Figure 6.6: The macro, micro and total porosities of porous scaffolds prepared from 63-75, 90-106 and 150-180µm fraction porogens as determined by the volumetric, gravimetric and theoretical methods described in the text (% ± SEM).

Stellenbosch University http://scholar.sun.ac.za

6.4.4 Rat subcutaneous implants

6.4.4.1 Histology

Hematoxylin and eosin stains of the explanted porous disks indicated that there was an inverse correlation between the number and size of multinucleated FBGC and pore size (Fig 6.7 a-b). This trend in an inflammatory response was more clearly perceived in sections that were immunoperoxidase-stained with the ED1 antibody (Fig 6.7 c-d). There were substantially fewer macrophages in the high pore-size (129μm) relative to the low pore-size (66 μm) disks. A tendency for the ED1 antibody to stain only limited portions of FBGCs was observed. The incomplete staining was variable and appeared to be more frequent in the 157μm explants. Capillaries invading the disks were visualised with GSL-1 lectin staining. GSL-1 also reacts with FBGCs but vessels could be unequivocally identified by the presence of a lumen (Fig 6.7 e-f). Vessels were present throughout the depth of the disks, with a slightly higher occurrence just below the interface between the polyurethane and surrounding tissue. There was no intimation of relation between pore size and vascularisation. Erythrocytes were evident in a substantial proportion of vessels suggesting the existence of organised capillary beds in at least some areas of the implants. Mature vessels vested with mural smooth muscle cells were identified through a positive reaction with the monoclonal α-SMCA antibody (Fig 6.7 g-h). Arterioles were evenly distributed throughout the disks and appeared to be at similar levels across the three pore-sizes implanted.

6.4.4.2 Quantification of indexes

The results of the effect of pore size on the vascular (VI), arteriolar (AI), inflammatory response (IRI) and foreign body giant cell indexes (FBGCI) are shown in Figure 6.8. The FBGCI decreased by 21% between the 66 μm and 157 μm pore size scaffolds (5.7±0.5 to 4.5±0.1% for the two pore sizes, respectively, $p< 0.02$). There was an even larger decrease of 56% in the IRI, as evident in the qualitative examination of the ED1 antibody stained sections, between these two groups (4.0±1.1 to 1.8±0.3% for 66m and 157μm pores respectively, $p< 0.05$). The vascular and arteriolar indices did not change significantly with pore-size variation. The proportion of vessels that were arterialised was 43.7±4.4%, on average, across all pore sizes.

Stellenbosch University http://scholar.sun.ac.za

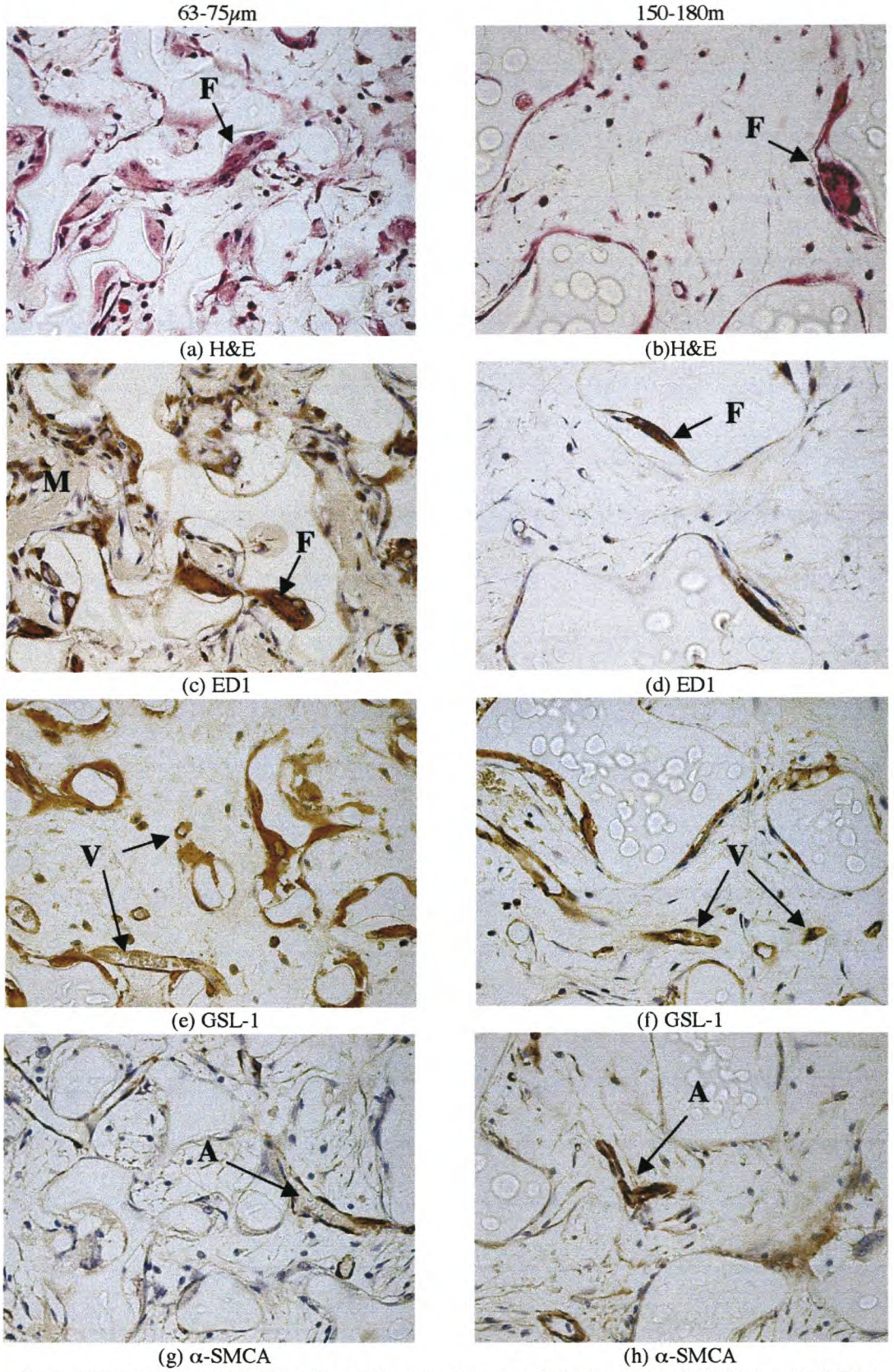

Figure 6.7: Representative histological images depicting (a,b) Hematoxylin & Eosin, (c,d) ED1 antibody, (e,f) GSL-1 lectin, and (g,h) α-SMCA stained sections of the polyurethane disks. Left column: 66μm porosity. Right column: 157μm porosity. (F=FBGC, V=Vessel, A=Arteriole and M=Macrophage)

Stellenbosch University http://scholar.sun.ac.za

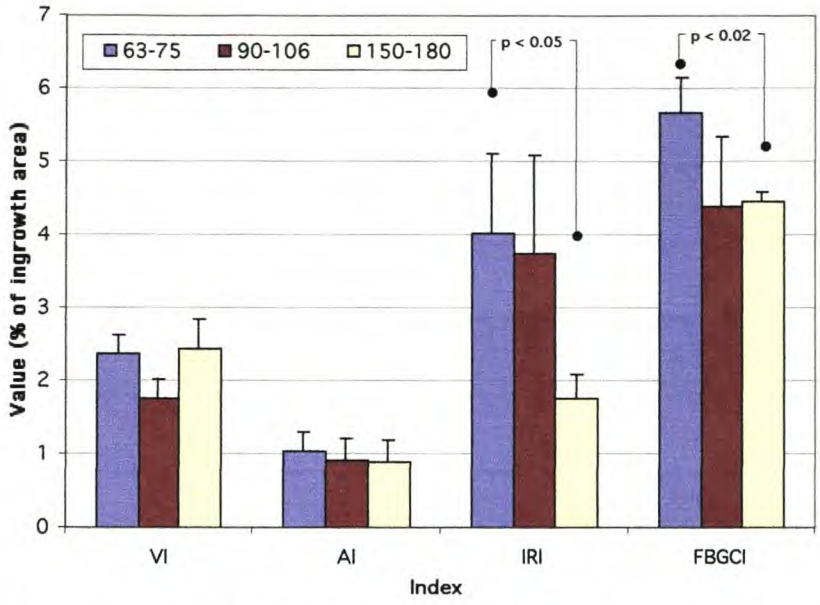

Figure 6.8: The Vascularization (VI), Arteriole (AI), Immune response (IRI) and foreign body giant cell (FBGCI) indexes of tissue growth into porous scaffolds prepared from 63-75, 90-106 and 150-180μm fraction porogens (% area).

6.5 Discussion

In the past few decades, the field of biomaterials research has expanded to include a wide range of prosthetic scaffolds such as orthopaedic, cardiovascular and aesthetic implants. In most of these implants, complete integration or at least silent acceptance by the recipient organism is a key goal. Integration and quiescent acceptance, however, often imply both the ability of tissue to 'invade' the prosthetic implant and the absence of an inflammatory rejection response. While porosity is an evident prerequisite for tissue ingrowth, there is evidence that space dimensions may influence the degree of foreign-body inflammation [20, 21]. As much as porosity itself was addressed in numerous approaches towards the creation of polymer scaffolds, pore dimensions were undefined and often random, thus preventing researchers from establishing a correlation between space dimensions and inflammation. By combining well-defined spherical porogens with a refined method of ethanol phase inversion, the authors were able to:

- create well defined, interconnecting, dodecahedron-shaped, ingrowth spaces within distinct narrow size-ranges,
- reduce the 'micro-porosity' associated with phase inversion to less than 2% and thus create a material less prone to mechanical failure,
- prove a correlation between space dimensions and inflammation by halving the macrophage response through doubling of space diameters and
- refute the connotation that inflammation is a prerequisite for vascular ingrowth.

The definition of the macropores was achieved through the use of spherical porogen beads of uniform spherical shape. They resembled pentagonal dodecahedra often used to describe the structure of foams. The spherical beads could, unlike irregular salt crystals often used in similar techniques, be fractionated into very narrow size-distributions that allowed for the regular packing of beads. The close packing ensured high porosities while the uniform bead-size was replicated in the scaffold's macropores.

Stellenbosch University http://scholar.sun.ac.za

In a ternary polymer/solvent/non-solvent phase separation, the relative rates at which solvent is exchanged for non-solvent determines the degree of microporosity, and also indirectly influences the size of the macrovoids produced by the porogen. In the present case, the microporosity was minimised by the choice of a non-solvent (ethanol) that enters the polymer solution at a rate lower than that at which the solvent (NMP) leaves. A low degree of microporosity is important in the maintenance of the mechanical properties of the scaffold, as they (the micropores) weaken the structure without contributing to the useful porosity available for ingrowth. This is a particularly important factor in the development of vascular grafts, where structural integrity and compliance are crucial. In other applications, where the scaffold is intended to be degradable and mechanical strength is not critical (e.g. in vitro organogenesis), increased microporosity may be achieved by careful selection of solvent/non-solvent pairs, and thereby beneficially decrease the mass of synthetic material to be degraded.

The most significant outcome of an increase in pore size within the polyurethane foam was a reduction in the inflammatory potential of the material. Strikingly, this occurs at what may be considered two temporal stages in the inflammatory response, namely the more immediate reply of the invading mononuclear macrophage and the endpoint of FBGC formation. The FBGC has been shown to directly induce cracking in implanted polyurethane at its site of adhesion [22] and therefore any reduction in FBGC presence could have a direct impact on the long-term stability of polyurethane-based prosthetic implants. There is much debate in the literature on what the consequences of the macrophage presence are for prosthetic implants [23]. They are generally considered to be pro-angiogenic due to their release of factors such as the potent angiogenic factor vascular endothelial growth factor (VEGF) when exposed to the hypoxic environment that must initially exist within an implant. Other stimulatory factors for tissue ingrowth known to be secreted by hypoxic macrophages are the fibroblast growth factors (acidic and basic; a-FGF and b-FGF) and platelet-derived growth factor (PDGF). The latter has been shown to recruit smooth muscle cells. Therefore it is of interest that the vascularisation and arteriolarization of the high-porosity implants were not impaired by their relatively decreased content of macrophages. This could be of particular significance for prosthetic vascular grafts where it has been argued that the healing of a graft requires transmural tissue ingrowth [24]. Certainly, transmural vascularisation is the most probable candidate for their spontaneous endothelialization. The ability of an increase in pore size to 129μm diameter to overcome the possible reduction in pro-angiogenic signals is a promising sign. The introduction of a pro-angiogenic ingrowth matrix within the pores which releases cytokines may further enhance this favourable trend.

Although the porous structures described in the present study were produced from a biostable polymer and were primarily intended for the evaluation of healing responses to implantable devices such as vascular grafts, the methods used in their production are applicable to the production of biodegradable scaffolds useful in cell transplantation and organogenesis.

6.6 References

1. Nam, Y. and Park, T., *Porous biodegradable polymeric scaffolds prepared by thermally induced phase separation.* J Biomed Mater Res, 1999. **47**(1): p. 8-17.
2. Mikos, A.G., Bao, Y., Cima, L.G., Ingber, D.E., Vacanti, J.P., and Langer, R., *Preparation of poly(glycolic acid) bonded fiber structures for cell attachment and transplantation.* J Biomed Mater Res, 1993. **27**(2): p. 183-9.
3. Wintermantel, E., Mayer, J., Blum, J., Eckert, K.L., Luscher, P., and Mathey, M., *Tissue engineering scaffolds using superstructures.* Biomaterials, 1996. **17**(2): p. 83-91.
4. Leidner, J., Wong, E.W., MacGregor, D.C., and Wilson, G.J., *A novel process for the manufacturing of porous grafts: process description and product evaluation.* J Biomed Mater Res, 1983. **17**(2): p. 229-47.
5. Annis, D., Bornat, A., Edwards, R.O., Higham, A., Loveday, B., and Wilson, J., *An elastomeric vascular prosthesis.* Trans Am Soc Artif Intern Organs, 1978. **24**: p. 209-14.
6. Hiratzka, L.F., Goeken, J.A., White, R.A., and Wright, C.B., *In vivo comparison of replamineform, Silastic, and bioelectric polyurethane arterial grafts.* Arch Surg, 1979. **114**(6): p. 698-702.

Stellenbosch University http://scholar.sun.ac.za

7. Berkowitz, H.D., Perloff, L.J., and Roberts, B., *Pseudointimal development on microporous polyurethane lattices.* Trans Am Soc Artif Intern Organs, 1972. **18**(0): p. 25-9.
8. Kowligi, R.R., von Maltzahn, W.W., and Eberhart, R.C., *Fabrication and characterization of small-diameter vascular prostheses.* J Biomed Mater Res, 1988. **22**(3 Suppl): p. 245-56.
9. Schugens, C., Maquet, V., Grandfils, C., Jerome, R., and Teyssie, P., *Polylactide macroporous biodegradable implants for cell transplantation. II. Preparation of polylactide foams by liquid-liquid phase separation.* J Biomed Mater Res, 1996. **30**(4): p. 449-61.
10. Hayashi, K., Takamizawa, K., Saito, T., Kira, K., Hiramatsu, K., and Kondo, K., *Elastic properties and strength of a novel small-diameter, compliant polyurethane vascular graft.* J Biomed Mater Res, 1989. **23**(A2 Suppl): p. 229-44.
11. Murabayashi, S., Kambic, H., Harasaki, H., Morimoto, T., Yozu, R., and Nose, Y., *Fabrication and long-term implantation of semi-compliant small vascular prosthesis.* Trans Am Soc Artif Intern Organs, 1985. **31**: p. 50-4.
12. Hinrichs, W.L., Kuit, J., Feil, H., Wildevuur, C.R., and Feijen, J., *In vivo fragmentation of microporous polyurethane- and copolyesterether elastomer-based vascular prostheses.* Biomaterials, 1992. **13**(9): p. 585-93.
13. Uchida, N., Kambic, H., Emoto, H., Chen, J.F., Hsu, S., Murabayshi, S., Harasaki, H., and Nose, Y., *Compliance effects on small diameter polyurethane graft patency.* J Biomed Mater Res, 1993. **27**(10): p. 1269-79.
14. Lommen, E., *Artificial skin.* 1988, University of Groningen: Groningen.
15. Beahan, P. and Hull, D., *A study of the interface between a fibrous polyurethane arterial prosthesis and natural tissue.* J. Biomed. Mater. Res., 1983. **16**: p. 827-838.
16. White, R., *Evaluation of small diameter graft parameters using replamineform vascular prostheses*, in *Vascular grafting, clinical applications and techniques*, C. Wright, Editor. 1983: Boston. p. 315-325.
17. Leidner, J. and Wong, E., *A novel process for the manufacturing of porous grafts: Process description and product evaluation.* J. Biomed. Mater. Res., 1983. **17**: p. 229-247.
18. White, R., Hirose, F., Sproat, R., Lawrence, R., and Nelson, R., *Histopathologic observations after short-term implantation of two porous elastomers in dogs.* Biomaterials, 1981. **2**(3): p. 171-6.
19. Zhang, Y. and Zhang, M., *Synthesis and characterization of macroporous chitosan/calcium phosphate composite scaffolds for tissue engineering.* J. Biomed. Mater. Res., 2001. **55**: p. 304-312.
20. Matlanga, B., LP and TN, S., *Tissue response to implanted polymers: The significance of shape.* J Biomed Mater Res, 1976. **10**: p. 391-397.
21. Schakenraad, J. and KH, L., *The influence of porosity and surface roughness on biocompatibility*, in *Tissue engineering of vascular grafts*, P. Zilla and Greisler, H., Editors. 1999, RG Landes: Austin. p. 513-530.
22. Zhao, Q., Topham, N., Anderson, J., Hiltner, A., Lodoen, G., and Payet, C., *Foreign-body giant cells and polyurethane biostability: in vivo correlation of cell adhesion and surface cracking.* J Biomed Mater Res, 1991. **25**(2): p. 177-83.
23. Davids, L., Dower, T., and Zilla, P., *The lack of healing in conventional vascular grafts*, in *Tissue engineering of vascular grafts*, P. Zilla and Greisler, H., Editors. 1999, RG Landes: Austin. p. 3-44.
24. Greisler, H.P., *Arterial regeneration over absorbable prostheses.* Arch Surg, 1982. **117**(11): p. 1425-31.

Stellenbosch University http://scholar.sun.ac.za

CHAPTER 7

Graft copolymerisation of acrylic acid and acrylamide as a spacer for the subsequent immobilization of biomolecules

7.1 Abstract

Copolymers of acrylic acid (Aac) and acrylamide (Aam) may be readily grafted to the surfaces of solid and porous polyurethanes by the use of ceric ion initiation. Unwanted gelation of the grafting solution, especially when porous substrates are used, could be successfully inhibited by the addition of a cupric salt. Electronic spectroscopy for chemical analysis (ESCA) of polyurethanes grafted with solution containing three feed compositions (20, 50 and 80 mol% Aac respectively) showed enrichment in Aac in the copolymer (relative to the feed). This implied a preference of both Aac and Aam terminated radical chains for the Aac monomer, and thus $r_1>1>r_2$. Reactivity ratios were determined by the intersection and linearization methods. Average values of $r_1=1.04$, $r_2=0.29$ and $r_1=1.40$, $r_2=0.48$ were obtained for grafting onto solid and porous polyurethane structures respectively. Reconstruction of copolymer composition curves based on the calculated reactivity ratios showed good fits with the copolymer compositions determined by ESCA analysis. Of the various reactivity ratios available in the literature for this comonomer pair, those derived from Q-e values ($Q_1=1.15$, $Q_2=1.18$, $e_1=0.77$, $e_2=1.30$) were closest to the values obtained in this study. Evaluation of composition-conversion curves revealed that the difference between the average (F_{1av}) and instantaneous copolymer composition (F_1) was less than 1%, up to a conversion of 30%. Thus the assumption needed for the calculation of reactivity ratios, i.e. that F_1 could be equated to F_{1av} (as calculated from ESCA results) at low conversion, was valid.

7.2 Introduction

Surface modification is a versatile technique by which the chemical and physical properties of biomaterials may be altered to improve compatibility and integration (See 3.5.1.3). Apart from being useful materials for the attenuation of protein and macrophage adhesion [1], acrylic acid on its own, or as a copolymer with acrylamide, has been used as an interim step to the covalent immobilization of bioactive molecules such as collagen [2-5] and heparin [5-7].

The copolymerisation of two monomers is characterized by their reactivity ratios, i.e. the relative preference each monomer has for propagation with another of the same type (as opposed to propagating with the other monomer). The reactivity ratios may be used not only to determine the relative amount of each monomer that will be taken up in the copolymer for any given feed composition, but also how the feed and copolymer compositions change with conversion of the monomers. A concise summary of copolymerisation theory, as applicable to the current study, is given in Appendix 5.

The accurate determination of reactivity ratios is not a trivial process, and has to be performed for each monomer pair under consideration. The reaction conditions (solvent, temperature, concentration etc.) may greatly affect the reactivity of the monomers, as may be seen in the listing of reactivity ratios r_1 and r_2 for the monomer pair acrylic acid (M_1) and acrylamide (M_2) respectively. (Table 7.1)

Stellenbosch University http://scholar.sun.ac.za

Table 7.1: List of historical r_1 and r_2 values for acrylic acid (M_1) and acrylamide (M_2)

r1	r2	Reference
3.8	0.58	[8]
1.676	0.465	[9]
1.644	0.445	[8]
1.466*	0.515*	[10]
1.376	0.598	[9]
0.341	1.346	[8]
0.333	1.358	[9]
0.29	1.06	[8]
0.289	1.085	[9]
* Calculated from Q_1=1.15, Q_2=1.18, e_1=0.77, e_2=1.30		

The ceric ion was an effective initiator for the graft polymerisation of polyurethane substrates. Initiation occurs through formation of free radical on the hard segment carbamate via complex formation with the ceric ion, as shown in Figure 7.1 [11].

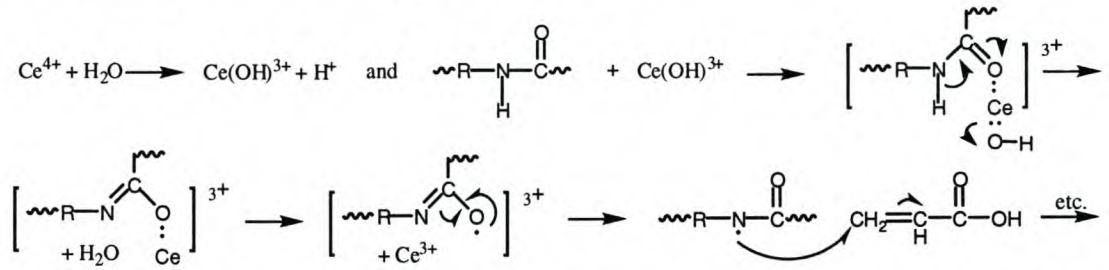

Figure 7.1: Mechanism for the ceric ion-induced free radical initiation of PU substrates for graft polymerisation [11].

The aim of this study is to determine a set of reactivity ratios for the graft copolymerisation of acrylic acid and acrylamide onto solid and porous polyurethane substrates using ceric ion initiation, and to compare these values to those obtained by previous researchers for bulk and solution polymerisation processes involving the same monomers. The efficacy of cupric salts to inhibit the gellation of reaction mixtures during graft polymerisation [12], will also be evaluated.

7.3 Materials and methods

7.3.1 Acrylic acid/Acrylamide grafting

After cleaning in isopropanol (IPA, 10min, RT) and multiple rinses with deionised water (DI), solid PU samples (8x8x0.2mm) and porous polyurethane disks (see Chapter 6) were immersed in the grafting solution containing acrylic acid (either 4.2M, 2.5M or 0.8M, Aldrich, USA), acrylamide (either 0.8M, 0.5M or 4.2M, Aldrich), $Cu(NO_3)_2$ (0.1M, Saarchem Holpro, RSA) and cerium ammonium nitrate (CAN) (0.06M, Saarchem, $(NH_4)_2[Ce(NO_3)_6]$). Oxygen was removed from the grafting solution before the addition of the cerium salt by the bubbling of Argon gas at 1 l/min for 10 min. The reaction vessels were sealed and grafting was continued for 35 min at room temperature, after which the samples were rinsed in DI water, washed in borate buffer (0.1M, pH=9, 50°C, 1hr), rinsed again in deionised (DI) water, and finally dried in air. All the steps, apart from the drying, were performed in an ultrasonic bath to ensure solution/solvent penetration and mixing.

Solid and porous samples were also grafted without the addition of the copper salt (conditions otherwise identical).

Stellenbosch University http://scholar.sun.ac.za

7.3.2 Surface analysis and reactivity ratio determination

Electron spectroscopy for chemical analysis (Physical Electronics Quantum 2000 Scanning ESCA Microprobe, 20W, 45°, CSIR, Pretoria) was performed on the solid (n=2) and porous (n=2) hydrogel-grafted samples to determine the atomic percentages of C, N and O in the surface layer. These conditions generally result in a depth of analysis of 2-4nm.

From these values (after equating instantaneous and average copolymer compositions: $F_{1av}= F_1$; $F_{2av}=F_1$ due to low conversions) and the molar fractions of each monomer in the feed solution (f_1^0, f_2^0), the reactivity ratios (r_1, r_2) of the monomers were determined by the approximation method, the Mayo-Lewis intersection method, and the Fineman-Ross linearization method. Throughout the following section acrylic acid was taken as monomer 1 (M_1):

Approximation method (See A5.2.3.1) [13]:

$$r_1 = f_2/F_2 \quad \text{and} \quad r_2 = f_1/F_1 \tag{7.1}$$

Intersection method (See A5.2.3.3) [13]

$$r_1 = r_2\left(\frac{F_1 f_2^2}{F_2 f_1^2}\right) + \left(\frac{f_2}{f_1}\right)\left(\frac{F_1}{F_2} - 1\right) \tag{7.2}$$

Linearization method (See A5.2.3.4) [14]:

$$\frac{f_1 (F_2 - F_1)}{f_2 F_1} = \left(-\frac{F_2 f_1^2}{F_1 f_2^2}\right) r_1 + r_2 \tag{7.3}$$

7.3.3 Sequence length and composition-conversion calculation

The instantaneous sequence length distribution ($N_{1;x}$) and average sequence lengths (x_{1av}; x_{2av}) for each monomer was calculated according to (See Appendix 5.2.1.6):

$$N_{1;x} = P_{11}^{x-1} P_{12} \quad \text{and} \quad N_{2;x} = P_{22}^{x-1} P_{21} \tag{7.4a,b}$$

$$x_{1av} = \frac{1}{P_{12}} \quad \text{and} \quad x_{2av} = \frac{1}{P_{21}} \tag{7.5a,b}$$

where

$$P_{11} = \frac{r_1 f_1}{r_1 f_1 + f_2} \quad \text{and} \quad P_{12} = \frac{f_2}{r_1 f_1 + f_2} \tag{7.6a,b}$$

$$P_{22} = \frac{r_2 f_2}{r_2 f_2 + f_1} \quad \text{and} \quad P_{21} = \frac{f_1}{r_2 f_2 + f_1} \tag{7.7a,b}$$

The calculated reactivity ratios were also used to plot the instantaneous copolymer composition against the feed composition (F_1 vs. f_1). The feed (f_1) and copolymer compositions (instantaneous (F_1) and average (F_{1av})) were subsequently plotted against the conversion (X) in order to determine the compositional drift (See A5.2.2):

$$F_1 = \frac{(r_1 - 1) f_1^2 + f_1}{(r_1 + r_2 - 2) f_1^2 + 2(1 - r_2) f_1 + r_2} \quad \text{and} \quad F_{1av} = \frac{f_1^0 - f_1(1 - X)}{X} \tag{7.8a,b}$$

$$X = 1 - \left[\left(\frac{f_1}{f_1^0}\right)^{\alpha}\left(\frac{f_2}{f_2^0}\right)^{\beta}\left(\frac{f_1^0 - \delta}{f_1 - \delta}\right)^{\gamma}\right] \tag{7.9}$$

Stellenbosch University http://scholar.sun.ac.za

7.4 Results and discussion

7.4.1 Graft copolymerisation

The success of the hydrogel grafting (f_1^0=0.8; M^0=5M, with copper salt) is evident in Figure 7.2. The internal surfaces of the unmodified porous structure has a smooth appearance, while the poly(acrylic acid-co-acrylamide grafted sample has a cobblestone appearance after dehydration, gold sputtering and visualization with the scanning electron microscope (SEM). Atomic force micrographs (AFM) of the solid PU before and after grafting show similar undulated surfaces on the grafted samples.

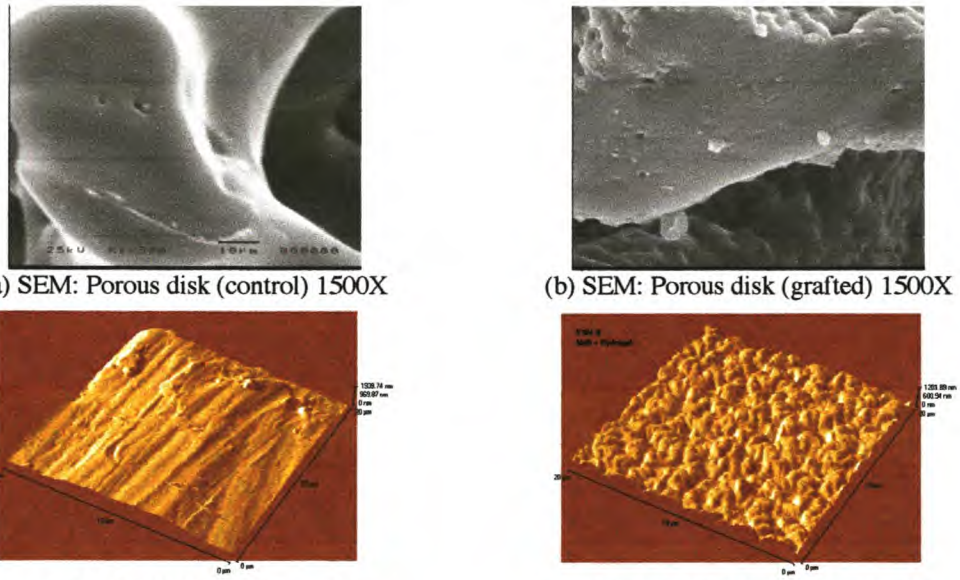

(a) SEM: Porous disk (control) 1500X (b) SEM: Porous disk (grafted) 1500X

(c) AFM: Solid shim (control) (d) AFM: Solid shim (grafted)

Figure 7.2: Visualization of porous (a,b) and solid (c,d) M48 substrates before and after graft copolymerisation with Aac and Aam. ***([M_{10}]=5M; f_1^0=0.8; with $Cu(NO_3)_2$)***

Graft polymerisation can also be performed without the addition of cupric ions in the reaction mixture [5]. In the absence of the cupric ions, however, the polymerisation of the monomer(s) in the solution surrounding the sample competes with the grafting reaction, and gelation of the reaction mixture occurred (own experience). With solid samples, sufficient grafting could be obtained (without the use of cupric ions) before gellation, and even when some gellation did occur, it was readily removed from the planar surfaces. When the reaction mixtures without cupric salts were used to graft porous samples, however, it was found that gellation invariably occurred within the porous structure before sufficient grafting could be achieved. Cupric and ferric ions act as free-radical scavengers by transferring electrons from propagating radical polymer chains to their incomplete d-shells [12]. This inhibitory effect is, however, greater in the bulk solution than in the graft, and is thus a valuable tool for the prevention of gel formation during graft polymerisation. The effectiveness of the copper nitrate used to graft copolymerise Aac and Aam onto the exposed surfaces (both internal and external) without unwanted blocking of the pores, is evident from the lack of ungrafted gel in the porous structure shown in Fig. 7.3b. All further analysis was performed on samples grafted with the addition of $Cu(CO_3)_2$ (to prevent blocking of the pores).

7.4.2 Determination of reactivity ratios

The oxygen to nitrogen (O/N) ratios of the PAac-co-PAam grafted surfaces (as calculated from the ESCA data), and the calculated average copolymer compositions, are tabulated against the

Stellenbosch University http://scholar.sun.ac.za

feed composition in Table 7.2. The molar fractions of monomer 1 (Aac) in the copolymer ($F1_{av}$) were higher than in the corresponding feeds (f_1^0).

Table 7.2: Copolymer compositions of grafted PU samples as determined from ESCA (Value±SEM)

f_1^0	O/N solid	O/N porous	F_{1av} solid	F_{1av} porous
0.8	10.375±1.375	12.807±1.901	0.824±0.022	0.855±0.020
0.5	4.261±0.630	4.228±0.491	0.620±0.046	0.617±0.036
0.2	2.101±0.134	1.928±0.003	0.355±0.028	0.317±0.001

Graphs obtained by the employment of the intersection and linearization methods are included in Figure 7.3. Although the three lines generated by eq. 7.2 did not intersect at a single point (solid polyurethane), the intersection did occur in a distinct region on the r_1,r_2 plane (Fig. 7.3a). For the grafting of the porous polyurethane, the intersections of the respective lines were much closer to a single point (Fig 7.3c), as attested by the standard error of the means given in Table 7.3. The R^2 values obtained for lines generated by eq. 7.3 (very close to unity) for both the solid and porous samples indicate a good correlation between the linearization model and the experimental data obtained (Fig 7.3b and d).

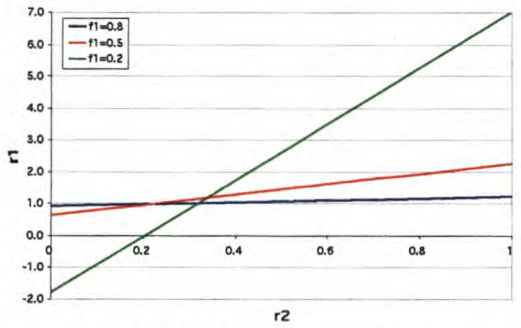

(a) Solid PU; Intersection

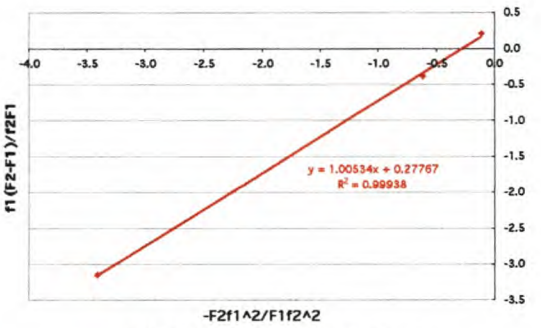

(b) Solid PU; Linearization

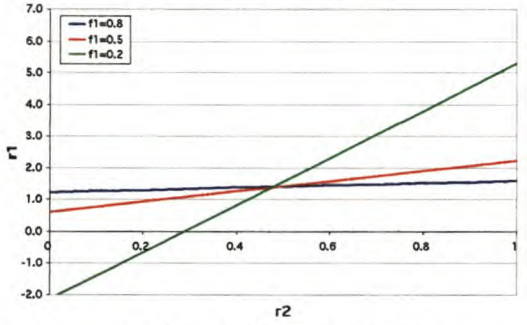

(c) Porous PU; Intersection

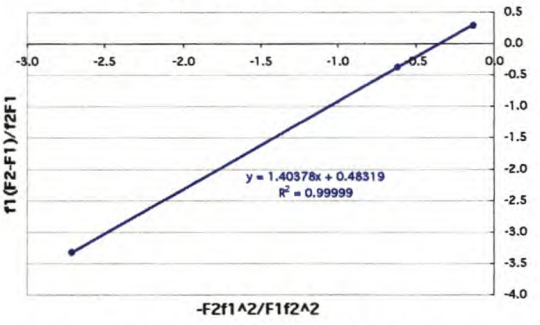

(d) Porous PU; Linearization

Figure 7.3: Graphical determination of reactivity ratios by the intersection and linearization methods

The approximation method, which resulted in r_1 and r_2 values that were appreciably higher than the other two methods (Table 7.3), did not fit the experimental data well. The former is based on the assumption that the copolymer composition is almost exclusively dependent on r_1 when low concentrations of M_2 are used (and on r_2 when M_1 is low). This method was used only to obtain approximate values and will not be discussed further. The intersection and linearization methods produced similar reactivity ratios. There was, however, an appreciable difference in the reactivity ratios (with either of these two methods) between the substrates used (solid vs. porous). Both the intersection and linearization method produced lower r_1 and r_2 values for the solid samples than on the porous disk. On both the solid and porous substrates, since $r_1>1>r_2$, both of the active centres have a preference for addition to one of the monomers, in this case M_1. This leads to the formation of a copolymer that is always enriched in Aac relative to the feed, as seen in Table 7.2.

Stellenbosch University http://scholar.sun.ac.za

Table7.3: Reactivity ratios as determined by the approximation, intersection and linearization methods

	Approximation	Intersection	Linearization
r_1 solid	1.138	1.061±0.061	1.005
r_2 solid	0.563	0.292±0.037	0.278
r_1 porous	1.381	1.397±0.008	1.404
r_2 porous	0.631	0.482±0.005	0.483

The reconstructed copolymer composition curves (Fig. 7.4), based on the reactivity ratios given in Table 7.3, show how well both the intersection method and linearization method data fit the experimentally derived copolymer fractions listed in Table 7.2.

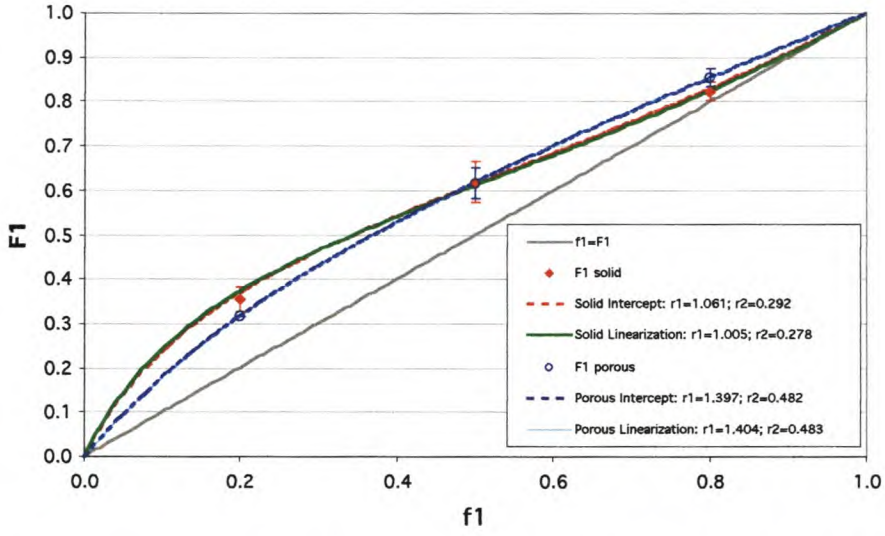

Figure 7.4: Copolymer composition (F_1) vs. feed composition (f_1) for poly acrylic acid-co acrylamide grafted to solid and porous polyurethanes as reconstructed from reactivity ratios by the intersection and linearization methods.

Figure 7.5 shows copolymer composition curves reconstructed from selected reactivity ratios from the literature (See Table 7.1). The best fit to the experimental data (for the porous PU) is obtained by using the reactivity ratios derived from the Q and e values of Ham et al. (r_1=1.466; r_2=0.515) [10].

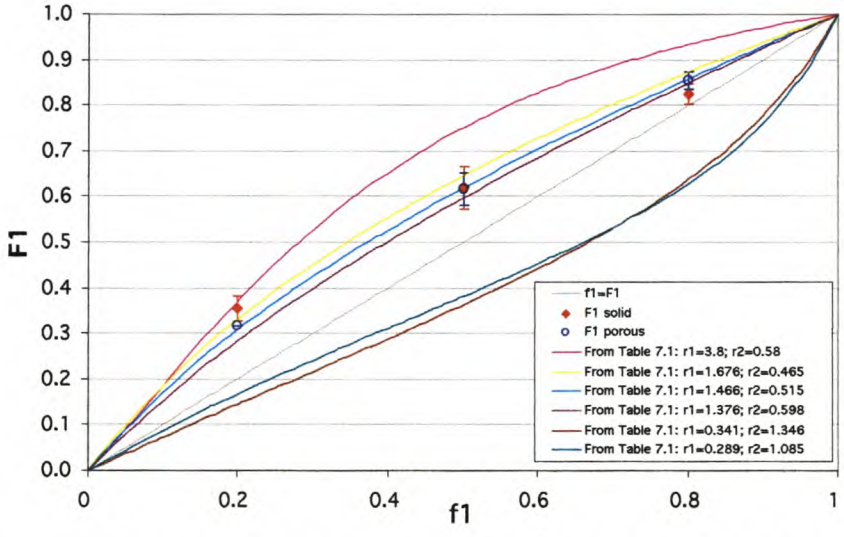

Figure 7.5: Copolymer composition (F_1) vs. feed composition (f_1) for poly acrylic acid-co- acrylamide as calculated from reactivity ratios obtained from the literature.

Stellenbosch University http://scholar.sun.ac.za

7.4.3 Determination of instantaneous sequence distributions

Whereas the reactivity ratios and copolymer compositions show the overall composition of the copolymers, valuable insight into a further aspect, namely the distribution of the two monomers in the polymer chain, may be obtained by analysing the sequence distributions. Figure 7.6 shows the instantaneous sequence distributions and average sequence lengths of both monomers taken up in the copolymer at feeds compositions of f_1^0=0.8, 0.5 and 0.2 respectively. It is interesting to note that, for a feed containing 80% Aac, 90% of the Aam units appear as single units flanked by Aac, while the average length of Aac units is 6.6.

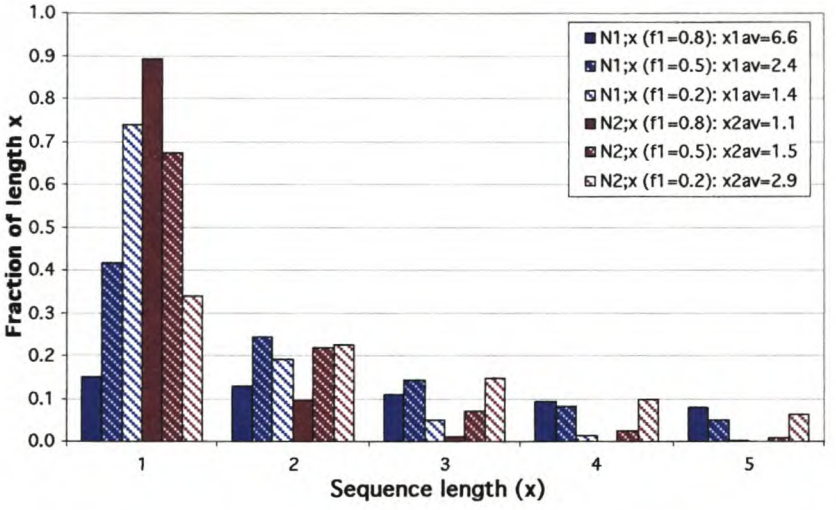

Figure 7.6: Instantaneous sequence distributions and average sequence lengths of PAac-co-PAam grafted to M48 (M_1=Aac; M_2=Aam; r_1=1.404; r_2=0.483; $[M_0]$=5M)

74..4 Influence of conversion on composition

The composition-conversion curve below (Fig. 7.7) has been calculated using the reactivity ratios obtained by using the linearization method (porous substrate). It shows the change in feed composition (f_1), instantaneous copolymer composition (F_1) and average copolymer composition (F_{1av}) as a function of the conversion (X). The difference between the average and instantaneous copolymer compositions is less than 1% up to a conversion of 0.3. Thus, the assumption of F_1=F_{1av} (for low conversions) used to determine the reactivity ratios is valid.

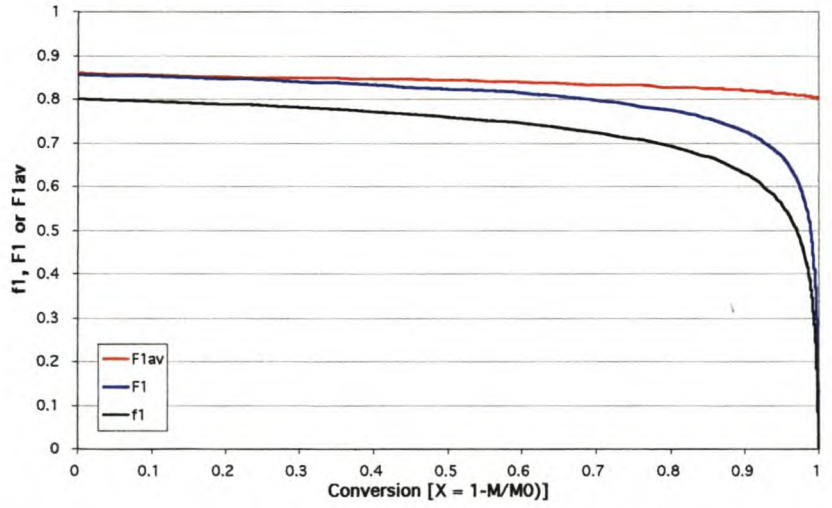

Figure 7.7: Composition-conversion curves for poly acrylic acid-co acrylamide grafted to porous polyurethane scaffolds as calculated from r_1=1.404 and r_2=0.483. ($[M_{10}]$=5M; f_1^0=0.8)

Stellenbosch University http://scholar.sun.ac.za

7.5 References

1. Yun, J., DeFife, K., Colton, E., Stack, S., Azeez, A., Cahalan, L., Verhoeven, M., Cahalan, P., and Anderson, J., *Human monocyte/macrophage adhesion and cytokine production on surface-modified poly(tetrafluoroethylene/hexafluoropropylene) polymers with and without protein preadsorption.* J Biomed Mater Res, 1995. **29**(2): p. 257-68.
2. Lee, S., Hsiue, G., Chang, P., and Kao, C., *Plasma-induced grafted polymerisation of acrylic acid and subsequent grafting of collagen onto polymer film as biomaterials.* Biomaterials, 1996. **17**(16): p. 1599-608.
3. Kinoshita, Y., Kuzuhara, T., Kirigakubo, M., Kobayashi, M., Shimura, K., and Ikada, Y., *Soft tissue reaction to collagen-immobilized porous polyethylene: subcutaneous implantation in rats for 20 wk.* Biomaterials, 1993. **14**(3): p. 209-15.
4. Okada, T. and Ikada, Y., *Tissue reactions to subcutaneously implanted, surface-modified silicones.* J Biomed Mater Res, 1993. **27**(12): p. 1509-18.
5. Hendriks, M., *Development of biomaterials with enhanced infection resistance. A surface modification approach.* 1996, Eindhoven University of Technology: Eindhoven. p. 181.
6. Sapatnekar, S., Kieswetter, K., Merritt, K., Anderson, J., Cahalan, L., Verhoeven, M., Hendriks, M., Fouache, B., and Cahalan, P., *Blood-biomaterial interactions in a flow system in the presence of bacteria: effect of protein adsorption [published erratum appears in J Biomed Mater Res 1995 May;29(5):679].* J Biomed Mater Res, 1995. **29**(2): p. 247-56.
7. Lindhout, T., Blezer, R., Schoen, P., Willems, G., Fouache, B., Verhoeven, M., Hendriks, M., Cahalan, L., and Cahalan, P., *Antithrombin activity of surface-bound heparin studied under flow conditions.* J Biomed Mater Res, 1995. **29**(10): p. 1255-66.
8. in *Polymer Handbook*, J. Brandrup, Immergut, E., and Grulke, E., Editors. 1999, Wiley Interscience: New York.
9. Greenley, R., *Recalculation of some reactivity ratios.* J Macromol Sci-Chem, 1980. **A14(4)**: p. 445-515.
10. Ham, G., *Copolymerization*, in *Encyclopedia of Polymer Science and Technology. Plastics, Resins, Rubbers, Fibers*, H. Mark, Gaylord, N., and Bikales, N., Editors. 1966, Interscience Publishers: New York. p. 165-244.
11. Feng, X., Sun, Y., and Qiu, K., *Reactive site and mechanism of graft copolymerization onto poly(ether urethane) with ceric ion as initiator.* Macromolecules, 1985. **18**: p. 2105-2109.
12. Ratner, B. and Hoffman, A., *The effect of cupric ion on the radiation grafting of N-Vinyl-2-pyrrolidone and other hydrophilic monomers onto silicone rubber.* Journal of Applied Polymer Science, 1974. **18**: p. 3183-3204.
13. Tidwell, P. and Mortimer, G., *An improved method of calculating copolymerization reactivity ratios.* Journal of Polymer Science Part A, 1965. **3**: p. 369-387.
14. Fineman, M. and Ross, S., *Linear method for determining monomer reactivity ratios in copolymerization.* Journal of Polymer Science, 1950. **5**: p. 259-262.

Stellenbosch University http://scholar.sun.ac.za

CHAPTER 8

Surface pacification of porous scaffolds

8.1 Abstract

Porosity and surface chemistry are known determinants of the healing response towards devices used in tissue engineering applications. In order to evaluate the effect of these two parameters on novel porous polyurethane scaffolds, disks containing three distinctly different pore sizes (66.4±1.3, 84.2±1.7 and 157.0±2μm), as well as large porosity disks (157.0±2.4μm) modified with collagen, heparin or a combination of collagen and heparin by covalent surface attachment, were produced. Disks (n=6) were implanted in the subcutaneous rat model for 14 days to evaluate neo-vascularization and inflammatory response.

By increasing the pore size from 84.2±1.7 to 157.0±2μm, and additionally pacifying the surface by collagen attachment, the inflammatory response (based on foreign body giant cell index, FBGCI) could be decreased by 80% ($p<0.002$). More importantly, this dramatic decrease could be achieved without any significant decrease in the vascularization of the implanted devices.

The immobilization of heparin or the combination of collagen and heparin had no significant effect on FBGCI.

The long-term outcome of porous prosthetic devices depends to a large degree on the ingrowth of surrounding tissue into the porous structure and successful incorporation of the device in vivo. This incorporation, in turn, is influenced by the inflammatory response elicited by the foreign body, and the successful vascularization of the ingrown tissue. The current results provide a means to minimise the inflammatory response without adversely affecting the neo-vascularization.

8.2 Introduction

The injury associated with the implantation of prosthetic devices leads to sequential events whereby acute inflammation and chronic inflammation are normally followed by the formation of granulation tissue, foreign body reaction and fibrosis. [1]. The inflammatory response is often exacerbated in porous polymeric scaffolds used in tissue engineering applications due to the increased surface area presented to the host. Factors that influence the reaction include the physical properties (shape, size, porosity, mechanical properties) and the chemical nature of the scaffold.

It was previously shown that the inflammatory response following implantation in the rat model (28 day implants) could be significantly reduced by an increase in the pore size in polyurethane scaffolds containing well-defined, interconnected pores. [2] (See also Chapter 6).

Shimizu reported favourable integration of various polymers of in vivo by the use of telopeptide-poor collagen immobilized by a lamination process [3, 4]. A group headed by Ikada at Kyoto University later developed a technique whereby collagen was covalently attached via its amine functionality to silicone [5] and polyethylene [6] implants via a grafted poly(acrylic acid) spacer. They claimed the method to be superior to that of Shimizu, as the covalent attachment proved to be more stable than the laminated structure that tends to delaminate in aqueous environments. Lee et al. also grafted collagen to PU via plasma-induced acrylic acid grafting, and reported improved cell adhesion [7]. An alternative method of linking collagen to PU with epoxides was demonstrated by Huang et al [8].

The most widely used function of heparin is related to its antithrombogenicity achieved through its interaction with anti-thrombin III (ATIII), and the subsequent interaction with thrombin that

Stellenbosch University http://scholar.sun.ac.za

interrupts the coagulation cascade [9]. It has been demonstrated that a unique pentasaccharide sequence in heparin is required for this interaction (Fig. 8.1).

Heparin is an anionic polysaccharide consisting of partially sulphonated, alternating, D-glucosamine and glycuronic (L-iduronic and D-glucuronic) acid residues. Consequently it may be immobilized through ionic means (with cationic substances) or covalent means through its hydroxyl, carboxyl and amino functions. Ionic methods include the deposition of the water-insoluble complexes of heparin and certain cationic surfactants [10, 11] and the deposition of heparin after the pre-treatment of surface with cationic surfactants [12, 13]. The most widely used ionic method involves the pre-treatment with 1-5% tridodecylmethylammonium chloride (TDMAC) in lipophilic solvents [14].

Covalent attachment onto cyanogen bromide activated poly(vinyl alcohol) [15, 16] and cyanuric acid activated agarose [17] via hydroxyl and/or amino groups in heparin have been reported. The carboxyl functions, after activation with a water-soluble carbodiimide, provide an alternative attachment site [18-20]. Additional reactive functionality, through which heparin may be covalently immobilized onto aminated surfaces through reductive amination, may be introduced through partial oxidation of glycol functions to the corresponding aldehydes [21].

Yet another method involves the attachment of heparin via polyethylene oxide spacers after functionalisation with isocyanates [22]. The use of PEO spacers is reported to decrease platelet adsorption by increasing the hydrophilicity, and to increase the bioactivity of the heparin. In addition, the bioactivity has been shown to increase with spacer length.

As the use of the abovementioned covalent immobilization methods have the risk of interfering with the pentasaccharide ATIII-binding sequence, a new method, termed end-point attachment was developed [23, 24]. It involves the partial degradation of heparin with nitrous acid to form fragments with reactive aldehyde groups at the reducing terminal residues. These fractions were then coupled to the aminated surface through reductive amination.

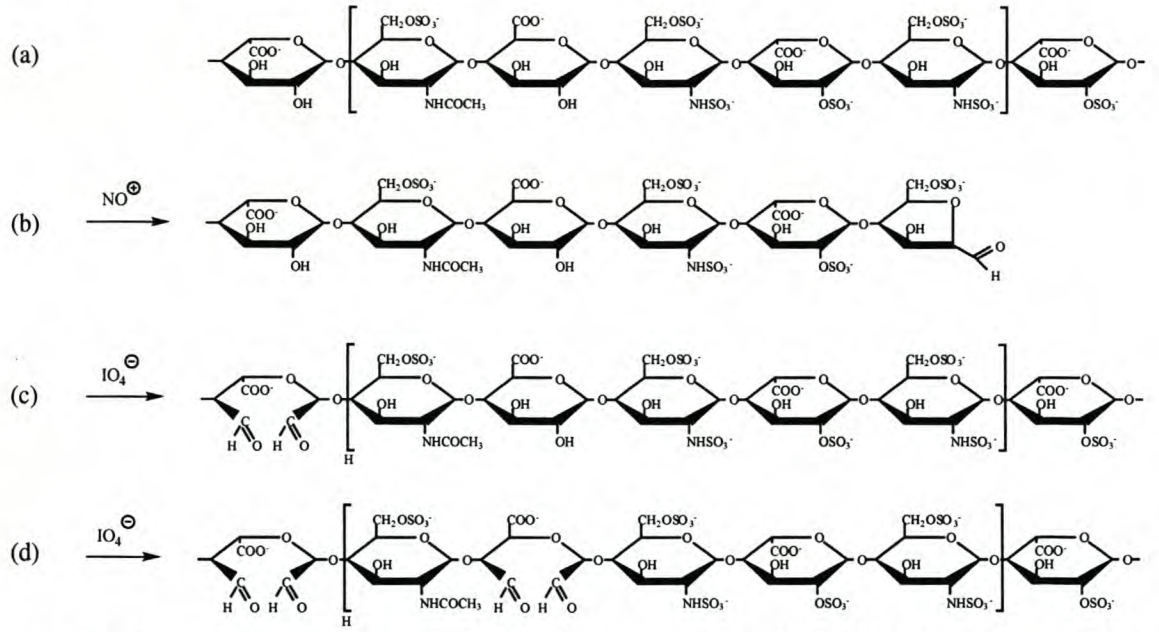

Figure 8.1: Chemical structure of heparin showing (a) the pentasaccharide ATIII binding sequence; (b) nitrous acid degradation; and (c) periodate oxidation. Note the possibility of oxidizing the glycol functionality in the pentasaccharide (d).

Although these methods were developed mainly to impart antithrombotic properties to substrates, immobilized heparin may also be used for the incorporation and protection of heparin-binding growth factors [25].

Stellenbosch University http://scholar.sun.ac.za

The overall objectives of the present study was to determine the effect of three surface modification treatments on the inflammatory response towards and neo-vascularization potential of porous polyurethane scaffolds containing large (150-180μm) pores. The first treatment, namely collagen immobilization, has previously been shown to facilitate the incorporation of polymeric devices in vivo, and was used in this study to determine whether the inflammatory response toward porous polyurethane scaffolds (with relatively high surface areas) could be mitigated by using this biomolecule. The effect of heparin immobilization, with the eventual goal of using it as a substrate for growth factor binding, was evaluated either with or without collagen pre-treatment. The secondary objective was to re-evaluate the inflammatory response toward porous polyurethane scaffolds containing various pore sizes (after a shorter implantation period than previously used).

8.3 Materials and methods

8.3.1 Porous scaffold Production

Porous polyurethane scaffolds were produced by a phase inversion/porogen extraction method as described earlier [2]. Briefly, a cylindrical column of sized gelatin beads (63-75μm, 90-106μm and 150-180μm respectively) was infiltrated with a 20% (m/m) solution of segmented polyurethane, and the resultant polymer/solvent/porogen rods were demoulded and precipitated by immersion in ethanol. Subsequent porogen extraction, followed by extensive washing and drying resulted in the porous scaffold. A thin impenetrable skin (±50μm) of polyurethane was applied to the outer surface of the cylindrical porous rods. After slicing disks of uniform thickness (2mm) from the rods, surface modification (where applicable), and sterilization by ethylene oxide (ETO) exposure, the in vitro and in vivo evaluations were performed.

8.3.2 Surface modification

8.3.2.1 Acrylic acid/Acrylamide grafting

After cleaning in isopropanol (IPA, 10min, RT) and multiple rinses with deionised water (DI), porous polyurethane disks prepared from a 150-180μm porogen size fraction were immersed in the grafting solution containing acrylic acid (4.2M, Aldrich, USA), acrylamide (0.8M, Aldrich), $Cu(NO_3)_2$ (0.1M, Saarchem Holpro, RSA) and cerium ammonium nitrate (CAN) (0.06M, Saarchem, $(NH_4)_2[Ce(NO_3)_6]$). Oxygen was removed from the grafting solution before the addition of the cerium salt by the bubbling of Argon gas at 1 l/min for 10 min. The reaction vessels were stoppered and grafting was continued for 35 min at room temperature, after which the samples were rinsed in DI water, washed in borate buffer (0.1M, pH=9, 50°C, 1hr), rinsed again in DI water, and finally dried in air. All the preceding and subsequent coupling steps, apart from the drying, were performed in an ultrasonic bath to ensure solution/solvent penetration and mixing.

8.3.2.2 Collagen immobilization

Collagen was covalently coupled to the poly(acrylic acid-co-acrylamide) (PAac-co-PAam) samples after activation of the carboxyl groups with a water-soluble carbodiimide. Activation was achieved by exposure of grafted samples to a 0.01M 1-(3- dimethylaminopropyl)-3-ethyl carbodiimide (EDC) and 0.01M N-Hydroxysuccinimide (NHS) in an 0.02M morpholino-ethanesulfonic acid (MES) buffer (pH=4.5, RT, 5min). (See Appendix 7). After removal of samples from the activation solution, and further removal of excess solution from the substrates by blotting on lint-free towelling, collagen coupling was achieved through exposure to a solution containing 0.5mg/ml collagen (Type I, calf skin, Fluka) in an 0.02M MES buffer for 24h at room temperature. The samples were consecutively rinsed in DI, 0.025M phosphate buffered saline (PBS, pH=7.4) and DI, and subsequently dried in air at room temperature.

Stellenbosch University http://scholar.sun.ac.za

8.3.2.3 Heparin immobilization

PAac-co-PAam grafted samples were exposed to an 0.5M EDA solution in an 0.5M MES buffer containing 0.05M EDC (pH=5.0, 2h, RT), and subsequently rinsed in DI prior to heparinization. Collagen-coated samples were heparinized without further pre-treatment.

Sodium heparin (5mg/ml, Diosynth, Netherlands) was oxidised in a phosphate buffer (0.05M, pH=6.8) containing sodium periodate (0.165mg/ml, 16h, RT, dark, Saarchem). After oxidation, the solution containing the oxidized heparin was diluted to 2mg/ml by addition of acetate buffer (0.4M, pH=4.6). The diluted heparin solution was pre-heated to 50°C, 0.01M sodium cyanoborohydrate ($NaCNBH_3$, Saarchem) was added, and after 10min aminated or collagen-coated samples were exposed to the resultant solution for 2h at 50°C (Fig 8.2). The samples were consecutively rinsed in DI, 1M saline and DI, and dried by exposure to an ethanol gradient (10 min each in 25%, 50% and 96%) and subsequent air-drying.

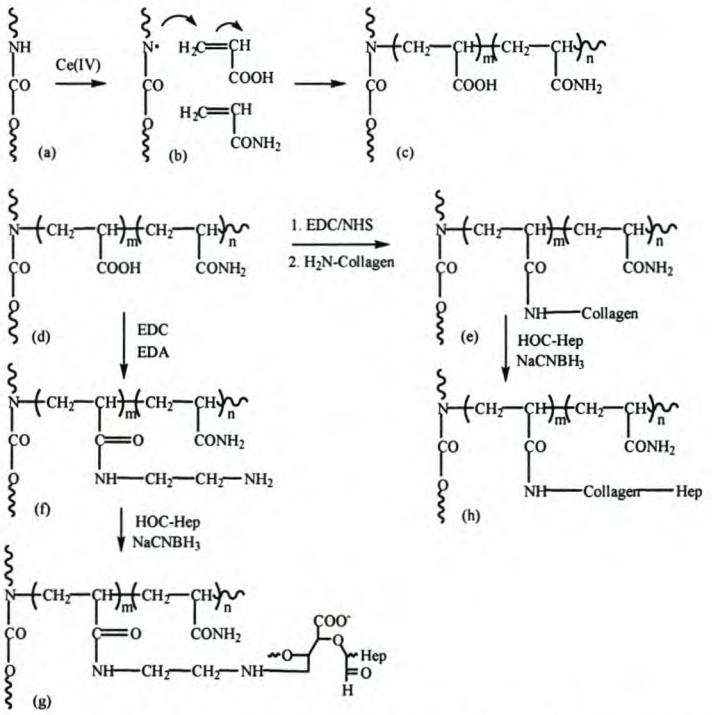

Figure 8.2: Reaction scheme for the immobilization of collagen, heparin, and a combination of collagen and heparin onto polyurethanes via acrylic acid/acrylamide grafting.

8.3.2.4 Staining Techniques

Staining techniques were employed to establish the success of each of the surface modification steps outlined above. All samples were incubated in Toluidine Blue (TB, Saarchem, 0.02% in 0.05M Tris buffer, pH=7.9), Ponceau S (PS, 0.02% in DI water) and Coomassie Blue R250 (CB, 0.25% in 40%MeOH, 7% HOAc, rest DI) for 5min at room temperature. Collagen treated samples were further stained with Azan trichrome (40°C, 2hr.), using PAac-co-PAam grafted samples as controls. All samples were then well rinsed in DI and dried before visual comparison.

8.3.3 Rat subcutaneous implants/explants

Six (n=6) disks prepared from each porogen-size fraction (63-75, 90-106 and 150-180 μm), as well as those that additionally received collagen, heparin, or collagen and heparin modification, were implanted subcutaneously in young male Wistar rats (± 200 g). Following induction of general anaesthesia with an intramuscular injection of a ketamine/xylazine mixture, the dorsal side of the animal was shaved. Using aseptic technique, three 1-cm longitudinal incisions were made through the skin at either side of the dorsal midline. A subcutaneous pocket for each disk

Stellenbosch University http://scholar.sun.ac.za

was prepared by gentle blunt dissection. The disks were implanted and the skin incisions were closed with single 3/0 Prolene sutures. After 14 days of implantation, the animals were sacrificed by inhalation of carbon dioxide. Disks were explanted with their surrounding fibrous capsules and fixed in 10% buffered formalin.

8.3.4 Evaluation of neovascularisation and inflammation

After 24h fixation in 10% formalin, the disks were bisected perpendicular to their ingrowth faces, paraffin embedded and 5 μm sections obtained. Sections were deparaffinised and stained with a biotinylated Griffonia simplicifolia lectin (GSL-1) (Vector Laboratories, Burlingame, CA, USA) that shows specificity for endothelial cells. Multinucleated foreign body giant cells (FBGC) were identified on hematoxylin and eosin stained sections. To quantify the inflammatory response (FBGC content) and neovascularisation (GSL-1 positive cells), the relevant stained sections were subjected to image analysis. For each section, a blinded observer captured 18 regions (300 X 350μm: neovascularisation; 150 X 175 μm: FBGC content) with a Leitz DM RB microscope. The areas of positively identified elements were quantified with Qwin image analysis software and normalised to the available ingrowth area, generating a vascularisation index (VI) and a FBGC index (FBGCI). Indexes were defined as the percentage area (relative to the available ingrowth area) occupied by the relevant features.

8.3.5 Statistical analysis

Data are expressed as means ± standard error of means (SEM). The comparisons of VI and FBGCI between groups were by Student's unpaired t-tests. One-sided p-values were determined in all cases. A significance level of 0.05 or less was accepted as being statistically significant.

8.4 Results

8.4.1 Porous scaffolds

8.4.1.1 Scaffold Structure

Figure 8.3 shows a semicircular section of a porous disk containing well-defined macropores with a high degree of inter-pore interconnectivity. The average diameter of the disks was 5.3±0.1mm, and the thickness of the outer skin an average of 53±2μm. The dodecahedral structure of the macropores, the abundance of interconnecting windows, and the low degree of microporosity are evident from the higher magnification micrograph depicted in the insert. The micropores were all below 10μm in size, and have limited connectivity with the macropores.

Stellenbosch University http://scholar.sun.ac.za

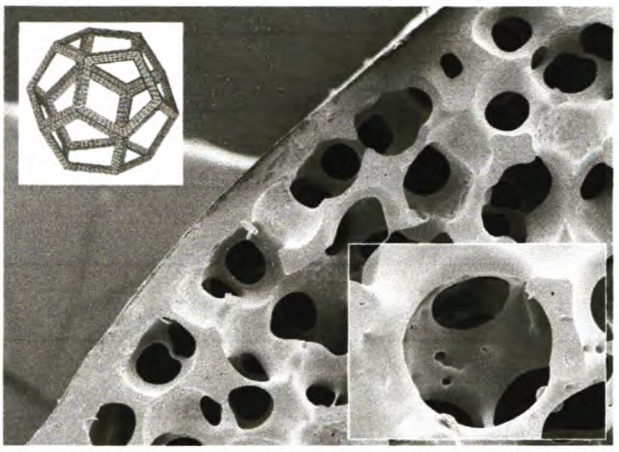

Figure 8.3: Scanning electron micrograph of a peripheral section of a porous disk prepared from a 150-180µm porogen size fraction (Orig. Mag = 333x), showing the porous structure and external skin. A pentagonal dodecahedron and a close-up view of an actual pore are shown as inserts.

8.4.2 Surface modification

None of the control samples adsorbed the Toluidine Blue (TB), Ponceau S (PS) or Coomassie Blue (CB) stains (Figure 8.4). The uniform uptake of the cationic TB after poly(acrylic acid-co-acrylamide) grafting (A2) shows that the grafting was successful throughout the structure. The positive staining achieved with anionic stain PS at B3 (together with the negative TB stain at A3) shows that the majority of the free carboxyl groups present on the hydrogel were capped by amines after the ethylene diamine coupling step. The increased uptake of Azan stain in D5 (compared to D2: other half of the same disk) shows successful collagen coupling, while the bathochromatic shift from A2 to A4 is indicative of successful heparin coupling.

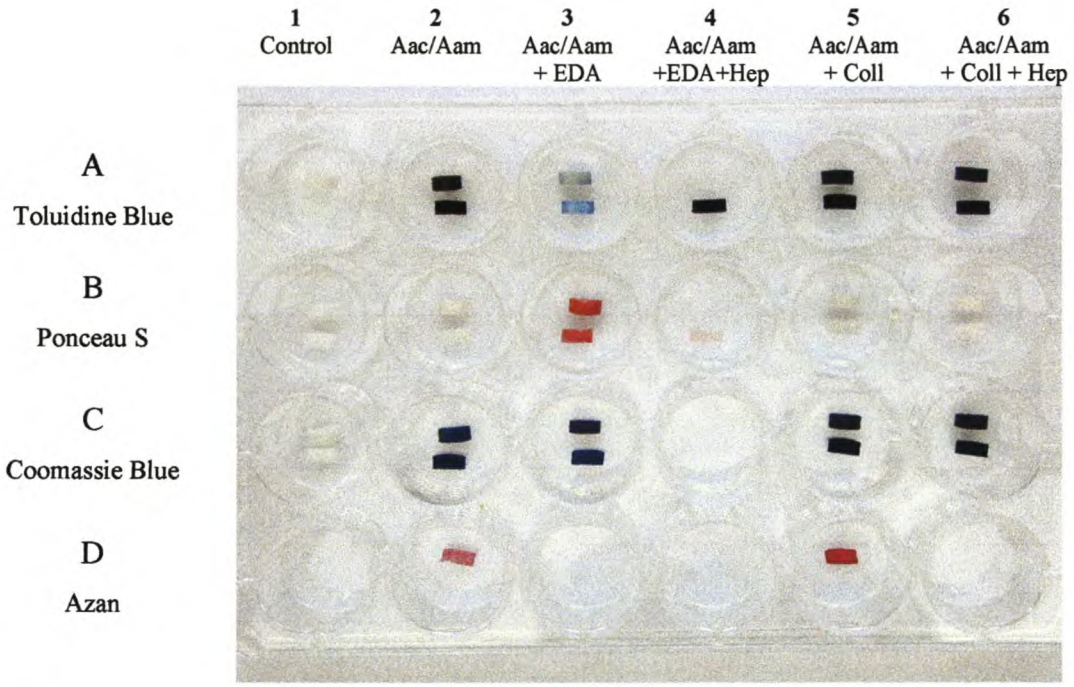

Figure 8.4: Toluidine Blue, Ponceau S, Coomassie Blue, and Azan stains of surface-modified disks at various stages of modification

Stellenbosch University http://scholar.sun.ac.za

8.4.3 Rat subcutaneous implants

8.4.3.1 Histological Analysis

Representative histological sections stained with GSL-1 lectin (GSL-1) and haematoxylin and eosin (H&E) are shown in Figure 8.5. The areas occupied by the polyurethane (P), as well as the microporosity (M) resulting from the phase-inversion process used during fabrication, are clearly seen in the various sections. The increase in pore size with increasing size of porogen used, as well as the presence of the collagen (C), heparin (H) and collagen/heparin (CH) surface modification layers were visually discernable.

GSL-1 stained sections show the presence of capillary vessels (V) throughout the porous structures. Although some cross-reactivity of the GSL-1 stain was evident for foreign body giant cells, the vessels were unequivocally identified at higher magnification by the presence of lumens. There was no visual evidence of the effect of either pore size or surface modification on the number of vessels present in the structures.

Foreign body giant cells (FBGC), as identified on hematoxylin and eosin (H&E) stained samples (F), are also shown in Figure 8.5. There is some indication of a decrease in FBGC formation with an increase in pore size, and a marked decrease in foreign body giant cells (F) when the large porosity scaffolds (Fig 8.5f) were pacified by collagen immobilization (Fig. 8.5h).

Stellenbosch University http://scholar.sun.ac.za

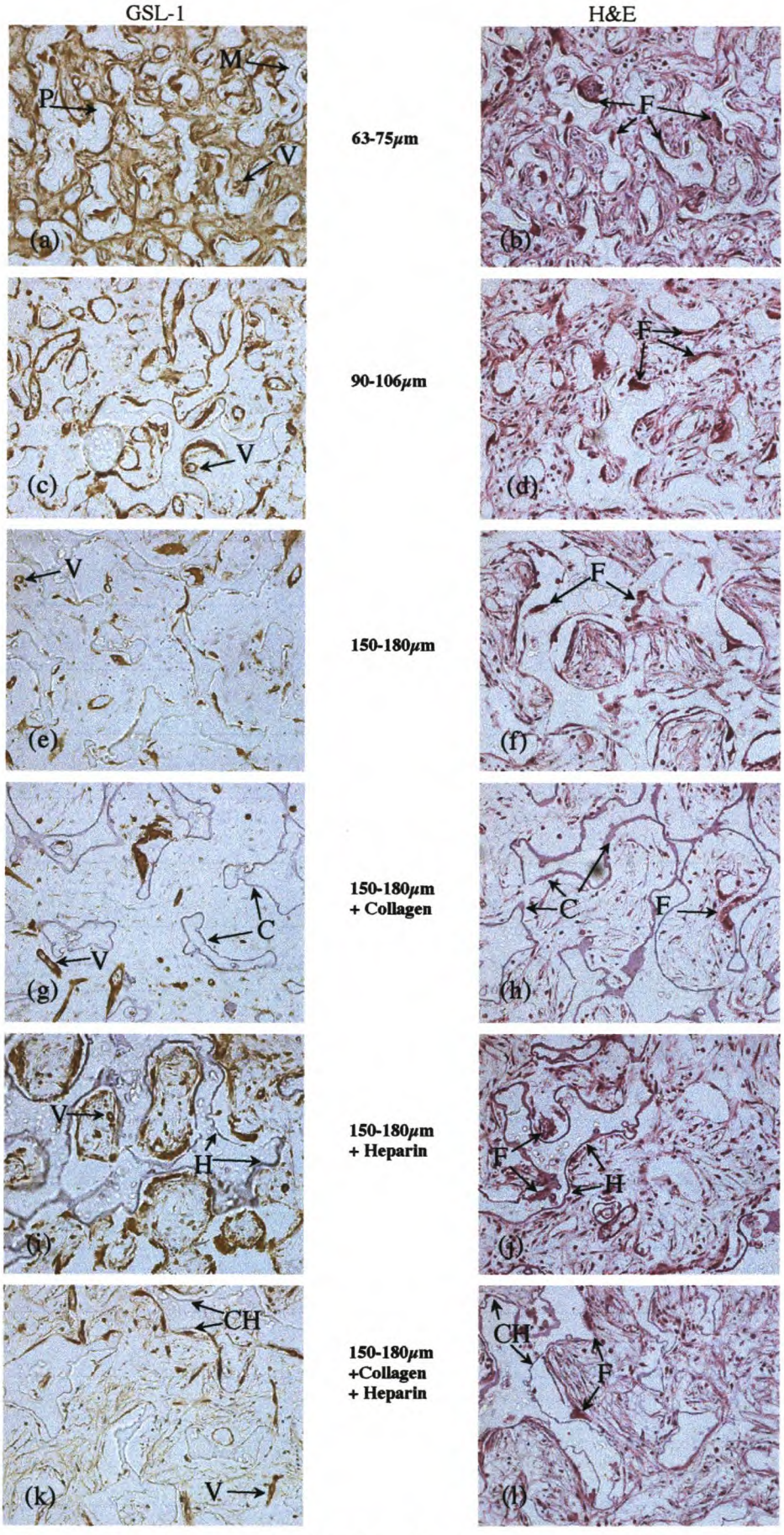

Figure 8.5: Histological micrographs of small, medium and large porosity disks, as well as large porosity disks after collagen, heparin and collagen plus heparin immobilization.

Stellenbosch University http://scholar.sun.ac.za

8.4.3.2 Quantification of indexes

Figure 8.6 summarizes the effects of pore size and surface modification on the Vascular Index (VI) and foreign body giant cell index (FBGCI), respectively. The VI was not significantly influenced by either the pore size or any of the surface modification treatments. After 14d of implantation, the FBGCI showed no significant change when the pore size was increased from 63 to 90μm, whereas a decrease from 5.43±1.06 to 3.14±0.95% was observed when the pore size was increased from 90 to 150μm (p=0.069). A further decrease in foreign body giant cell content to 1.55±0.45% was observed when the large porosity disks were pacified by collagen immobilization. In total, an 80% decrease was achieved by the combined increase in pore size (90 to 150μm) and the covalent immobilization of collagen.

Heparin immobilization on the large porosity scaffolds had no significant effect on FBGCI, and although the foreign body giant cell content of the collagen/heparin group (2.00±1.11%) was not statistically lower than that of the unmodified group (3.14±0.95%), it was also not significantly higher than that of the group that received collagen alone.

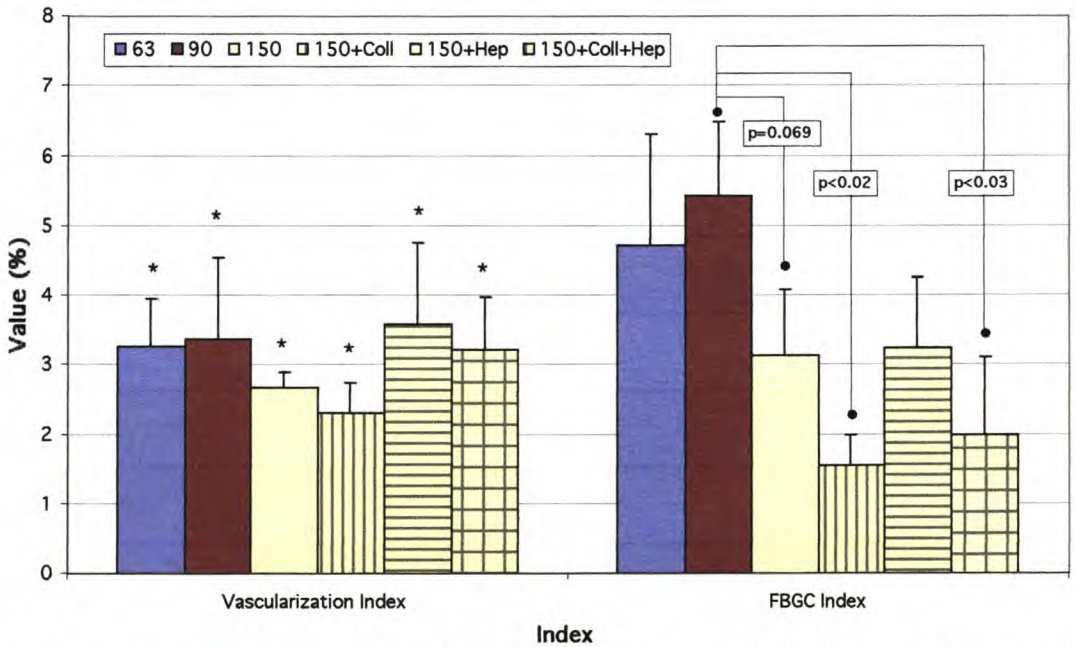

Figure 8.6: Vascularization and foreign body giant cell indexes of explanted polyurethane disks showing the influence of pore size and surface modification on the healing response.

8.5 Discussion

Porosity and surface chemistry have been shown to be important parameters that determine the healing response toward porous devices intended for tissue engineering applications. Not only is porosity *per se* essential for the successful incorporation of a device into living tissue, the nature of the porosity is also of great importance. The present study (together with previous findings) shows that large (±150μm), interconnecting pores of well-defined shape are conducive to the ingrowth of capillary vessels that are in turn essential to the viability of other ingrowing tissue types. Although the decrease in FBGCI with increased pore size (90-106 to 150-180μm) was not significant at the 95% confidence level, a previous study has shown this decrease to be statistically significant after longer implantation periods (28d). (See Chapter 6)

In addition to angio-permissive porosity, the long-term integration of devices requires the minimization of acute and chronic inflammatory responses toward the implanted device. If this reaction is not controlled, implanted devices elicit the formation of granulation tissue that in turn leads to a fibrotic response that may impede the performance of the device. As the relative area

Stellenbosch University http://scholar.sun.ac.za

of the implant exposed to surrounding tissue is orders of magnitude larger in porous scaffolds than would be the case with solid implants, the need for surface pacification is proportionally increased.

Apart from the stated requirements, porous structures used as tissue engineering scaffolds are required to fulfil their primary objective that may depend on other parameters. The development of a tissue engineered vascular prosthesis, which constitutes the overall project of which the current study forms a part, is a case in point. In order for them (vascular prostheses) to perform their primary function of re-establishing blood flow to the distant vasculature, a number of other requirements (mechanical strength, compliance, chemical stability) need to be met. Material choice is often influenced by these requirements. Hence, a method that allows for the alteration of the polymer/tissue interaction without undue influence on the parameters influencing the primary function of the device is invaluable. Surface modification provides such a tool.

Thus surface modification provides a means of "hiding" the inflammatory material without unduly changing its bulk properties. Depending on the choice of modifying material, the action of the modified surface may be passive or active. Grafted hydrogels have been shown to favourably influence polymer/tissue interaction by providing a passive hydrophilic surface layer. In order to provide active interactions, biologically derived substances such as proteins and glycosaminoglycans (or surface active drugs) are required.

Collagen is a biologically derived protein that was chosen as a surface modifying agent in order to mimic the native environment in which cells live, i.e. the extracellular matrix (of which it is a component). The large decrease in FBGC formation with the immobilization of collagen (via a hydrogel layer) shows the potential of this biomolecule to decrease foreign body reactions and thus improve the healing response towards implanted devices. It is notable that this could be achieved without adversely affecting the neo-vascularization in the scaffolds.

Although heparin is generally used as an anti-thrombotic agent, the use of this polysaccharide in the current study was to determine its effect on vascularization and inflammatory response for possible later use as a means of immobilizing and stabilizing heparin-binding growth factors that have the potential of upregulating the neo-vascularization. The finding that the immobilization of heparin did not increase the FBGC formation, and more importantly that the combination of collagen and heparin did not elicit significantly higher FBGCI than the best group (collagen alone), is significant.

8.6 References

1. Anderson, J. *Inflammatory response to implants.* in *Society for Biomaterials: 27th Annual Meeting.* 2001. St Paul, Minnesota.
2. Bezuidenhout, D., Davies, N., and Zilla, P., *Effect of well-defined dodecahedral porosity on inflammation and neo-vascularization.* ASAIO Trans, 2001. **Submitted**.
3. Shimizu, Y., Abe, R., Teramatsu, T., Okamura, S., and Hino, T., *Studies on copolymers of collagen and a synthetic polymer. First report- -experimental study on biocompatibility of laminar copolymers of collagen and a synthetic polymer.* Biomater Med Devices Artif Organs, 1977. **5**(1): p. 49-66.
4. Shimizu, Y., Miyamoto, Y., Teramatsu, T., Okamura, S., and Hino, T., *Studies on composites of collagen and a synthetic polymer. Second report - mode of reaction of a laminar composite with living tissue, and results of long-term implantation.* Biomater Med Devices Artif Organs, 1978. **6**(4): p. 375-91.
5. Okada, T. and Ikada, Y., *Tissue reactions to subcutaneously implanted, surface-modified silicones.* J Biomed Mater Res, 1993. **27**(12): p. 1509-18.
6. Kinoshita, Y., Kuzuhara, T., Kirigakubo, M., Kobayashi, M., Shimura, K., and Ikada, Y., *Soft tissue reaction to collagen-immobilized porous polyethylene: subcutaneous implantation in rats for 20 wk.* Biomaterials, 1993. **14**(3): p. 209-15.
7. Lee, S., Hsiue, G., Chang, P., and Kao, C., *Plasma-induced grafted polymerization of acrylic acid and subsequent grafting of collagen onto polymer film as biomaterials.* Biomaterials, 1996. **17**(16): p. 1599-608.
8. Huang, L., Lee, P., Chen, L., and Hsieh, K., *Comparison of epoxides on grafting collagen to polyurethane and their effects on cellular growth.* J Biomed Mater Res, 1998. **39**(4): p. 630-6.

Stellenbosch University http://scholar.sun.ac.za

9. Larm, O., Larson, R., and Olsson, P., *Highlights in the history of heparin*, in *Heparin*, D. Lane and Lindahl, U., Editors. 1989, Edward Arnold: London. p. 1-23.
10. Gott, V., Whiffen, J., and Dutten, R., *Heparin bonding on colloidal graphite surfaces.* Science, 1963. **142**: p. 1297.
11. Ericsson, J., Gillberg, G., and Lagergren, H., *A new method for preparing nonthrombogenic surfaces.* Journal of Biomedical Material Research, 1967. **1**: p. 301.
12. Barbucci, R., Benvenuti, M., Casini, G., Ferruti, P., and Nocentini, M., *Preparation and FTIR characterization of polyurethane surfaces grafted with heparin-complexing poly(amino-amine) chains.* Macromolecular Chemistry, 1985. **186**: p. 2291.
13. Leininger, R., Cooper, C., and Grode, G., *Nonthrombogenic plastic surfaces.* Science, 1966. **152**(1325).
14. Grode, G., Andersson, S., grotta, H., and Falb, R., *Nonthrombogenic surfaces via a simple coating process.* Transactions American Society for Artificial Internal Organs, 1969. **15**(1).
15. Schmer, G., *The biological activity of covalently immobilized heparin.* Trans Am Soc Artif Intern Organs, 1972. **18**: p. 321-4 333.
16. Miyura, Y., Aoyugi, S., Kusada, Y., and Miyamoto, K., *The characteristic of anticoagulants by covalently immobilized heparin.* Journal of Biomedical Material Research, 1980. **14**: p. 619.
17. Finlay, T., Troll, V., and Hodgkins, L., *Immobilization of heparin with trichloro-s-triazine: purification of mouse antithrombin.* Analytical Biochemistry, 1980. **108**: p. 354.
18. Danishefski, I. and Tzeng, F., *Preparation of heparin-linked agarose and its interaction with plasma.* Thrombosis research, 1974. **4**: p. 237.
19. Lindon, J., Salzman, E., Merril, E., Dincer, A., Labarre, D., Bauer, K., and Rosenberg, R., *Catalytic activity and platelet reactivity of heparin covalently bobded surfaces.* Journal of laboratory and Clinical medicine, 1985. **105**(2): p. 219.
20. Heyman, P., Cho, C., McRea, J., and Olsen, D., *Heparinized polyurethanes.* Journal of Biomedical Material Research, 1985. **19**: p. 419.
21. Solomon, D., Hu, C., McGary, C., and Lentz, D. *Covalently immobilized heparin, chemistry and characterization.* in *Transactions of the 10th European Congress on Biomaterials*. 1986.
22. Rattner, B. and Hoffman, A., *Nonthrombogenic treatments and Strategies*, in *Biomaterials Science. An Introduction to Material in Medicine*, B. Ratner, Hoffman, A., Schoen, F., and Lemons, J., Editors. 1996, Academic Press: San Diego. p. 297-308.
23. Hoffman, J., Larm, O., and Scholander, E., *A new method for covalent coupling of heparin and other glycosaminoglycans to substrates containing primary amino groups.* Carbohydrate Research, 1983. **117**: p. 328.
24. Larm, O., Larsson, R., and Olsson, P., *A new non-thrombogenic surface prepared by selective covalent binding of heparin via a modified reducing terminal residue.* Biomater Med Devices Artif Organs, 1983. **11**(2-3): p. 161-73.
25. Sommer, A. and Rifkin, D., *Interaction of heparin with human basic fibroblast growth factor: protection of the angiogenic protein from proteolytic degradation by a glycosaminoglycan.* J Cell Physiol, 1989. **138**(1): p. 215-20.

Stellenbosch University http://scholar.sun.ac.za

CHAPTER 9

Establishment of an animal model for the differentiation between transanastomotic and transmural healing

9.1 Abstract

Historically, animal models used in the evaluation of synthetic vascular grafts did not sufficiently mimic the healing responses encountered in humans. Their use further often precluded accurate assessment of and differentiation between transanastomotic and transmural healing. An isolated chacma-baboon femoral model that would allow for the differentiation between these two healing modes is proposed.

Thus, 2cm test segments of the graft material under investigation was interposed between two 3cm segments of low porosity (30μm internodal distance) expanded polytetrafluoroethylene (ePTFE). The resulting 8cm composite grafts were implanted in the femoral artery of adult chacma baboons (>20kg) after standard access, excision and end-to-end interposition. The baboon femoral artery promised limited disruption of blood flow patterns due to good size matching. The isolating segments allowed no transmural ingrowth and further limited transanastomotic pannus outgrowth to levels similar to those observed in humans. A full regimen for the qualitative and quantitative evaluation (involving scanning electron micrography and specific histological staining techniques) of surface and transmural healing is proposed.

9.2 Introduction

Problems pertaining to the use of dog and other animal models, such as the yellow baboon, used to evaluate vascular grafts intended for human use have been elucidated in Chapter 3. Briefly, the use of some models led, particularly in dogs, to the full *transanastomotic* healing of grafts, whereas similar grafts showed little or no midgraft healing in humans. Another model, the yellow baboon, allowed for complete *transmural* healing of large porosity grafts; a phenomenon that is also not mirrored in clinical applications. In other cases, it was not possible to distinguish between the two modes of healing. These discrepancies between commonly used animal experimental models and the human response have prompted this investigation into an alternative vascular graft evaluation model. It was primarily designed to evaluate the extent and nature of transmural ingrowth, a mode of healing thought to be critical in the development of the next generation of vascular grafts, while simultaneously eliminating the obfuscating effects of transanastomotic outgrowth.

Features of the proposed model include:

- The use of the chacma baboon, a senescent animal model that has been shown to most closely resemble the healing responses of humans
- The use of the femoral position. This position provides a close match to the size of the grafts under investigation (4mm ID), ease of access and minimum risk of complications.
- A composite graft consisting of (See Fig. 9.1):
  - Proximal and distal isolation segments of 30μm ePTFE. This material has been shown to be not only resistant to transmural ingrowth in all animals, but also to transanastomotic endothelialization in the chacma baboon
  - A central section (2cm) consisting of the graft material under investigation. The central section is attached to the isolating sections by application of an adhesive that simultaneously seals the anastomoses and thus prevents ingrowth into the anastomotic juncture.

Stellenbosch University http://scholar.sun.ac.za

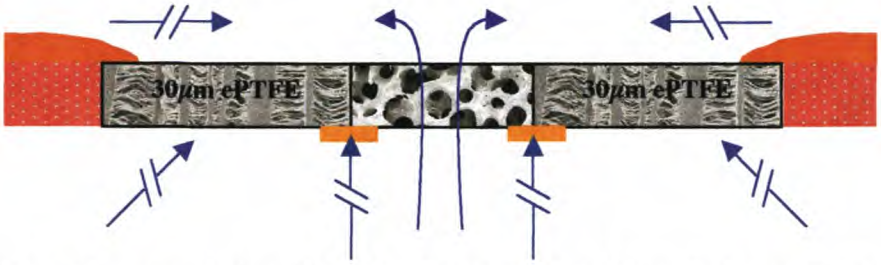

Figure 9.1: Schematic representation of the isolated graft model used to evaluate the efficacy of graft sections toward transmural healing

This chapter gives a full account of materials and methods used in graft production, implantation, explantation, and post-explant evaluation. The results will, however, be limited to the testing of the model, and selected results only will be used to illustrate the method and its effectiveness in preventing excessive transanastomotic outgrowth. Specific results on the transmural healing patterns achieved with ePTFE and PU test segments will be described in Chapters 10 and 11, respectively.

9.3 Materials and Methods

9.3.1 Graft Production

Test sections of ePTFE (from the indicated source) or polyurethane vascular grafts (as described in Chapter 5), nominal size: 4mmID, 2cm length, were interposed between two sections of 30μm ePTFE grafts (Atrium, 4mm, 30μmIND, 3cm length) in order to isolate the test section from the native artery. The anastomoses between the two synthetic materials were affected by repeated application of a polyurethane solution (5% M48 in $CHCl_3$) to the anastomotic area after immobilization of the three sections on a stainless steel mandrel. All grafts were sterilized by standard ethylene oxide exposure (Groote Schuur Hospital).

9.3.2 Implantation

9.3.2.1 Assignment

Isolated test grafts were implanted in chacma baboons (>20kg, male/female) by the method described below. Assignment of grafts to recipients and implant positions was done according to a rotational scheme. The group sizes were deemed to be too small for random assignment, and logical combinations of treatments were assigned on the basis that no animal received two grafts from the same group.

9.3.2.2 Pre-Implant/Explant Procedure

Animals were starved for 24h prior to the implant/explant date and subsequently injected with Temgesic prior to transport to the operating theatre. An i.v line was installed, an ECG transducer attached, Ketamine was administered and the animals were incubated (3-4l/min, 15mbar, 1-2%Ethrane, O_2 flow 4-5l/min). Following the injection of heparin, access was gained to the superficial femoral arteries via standard access.

9.3.2.3 Implant Procedure

Two vascular-clamps (proximal: 1cm after femoral bifurcation and distal 9cm from proximal) were placed on the superficial femoral artery, a 7cm section of the artery was excised, and the graft interposed end-to-end with one 7/0 Prolene running suture (proximal end first) after rehydrating (PBS) and trimming to correspond to the length of the excised vessel. After de-aeration by removal of the distal clamp, the blood was allowed to clot in the graft wall.

Stellenbosch University http://scholar.sun.ac.za

Subsequent removal of the proximal clamp restored the blood flow to the distal vasculature. Following the enclosure of the graft in the quadriceps, the skin was closed (in layers) with a 3/0 Maxon running suture. Early occlusion was prevented by administration of ASA (300 mg) orally through an NG tube at the time of completion of operation. The animals were weaned off the ventilator as soon as their own respiration was sufficient. Daily oral administration of ASA was continued for the duration of the implant. Regular visual monitoring of the animals' well-being and dietary habits was performed.

9.3.2.4 Explant Procedure

After the desired implantation time, the animals were again anaesthetised and access was gained to the implant sites. The femoral arteries were cannulated proximal and distal to the implant position, and the veins ligated to prevent back-flow during subsequent rinsing and fixation steps. After sacrificing the animal by injection of potassium chloride, and confirmation of death by ECG, the grafts were rinsed with 100ml PBS to remove excess blood, and subsequently flushed with 100ml of a 10% formalin solution to effect the in situ fixation of cellular and extracellular materials present on the lumenal surface. The grafts were then excised with the surrounding tissue and with 3cm of natural vessel on each end. Grafts were assessed for patency by ligation of side branches and injection of PBS from the proximal end. The explanted grafts were marked with a Liga-clip to identify the proximal end and placed in 10% formalin for 24h fixation.

Following fixation and removal of excess surrounding tissue, a macrophotograph of the intact graft was captured (Fig 9.2A). A 3-5mm longitudinal strip was dissected from the graft to determine the exact position of the test section and patency assessment. A second macrophotograph was taken at this point (B). After removal of a 3-5mm transverse section from the test section (L3), the rest of the graft was dissected into the sections shown in Figure 9.2D. Sections destined for light microscopy (L1...L5) were transferred to separate vials containing 10% formalin for further preparation. Samples for scanning electron microscopy (SEM) and transmission electron microscopy (TEM) were further fixed in a 2.5% solution of glutaraldehyde (GA).

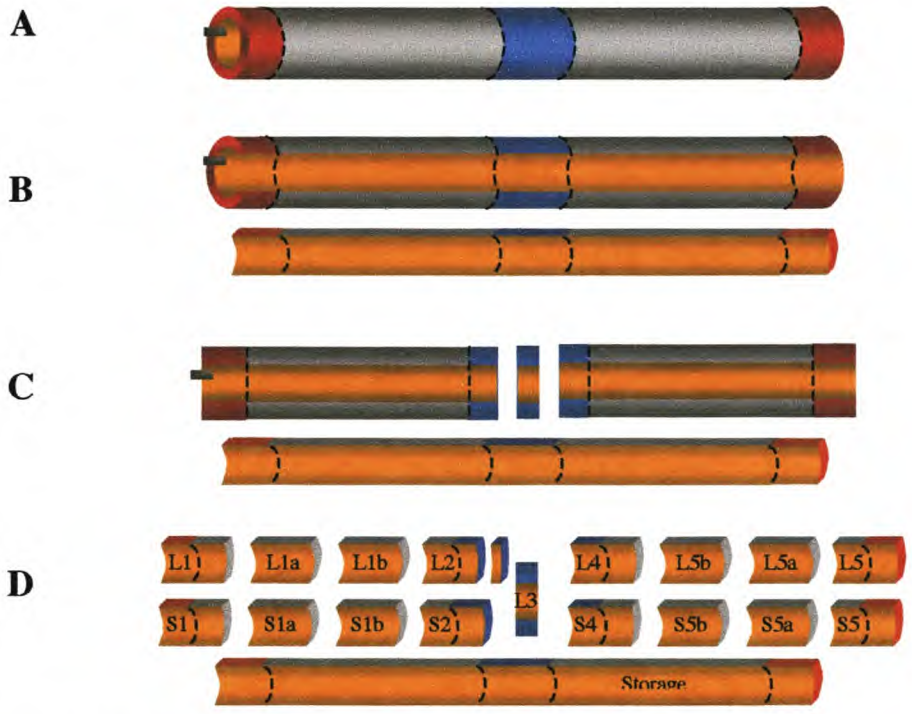

Figure 9.2: Schematic representation of the preparation of samples from explanted grafts for light microscopy (L), scanning electron microscopy (S), transmission electron microscopy (TEM), and storage.

Stellenbosch University http://scholar.sun.ac.za

9.3.2.5 Evaluation of Neovascularisation and Inflammatory Response

(A) Surface Healing

Sections denoted S in Figure 9.2 (S1, S1a...S5, S5a...) were prepared for SEM analysis by critical-point drying Balzars Union CPD020) and sputter coating with gold (Polaron SC500). Their surfaces were evaluated using a Jeol scanning electron microscope coupled to an Orion image capturing system and NIH image analysis software. The percentage of the sample covered by endothelium and thrombus were noted and quantified (were applicable).

(B) Transmural Healing

The sections denoted L were prepared for light microscopy by conventional imbedding and staining methods. The orientations of sections prepared from the samples are shown in Fig 9.3.

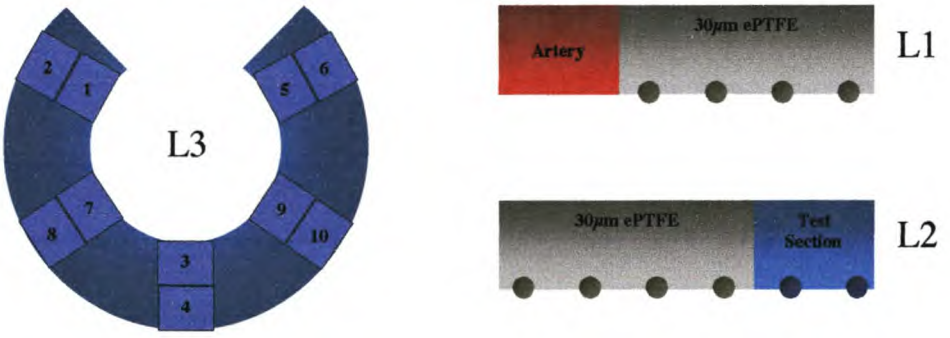

Figure 9.3: Schematic representation of the mounting orientations of explanted graft sections and areas used for image analysis.

The range of staining techniques employed throughout the study, the cellular and extracellular material targeted by these stains, are listed together with the quantification parameter in Table 9.1.

Table 9.1: Listing of stains and antibodies used in detecting distinguishing features during histological processing and image analysis.

Stain/Antibody	Target features	Cross-reactivity	Quantification
Fibronectin	Fibrin	-	-
CD-31	EC	-	VI
Actin	SMC	-	AI
H&E	general	Various	FBGCI
HAM-56	FBGC/Mac	-	FBGCI
Factor VIII	Fibrin/EC	-	-
Azan trichrome	Collagen (Blue)	Nuclei/RBC's/Fibrin (Red) SMC (Orange/Red)	-

GSL-1: *Griffonia simplicifolia lectin (Vector Laboratories, CA, US)*
CD-31: *Pecam-1 (Platelet endthelialo cell adhesion molecule)*
Actin: *Smooth muscle cell actin (α-SMCA) (Research Diagnostics, NJ, USA)*
H&E *Hematoxylin and Eosin*
Azan: *Trichrome Masson: Azocarmine / Orange-G / Aniline Blue (Sigma, USA)*

EC: *Endothelial cells*
SMC: *Smooth muscle cells*
FBGC: *Foreign body giant cells*
VI: *Vascularization Index*
AI: *Arteriolarization Index*
FBGCI: *FBGC Index*

Stellenbosch University http://scholar.sun.ac.za

For each section, a blinded observer captured the depicted regions (Fig. 9.3) (300 X 350μm: neovascularization, arteriolarization; 150 X 175 μm: inflammatory response, FBGC content) with a Leitz DM RB microscope. The areas of positively identified elements were quantified with Qwin image analysis software and normalised to the available ingrowth area, generating a vascularization index (VI) and a FBGC index (FBGCI). Indexes were defined as the percentage area (relative to the available ingrowth area) occupied by the relevant features.

9.3.6 Statistical Analysis

Data are expressed as means ± standard error of means (SEM). The comparisons of VI, AI and FBGCI between groups were by Student's unpaired t-tests. One-sided p-values were determined in all cases. A significance level of 0.05 or less was accepted as being statistically significant.

9.4 Results

9.4.1 Composite graft production

Figure 9.4 shows composite grafts prepared by the interposition of test segments between isolating low-porosity ePTFE segments. The polyurethane sealant provided for both a structurally sound connection and an impenetrable layer. The high porosities of the test segments (as opposed to the flanking segments), and the extent of the applied sealant, are clearly visible in the high magnification macrographs.

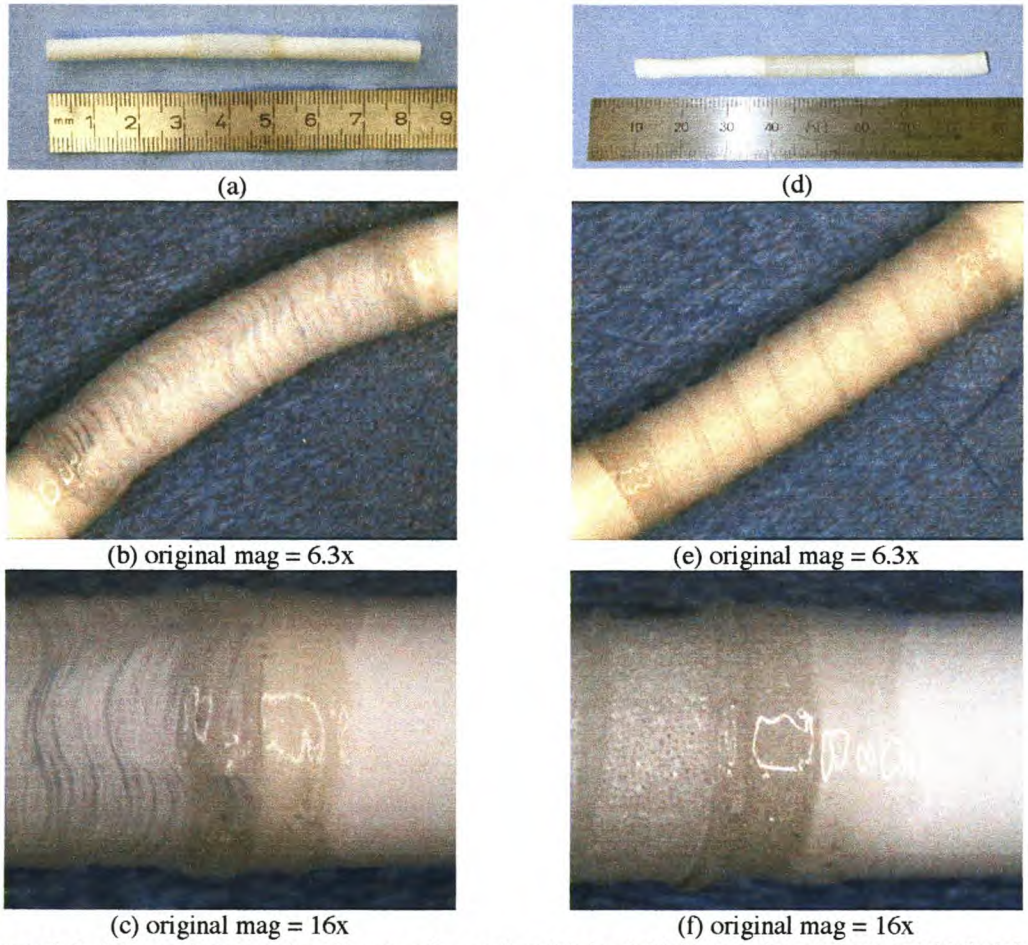

Figure 9.4: Macrophotographs of composite grafts with (a-c) high porosity ePTFE and (d-f) PU test segments interposed between low porosity ePTFE segments

Stellenbosch University http://scholar.sun.ac.za

9.4.2 Baboon femoral implants

Although the size of the exposed implant site, and the length of the femoral artery that was excised prior to implantation, did not always accommodate the full length (8cm) of the composite synthetic graft, slight trimming of the graft ends was sufficient to establish a good fit (Fig 9.5) Even though the high porosity and permeability of the test segments resulted in the initial free-flow of blood through the central section after removal of the distal clamp, haemostasis in the wall was generally achieved within 5-10 minutes. The subsequent removal of the proximal clamp occasionally resulted in some further bleeding due to the increased pressure. Bleeding at the anastomoses was stopped by the application of additional sutures, while renewed loss of blood through the mid-section of the graft wall was stopped by the topical application of aprotinin-impregnated pledges. Blood was not immediately able to penetrate the isolating, low-porosity ePTFE, as was evident from the continued white colour of these sections in Fig 9.5. The good size-matching between the grafts and femoral artery can be seen in Fig 9.5 b and c.

(a) (b) (c)

Figure 9.5: Macrophotographs of isolated grafts implanted in the bilateral femoral position in the chacma baboon.

9.4.3 Surface analysis

An explanted graft containing an adherent outer capsule is shown in Figure 9.6. Careful longitudinal dissection allowed for the visual evaluation of the lumenal surface and for the assessment of graft patency. The graft shown below contained no thrombotic deposits apart from a thin white layer directly on the surface, and was patent throughout.

(a) (b) (c)

Figure 9.6: Macrophotographs of an explanted composite graft containing a high-porosity ePTFE test section.

Further detailed analysis of the graft surface was possible by scanning electron microscopy. Although the nature of the surfaces depicted in the micrographs (Figure 9.7) is not visible at the low magnification shown, it was possible to distinguish between different surface features (e.g. endothelial cells, exposed graft, and fibrin deposits) at higher magnification.

Stellenbosch University http://scholar.sun.ac.za

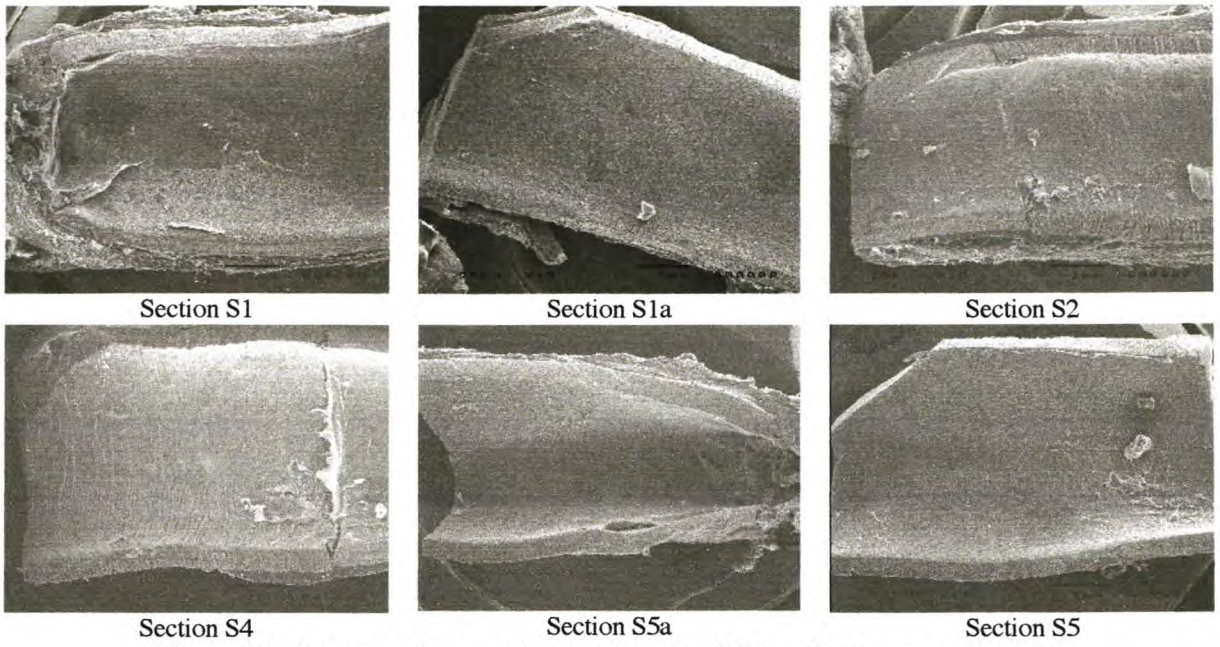

Figure 9.7: Scanning electron micrographs of the full length of a composite graft.

The efficacy of the low-porosity flanking sections in preventing excessive transanastomotic endothelialization is shown in Figure 9.8. After 14 days of implantation, both the proximal and distal endothelialization was limited to below 5mm. Extension of the implant duration to 21 days resulted in an increase in the proximal transanastomotic endothelialization to approximately 10mm. This distance is, however, much lower than the length of the isolating segments. The insert depicts a micrograph of pannus tissue growing across the anastomosis between the natural artery and the graft.

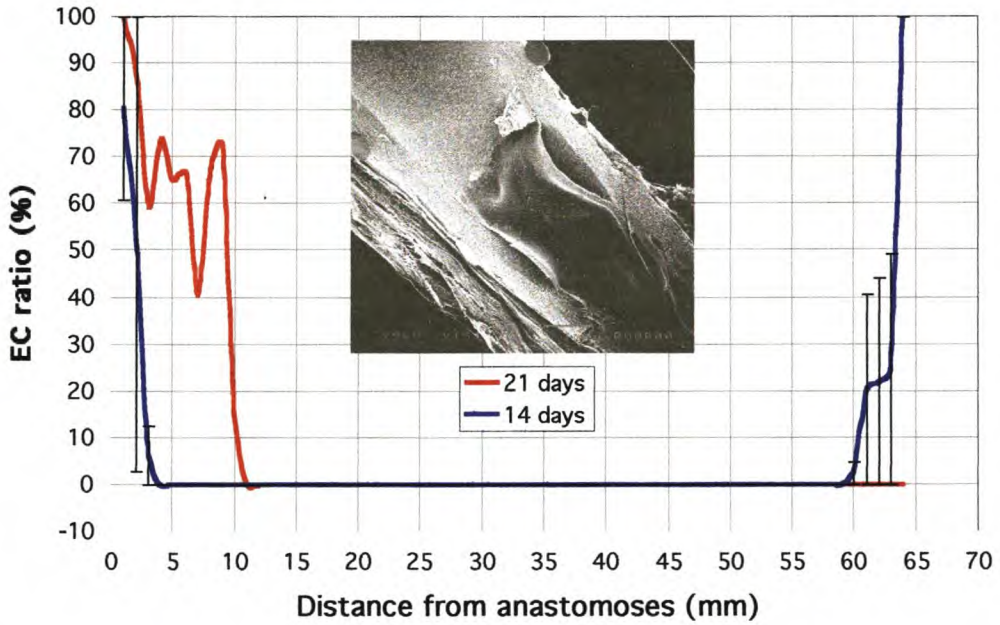

Figure 9.8: Extent of transanastomotic endothelialization on low-porosity (30μm) isolating ePTFE sections of a composite vascular graft.

Stellenbosch University http://scholar.sun.ac.za

CHAPTER 10

High porosity ePTFE

Are increased ingrowth-spaces alone sufficient for transmural healing?

10.1 Introduction

The lack of transmural healing in standard ePTFE grafts has been shown to result from the restricted ingrowth spaces available for tissue ingrowth (see Chapters 2 and 3). Although higher porosities (60μm) allow full transmural capillary ingrowth in the yellow baboon, the ingrowth is restricted to the outer two-thirds of the wall in the chacma baboon. Davids et al. explained these phenomena after a detailed analysis of the available ingrowth dimensions in low (30μm) and high (60μm) ePTFE prostheses [1]. In Figure 10.1 (a), the dimensions of the minimum continual ingrowth channels in 30μm ePTFE are close to the mean diameter of capillary vessels, and far below the spaces needed for arteriolar ingrowth. Large porosity ePTFE, on the other hand, were shown to contain spaces large enough for the ingrowth of both capillaries and arterioles (Gigure 10.1 b).

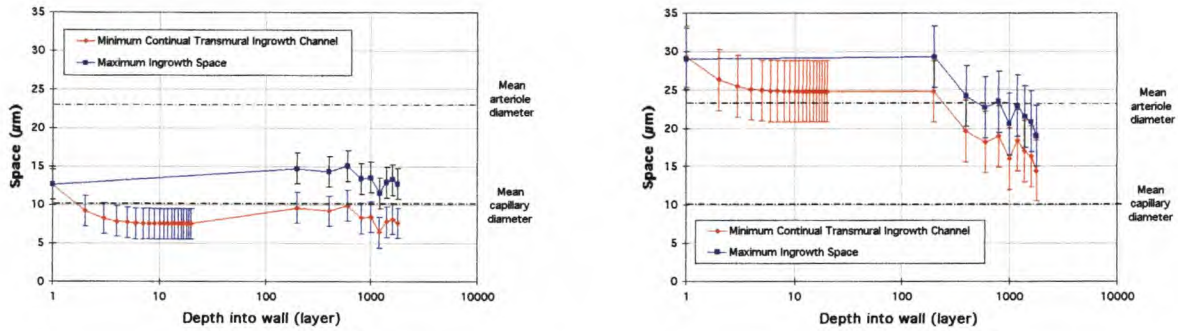

(a) 30μm ePTFE (b) 60μm ePTFE

Figure 10.1: Ingrowth dimensions of (a) standard and (b) large porosity ePTFE [1]

The current study was designed to reinvestigate the transmural healing response in the isolated chacma baboon model (see Chapter 9), and to determine whether an increase in pore size alone would lead to improved healing. The hypothesis that the lumenal sealing of the graft surface (in order to prevent the build-up of impenetrable fibrin deposits) would further improve full transmural ingrowth was also to be tested.

10.2 Materials and methods

The methods used in graft production, implantation and analysis have been described in detail in Chapter 9. Thus only the specific parameters pertaining to this study, and additional procedures not described earlier, will be given.

Both standard (30μm nominal IND) and a new, very large porosity (nominal IND=150μm), ePTFE grafts were obtained by special request from a leading ePTFE graft manufacturer. The large porosity grafts were interposed between two segments of low porosity material by methods described in Chapter 9. Five grafts of this type were implanted in the femoral baboon model for durations for 4h, 7days, 14 days, 21 days and 28 days, respectively. In addition, the central section of another graft was sealed with a thin layer of polyurethane and implanted for 14 days. Although the implants were limited to one graft per time period, these pilot implants allowed for the determination of basic trends while limiting the number of primate experiments. Skinning of

Stellenbosch University http://scholar.sun.ac.za

the 150μm grafts was achieved by the repeated application of a 5% solution of polyurethane (M48) to the lumenal surface and drying at elevated temperatures between application steps. Analysis of graft porosities (internodal distances) was achieved by standard image analysis techniques of scanning electron micrographs. Internodal distances are expressed as means±standard error of the means.

The average internodal distances (IND) of the 30μm nominal IND grafts were 22.3μm±0.9μm and 25.1±1.1μm, while those of the 150μm grafts were very close to the claimed IND (148±3.9 and 146±3.1 on the lumenal and ablumenal surfaces respectively) (See Figure 10.2 a,b,e,f). Thus the large-porosity grafts contained ingrowth spaces that were more that 6 times that of the low porosity material (as defined by the IND). Apart from this difference in dimensions, there was also a distinct difference in the transmural structure of the grafts. While the low-porosity material contained nodes that were fairly randomly distributed through the graft wall, the nodes in the high-porosity grafts were more parallel to one another, and if one disregards the impediment created by the fibrils, they defined distinct channels that connected the lumenal surface to the ablumenal surface (Fig 10.2 c and f).

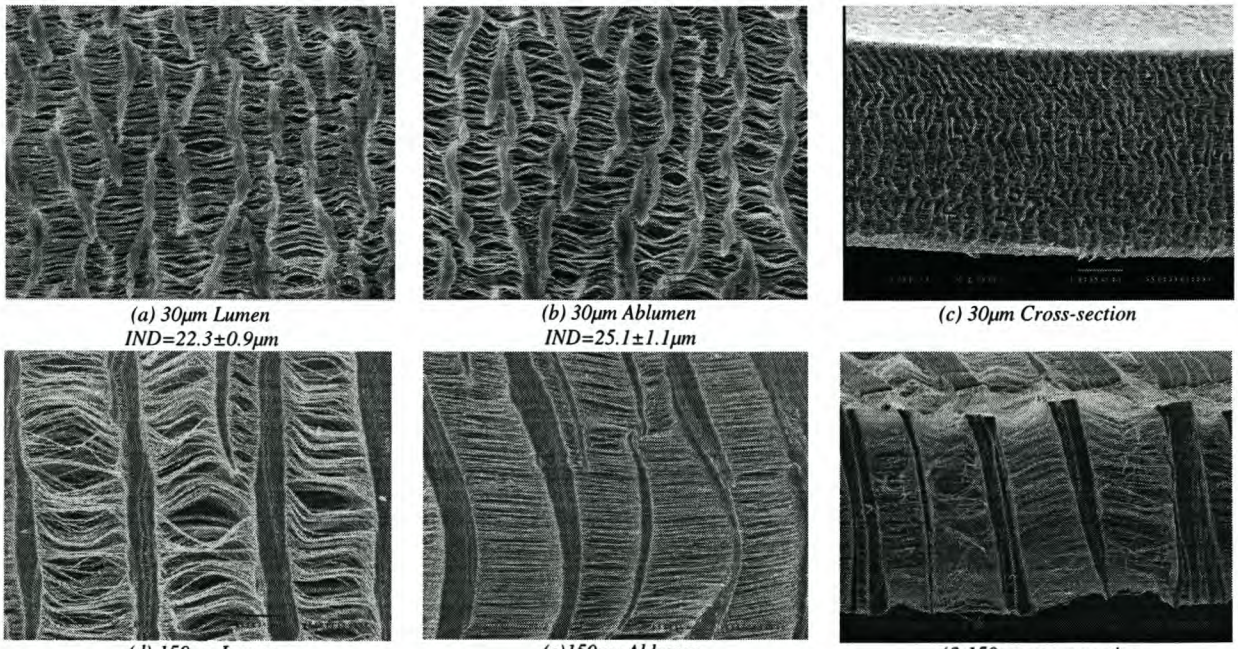

(a) 30μm Lumen IND=22.3±0.9μm
(b) 30μm Ablumen IND=25.1±1.1μm
(c) 30μm Cross-section
(d) 150μm Lumen IND=148±3.9μm
(e)150μm Ablumen IND=146±3.1μm
(f) 150μm cross-section

Figure 10.2: Scanning electron micrographs of 30μm and 150μm nominal IND ePTFE vascular grafts

10.3 Results and discussion

The healing patterns of the three graft types, namely 30μm, 150μm, and 150μm porosity ePTFE with a lumenal sealant, are described with reference to the respective figures below (Figures 10.3, 10.5 and 10.7). The responses are further summarized in the attached schematics (Figures 10.4, 10.6 and 10.8) and text that follows each of these figures.

Stellenbosch University http://scholar.sun.ac.za

10.3.1 Low porosity 30μm ePTFE

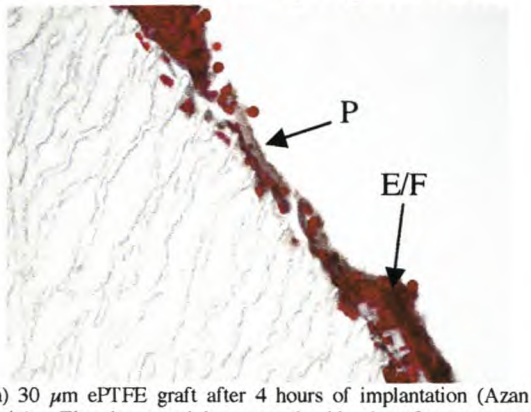

(a) 30 μm ePTFE graft after 4 hours of implantation (Azan stain). The dense red layer on the blood surface presents erythrocytes (E) and fibrin while the greyish grainy depositions are platelets (P). The narrow PTFE spaces have not allowed the penetration of any white or red blood cells into the depth of the graft.

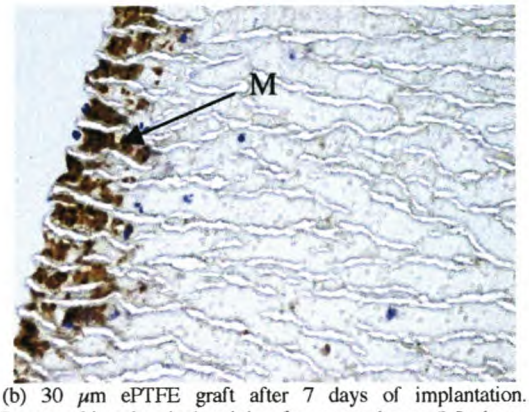

(b) 30 μm ePTFE graft after 7 days of implantation. Immuno-histochemical staining for macrophages (M) shows that the spaces are even too narrow to allow the penetration of white blood cells. Only a few erythrocytes and lymphocytes can be seen in the depth.

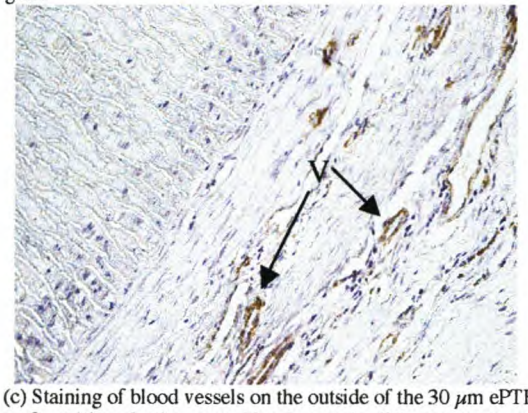

(c) Staining of blood vessels on the outside of the 30 μm ePTFE graft. Although the new blood vessels (V) are very well developed on the outside in the surrounding tissue, the narrow ePTFE spaces do not allow them to penetrate into the graft wall.

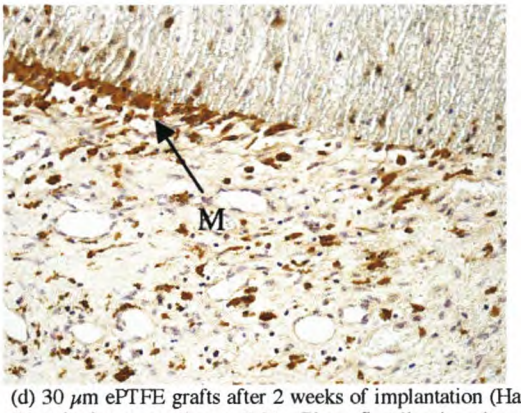

(d) 30 μm ePTFE grafts after 2 weeks of implantation (Ham 56 stain for macrophages (M)). These first-line invaders of white blood cells accumulate on the outside of the graft because of the inability to penetrate into the narrow spaces of the 30 μm graft.

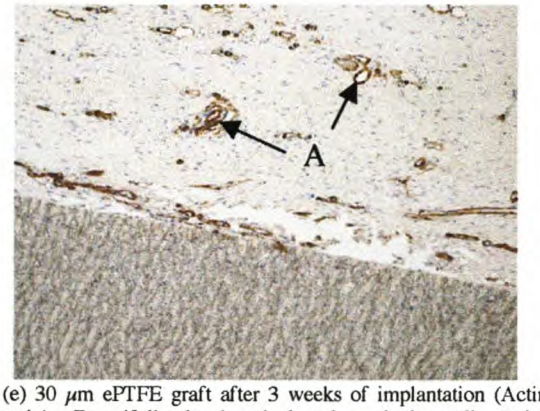

(e) 30 μm ePTFE graft after 3 weeks of implantation (Actin stain). Beautifully developed, densely-packed, small arteries (A) on the outside of the graft which cannot penetrate into the graft wall because of the narrowness of the spaces.

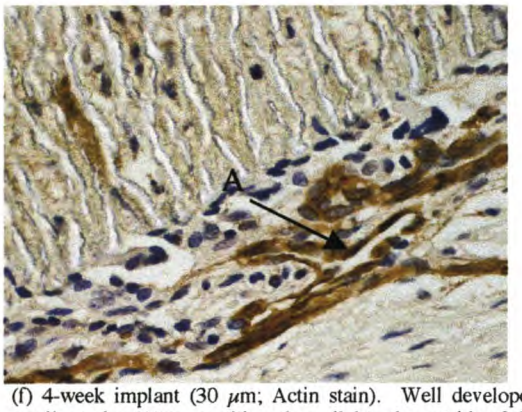

(f) 4-week implant (30 μm; Actin stain). Well developed small arteries (A) are positioned parallel to the outside of the graft. Artery penetration into the graft wall is restricted by limited ingrowth spaces.

Figure 10.3: Histological analysis of 30μm porosity ePTFE vascular grafts

Stellenbosch University http://scholar.sun.ac.za

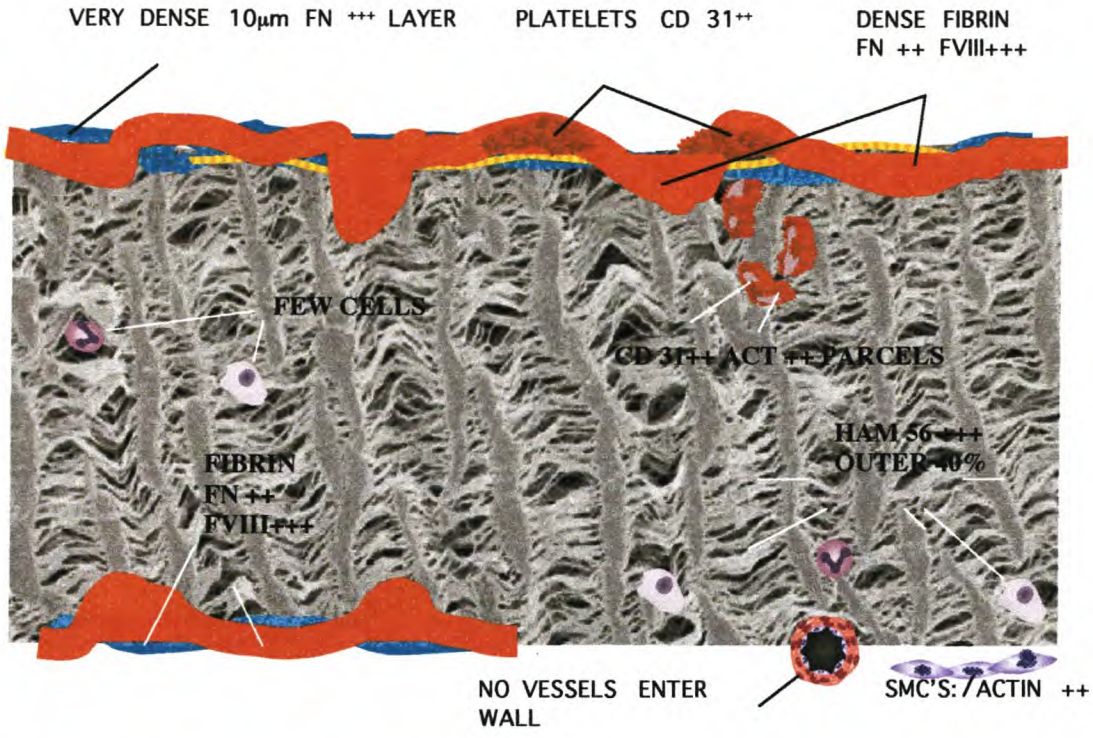

Figure 10.4: Schematic representation of lack of healing events in 30µm porosity ePTFE grafts. There are fibrin depositions on both surfaces particularly on the blood surface. This thin thrombus layer consists primarily of fibrin and red blood cells with a few areas of platelets. No blood vessels enter the graft wall further than a few micrometers. The spaces between the ePTFE nodes and fibres are not only too narrow for arterioles and capillaries, but also for single white blood cells such as macrophages.

In our non-human primate model it became very obvious that the low porosity 30 μm ePTFE grafts feature all the negative aspects of graft healing without allowing the healing process itself to occur even at the lowest of all levels.

- Fibrin deposition: The infiltration of fibrin from the blood into the graft wall occurs to the same degree as in high-porosity grafts. Given the inhibitory effect of compacted fibrin on tissue ingrowth, it is obvious that the low porosity and the hydrophobicity of the ePTFE material were not capable of counteracting this detrimental aspect of graft healing.
- Ingrowth spaces: The well healed surrounding tissue with an abundance of capillaries and arterioles clearly demonstrates that a healing process is well underway. Since not only capillaries were incapable of growing into the interstitial spaces of the graft but also, to a large extent, inflammatory cells, low-porosity 30 μm ePTFE grafts can be described as non-healing conduits.
- Compliance: The negative influence of the complete lack of compliance of expanded polytetrafluoroethylene grafts did not have to any visible influence on the healing because porosity already completely inhibited any cellular ingrowth.

Stellenbosch University http://scholar.sun.ac.za

10.3.2 High-porosity 150μm ePTFE: unsealed blood surface

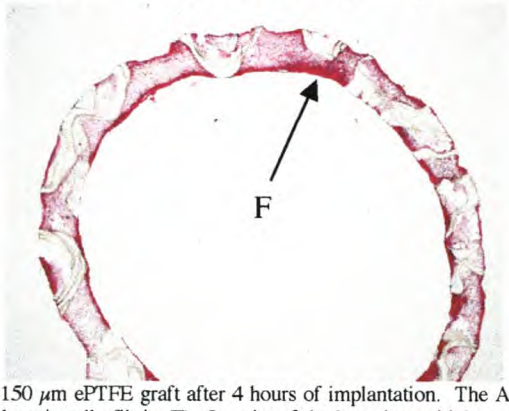

(a) 150 μm ePTFE graft after 4 hours of implantation. The Azan stain marks primarily fibrin (F). In spite of the huge interstitial spaces in the graft wall, the fibrin accumulation is primarily at the blood surface.

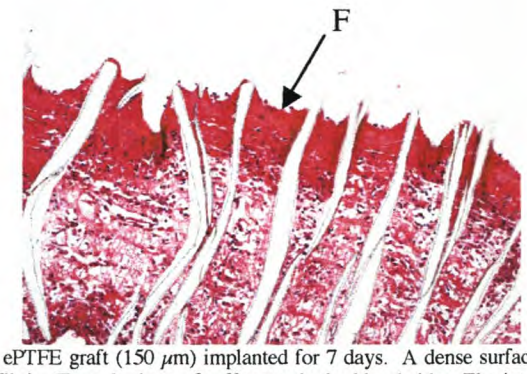

(b) ePTFE graft (150 μm) implanted for 7 days. A dense surface layer of fibrin (F) seals the graft off towards the blood side. The interstitial spaces of the graft wall are only filled by a very loose material.

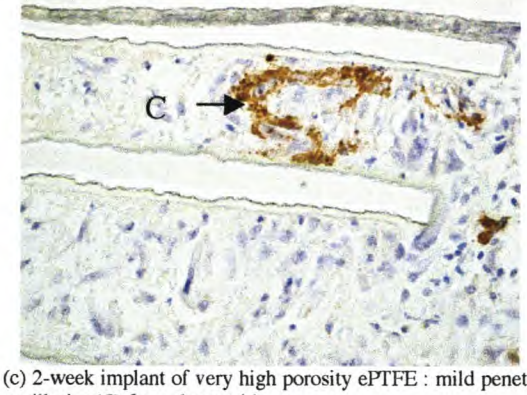

(c) 2-week implant of very high porosity ePTFE : mild penetration with capillaries (C) from the outside.

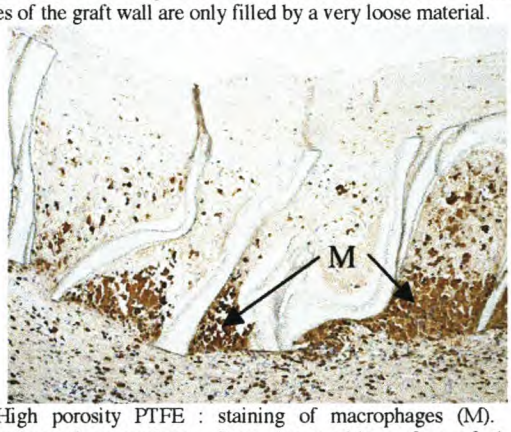

(d) High porosity PTFE : staining of macrophages (M). Dense infiltration of macrophages from the outside surface of the graft, indicating that the lack of an inflammatory reaction in 30 μm ePTFE was not due to the ePTFE material but to the narrow spaces.

Figure 10.5: Histological analysis of 150µm porosity ePTFE vascular grafts

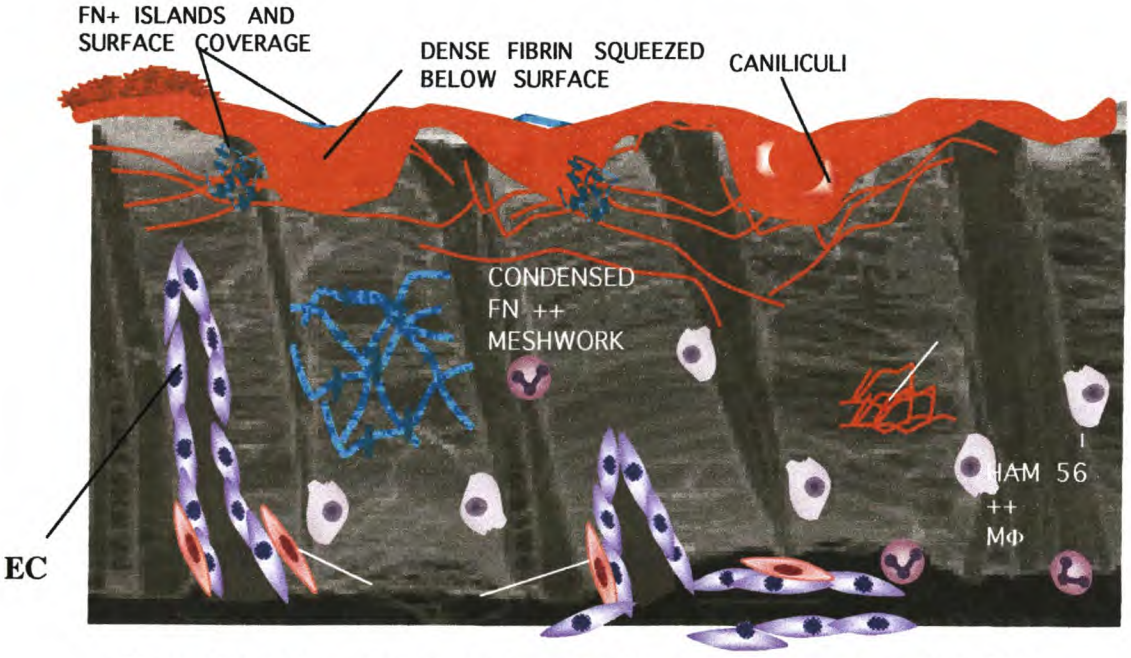

Figure 10.6: Schematic representation of healing events in 150 µm porosity ePTFE. The wide ingrowth spaces of the interstices of the graft wall allow the penetration by capillaries. The blood surface is nevertheless equally sealed with a dense layer of fibrin, something already seen in 30 micrometer ePTFE. In spite of a moderate density of penetrating capillaries, hardly any arterioles are seen growing into the graft wall.

Stellenbosch University http://scholar.sun.ac.za

The porosity of the 150μm ePTFE grafts created ingrowth spaces almost 3 times larger than those in any previously-used, so-called high porosity ePTFE grafts (60μm). Our implantation results clearly confirmed that the spaces available are sufficient for the penetration with micro-capillaries and arterioles. Overall, the healing was only modestly occurring, with a massive build-up of compacted fibrin at the blood surface.

- Fibrin deposition: Similar to all other high-porosity grafts, an almost acellular, highly compacted fibrin layer was building up in the inner third of the graft wall, completely preventing cellular ingrowth in this area.
- Ingrowth spaces: Both arterioles and capillaries were occasionally seen throughout the graft wall except in the area of the compacted fibrin. This indicates that the spaces are theoretically available for ingrowth. Nevertheless, no circularly aligned parcels of smooth muscle cells as seen in the polyurethane grafts could be detected. The reason for this lack of muscularisation of the graft wall may – apart from the lack of compliance – lie in the combined physical obstruction of circular ingrowth paths by solid transmural nodes and by a still relatively dense fibrillar meshwork.
- Compliance: The modestly developed ingrowth of blood vessels in spite of ingrowth permissive interstitial spaces stands in stark contrast to the ingrowth events observed in the compliant polyurethane grafts. In view of the proven stimulatory effect of pulsatile stress and strain on the proliferation of vascular wall cells, this retarded development of the new artery wall is most likely the result of the complete lack of compliance in ePTFE grafts.

10.3.3 High-porosity150μm ePTFE: sealed blood surface

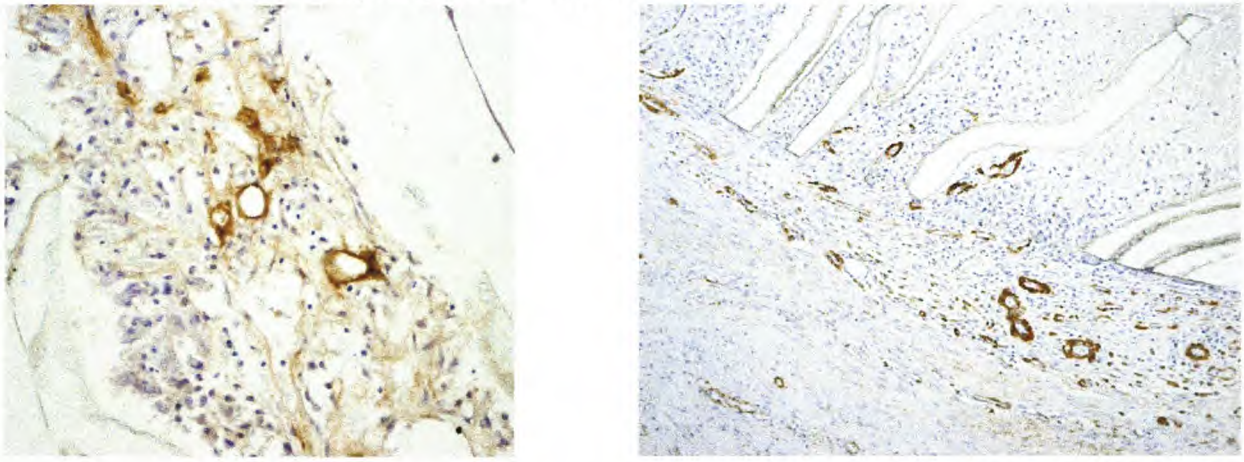

Surface skinned 150 μm ePTFE grafts. One can see the thin layer of heparin grafted to the blood surface. Underneath the protecting surface sealant capillaries have infiltrated the graft wall all the way to the blood surface

Figure 10.7: Histological analysis of 150μm porosity ePTFE vascular grafts containing a lumenal skin

Stellenbosch University http://scholar.sun.ac.za

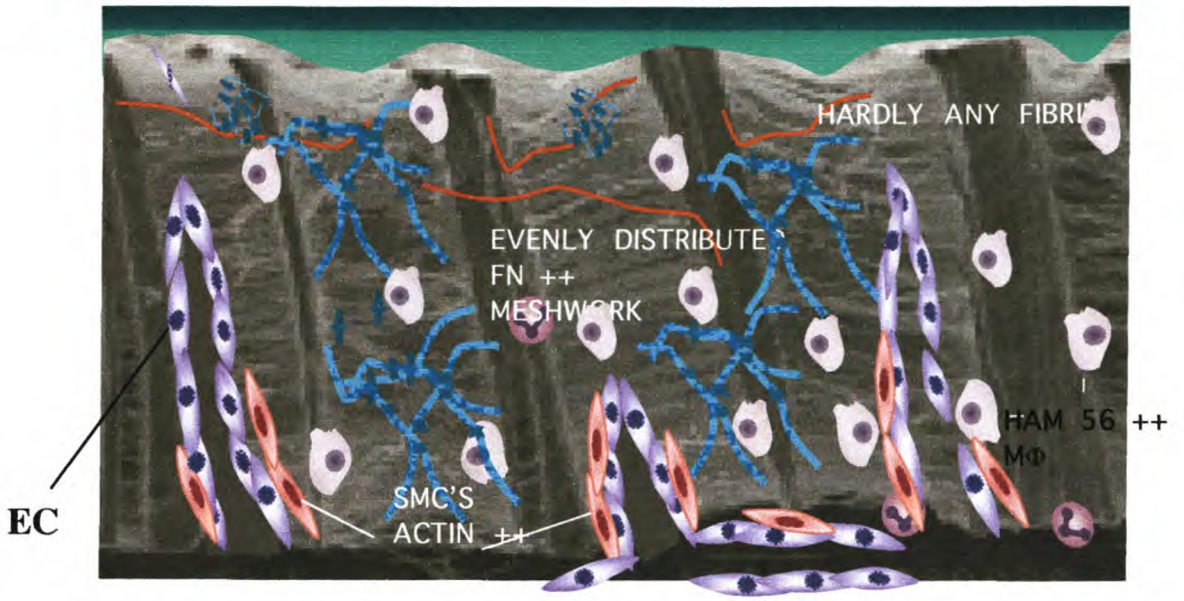

Figure 10.8: Schematic representation of healing events in skinned, high-porosity PTFE grafts. The surface sealing which prevents the build-up of hostile fibrin results in a much better capillary penetration of the entire graft wall. However, vessel density is still very modest and smooth muscle cells are very scarce.

In contrast to the unsealed grafts, the inner third of the graft wall is not blocked by compacted fibrin. Cellular ingrowth goes all the way from the outside adventitial area to the sealant layer at the blood surface. Overall, the healing of the graft wall is still only moderately expressed and most importantly, no smooth muscle cell proliferation or orientation characterises this healing. Therefore, in spite of surface protection and availability of ingrowth permissive interstitial spaces, no new artery wall is being formed.

- Fibrin deposition: Through surface sealing the infiltration of compacted fibrin matrices is completely inhibited. As a result, the overall healing of the graft wall is clearly superior to that of the non-sealed control grafts.
- Ingrowth spaces: similar to the unsealed, high-porosity ePTFE grafts interstitial spaces clearly allow the penetration of both capillaries and arterioles throughout the graft wall. It must be considered as a possibility that the complete lack of arteriolarization by the infiltration of the spaces with the smooth muscle cells is partly caused by the impenetrable transmural nodular barriers and the dense fibrils that are only maximally stretchable in the middle ground between two nodes.
- Compliance: In spite of the facilitating effect of the surface shield with regards to the prevention of fibrin insudation, graft healing is disappointing in view of the fact that spaces are at least theoretically ingrowth-permissive and of the strong biological response of vascular wall cells to pulsatile stretching. It must be assumed that the lack of arteriolarization of the graft wall is primarily due to the non-compliant nature of ePTFE grafts.

10.4 Reference

1. Davids, L., Dower, T., and Zilla, P., *The lack of healing in conventional vascular grafts*, in *Tissue engineering of vascular grafts*, P. Zilla and Greisler, H., Editors. 1999, RG Landes: Austin. p. 3-44.

Stellenbosch University http://scholar.sun.ac.za

CHAPTER 11

High-porosity PU grafts

Combination of increased spaces, dodecahedral structure and compliance.

11.1 Introduction

Porous polyurethane grafts have been used for the past 30 years as experimental substitutes for commercially available Dacron and ePTFE prostheses (See Chapter 5). The in vivo evaluation of these grafts was predominantly performed in the canine model (carotid, aortic, femoral/iliac and vena cava positions), although the rat aortic, ovine carotid and porcine aortic models have also been employed.

The most commonly reported healing response involved the formation of what is described as a glistening neo-intima (or pseudo intima) on the lumenal surface of grafts implanted in animal models [1-12]. The full endothelialization of the grafts were either obtained in many cases [2, 13-16], or assumed without further confirmation [17]. Although the origin of these surface-healing layers was not identified, the lack of sufficient interconnected porosity, combined with the use of animals models that allow extensive transanastomotic outgrowth, indicate that the surface tissue originated from the native artery rather than from the perigraft tissue.

The high patency rates achieved with various PU graft types may also be attributed to the successful transanastomotic surface healing in these models. One hundred percent (100%) patency was achieved in short (<12months) [2, 15, 18-20], medium (12 months) [4, 21], and long-term (10years) [14] implants in various animal models. A number of the reviewed grafts did, however, exhibit much lower patency rates. Apart from one study in which all (of 4) grafts were occluded [22], the patency rates were, however, generally close to or above 50% [1, 3, 23-25].

In order to decrease thrombogenicity, a number of workers have pre-seeded PU grafts with endothelial cells. Hess et al. [26] and Stansby et al. [27] successfully seeded Vascugraft and Pulse-Tec grafts with ECs, but did not perform in vivo studies. When in vivo studies were performed on EC seeded PU grafts, the results were encouraging but not striking. While one study showed the absence of thrombus formation in a 24hr canine AV shunt model [28], and another could slightly improve patencies (non-seeded controls) [29], the seeded, multicellular lining on the lumen became detached after 5 weeks in the canine carotid artery model used by Williams et al. [10].

The current study was designed to evaluate a novel polyurethane vascular prosthesis in the isolated chacma baboon model. The model was designed to more accurately mimic the healing responses observed in humans by eliminating the effect of transanastomotic outgrowth (See Chapter 9). The main aim of the study was to determine whether full transmural healing (ingrowth of capillaries, arterioles and smooth muscle cells) could be achieved (as opposed to transanastomotic outgrowth) by providing large, well-defined, interconnected pores in the graft wall. Secondary objectives were to determine (i) the effect of a lumenal sealant, (ii) whether the three-dimensional porous structure, that provides equal opportunity for growth in all directions, would allow for the spontaneous helical orientation of smooth muscle cells in the graft wall, and (iii) whether the pulsatile stress/strain resulting from compliance achieves the biological effects promised by in vitro experiments [30].

Stellenbosch University http://scholar.sun.ac.za

11.2 Materials and methods

Polyurethane vascular grafts (M48, 150μm pores, 4mm ID, 2cm length) were produced by the method described in section 5.4.4.3 B(ii) and reinforced by the helical winding of a polyurethane fibre (200μm, 2.5mm pitch) (See 5.4.4.6). The lumenal surfaces of four of the grafts were sealed by the repeated application of a polyurethane solution (5% M48 in $CHCl_3$) (Fig 11.1), and heparin was immobilized on the inner surfaces of the sealant layer as described previously (See 8.3.2.1 and 8.3.2.4), with the exception that the grafting was performed for 60min, and that grafting and heparinization occurred in a flow reactor that limited the modification to the inner surface.

All grafts were subsequently interposed between 3cm sections of low porosity ePTFE, sterilized by standard ETO exposure, degassed and implanted into the femoral position of adult chacma baboons (>20kg) by end-to-end anastomoses (See Chapter 9). The unskinned grafts were implanted for a duration of 4 hours (n=1), 7 days (n=1), 14 days (n=2), 21 days (n=1) and 28 days (n=2) while grafts containing a heparinized lumenal sealants were implanted for 4 hours (n=1), 7 days (n=1), 21 days (n=1) and 28 days (n=1) respectively. Graft explant and evaluation was performed as described in Chapter 9.

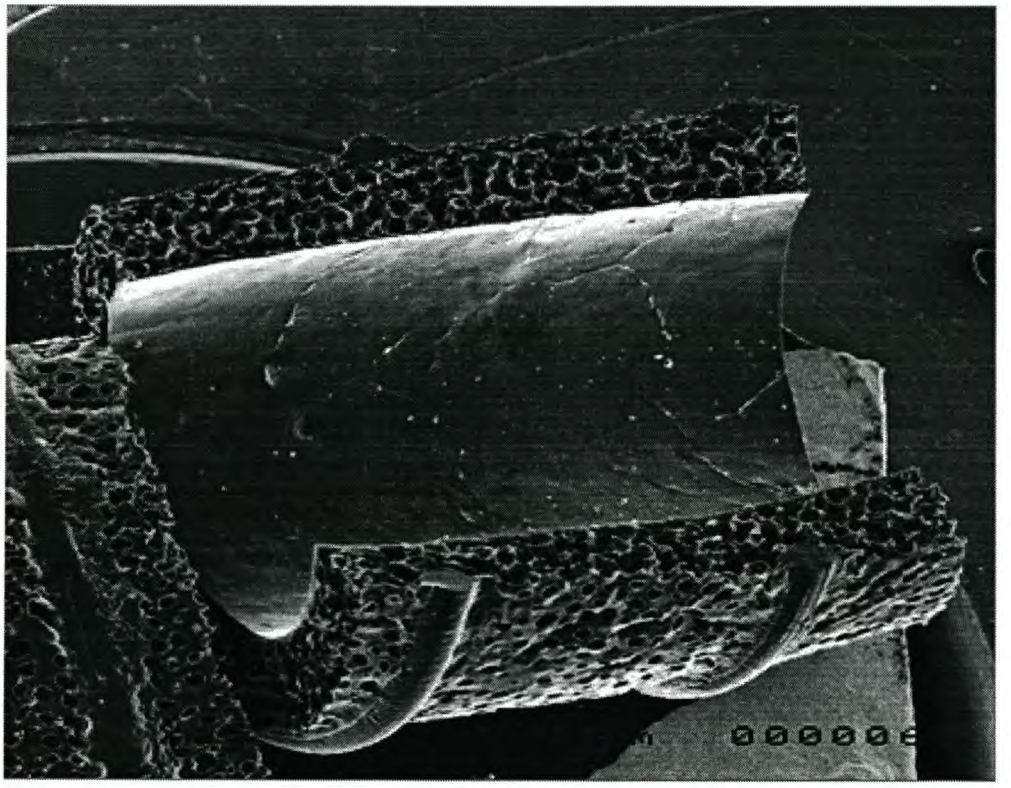

Figure 11.1: Scanning electron micrographs of a PU graft containing a PU surface sealant.

11.3 Results and discussion

The healing patterns of the two graft types, namely 150μm PU and 150μm porosity PU with a lumenal sealant, are described with reference to the respective figures below (Figures 11.2 and 11.4). The responses are further summarized in the attached schematics (Figures 11.3 and 11.5) and text that follows each of these figures.

Stellenbosch University http://scholar.sun.ac.za

11.3.1 150μm Polyurethane: unsealed blood surface

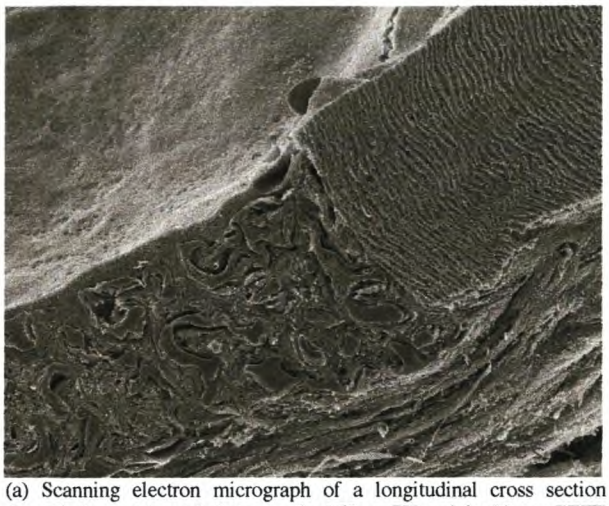

(a) Scanning electron micrograph of a longitudinal cross section through the anastomosis between the 150μm PU and the 30μm ePTFE isolating segment. The healing throughout the graft wall is evident.

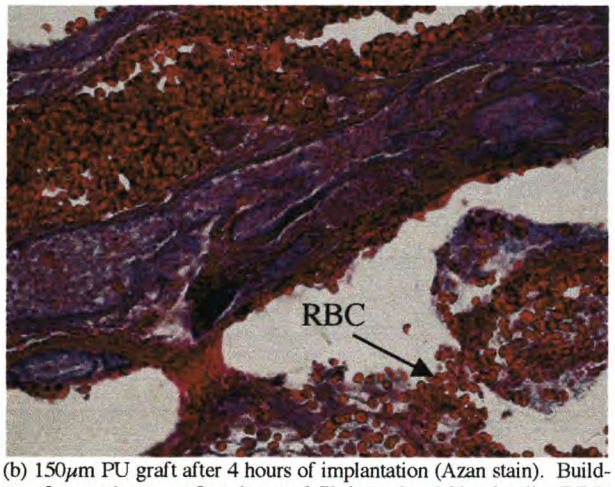

(b) 150μm PU graft after 4 hours of implantation (Azan stain). Build-up of a moderate surface layer of fibrin and red blood cells (RBC) whereby blood platelets and erythrocytes are contained in parcels

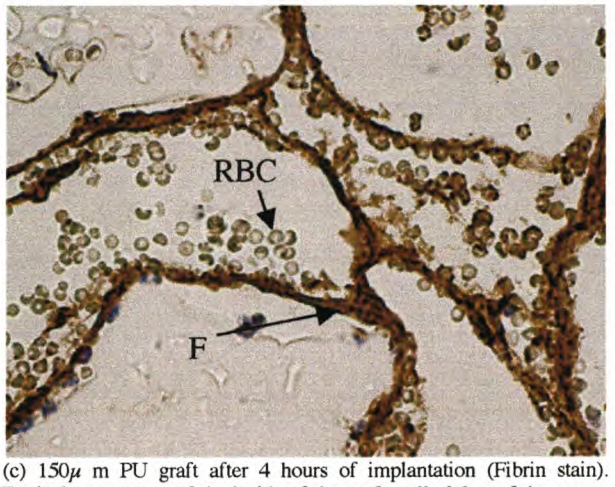

(c) 150μ m PU graft after 4 hours of implantation (Fibrin stain). Typical appearance of the inside of the graft wall. Most of the spaces are empty with thin membranes of fibrin (F) surrounding RBCs.

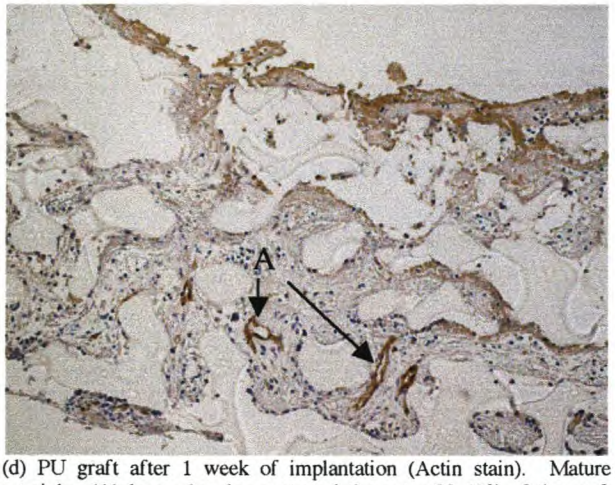

(d) PU graft after 1 week of implantation (Actin stain). Mature arterioles (A) have already penetrated the outer 30-40% of the graft wall.

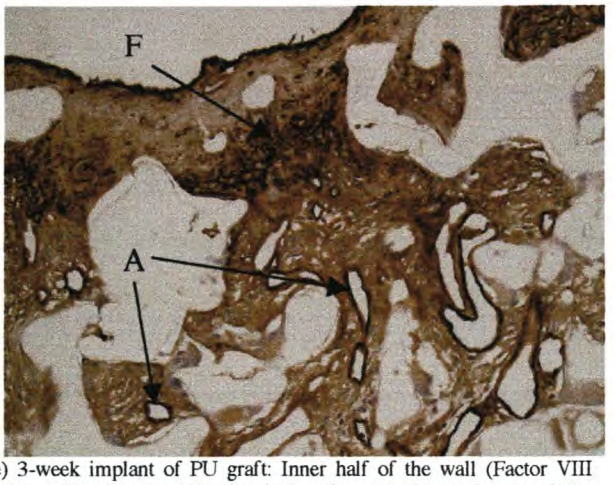

(e) 3-week implant of PU graft: Inner half of the wall (Factor VIII stain). The immunohistochemical stain strongly marks the dense surface layer consisting of compacted fibrin (F). Underneath a dense convolute of blood vessels (V) can be seen reaching all the way through the wall to the compacted surface fibrin.

Figure 11.2: Histological analysis of 150μm polyurethane grafts

Stellenbosch University http://scholar.sun.ac.za

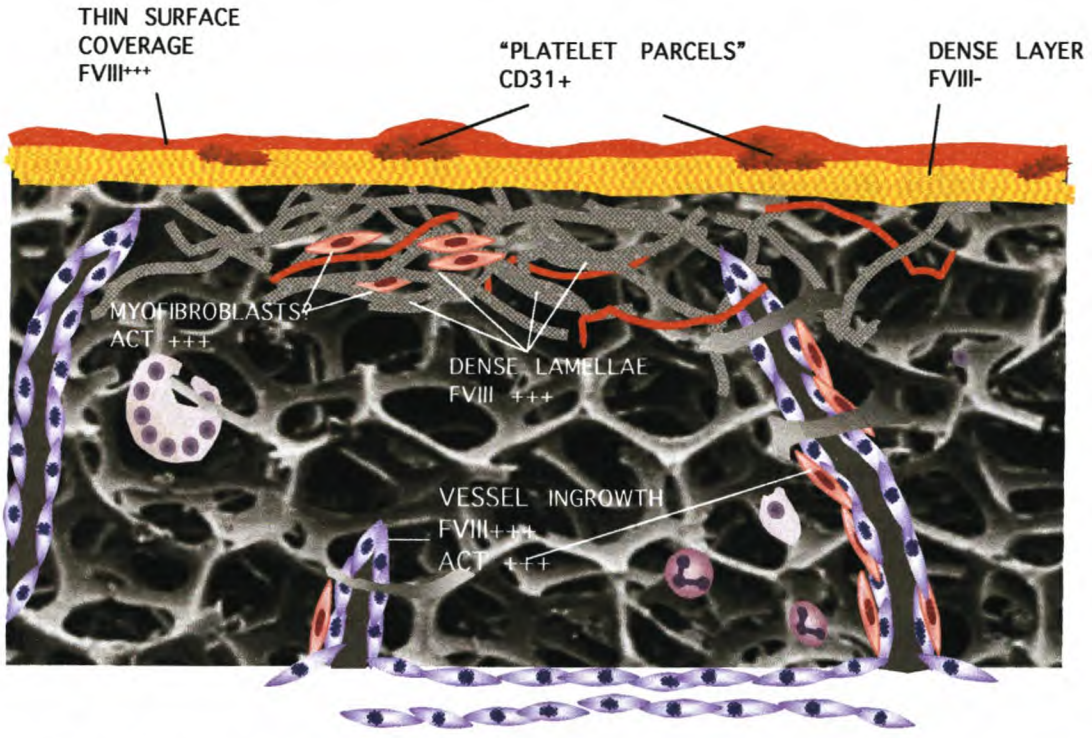

Figure 11.3: Schematic representation of the healing events in 150µm PU grafts.
A distinct number of capillaries penetrate the entire graft wall, but only a minority of them represent arterioles with smooth muscle cells. An impenetrable layer is built up on the blood surface, preventing any further ingrowth and influencing the healing pattern of the graft. Only few SMCs align along the compacted fibrin layer.

In contrast to ePTFE grafts where the fibrils are only maximally stretchable in the middle ground between 2 nodes but converge towards their anchorage points at both nodes, ingrowth spaces in the polyurethane grafts evenly provide widely open interstitial spaces. The distinctly higher density of blood vessels in the interstices of the grafts is most likely the result of the combined freely communicating ingrowth spaces and the biological effect of stretching in a compliant graft.

- Fibrin deposition: As in all other high-porosity, non-sealed grafts, high-density compacted fibrin matrices build up in the inner third of the graft wall. These mostly acellular matrices appear to be completely impenetrable for cells.
- Ingrowth spaces: In contrast to ePTFE grafts, convolutes of capillaries and arterioles are criss-crossing the graft wall in all directions and up to much larger diameters. Furthermore, small bundles of smooth muscle cells are already visible in these non-sealed grafts in the inner third of the prosthesis. The orientation of those smooth muscle cells seems to be circular rather than longitudinal.
- Compliance: It is quite obvious that the few bundles of freely aligned, smooth-muscle cells are aligning themselves along the vectors of stress and strain. This indicates that compliance exerts a distinct biological effect on the graft wall. Moreover, vessel density is distinctly higher than in ePTFE grafts, even in those areas where ingrowth dimensions would be comparable. This again points towards the important role compliance plays with regards to the arteriolarization of a prosthetic graft wall.

Stellenbosch University http://scholar.sun.ac.za

11.3.2 150μm Polyurethane: sealed blood surface

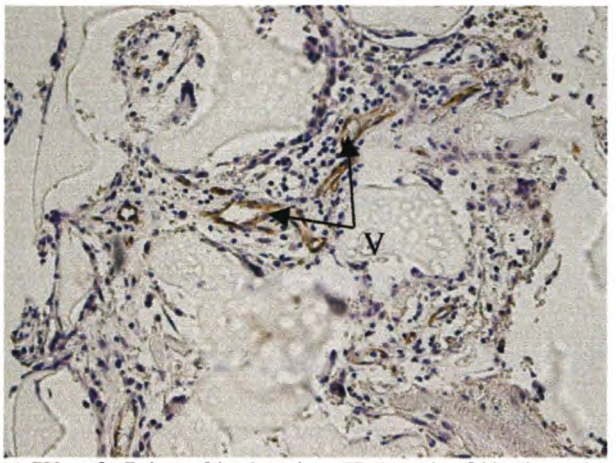

(a) PU graft: 7 days of implantation (CD 31 stain of blood vessels). This picture is a typical representative of the skinned PU implants showing that blood vessels rapidly penetrate through the entire graft wall to reach the outer surface of the skin.

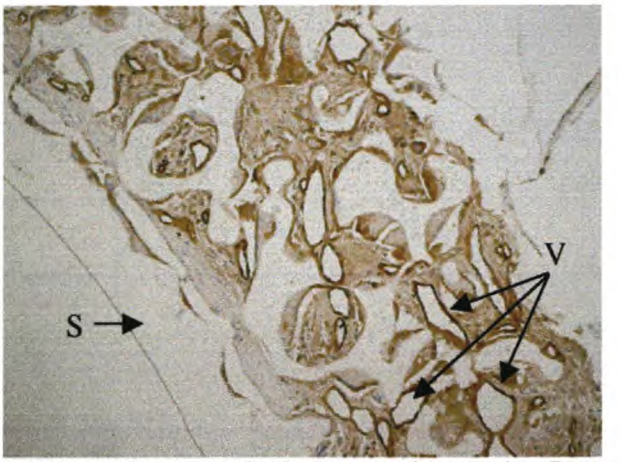

(b) Skinned 150μm PU graft: Blood vessel staining (21 days, Factor VIII). The entire graft wall is packed with blood vessels (V) which reach evenly from outside to inside. Furthermore one can already recognize the tissue bands underneath the lumenal skin (S).

(c) 4-week implant of surface skinned PU grafts. After 28 days of implantation, the previously dilated sinuses inside the graft wall have turned into mature vessels (V) typical of small arteries.

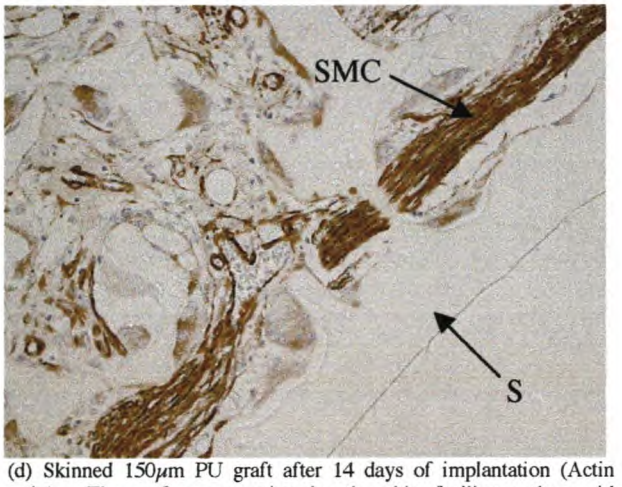

(d) Skinned 150μm PU graft after 14 days of implantation (Actin stain). The surface protection by the skin facilitates the rapid development of a circumferentially aligned, densely packed layer of SMCs close to the blood surface.

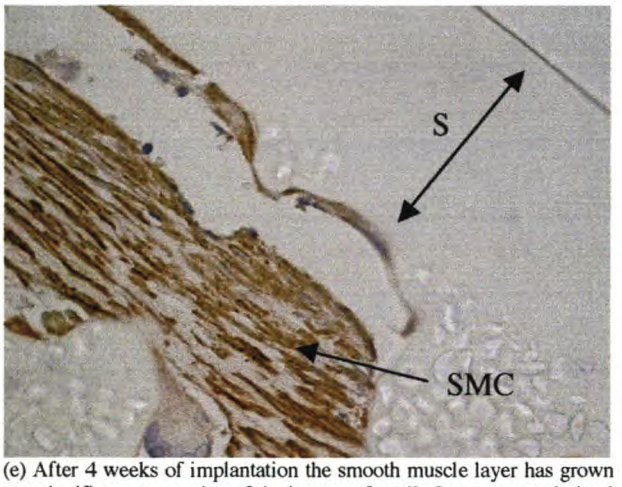

(e) After 4 weeks of implantation the smooth muscle layer has grown to a significant proportion of the inner graft wall. In contrast to intimal hyperplasia, the SMCs are already densely packed as they are in a native artery

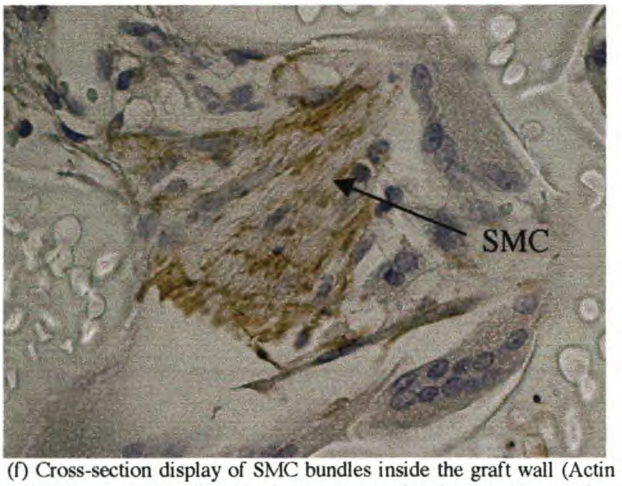

(f) Cross-section display of SMC bundles inside the graft wall (Actin stain; 4 weeks). This typical cross-sectional appearance of a longitudinally cut graft underlines once more that the SMC bundles are circumferentially aligned.

Figure 11.4: Histological analysis of lumenally skinned 150μm PU grafts

Stellenbosch University http://scholar.sun.ac.za

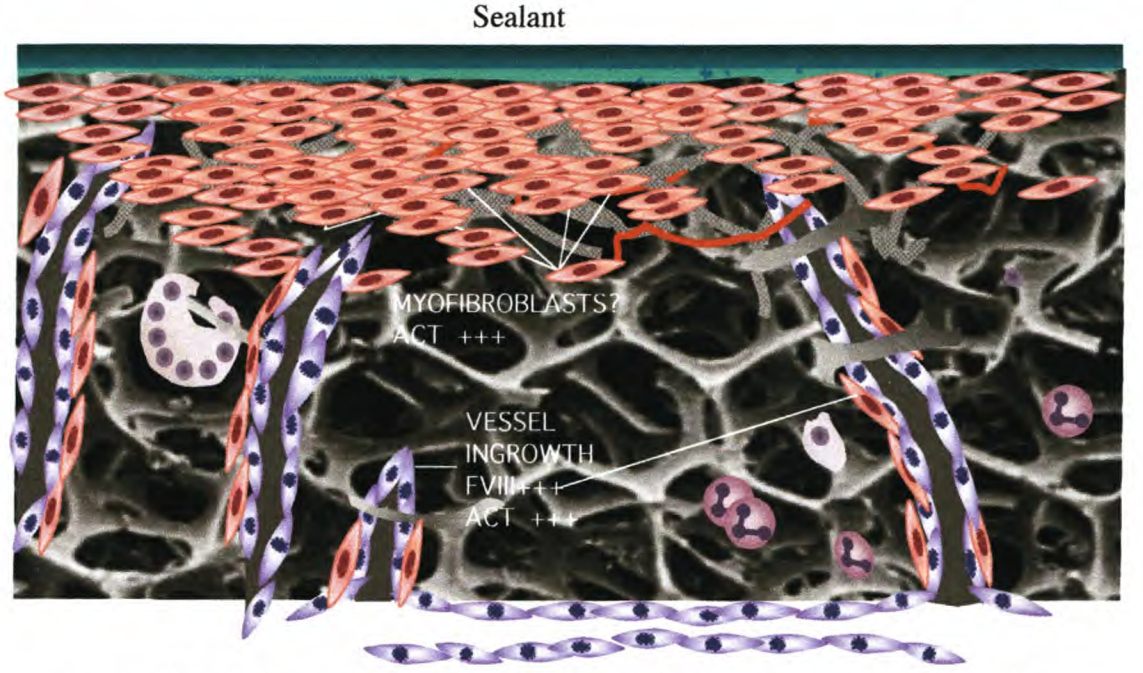

Figure 11.5: Schematic representation of healing events in 150 µm polyurethane grafts. The surfaces were sealed and thus protected against fibrin insudation. Capillaries penetrate through the entire graft wall from outside to the surface sealant within less than 2 weeks. The density of blood vessels is distinctly higher than in the non-sealed controls. Smooth muscle cells are present at a much higher number both as accompanying layer arterioles and as free cells in the interstices of the graft. Most strikingly, a densely packed layer of smooth muscle cells starts building up at the interface with the blood surface sealant as early as after 2 weeks of implantation. At 4 weeks these dense muscle bundles are occupying approximately one third of the graft wall and are circularly aligned. Their position coincides with the site of highest stress and strain.

Overall, surface protected polyurethane grafts with interconnected dodecahedral structures resulted in a partial transformation of the scaffold into a new artery within a very short period of 4 weeks. Since these results were obtained in the non-human primate, their relevance for human implants is obvious. In view of the fact that human graft implants are supposed to replace or bypass an artery for up to decades, such a rapid healing event promises to turn such a polyurethane scaffold into a hybrid artery during the very early phase of implantation. Two main aspects of our concept have been proven in these non-human primate implants, namely the importance of multi-directional ingrowth spaces and of compliance.

- Fibrin deposition: The surface sealant completely prevented the build-up of compacted fibrin, which was non-permissive for tissue ingrowth in the non-sealed grafts. As a consequence, those areas that show the highest stress and strain and are therefore the site of origin for the development of a muscular wall were not obstructed by the hostile fibrin matrix.
- Ingrowth spaces: The smooth muscle cell bundles and parcels which developed in the inner half of the graft surface were clearly circularly lined confirming in a powerful way how important it is to provide ingrowing muscle cells with ingrowth spaces which allow an orientation according to stress and strain principles rather than scaffold barriers.
- Compliance: In vitro experiments performed in our laboratory have previously shown that cyclic stress and strain has a twofold effect on smooth muscle cells. On the one hand the smooth muscle cells rapidly align themselves along the vectors of the stress and the strain. On the other hand, growth factors that are the driving force for the population of the graft wall with vascular cells are produced at threefold levels by the ingrowing vascular cells if they are exposed to cyclic stress and strain. Our calculations from the stress and strain models clearly predicted that the site of smooth muscle cell proliferation will be the innermost layer of the graft wall. The fact that this was exactly the site where the build up of

Stellenbosch University http://scholar.sun.ac.za

an arterial vascular wall commenced was further proof for the importance of compliance. Compared with the non-existence of any muscle build up in the wall of high porosity ePTFE grafts, the distinct presence of the smooth muscle cell rich arterial wall at an early stage underlines the role compliance plays in our polyurethane grafts once again.

The increased vascularization of the graft wall after lumenal sealing was confirmed by quantitative analysis. For all the implant durations shown (>14 days), the vascularization indexes of the skinned samples were greater than that obtained with the PU alone (Fig. 11.6). The increases were especially noticeable in the shorter implant groups. This indicates the increased speed at which the grafts are vascularized when a lumenal skin was present. A similar trend is observed for the arteriolar indexes. Although the 28-day implant showed lower arteriolarization than the control, the improved ability of the skinned graft to be invaded by arterioles is evident in the 14 and 21 day implants (Fig.11.7).

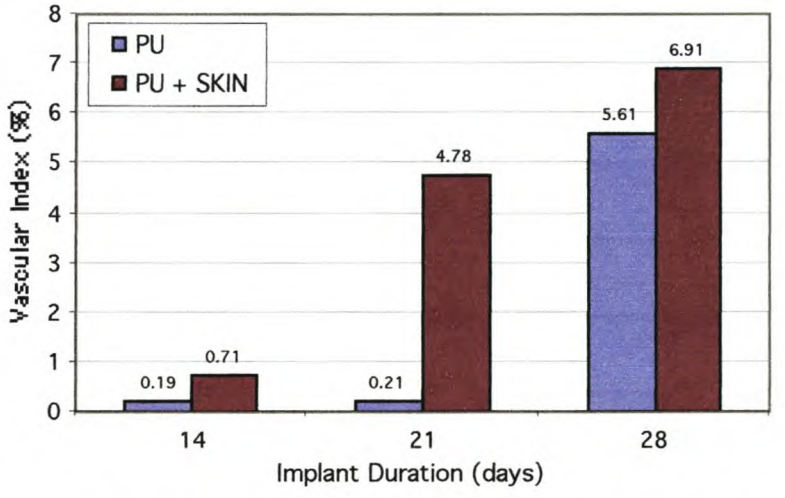

Figure 11.6: Comparison of vascularization indexes of skinned vs. non-skinned 150µm PU grafts

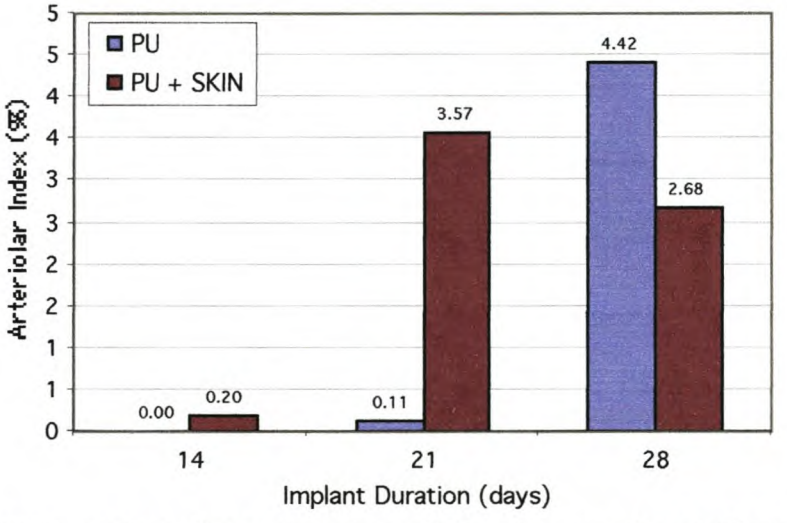

Figure 11.7: Comparison of arteriolar indexes of skinned vs. non-skinned 150µm PU grafts

Stellenbosch University http://scholar.sun.ac.za

Calculation of the stress distributions in the artery wall demonstrate that the maximum tensile stress is exactly in those regions of the graft wall where the thick smooth muscle cell bundles are found in the skinned PU grafts (Fig. 11.8 a) [31]. Furthermore the direction of the principle stress in a circumferential direction equally coincides with the alignment of the SMC bundles. This orientation of SMCs also coincides with the orientation found in a non-scaffolded ingrowth gel that was exposed to similar strains. These experiments by Kanda et al. [32] predicted the orientation of SMCs in a scaffold with unrestricted ingrowth spaces and sufficient compliance to freely exert tensile strain (Fig 11.8 b).

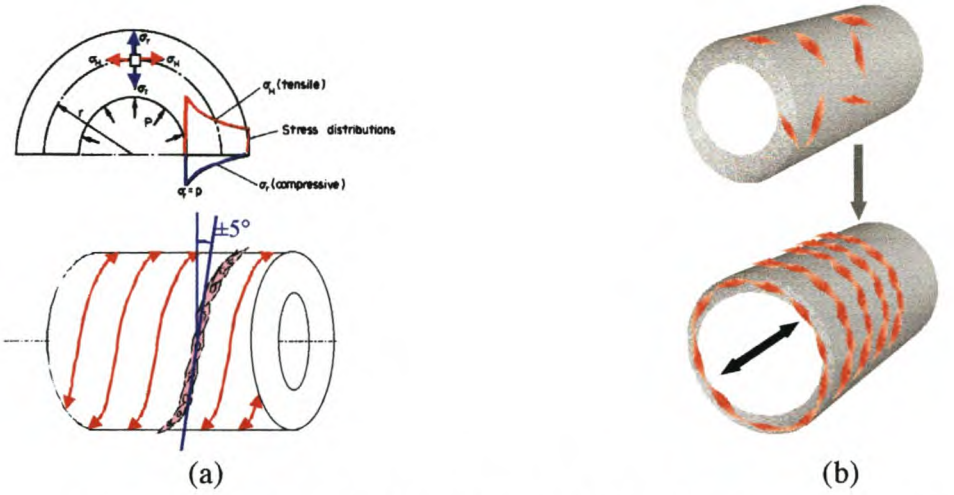

Figure 11.8: Orientation of smooth muscle cells resulting from applied stresses

Another explanation of the rapid development of oriented SMC bundles in the grafts was provided by Smith et al. [30], who showed not only the alignment of these cells in the direction of the applied stress (in vitro), but also an upregulation in vascular endothelial growth factor production with the application of cyclic stretch (Fig 11.9).

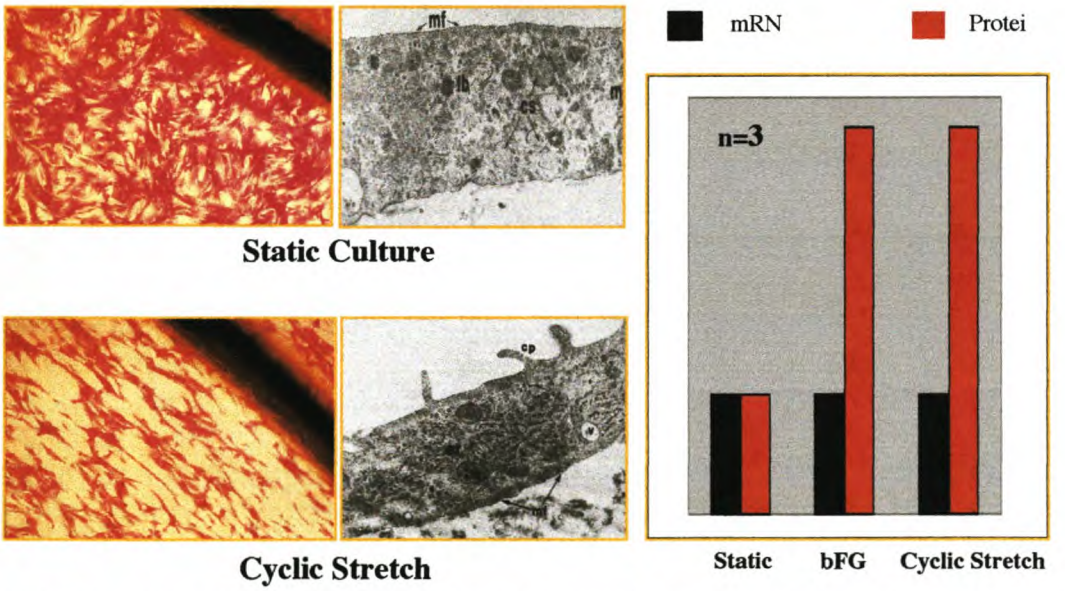

Figure 11.9: Orientation of smooth muscle cells and the upregulation of growth factor production resulting from applied stresses

Stellenbosch University http://scholar.sun.ac.za

11.4 Comparison of graft types

The healing responses towards the five graft types described in Chapters 10 and 11 are summarized in Table 11.1 for comparison. Apart from a thin lumenal fibrin layer deposited on the low porosity (30μm) ePTFE, the ingrowth spaces are insufficient for significant ingrowth of cellular material. Some capillary and SMC ingrowth could be achieved by increasing the IND from 30 to 150μm, and the application of the lumenal sealant on the high porosity ePTFE material led to further increases in capillary ingrowth and overall healing response. The lack of compliance and restrictive nodular structure did not, however, allow for the orientation of smooth muscle cells. The more open structure of the high porosity PU grafts, combined with compliance, led to an even further improvement in arteriolization and SMC penetration, with the result that these grafts showed overall improved healing over the high porosity ePTFE grafts. The high porosity PU grafts allowed for some SMC orientation, but full transmural healing was prevented by the presence of the fibrin layer. When the deposition of the fibrin layer was prevented by the application of the sealant on the PU grafts, full vascularization of the graft wall and helical SMC orientation was achieved. It may therefore be concluded that a combination of large, interconnected porosity, compliance, and the prevention of lumenal fibrin deposition are required to achieve full transmural neo-vascularization and circumferential SMC orientation.

Table 11.1: Comparison of in vivo healing responses obtained with ePTFE and PU vascular grafts in the isolated baboon femoral model.

Feature	30μm ePTFE	150μm ePTFE	1500μm ePTFE + Skin	150μm PU	150μm PU + Skin
Lumenal Fibrin Deposition	+	++	-	+	-
Compliance	-	-	-	++	+
Macrophage Penetration	-	+	+	+	+
Capillary Penetration	-	+	++	++	+++
Arteriole Penetration	-	+	+	++	+++
SMC Penetration	-	+	+	++	+++
SMC Orientation	-	-	-	+	++
Overall Response	1	2	3	4	5
-: minimal presence or absent	+; ++; +++: Increased levels of presence			1,2,3,4,5: Increased levels of healing	

11.4 References

1. Murabayashi, S., Kambic, H., Harasaki, H., Morimoto, T., Yozu, R., and Nose, Y., *Fabrication and long-term implantation of semi-compliant small vascular prosthesis.* Trans Am Soc Artif Intern Organs, 1985. **31**: p. 50-4.
2. Hiratzka, L.F., Goeken, J.A., White, R.A., and Wright, C.B., *In vivo comparison of replamineform, Silastic, and bioelectric polyurethane arterial grafts.* Arch Surg, 1979. **114**(6): p. 698-702.
3. White, R.A., White, E.W., Hanson, E.L., Rohner, R.F., and Webb, W.R., *Preliminary report: Evaluation of tissue ingrowth into experimental Replamineform vascular prostheses.* Surgery, 1976. **79**(02): p. 229-32.
4. Wilson, G.J., MacGregor, D.C., Klement, P., Lee, J.M., del Nido, P.J., Wong, E.W., and Leidner, J., *Anisotropic polyurethane nonwoven conduits: a new approach to the design of a vascular prosthesis.* Trans Am Soc Artif Intern Organs, 1983. **29**: p. 260-8.
5. Leidner, J., Wong, E.W., MacGregor, D.C., and Wilson, G.J., *A novel process for the manufacturing of porous grafts: process description and product evaluation.* J Biomed Mater Res, 1983. **17**(2): p. 229-47.
6. Kambic, H., Murabayashi, S., Yozu, R., Morimoto, T., Furuse, M., Harasaki, H., George, C., Helmus, M., Snyder, R., and Nose, Y., *Small vessel replacement with elastomeric protein composite materials: preliminary studies.* Trans Am Soc Artif Intern Organs, 1984. **30**: p. 406-10.
7. Gupta, B.S. and Kasyanov, V.A., *Biomechanics of human common carotid artery and design of novel hybrid textile compliant vascular grafts.* J Biomed Mater Res, 1997. **34**(3): p. 341-9.
8. van der Lei, B., Wildevuur, C.R., Dijk, F., Blaauw, E.H., Molenaar, I., and Nieuwenhuis, P., *Sequential studies of arterial wall regeneration in microporous, compliant, biodegradable small-caliber vascular grafts in rats.* J Thorac Cardiovasc Surg, 1987. **93**(5): p. 695-707.
9. Therrien, M., Guidoin, R., Adnot, A., and Paynter, R., *Hydrophobic and fibrillar microporous polyetherurethane urea prosthesis: an ESCA study on the internal and external surfaces of explanted grafts.* Biomaterials, 1989. **10**(8): p. 517-20.

Stellenbosch University http://scholar.sun.ac.za

10. Williams, S.K., Carter, T., Park, P.K., Rose, D.G., Schneider, T., and Jarrell, B.E., *Formation of a multilayer cellular lining on a polyurethane vascular graft following endothelial cell sodding.* J Biomed Mater Res, 1992. **26**(1): p. 103-17.
11. Cohn, D., Elchai, Z., Gershon, B., Karck, M., Lazarovici, G., Sela, J., Chandra, M., Marom, G., and Uretzky, G., *Introducing a selectively biodegradable filament wound arterial prosthesis: a short-term implantation study.* J Biomed Mater Res, 1992. **26**(9): p. 1184-204.
12. Edwards, A., Carson, R.J., Bowald, S., and Quist, W.C., *Development of a microporous compliant small bore vascular graft.* J Biomater Appl, 1995. **10**(2): p. 171-87.
13. Hess, F., Jerusalem, C., Steeghs, S., Reijnders, O., Braun, B., and Grande, P., *Development and long-term fate of a cellular lining in fibrous polyurethane vascular prostheses implanted in the dog carotid and femoral artery. A scanning and light microscopical study up to 53 months after implantation.* J Cardiovasc Surg (Torino), 1992. **33**(3): p. 358-65.
14. Marinescu, V., Pausescu, E., and Carnaru, S., *Long-term biological fate of polyurethane aortic prostheses.* Thorax, 1971. **26**(1): p. 108-11.
15. Lommen, E., Gogolewski, S., Pennings, A.J., Wildevuur, C.R., and Nieuwenhuis, P., *Development of a neo-artery induced by a biodegradable polymeric vascular prosthesis.* Trans Am Soc Artif Intern Organs, 1983. **29**: p. 255-9.
16. Hess, F., Jerusalem, C., and Braun, B., *The endothelialization process of a fibrous polyurethane microvascular prosthesis after implantation in the abdominal aorta of the rat. A scanning electron microscopic study.* J Cardiovasc Surg (Torino), 1983. **24**(5): p. 516-24.
17. Berkowitz, H.D., Perloff, L.J., and Roberts, B., *Pseudointimal development on microporous polyurethane lattices.* Trans Am Soc Artif Intern Organs, 1972. **18**(0): p. 25-9.
18. Akiyama, N., Esato, K., Fujioka, K., and Zempo, N., *A comparison of CORVITA and expanded polytetrafluoroethylene vascular grafts implanted in the abdominal aortas of dogs.* Surg Today, 1997. **27**(9): p. 840-5.
19. Underwood, C.J., Tait, W.F., and Charlesworth, D., *Design considerations for a small bore vascular prosthesis.* Int J Artif Organs, 1988. **11**(4): p. 272-6.
20. Hinrichs, W.L., Kuit, J., Feil, H., Wildevuur, C.R., and Feijen, J., *In vivo fragmentation of microporous polyurethane- and copolyesterether elastomer-based vascular prostheses.* Biomaterials, 1992. **13**(9): p. 585-93.
21. Annis, D., Bornat, A., Edwards, R.O., Higham, A., Loveday, B., and Wilson, J., *An elastomeric vascular prosthesis.* Trans Am Soc Artif Intern Organs, 1978. **24**: p. 209-14.
22. Zhang, Z., Marois, Y., Guidoin, R.G., Bull, P., Marois, M., How, T., Laroche, G., and King, M.W., *Vascugraft polyurethane arterial prosthesis as femoro-popliteal and femoro-peroneal bypasses in humans: pathological, structural and chemical analyses of four excised grafts.* Biomaterials, 1997. **18**(2): p. 113-24.
23. Kogel, H., Vollmar, J.F., Cyba-Altunbay, S., Mohr, W., Frosch, D., and Amselgruber, W., *New observations on the healing process in prosthetic substitution of large veins by microporous grafts--animal experiments.* Thorac Cardiovasc Surg, 1989. **37**(2): p. 119-24.
24. Allen, R.D., Yuill, E., Nankivell, B.J., and Francis, D.M., *Australian multicentre evaluation of a new polyurethane vascular access graft.* Aust N Z J Surg, 1996. **66**(11): p. 738-42.
25. Uchida, N., Kambic, H., Emoto, H., Chen, J.F., Hsu, S., Murabayshi, S., Harasaki, H., and Nose, Y., *Compliance effects on small diameter polyurethane graft patency.* J Biomed Mater Res, 1993. **27**(10): p. 1269-79.
26. Hess, F., Jerusalem, R., Reijnders, O., Jerusalem, C., Steeghs, S., Braun, B., and Grande, P., *Seeding of enzymatically derived and subcultivated canine endothelial cells on fibrous polyurethane vascular prostheses.* Biomaterials, 1992. **13**(10): p. 657-63.
27. Stansby, G., Berwanger, C., Shukla, N., Schmitz-Rixen, T., and Hamilton, G., *Endothelial seeding of compliant polyurethane vascular graft material.* Br J Surg, 1994. **81**(9): p. 1286-9.
28. Muller-Glauser, W., Lehmann, K.H., Bittmann, P., Bay, U., Dittes, P., von Segesser, L., and Turina, M., *A compliant small-diameter vascular prosthesis lined with functional venous endothelial cells.* ASAIO Trans, 1988. **34**(3): p. 528-31.
29. Poole-Warren, L.A., Schindhelm, K., Graham, A.R., Slowiaczek, P.R., and Noble, K.R., *Performance of small diameter synthetic vascular prostheses with confluent autologous endothelial cell linings.* J Biomed Mater Res, 1996. **30**(2): p. 221-29.
30. Smith, J., Davies, N., Willis, A., Sumpio, B., and Zilla, P., *Cyclic stretch induces the expression of vascular endothelial growth factor in vascular smooth muscle cells.* Endothelium, 2001. **8**(1): p. 41-47.
31. Yeoman, M., *Design and optimisation of a fabric reinforced porous prosthetic graft using finite element methods and genetic algorithms*, in *Mechanical Engineering*, University of Cape Town.
32. Kanda, K., Matsuda, T., and Oka, T., *Mechanical stress induced cellular orientation and phenotypic modulation of 3-D cultured smooth muscle cells.* Asaio J, 1993. **39**(3): p. M686-90.

Stellenbosch University http://scholar.sun.ac.za

CHAPTER 12

Conclusions

This study has resulted in an overall appreciation of the shortcomings of commercially available synthetic vascular prostheses in providing successful long-term outcomes in small-diameter applications. The conclusions that may be drawn from this study relating to the effect of the many variables that determine the healing responses toward, and hence outcomes associated with, vascular grafts are listed below.

- Conventional Dacron and ePTFE prostheses fail in small-diameter applications due to insufficient ingrowth spaces and compliance mismatching, resulting in the incomplete healing of the graft wall. Even though various researchers produced experimental polyurethane with sufficient compliance, transmural healing was not achieved due to a lack of ingrowth space and/or pore interconnectivity.
- A vascular graft should ideally contain unit pores that resemble open-faced pentagonal dodecahedra. These structures allow for the uninhibited ingrowth of tissue in all dimensions, and should theoretically allow for the helical re-orientation of radially ingrowing smooth muscle cells to resemble the structure of a natural artery. Helical re-orientation has been identified as a *sine qua non* for the mimicking of the structure and properties of natural blood vessels.
- Novel porous grafts, containing well-defined, interconnected pores could be produced by a variation of the phase inversion/porogen extraction technique. The compliance of the structure was achieved by using a thermoplastic elastomer (polyurethane).
- The pore size not only determines the extent of tissue ingrowth, but also the inflammatory response towards porous implants. A significant decrease in inflammatory response was achieved by merely increasing the pore size from 60 to 150μm. It is important to note that this decrease in inflammation was achieved without adversely affecting the neo-vascularization.
- The inflammatory response was further decreased by surface pacification. The combination of large pores and covalent collagen surface immobilization resulted in an 80% decrease in foreign-body giant cell formation.
- Conventional animal models (dogs and yellow baboons) used historically for the evaluation of vascular grafts failed to differentiate between transanastomotic and transmural healing. As the transmural outgrowth in the human stops within 1-2cm from the anastomosis, this healing mode should not be relied upon to improve graft outcomes. The senescent, isolated chacma baboon femoral model described in Chapter 9 has been shown to eliminate the interference of transanastomotic tissue on the healing response.
- Low-porosity (30μm) ePTFE does not allow much tissue ingrowth due to very limited ingrowth spaces. Although the 6-fold increase in the internodular distance did result in an improvement in wall healing, the fibrillar structure was not conducive to complete healing or cellular orientation. The build-up of impenetrable fibrin on the lumenal surface was identified as an inhibiting factor for full transmural healing. Although the elimination of this fibrin layer by the application of a lumenal sealant improved tissue ingrowth into high porosity ePTFE, the lack of compliance, combined with the restrictive structure, did not allow for the orientation of smooth muscle cells in the graft wall.
- Although capillaries and arterioles were able to penetrate most of the thickness of a high-porosity PU graft wall, their progress was inhibited by the formation of an impenetrable layer deposited and compacted by the blood in the lumen of the graft. Elimination of the hostile

Stellenbosch University http://scholar.sun.ac.za

fibrin layer, again by the lumenal sealing of the graft, resulted in the desired healing response. Not only were capillary and arteriolar vessels able to penetrate and populate the entire thickness of the graft wall, but also thick, helically oriented bands of organised smooth muscle cells were able to form within the porous structure. This response is believed to be a very important milestone in field of vascular grafting, as holds the key for tissue-engineered polymer/tissue composites that mimic natural vessels in form and function.

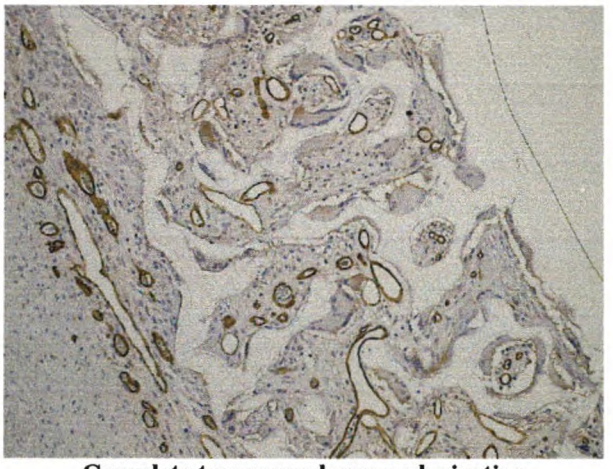

Complete transmural revascularization

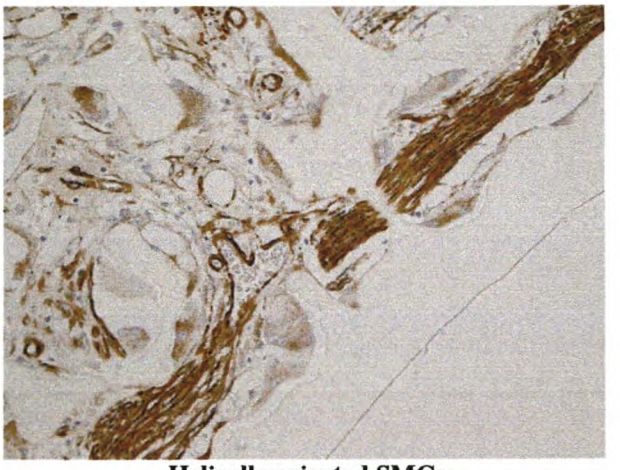

Helically oriented SMCs.

Stellenbosch University http://scholar.sun.ac.za

CHAPTER 13

Future Research

1. Material stability

The high surface to volume ratio of the porous grafts places high demands on the stability of the materials used in their production. Long-term studies are to be performed to confirm the stability of the polyurethanes in vivo.

2. Graft production

The phase inversion/porogen extraction technique was a valuable tool in the production of grafts containing the desired porosity for the proof of the concept. Large-scale production of vascular grafts will require up-scaling of the present process (already initiated by the author) or reinvestigation of the foam-extrusion process.

The biostable lumenal sealant used in this study allowed for the proof of the hypothesis that healing may be improved by eliminating the fibrin deposition on the blood-contacting surface of the grafts. In order to allow for the migration of the ingrowing tissue onto the lumenal surface and to create a viable endothelium, research into the development of biodegradable sealants is needed. The degradable sealant should be non-thrombogenic, and should be engineered to degrade only when the ingrowing perigraft tissue reaches its outer surface.

Accurate in vitro and in vivo compliance measurement and mathematical modelling are invaluable tools in the development of vascular grafts. Initial investigations into these fields have been performed by other researchers in our laboratories. A further study, involving the use of both finite element analysis and compliance measurement to optimise graft compliance by the application of adventitial reinforcement, already forms the basis of a current study by another Ph.D student.

3. Ingrowth matrixes

Ingrowth matrixes, capable of facilitating the ingress of the desired cell types into the porous prostheses, may allow for the further improvement of graft healing patterns. The development of such matrixes is the subject of an ongoing project by one of the groups in our unit (in conjunction with international collaborators).

4. Long-term primate studies

Long-term implantation of the prosthetic grafts should be performed to follow the healing patterns resulting from continued cellular ingrowth and reorganisation

Stellenbosch University http://scholar.sun.ac.za

APPENDIX 1

Relationship between volumetric and diameter compliance of vascular grafts.

$$
\begin{aligned}
C_V &= \frac{\Delta V}{V_d \Delta P} \\
&= \frac{\Delta V_s - \Delta V_d}{V_d \Delta P} \\
&= \frac{\Delta D_s^2 - \Delta D_d^2}{D_d^2 \Delta P} \\
&= \frac{(D_d + \Delta D)^2 - \Delta D_d^2}{D_d^2 \Delta P} \\
&= \frac{\Delta D_d^2 + 2D_d \Delta D + \Delta D^2 - \Delta D_d^2}{D_d^2 \Delta P} \\
&= \frac{2D_d \Delta D + \Delta D^2}{D_d^2 \Delta P} \\
&= \frac{2D_d \Delta D}{D_d^2 \Delta P} + \frac{\Delta D^2}{D_d^2 \Delta P} \\
&= \frac{2\Delta D}{D_d \Delta P} + \frac{\Delta D^2}{D_d^2 \Delta P} \\
&= 2C_D + \frac{\Delta D^2}{D_d^2 \Delta P} \\
&\approx 2C_D
\end{aligned}
\qquad \text{(A1.1)}
$$

Stellenbosch University http://scholar.sun.ac.za

APPENDIX 2

Solubility of polyurethanes

Table A3.1: The solubility of Medtronic M48 (A), Chronoflex AL 55D (B), Chronoflex AL 75D(C) and Hydrothane (D) in various solvents.

ORGANIC SOLVENT		δ_d MPa$^{1/2}$	δ_p MPa$^{1/2}$	δ_h MPa$^{1/2}$	δ_t MPa$^{1/2}$	EXTENT OF SOLUBILITY			
						A M48	B C55	C C75	D Hyd
1.	Acetic acid	14.5	8	13.5	21.4	4	1	1	1
2.	Acetic anhydride	16	11.7	10.2	22.3	4	4	4	4
3.	Acetone	15.5	10.4	7	20	3	4	4	4
4.	Acetonitrile	15.3	18	6.1	24.4	4	4	4	4
5.	Acrylonitrile	16.4	17.4	6.8	24.8	4	4	4	4
6.	n-Amyl alcohol	16	4.5	13.9	21.7	3	4	4	4
7.	Aniline	19.4	5.1	10.2	22.5	-	1	2	2
8.	Benzene	18.4	1	2.1	18.5	2	4	2	4
9.	Benzaldehyde	19.4	7.4	5.3	21.4	1	1	2	2
10.	Benzyl alcohol	18.4	6.3	13.7	23.8	4	4	1	1
11.	n-Butanol	16	5.7	15.8	23.1	4	4	4	4
12.	Butyl acetate	15.8	3.7	6.3	17.4	3	4	4	-
13.	sec Butyl alcohol	15.8	5.7	14.5	22.2	4	4	4	4
14.	Chlorobenzene	18.6	4.3	4.1	19.5	2	4	4	3
15.	Chloroform	17.8	3.1	5.7	18.9	1	1	1	1
16.	m-Cresol	18	5.1	12.9	22.7	2	1	1	1
17.	Cyclohexane	16.7	0	0	16.7	2	4	-	4
18.	Cyclohexanone	17.8	6.3	5.1	19.6	1	2	2	3
19.	Dichloroethane	19	7.4	4.1	20.9	-	-	3	3
20.	Diethyl ether	14.5	2.9	5.1	15.8	3	-	4	4
21.	Diethylene glycol	16.2	14.7	20.5	30	4	4	4	4
22.	N,N dimethyl acetamide	16.8	11.5	10.2	22.7	1	1	1	1
23.	N,N dimethyl formamide	17.4	13.7	11.3	24.8	2	1	1	2
24.	Dimethyl sulfoxide	18.4	16.4	10.2	26.7	2	2	1	4
25.	1,4-Dioxane	19	1.8	7.4	20.4	1	2	2	2
26.	Ethanol	15.8	8.8	19.4	26.5	3	4	4	4
27.	Ethyl acetate	15.8	5.3	7.2	18.1	4	4	4	4
28.	Ethyl acetate	14.3	11.9	16.6	24.9	4	1	2	1
29.	Hexane	14.9	0	0	14.9	4	4	4	4
30.	Methylene chloride	18.2	6.3	6.1	20.2	2	1	2	1
31.	methyl ethyl ketone	16	9	5.1	19	3	-	4	1
32.	N-methyl-2-pyrrolidone	18	12.2	7.1	22.9	1	1	1	1
33.	Nitrobenzene	20	8.6	4.1	22.2	2	3	1	4
34.	Nitromethane	15.8	18.8	5.1	25.1	4	3	4	4
35.	n-Propanol	16	6.8	17.4	24.5	4	4	4	4
36.	Propylene glycol	16.8	9.4	23.3	30.2	4	4	3	4
37.	Pyridine	19	8.8	5.9	21.8	1	1	1	1
38.	Tetrahydrofurane	16.8	5.7	8	19.4	1	1	2	2
39.	Toluene	18	1.4	2	18.2	3	4	4	2
40.	Triethanolamine	17.2	15.6	21.3	31.5	4	4	4	4
41.	Trimethyl phosphate	16.8	16	10.2	25.3	4	4	4	4

(1) Good solvent
(2) Good swelling agent
(3) Poor swelling agent
(4) Non-solvent

Stellenbosch University http://scholar.sun.ac.za

APPENDIX 3

Derivation of the volumetric closed-porosity equation

$$
\begin{aligned}
P_{Vcp} &= \frac{V_{Vcp}}{V_{Vscaf}} \\
&= \frac{V_{Vcp}}{V_{Vskel}} \times \frac{V_{Vskel}}{V_{Vscaf}} \\
&= \left(\frac{V_{Vskel} - V_{Vpol}}{V_{Vskel}} \right) \left(\frac{V_{Vskel}}{V_{Vscaf}} \right) \\
&= \left(1 - \frac{V_{Vpol}}{V_{Vskel}} \right) \left(\frac{V_{Vskel}}{V_{Vscaf}} \right) \\
&= \left(1 - \frac{m_{scaf}}{\rho_{pol} V_{Vskel}} \right) \left(\frac{V_{Vskel}}{V_{Vscaf}} \right) \\
&= \left(1 - \frac{m_{scaf}}{\rho_{pol} (V_2 - V_1)} \right) \left(\frac{V_2 - V_1}{V_2 - V_3} \right)
\end{aligned}
\qquad \text{(A3.1)}
$$

Stellenbosch University http://scholar.sun.ac.za

APPENDIX 4

Derivation of the theoretical porosity equations

A4.1 Vacuum/pressure-cast scaffolds

Under the assumption of constant volume, the volume of the macropores equal the volume of the porogen, and the degree of macroporosity can be calculated as follows:

$$P_{Tmac} = \frac{V_{Tmac}}{V_{Tscaf}} = \frac{V_{Tpor}}{V_{Tscaf}} = \frac{\rho_{Bpor}}{\rho_{por}} \tag{A4.1}$$

The total porosity can be derived in terms of the solution and bead characteristics by:

$$P_{Ttp} = \frac{V_{Ttp}}{V_{Tscaf}} = \frac{V_{Tscaf} - V_{Tpol}}{V_{Tscaf}} = 1 - \frac{V_{Tpol}}{V_{Tscaf}} \tag{A4.2}$$

V_{pol} will first be derived in terms of the known parameters. By definition, under the stated assumptions:

$$\rho_{Bpar} = \frac{m_{par}}{V_{Tscaf}} \tag{A4.3}$$

$$\rho_{par} = \frac{m_{por}}{V_{Tpar}} \tag{A4.4}$$

$$\rho_{\text{soln}} = \frac{m_{\text{soln}}}{V_{\text{soln}}} \tag{A4.5}$$

$$\rho_{\text{pol}} = \frac{m_{\text{pol}}}{V_{\text{pol}}} \tag{A4.6}$$

$$x = \frac{m_{pol}}{m_{\text{soln}}} \tag{A4.7}$$

$$V_{Tscaf} = V_{por} + V_{\text{soln}} \tag{A4.8}$$

Substitution of (A4.5) and (A4.6) into (A4.7) and solving for V_{pol} yields:

$$V_{pol} = \frac{x\rho_{\text{soln}}}{\rho_{\text{pol}}} V_{\text{soln}} \tag{A4.9}$$

From (A4.8) and (A4.9):

$$V_{pol} = \frac{x\rho_{\text{soln}}}{\rho_{\text{pol}}} \left(V_{Tscaf} - V_{Tpar}\right) \tag{A4.10}$$

Substitution of (A4.10) into the originally derived equation for the total theoretical porosity (A4.2), and simplification, yields:

$$P_{Ttp} = 1 - \left[\left(\frac{x\rho_{\text{soln}}}{\rho_{\text{pol}}} \right) \left(1 - \frac{V_{Tpor}}{V_{Tscaf}} \right) \right] \tag{A4.11}$$

Finally, from (A4.1), it follows that:

$$P_{Ttp} = 1 - \left[\left(\frac{x\rho_{\text{soln}}}{\rho_{\text{pol}}} \right) \left(1 - \frac{\rho_{Bpor}}{\rho_{por}} \right) \right] \tag{A4.12}$$

Stellenbosch University http://scholar.sun.ac.za

A4.2 Paste-cast scaffolds

If particles are added to the polymer solution, and the sample cast from this mixture, the porosity can not be determined by using eq. (A4.12) above, since the scaffold volume (V_{Tscaf}) cannot be calculated from the bulk density of the particles (thus eq. (A4.3) does not apply in this case).

Thus substitution from eqs. (A4.6) and (A4.8) into eq. (A4.2) yields:

$$P_{Ttp} = 1 - \frac{m_{pol}/\rho_{pol}}{V_{por} + V_{soln}} \tag{A4.13}$$

Similar substitutions made from eqs. (A4.4) and (A4.5) yields:

$$P_{Ttp} = 1 - \frac{m_{pol}/\rho_{pol}}{m_{por}/\rho_{por} + m_{soln}/\rho_{soln}} \tag{A4.14}$$

From eq. (A4.7):

$$P_{Ttp} = 1 - \frac{m_{pol}/\rho_{pol}}{m_{por}/\rho_{por} + m_{pol}/x\rho_{soln}} \tag{A4.15}$$

Regrouping to obtain P_{Ttp} in terms of the particle/polymer ratio:

$$P_{Ttp} = 1 - \frac{1}{\frac{m_{por}}{m_{pol}}\frac{\rho_{pol}}{\rho_{par}} + \frac{\rho_{pol}}{x\rho_{soln}}} \tag{A4.16}$$

Alternately, the porosity can be calculated from the particle/solution ratio by recognising that:

$$\frac{m_{por}}{m_{soln}} = x\frac{m_{por}}{m_{pol}} \tag{A4.17}$$

Thus from (A4.15):

$$P_{Ttp} = 1 - \frac{x/\rho_{pol}}{\frac{m_{por}}{m_{soln}}\frac{1}{\rho_{par}} + \frac{1}{\rho_{soln}}} \tag{A4.18}$$

The theoretical macroporosity (P_{Tmac}) can be calculated from:

$$P_{Tmac} = \frac{V_{por}}{V_{tot}} \tag{A4.19}$$

From (A4.4), (A4.6), (A4.8), and (A4.19):

$$P_{Tmac} = \frac{m_{por}/\rho_{por}}{\frac{m_{par}}{\rho_{por}} + \frac{m_{soln}}{\rho_{soln}}} \tag{A4.20}$$

Which becomes:

$$P_{Tmac} = \frac{1}{1 + \frac{m_{soln}}{m_{por}}\frac{\rho_{por}}{\rho_{soln}}} \tag{A4.21}$$

Calculation of porogen content

Stellenbosch University http://scholar.sun.ac.za

For the vacuum casting method, the fraction of porogen in a dried graft (before porogen extraction) can be calculated from:

$$Por = \frac{m_{por}}{m_{por} + m_{pol}} = \frac{\rho_{por} V_{Tpor}}{\rho_{por} V_{Tpor} + x\rho_{sol\,n} V_{sol\,n}} \tag{A4.22}$$

By dividing the numerator and denominator by V_{Tscaf}, one obtains:

$$Por = \frac{\rho_{por} V_{Tpor} / V_{Tscaf}}{\rho_{por} V_{Tpor} / V_{Tscaf} + x\rho_{sol\,n} V_{sol\,n} / V_{Tscaf}} \tag{A4.23}$$

Since the volume of the porogen and volume of the solution makes up the volume of the graft:

$$\frac{V_{sol\,n}}{V_{Tscaf}} = \frac{V_{Tscaf} - V_{Tpor}}{V_{Tscaf}} = 1 - \frac{V_{Tpor}}{V_{Tscaf}} \tag{A4.24}$$

Substitution of eq A4.1 and A4.24 in A4.23 yields:

$$Por = \frac{\rho_{por}\rho_{Bpor} / \rho_{por}}{\rho_{por}\rho_{Bpor} / \rho_{por} + x\rho_{sol\,n}\left(1 - \left(\rho_{Bpor} / \rho_{por}\right)\right)} = \frac{\rho_{Bpor}}{\rho_{Bpor} + x\rho_{sol\,n}\left(1 - \left(\rho_{Bpor} / \rho_{por}\right)\right)} \tag{A4.25}$$

Stellenbosch University http://scholar.sun.ac.za

APPENDIX 5

Derivation of copolymerisation equations

A5.1 Introduction

Copolymerisation may be defined as a process whereby more than one distinctly different monomer is incorporated into the same polymer chain. The generic term copolymer is used to describe the product of such a process, whereas the terms bipolymer, terpolymer, quadripolymer etc. are used to describe copolymers containing two, three, four, or more, monomers. Although this definition may include the formation of many step-growth or condensation polymers, it is not useful to do so, and this discussion will concern itself only with the chain-growth copolymerisation of olefinic monomers. The discussion will further be limited to free-radical copolymerization of binary mixtures, on which most of the work has been based.

Since it is the kinetics, rather than the thermodynamics, of a free-radical copolymerization that determines the structure of the product, the copolymer composition and sequence distribution may be determined by obtaining a set of differential equations describing the rates at which the monomers are incorporated into the polymer. Various models have been developed to predict the chemical composition of copolymers. They include the terminal model, the penultimate model, the complex participation model, the complex dissociation model, and the depropagation model. Only the terminal model will be discussed.

A5.2 Terminal model

A5.2.1 Instantaneous copolymer composition

The terminal model, which has become the standard kinetic treatment for free-radical copolymerization systems, was independently published in 1944 by Mayo and Lewis [1], by Wall [2], and by Alfrey and Goldfinger [3]. The model assumes that the reactivity of the macroradical depends solely on the identity of the last-added monomer. Thus, for binary systems, the four chain propagation steps in the copolymerization of a mixture of monomers containing M_1 and M_2 are shown in eq. (A5.1):

$$\begin{aligned} M_1^\bullet + M_1 &\xrightarrow{k_{11}} M_1^\bullet \\ M_1^\bullet + M_2 &\xrightarrow{k_{12}} M_2^\bullet \\ M_2^\bullet + M_1 &\xrightarrow{k_{21}} M_1^\bullet \\ M_2^\bullet + M_2 &\xrightarrow{k_{22}} M_1^\bullet \end{aligned} \qquad \text{(A5.1)}$$

The rates of disappearance of M_1 and M_2 are then given by

$$-d[M_1]/dt = k_{11}[M_1^\bullet][M_1] + k_{21}[M_2^\bullet][M_1] \qquad \text{(A5.2)}$$

$$-d[M_2]/dt = k_{12}[M_1^\bullet][M_2] + k_{22}[M_2^\bullet][M_2] \qquad \text{(A5.3)}$$

If it is assumed that the radicals are low-concentration intermediates, that chains are long so that the major path by which radicals $M_1^\bullet$ and $M_2^\bullet$ are formed is by interconversion of one into the other, the following steady-state expression may be written:

$$d[M_1^\bullet]/dt = k_{21}[M_2^\bullet][M_1] - k_{12}[M_1^\bullet][M_2] = 0 \qquad \text{(A5.4)}$$

Division of eq. (A5.2) by eq. (A5.3), elimination of the radical concentrations via eq. (A5.4), and the subsequent introduction of the reactivity ratios r_1 and r_2 yield the following copolymerization equation:

Stellenbosch University http://scholar.sun.ac.za

$$\frac{d[M_1]}{d[M_2]} = \frac{[M_1]}{[M_2]} \times \frac{r_1[M_1]+[M_2]}{[M_1]+r_2[M_2]} \quad \text{(Mayo-Lewis equation)} \tag{A5.5}$$

where

$$r_1 = k_{11}/k_{12} \text{ and } r_2 = k_{22}/k_{21} \tag{A5.6}$$

Equation (A5.5), the differential copolymer composition equation, has widely become known as the Mayo-Lewis equation, and has been used to determine the reactivity ratios of many comonomer pairs.

Equation (A5.5) may also be rewritten in the following convenient forms (eqs. (A5.7) and (A5.10)):

$$\frac{F_1}{F_2} = \frac{r_1 f_1^2 + f_1 f_2}{r_2 f_2^2 + f_1 f_2} \tag{A5.7a}$$

by eliminating F_2:

$$F_1 = \frac{r_1 f_1^2 + f_1 f_2}{r_1 f_1^2 + 2 f_1 f_2 + r_2 f_2^2} \tag{A5.7b}$$

where

$$f_1 = [M_1]/([M_1]+[M_2]) = [M_1]/[M] \tag{A5.8}$$

and

$$F_1 = d[M_1]/(d[M_1]+d[M_2]) = d[M_1]/d[M] \tag{A5.9}$$

Skeist [4] proposed the following form (by eliminating f_2):

$$F_1 = \frac{(r_1-1)f_1^2 + f_1}{(r_1+r_2-2)f_1^2 + 2(1-r_2)f_1 + r_2} \tag{A5.10}$$

where

$$f_2 = 1 - f_1 \text{ and } F_2 = 1 - F_1 \tag{A5.11}$$

The dependence of the instantaneous copolymer composition on the feed composition for various r_1-r_2 pairs is clearly seen in Figure A5.1, which is the graphical representation of eq. (A5.10) for the following cases:

A5.2.1.1 $r_1 \approx r_2 \approx 0$ ($k_{11} << k_{12}$ and $k_{22} << k_{21}$)

Each of the two growing macroradicals shows a strong preference for cross-propagation. In the theoretical case where $r_1=r_2=0$, this preference is absolute, and each of the radicals will add only to the monomer that does not constitute its own active centre. This will result in the formation of a strictly alternating copolymer. The Mayo-Lewis equation simplifies to:

$$\frac{d[M_1]}{d[M_2]} = 1 \quad \text{or} \quad F_1 = F_2 = 0.5 \tag{A5.12}$$

which shows that the two monomers are consumed at the same rate, regardless of the composition of the monomers in the feed.

A5.2.1.2 $r_1=r_2=1$ ($k_{11}=k_{12}$; $k_{22}=k_{21}$)

In this case, neither of the radicals shows any preference for either of the monomers, so that the relative rate of monomer consumption depends solely on the relative composition of the

Stellenbosch University http://scholar.sun.ac.za

monomers in the feed. Equations (A5.5) and (A5.7) can then be simplified to eq. (A5.13), where the copolymer composition equals the monomer feed composition.

$$\frac{d[M_1]}{d[M_2]} = \frac{[M_1]}{[M_2]} \quad \text{or} \quad F_1 = f_1 \tag{A5.13}$$

This is equivalent to the early Wall [5] treatment with $\alpha=1$

A5.2.1.3 $r_1>1$; $r_2<1$

Both of the active centres have a preference for addition to one of the monomers, in this case M_1. This leads to the formation of a copolymer that is always enriched in M_1, relative to the feed. A similar argument can be made for the case ($r_1>1$; $r_2<1$).

If $r_1r_2=1$, or $k_{11}/k_{12}=k_{12}/k_{22}$, which is clearly a special case of ($r_1>1$; $r_2<1$), both active centres show **the same** preference for addition to the more reactive monomer. The Mayo-Lewis equation can then be simplified to:

$$\frac{d[M_1]}{d[M_2]} = r_1\frac{[M_1]}{[M_2]} \quad \text{or} \quad F_1 = \frac{r_1 f_1}{(r_1-1)f_1+1} \tag{A5.14}$$

This is equivalent to the earlier Wall [5] treatment with $\alpha=r_1$, and was later termed "ideal copolymerization" by the same author [2], who also pointed out the analogy between binary copolymerization and Raoult's law describing the boiling of a mixture of liquids.

A5.2.1.4 $r_1<1$; $r_2<1$

Each radical prefers cross-propagation to homopropagation, although this preference is not absolute. The tendency to alternate will increase as r_1 and r_2 approach zero. The cross-over point in a graph of F_1 vs. f_1, or the point where the copolymer composition curve crosses the diagonal representing the composition of the feed, can be determined by determining three the roots of eq. (A5.7) with $F_1=f_1$.: [2]

$$f_1 = 0 \tag{A5.15a}$$

$$f_1 = 1 \tag{A5.15b}$$

$$f_1 = F_1 = \frac{1-r_2}{(1-r_1)(1-r_2)} \tag{A5.15c}$$

The two solutions, $f_1=0$ and $f_1=1$, are trivial since they represent the two pure monomers. Since f_1 is a fraction, the third root only has a significance for $0<f_1<1$, which requires that:

$r_1<1$ and $r_2<1$ simultaneously, or

$r_1>1$ and $r_2>1$ simultaneously

Both conditions can be incorporated into one statement, namely:

$$(r_1-1)(r_2-1)>0$$

This composition can also be defined as the point where $d[M_1]/d[M_2]=[M_1][M_2]$. Substitution into eq. (A5.5) yields:

$$\frac{[M_1]}{[M_2]} = \frac{1-r_2}{1-r_1} \tag{A5.16}$$

Simple substitution of eqs. (A5.8) and (A5.11) shows that eq. (A5.16) is equivalent to eq. (A5.15c).

Stellenbosch University http://scholar.sun.ac.za

At this point the monomer and copolymer compositions are identical. Wall [2], in analogy to distillation, has termed the reaction under such conditions an **azeotropic copolymerization**.

A5.2.1.5 $r_1>1$; $r_2>1$

In this case, both types of radical prefer homopropagation to cross-propagation, and there will either be a tendency toward independent and concurrent homopolymerization, or toward the formation of copolymers containing long sequences of each monomer ("blocky: copolymers). There are very few, if any, cases where the r_1r_2 product is significantly greater than unity [6].

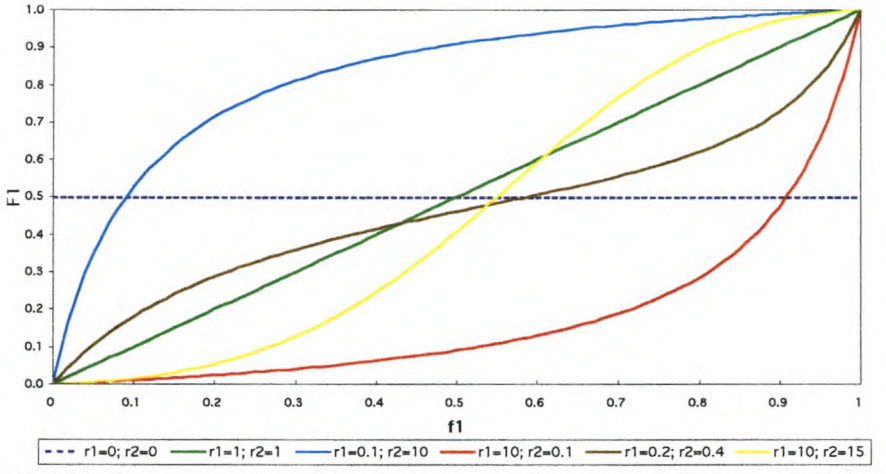

Figure A5.1: Graphical representation of instantaneous copolymer composition as a function of monomer composition for various reactivity ratio pairs.

A5.2.1.6 Instantaneous sequence distribution

Consider the first propagation step in eq. (A5.1) where $M_1^{\bullet}$ adds to M_1. The probability of this step occurring (P_{11}) is given by:

$$P_{11} = \frac{k_{11}[M_1^{\bullet}][M_1]}{k_{11}[M_1^{\bullet}][M_1] + k_{12}[M_1^{\bullet}][M_2]} \tag{A5.17}$$

Similar treatment of the other three propagation steps in eq. (A5.1), and subsequent simplification leads to the following four probabilities:

$$P_{11} = \frac{r_1[M_1]}{r_1[M_1]+[M_2]} = \frac{r_1 f_1}{r_1 f_1 + f_2} \tag{A5.18a}$$

$$P_{12} = \frac{[M_2]}{r_1[M_1]+[M_2]} = \frac{f_2}{r_1 f_1 + f_2} \tag{A5.18b}$$

$$P_{22} = \frac{r_2[M_2]}{r_2[M_2]+[M_1]} = \frac{r_2 f_2}{r_2 f_2 + f_1} \tag{A5.18c}$$

$$P_{21} = \frac{[M_1]}{r_2[M_2]+[M_2]} = \frac{f_1}{r_2 f_2 + f_1} \tag{A5.18d}$$

with

$$P_{11} + P_{12} = 1 \quad \text{and} \quad P_{22} + P_{21} = 1 \tag{A5.19}$$

Stellenbosch University http://scholar.sun.ac.za

Copolymer sequence distributions are usually expressed as the number-fractions of uninterrupted sequences of a given monomer (M_1 or M_2) that are of a particular length. An uninterrupted sequence of M_1 units of length x is formed when an $M_1^{\bullet}$-terminated macroradical adds (x-1) M_1 units followed by an M_2. The probability of such a sequence occurring can be determined by calculating the product of the probabilities of the independent steps that lead to the sequence. The number fraction of all M_1 sequences of which the length is x ($N_{1;x}$) then equals the probability that any particular M_1 sequence is of that length ($P_{1;x}$). A similar argument holds true for M_2 sequences. Thus:

$$N_{1;x} = P_{1;x} = P_{11}^{x-1} P_{12} \tag{A5.20a}$$

and

$$N_{2;x} = P_{2;x} = P_{22}^{x-1} P_{21} \tag{A5.20b}$$

The statistical approach toward copolymer composition is very useful, not only in the determination of sequence distributions, but also in the derivation of the instantaneous copolymer composition equation. In the derivation of the Mayo-Lewis equation (5) it was necessary to assume the steady-state condition stated in eq. (4). Even more complex steady-state assumptions are required for the derivation of composition equations for models where the effects of more remote units are considered (penultimate model, pen-penultimate model, etc.). Goldfinger and Kane [7] were the first to use the statistical approach to derive the copolymer composition equation for the terminal model without recourse to steady-state assumption.

The number average sequence length of M_1 (x_{1av}), which equals the "relative weight" of all M_1's (W_1), determined by the summation of the sequence fractions properly weighed according to the number of M_1 units in each sequence, is given by

$$W_1 = x_{1av} = \sum_{x=1}^{\infty} x N_{1;x} \tag{A5.21a}$$

and similarly:

$$W_2 = x_{2av} = \sum_{x=1}^{\infty} x N_{2;x} \tag{A5.21b}$$

which can be shown to correspond to (see Appendix 6):

$$W_1 = x_{1av} = \frac{1}{P_{12}} \tag{A5.22a}$$

and

$$W_2 = x_{2av} = \frac{1}{P_{21}} \tag{A5.22b}$$

The molecular composition of the copolymer can now be expressed as the ratio of the respective weight fractions.

$$\frac{F_1}{F_2} = \frac{W_1}{W_2} = \frac{P_{21}}{P_{12}} = \frac{f_1}{f_2} \times \frac{r_1 f_1 + f_2}{r_2 f_2 + f_1} \tag{A5.23}$$

Simple substitution shows that eq. (A5.23) is equivalent to the Mayo-Lewis equation.

A5.2.2 Composition drift

The copolymer compositions, sequence distributions, and average sequence lengths derived above are instantaneous values, and are therefore only adequate to describe the polymer properties at fixed (constant) feed compositions (and fixed reactivity ratios). Fixed feed

Stellenbosch University http://scholar.sun.ac.za

compositions can be maintained by continuously feeding the reactor at a rate that equals the polymerisation rate with a monomer mixture identical in composition to the copolymer being formed. If this is not done, there will be a continuous change or drift in feed (and hence polymer) composition as the reaction progresses, since the compositions of copolymer and feed generally differ. Exceptions are terminal-model copolymerisation in which azeotropic behaviour is observed. Fixed feed compositions in batch reactors can also be approximated by stopping copolymerization reactions at very low conversions (typically 5 to 10%), thereby limiting the effect of composition drift.

For obvious reasons, it is customary in practice to carry out polymerisations to high conversions, and the manner in which the copolymer composition varies as the reaction proceeds is of great importance. This relation can be obtained by integrating the differential composition equation (5) to yield [1]

$$\ln\frac{[M_2]}{[M_2^0]}=\frac{r_2}{1-r_2}\ln\frac{[M_2^0][M_1]}{[M_1^0][M_2]}-\frac{1-r_1r_2}{(1-r_1)(1-r_2)}\ln\frac{(r_1-1)[M_1]/[M_2]-r_2+1}{(r_1-1)[M_1^0]/[M_2^0]_0-r_2+1} \tag{A5.24}$$

Direct application of the integrated composition equation is difficult, and although computation may be made easier by simplifications or power-series approximation [8], the use of this equation is time consuming [6].

There is, however, a more convenient way of deriving a conversion-composition equation. The analogy between copolymerization and the boiling of a mixture of liquids has already been mentioned. Skeist [4] took this analogy further by using the Raleigh equation, which relates the composition and yield in distillation processes, to derive the relation between the composition and conversion of copolymerization reactions. Consider a mixture of monomers M_1 and M_2, of mole fractions f_1 and f_2 respectively, such that the polymer originally formed is enriched in M_1 relative to the feed ($F_1>f_1$). If there is a total of M moles of monomers present, the number of moles of M_1 will be f_1M.

When dM moles have polymerised, the polymer will contain F_1dM moles of M_1. At this time, the number of moles of M_1 in the feed will be reduced to $(M-dM)(f_1-df_1)$. A material balance of M_1 dictates that:

$$f_1M-(f_1-df_1)(M-dM)=F_1dM \tag{A5.25}$$

Ignoring the product of the differentials, Skeist [4] showed that:

$$\ln\frac{M}{M^0}=\int_{f_1^0}^{f_1}\frac{df_1}{F_1-f_1}\ \text{Skeist Equation} \tag{A5.26}$$

This conversion-composition equation (26) is model independent and can be used to determine the conversion, irrespective of which model was used to calculate the instantaneous copolymer compositions. Thus, if F_1 is calculated at suitable intervals for $0<f_1<1$ by using the appropriate model, graphical or numeric integration of the function $1/(F_1-f_1)$ between the desired values of f_1 yields $\ln(M/M^0)$. The conversion, X, can then easily be calculated form:

$$X=1-\frac{M}{M^0} \tag{A5.27}$$

Meyer and Lowrey [9] have obtained an analytical solution to Skeist's equation for the terminal model by substitution of eq. (A5.10) into eq. (A5.26) and subsequent integration. This yields:

$$\frac{M}{M^0}=\left(\frac{f_1}{f_1^0}\right)^{\alpha}\left(\frac{f_2}{f_2^0}\right)^{\beta}\left(\frac{f_1^0-\delta}{f_1-\delta}\right)^{\gamma}\ \text{(Meyer-Lowry equation)} \tag{A5.28}$$

where

Stellenbosch University http://scholar.sun.ac.za

$$\alpha = r_2/(1-r_2)$$
$$\beta = r_1/(1-r_1)$$
$$\gamma = (1-r_1r_2)/(1-r_1)(1-r_2)$$
$$\delta = (1-r_2)/(2-r_1-r_2)$$

The average composition of the total polymer formed at that point, F_{1av}, then follows either by:

- graphical integration of F_1 vs. M_1, or
- by calculating the difference between the composition and amount of residual monomers and those originally present. Thus:

$$F_{1av} = \frac{M_1^0 - M_1}{M^0 - M}$$
$$= \frac{f_1^0 M^0 - f_1 M}{M^0 - M}$$
$$= \frac{f_1^0 - f_1(M/M^0)}{1-(M/M^0)}$$

or, by substituting eq. (27):

$$F_{1av} = \frac{f_1^0 - f_1(1-X)}{X} \qquad \text{(A5.29)}$$

A5.2.3 Determination of reactivity ratios

Reactivity ratios are generally determined by the preparation of copolymers from known feed compositions (f_1; f_2), analysis of the copolymer composition (F_{1av}; F_{2av}), and subsequent calculation of the ratios (r_1; r_2) by manipulation of the appropriate copolymerisation equations. Since the use of the integrated forms of the copolymerization equations is impracticable, constant feed compositions are approximated by limiting the reactions to low conversions. Under these conditions:

$$f_1 \approx f_1^0 \approx const \qquad \text{(A5.30)}$$

and thus

$$F_1 \approx F_{1av} \qquad \text{(A5.31)}$$

A5.2.3.1 Approximation method

The approximation method depends on the fact that the composition of the copolymer is almost exclusively dependent on r_1 when low concentrations of M_2 are used [10]. Under these circumstances, it can be shown that:

$$r_1 = f_2/F_2 \qquad \text{(A5.32)}$$

The advantage of this method is that it allows for quick estimation of the reactivity ratio r_1 by performing a single experiment, but sensitive analytical procedures are required to accurately determine the mole fraction of monomer 2 incorporated into the polymer (F_2). The method is also based on the assumption that the system obeys the usual copolymerisation mechanism without any means of independently evaluating the validity of the assumption, and may be seriously biased if $r_1<0.1$ or $r_1>10$.

Similarly, at low concentrations of M_1, r_2 may be obtained from:

$$r_2 = f_1/F_1 \qquad \text{(A5.33)}$$

Stellenbosch University http://scholar.sun.ac.za

A5.2.3.2 Curve-fitting method

This method comprises preparing a graph of observed copolymer compositions (F_1) versus monomer composition (f_1) and then drawing a curve represented by eq A5.7a for selected r_1 and r_2 values. This process is repeated for other r_1, r_2 pairs until a good fit to the experimental data is achieved. The method provides the observer with:

- a visual check on the validity of the model as the data is generally collected over a wide range of monomer compositions,
- a qualitative measure of the experimental error (assuming the validity of the model), and
- a qualitative measure of how well the reactivity ratios are estimated.

Extensive iterative calculations and subjective weighing of data (in the determination of how good the fit is) are major disadvantages.

Tidwell and Mortimer proposed a non-linear least-squares method (based the Gauss-Newton non-linear least-squares procedure) to remove observer subjectivity and to quantitatively determine the confidence limits for the r1, r2 set [10]. These authors have also given guidelines to the planning of experimental conditions. Two concentrations of M2 (f21 and f22) that will lead to precise estimates of the reactivity ratios are calculated. The first method relies on maximizing the modulus of the determinant of a 2x2 matrix with elements consisting of the partial derivatives of functions of (f21, f22, r1, and r2) with respect to r1 and r2. They have also provided a table of computations that maximise the modulus for selected r1, r2 values in order to facilitate future experimental work without the need for further calculation.

A somewhat less exact, but much simpler method, involves the estimation of experimental conditions such that:

$$f_{21} \approx r_1/(2+r_1) \tag{A5.34a}$$

and

$$f_{22} \approx 2/(2+r_2) \tag{A5.34b}$$

A5.2.3.3 Intersection method

Mayo and Lewis proposed the rearrangement of eq A5.7a to yield [10]:

$$r_1 = r_2\left(\frac{F_1 f_2^2}{F_2 f_1^2}\right)+\left(\frac{f_2}{f_1}\right)\left(\frac{F_1}{F_2}-1\right) \tag{A5.35}$$

Thus, if for each experimental data set, r1 (ordinate) was plotted against r2 (abscissa), a line with slope ($F_1f_2^2/F_2f_1^2$) and intercept (f_2/f_1)[(F_1/F_2)-1] would ensue. Theoretically (and in the absence of experimental errors) these lines should intercept at a single point on the r1, r2 plane.

A5.2.3.4 Linearization method

Yet another re-arrangement of eq 7a, proposed by Fineman and Ross [11] yields:

$$\frac{f_1\,(F_2-F_1)}{f_2\,F_1}=\left(-\frac{F_2 f_1^2}{F_1 f_2^2}\right)r_1 + r_2 \tag{A5.36}$$

Consequently, a plot of $f1(F_2\text{-}F_1)/f2F1$ versus $-F_2f_1^2/F_1f_2^2$ would yield a straight line with slope r_1 and intercept r_2.

A5.2.3.5 The Q-e scheme

The reactivity of monomers with free radicals involves resonance, polar and steric factors. Although the Q-e scheme does not accommodate steric factors, it is an attempt to combine the effects of resonance stabilization and polarity on the reactivity of monomers with free radicals in

Stellenbosch University http://scholar.sun.ac.za

a semiquantitative fashion. Whereas copolymerization theory allows the description of monomer pair reactivities by relative reactivity ratios for that particular pair, the Q-e scheme is an attempt to characterize each individual monomer with a set of numerical constants.

The central assumption of the scheme is that the rate constant, k_{ij} for the attack of radical i upon monomer j is given by:

$$k_{ij} = P_i Q_j \exp(-e_i e_j) \tag{A5.37}$$

Where P_i is characteristic of radical i; Q_j is the mean reactivity of monomer j; and e_i and e_j are measures of the polarity of the radical and monomer, respectively. When eq 5.37 is applied to the relative rate constants for a given radical i with monomers j and k, the radical reactivity factor cancels out:

$$\frac{k_{ij}}{k_{jk}} = \frac{Q_j}{Q_k} \exp(-e_i(e_j - e_k)) \tag{A5.38}$$

Thus the relative reactivity ratios, r1 and r2, of a binary system may be written as:

$$r_1 = \frac{k_{11}}{k_{12}} = \frac{Q_1}{Q_2} \exp(-e_1(e_1 - e_2)) \tag{A5.39}$$

$$r_2 = \frac{k_{22}}{k_{21}} = \frac{Q_2}{Q_1} \exp(-e_2(e_2 - e_1)) \tag{A5.40}$$

Each monomer is characterised by two numbers, Q and e, from which the reactivity ratios of any chosen monomer pair can be estimated, even before any experiment with the particular pair is carried out (as long as each monomer has previously been copolymerised with any other monomer). Styrene was chosen as the standard and assigned values of Q = 1.00 and e = -0.80. Values of Q generally increases with increased resonance stabilization, while e values become less negative as groups attached to the double bond become more electron-attracting [12].

(i) Resonance stabililization

A fundamental premise inherent in the Q-e scheme is that resonance stabilization affects the reactivity of both monomer and corresponding radicals, but in reverse ways [13]. Thus, conjugation in a monomer leads to high reactivity of the monomer with radicals in general, and low reactivity of the corresponding radical to monomers in general. Unconjugated monomers, on the other hand, possess low reactivity towards radicals, while their corresponding radicals possess high reactivity towards monomers in general.

The effect of delocalization can be further illustrated by the series of R-groups below (in the monomer $RCH{=}CH_2$ and the corresponding radical), arranged in decreasing delocalization potential. R-groups with high delocalisation potential (egg $-CH_6$) increase the stability of the radical (and thus decrease the reactivity thereof), while a group such as $-OCOCH_3$ decreases the stability of the radical (and thus increases the reactivity thereof). Thus:

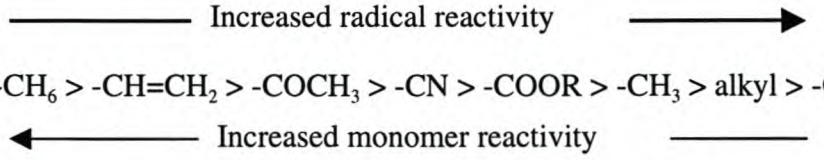

Suppression of radical reactivity toward a monomer is, however, stronger than the enhancement of monomer reactivity toward a radical [12]. The styrene radical, for example, is 1000 times less reactive toward a given monomer than the vinyl acetate radical, whereas the styrene monomer is only 50 times more reactive than the vinyl acetate monomer toward a given radical.

Stellenbosch University http://scholar.sun.ac.za

(ii) Polar effects

The polarity of the R-group also influences the nature of the copolymer. Strong electron-withdrawing groups (ester, acid, ketone, nitrile) reduce the electron density of the double bond, while electron-donating groups (alkyl, ether, acetate) have the opposite effect. Thus acrylonitrile and methyl vinyl ketone with similar polarities form random copolymers, whereas acrylonitrile and methyl vinyl ethers with opposite polarities generally form alternating copolymers.

Stellenbosch University http://scholar.sun.ac.za

APPENDIX 6

Derivation of average weight equation

$$W_1 = \sum_{x=1}^{\infty} xN_{1;x}$$

$$= \sum_{x=1}^{\infty} xP_{11}^{x-1}P_{12}$$

$$= \frac{1-P_{11}}{P_{11}} \sum_{x=1}^{\infty} xP_{11}^{x}$$

Expansion of the series leads to:

$$W_1 = \frac{1-P_{11}}{P_{11}} \left(P_{11} + 2P_{11}^2 + 3P_{11}^3 + \ldots + xP_{11}^x + \ldots\right)$$

$$= 1 - P_{11} + 2P_{11} - 2P_{11}^2 + 3P_{11}^2 - 3P_{11}^3 + \ldots + xP_{11}^{x-1} - xP_{11}^x + \ldots$$

$$= 1 + P_{11} + P_{11}^2 + P_{11}^3 + \ldots + P_{11}^x + \ldots$$

And its summation:

$$W_1 = \frac{1}{P_{11}} \sum_{x=1}^{\infty} P_{11}^x$$

Now consider:

$$\sum_{k=1}^{n} P_{11}^k = P_{11} + P_{11}^2 + P_{11}^3 + \ldots + P_{11}^n$$

and

$$\sum_{k=1}^{n} P_{11}^{k+1} = P_{11}^2 + P_{11}^3 + P_{11}^4 + \ldots + P_{11}^{n+1}$$

so that

$$\sum_{k=1}^{n} P_{11}^k - \sum_{k=1}^{n} P_{11}^{k+1} = P_{11} - P_{11}^{n+1}$$

$$\sum_{k=1}^{n} P_{11}^k - P_{11} \sum_{k=1}^{n} P_{11}^k = P_{11} - P_{11}^{n+1}$$

$$\sum_{k=1}^{n} P_{11}^k \left(1 - P_{11}\right) = P_{11} - P_{11}^{n+1}$$

$$\sum_{k=1}^{n} P_{11}^k = \frac{P_{11} - P_{11}^{n+1}}{1 - P_{11}}$$

$$\frac{1}{P_{11}} \sum_{k=1}^{n} P_{11}^k = \frac{1 - P_{11}^n}{1 - P_{11}}$$

Stellenbosch University http://scholar.sun.ac.za

APPENDIX 7

Reaction mechanisms and side reactions for the EDC/NHS activation of carboxylic acids

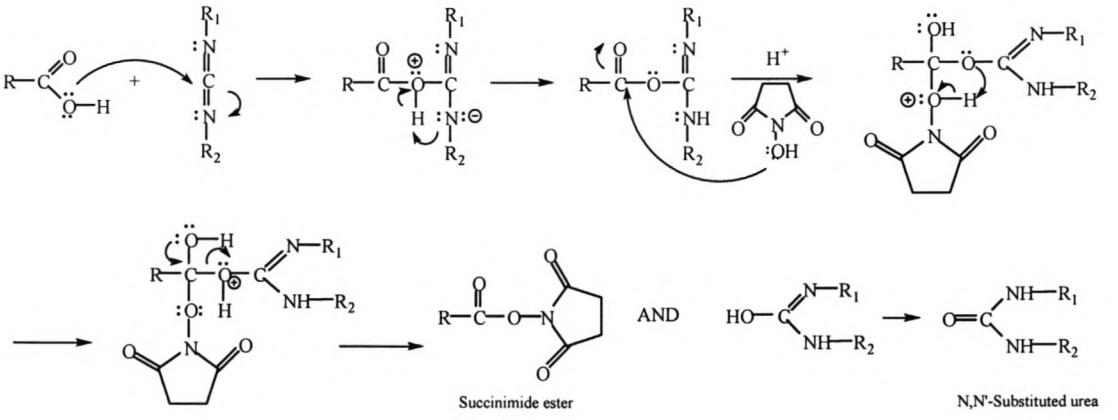

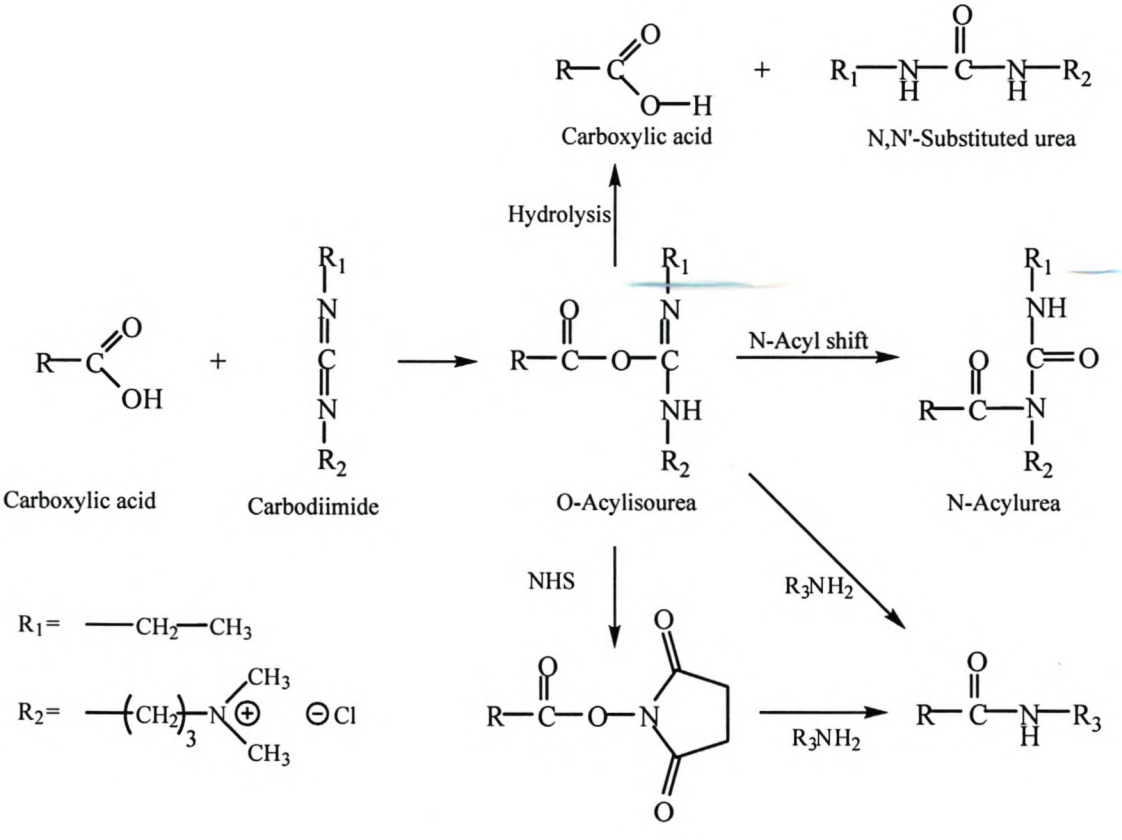

Stellenbosch University http://scholar.sun.ac.za

References

1. Mayo, F. and Lewis, F., *Copolymerization. 1. A basis for comparing the behavior of monomers in copolymerization; the copolymerization of styrene and methyl methacrylate.* Journal of the American Chemical Society, 1944. **66**(Sept): p. 1594-1601.
2. Wall, F.T., *The structure of copolymers. II.* Journal of the American Chemical Society, 1944. **66**(Dec): p. 2050-2057.
3. Turner, A. and Goldfinger, G., *The mechanism of copolymerization.* The Journal of Chemical Physics, 1944. **12**(6): p. 205-209.
4. Skeist, I., *Copolymerization: the composition distribution curve.* Journal of the American Chemical Society, 1946. **68**(Sept): p. 1781-1785.
5. Wall, F.T., *The structure of vinyl copolymers.* Journal of the American Chemical Society, 1941. **63**: p. 1862-67.
6. Mayo, F. and Walling, C., *Copolymerization*, in *Chemical Reviews*, R. Shriner and Kelley, L., Editors. 1950, The Williams & Wilkins Company: Baltimore. p. 192-287.
7. Goldfinger, G. and Kane, T., *Letter to Editors: Derivation of the copolymerization equation without steady-state assumptions.* Journal of Polymer Science, 1948. **3**: p. 462-463.
8. Walling, C. and Briggs, E., *Copolymerization III. Systems containing more than two monomers.* Journal of the American Chemical Society, 1945. **67**(Oct): p. 1774-1779.
9. Meyer, V. and Lowry, G., *Integral and differential binary copolymerization equations.* Journal of Polymer Science : Part A, 1965. **3**: p. 2843-2851.
10. Tidwell, P. and Mortimer, G., *An improved method of calculating copolymerization reactivity ratios.* Journal of Polymer Science Part A, 1965. **3**: p. 369-387.
11. Fineman, M. and Ross, S., *Linear method for determining monomer reactivity ratios in copolymerization.* Journal of Polymer Science, 1950. **5**: p. 259-262.
12. Swift, G. and Hughes, K., *Solubility parameters - Solution polymerization*, in *Encyclopedia of Polymer Science and Technology.*, Interscience Publishers: New York. p. 402-417.
13. Ham, G., *Copolymerization*, in *Encyclopedia of Polymer Science and Technology. Plastics, Resins, Rubbers, Fibers*, H. Mark, Gaylord, N., and Bikales, N., Editors. 1966, Interscience Publishers: New York. p. 165-244.